1972

Analysis of a hydrogen-oxygen semi-closed rankine cycle propulsion plant for deep submersibles.

Reese, Ronald Malcolm.

Massachusetts Institute of Technology

---

http://hdl.handle.net/10945/15979

ANALYSIS OF A HYDROGEN - OXYGEN SEMI - CLOSED RANKINE CYCLE PROPULSION PLANT FOR DEEP SUBMERSIBLES

VOLUME I

RONALD MALCOLM REESE

ANALYSIS OF A HYDROGEN-OXYGEN SEMI-CLOSED RANKINE CYCLE PROPULSION PLANT FOR DEEP SUBMERSIBLES

by

Ronald Malcolm Reese

B.S., U.S. Naval Academy
(1960)

S.M., Nav.E., Massachusetts Institute of Technology
(1970)

Submitted in Partial Fulfillment of the Requirements
for the degree of Doctor of Philosophy
at the
Massachusetts Institute of Technology
(June 1972)

ANALYSIS OF A HYDROGEN-OXYGEN SEMI-CLOSED RANKINE CYCLE PROPULSION PLANT FOR DEEP SUBMERSIBLES

Ronald Malcolm Reese

Submitted to the Department of Ocean Engineering on May 5, 1972,
in partial fulfillment of the requirements for the degree of
Doctor of Philosophy.

ABSTRACT

A semi-closed Rankine cycle propulsion plant for the propulsion of a small deep diving submersible vehicle is analyzed. The propulsion plant is fueled by cryogenic hydrogen and oxygen.

Weights and volumes, efficiencies of various plant components are estimated, and the plant is compared with competitive propulsion plants for a 50 kw, 1000 kwh mission at depths of 8000 and 20,000 feet. Weight of the plant in air is about 5500 pounds heavier than a comparable Brayton cycle propulsion plant at the 20,000 foot depth and about twice the weight of a hydrogen-oxygen fuel cell plant. It is about half the weight of a comparable silver-zinc battery system. At the 8000 foot depth it is about 1000 pounds heavier than the Brayton cycle plant.

A porous plug combustion chamber employing premixed hydrogen, oxygen and steam is evaluated, and a novel three-four disk axial impulse re-entry turbine is designed using turbine interstage leakage equations developed. A computer analysis of film condensation with superheated steam in the presence of three non-condensable gases is presented for a horizontal tube and shell condenser.

Thesis Supervisor: A. Douglas Carmichael
Title: Professor of Power Engineering

ACKNOWLEDGEMENTS

The research work performed in this thesis was sponsored by the Department of the Navy, Naval Ship Systems Command, Washington, D.C.

I wish to thank Professor A.D. Carmichael, the thesis supervisor, for his great assistance in the course of this thesis. I also thank Professor W.M. Rohsenow for his assistance in the area of heat transfer, and Professor D.B. Stickler in the area of combustion, and Professor J.L. Smith in the area of cryogenics.

The assistance of Mr. John Freund and Mr. Daniel Spadone of the Naval Ship Systems Command in obtaining release of portions of government contractor reports in the field of deep submergence power plants is much appreciated. The assistance of Mr. B. James Lowe and his staff at the Westinghouse Underseas Division, Ocean Research and Engineering Laboratory, Annapolis, Maryland was very valuable.

In the area of computer work I would like to thank the staff of the Massachusetts Institute of Technology Information Processing Center for their assistance, and Mr. Michael Aughey of the Naval Ship Engineering Center, Washington, D.C. for his assistance in obtaining a steam table computer program. The assistance of Lieutenant R.P. Gill, USN, in providing a computer optimization program for a pattern search is also appreciated.

The assistance of Dr. George Moore of the General Electric Research and Development Center, Schenectady, New York, in

reviewing the porous plug combustion chamber design is greatly appreciated.

Finally, I would like to thank Miss Sandra Vivolo for her preparation of the final manuscript and my wife, Ann, for her great help in the preparation of the rough copy.

TABLE OF CONTENTS

Abstract 2

Acknowledgements 3

List of Figures 6

List of Tables 9

Chapter I - Introduction 12

Chapter II - Previous Work 16

Chapter III - Method of Analysis 22

Chapter IV - Thermodynamic Assessment 30

Chapter V - Combustion Chamber 48

Chapter VI - Condenser and Related Equipment 64

Chapter VII - Expander Selection and Design 112

Chapter VIII - Auxiliary/Emergency Power and Transmission System 160

Chapter IX - Reactant Storage and Feed System 173

Chapter X - Regenerator 186

Chapter XI - Encapsulation and Weight and Volume Summary 190

Chapter XII - Conclusions 200

Appendix A - Liquid Propellant Rocket Combustion Chamber 205

Appendix B - Porous Plug Burner Combustion Chamber 228

Appendix C - Re-Entry Turbine Analysis 272

Appendix D - Condenser Analysis 306

Biography 426

LIST OF FIGURES

Figure I-1 Basic Semi-Closed Rankine Cycle 14

Figure III-1 Mission Power Profile 25
Figure III-2 Propulsion Power Curve Versus Vehicle Speed 26

Figure IV-1 Cycle with Regeneration 31
Figure IV-2 Enthalpy-Entropy Diagram for Recirculation Flow 32
Figure IV-3 Effect of Turbine (Expander) Inlet Temperature and Pressure 37
Figure IV-4 Effect of Combustion Chamber Pressure 39
Figure IV-5 Effect of Regeneration 40
Figure IV-6 Effect of Varying Regenerator Effectiveness on Overall Thermal Efficiency 42
Figure IV-7 Effect of Condenser Pressure 43
Figure IV-8 Effect of Expander Efficiency on Overall Thermal Efficiency 44

Figure V-1 Liquid Propellant Rocket Combustion Chamber 51
Figure V-2 Schematic Diagram of a High Pressure Porous Plug Combustion Chamber 55

Figure VI-1 Possible Arrangement for Condensation Directly on the Inner Surface of the Pressure Vessel Wall 66
Figure VI-2 External Condenser Arrangement 67
Figure VI-3 Schematic Diagram of Skin Cooler 72
Figure VI-4 Condenser Area Versus Flow Rate 87
Figure VI-5 Condenser Area Versus Flow Rate at Low Steam Flow Rates 88
Figure VI-6 Standard Condenser Weight Versus Steam Rate, Coolant Temperature, 75°F 90

Figure VI-7 Schematic Diagram of Standard Condenser 91

Figure VI-8 Schematic Diagram of Deep Sea Condenser 93

Figure VI-9 8000 Ft. Depth Deep Sea Condenser, Weight Versus Steam Rate 94

Figure VI-10 20,000 Ft. Depth Deep Sea Condenser, Weight Versus Steam Rate 95

Figure VI-11 Condenser Volume Versus Steam Rate 97

Figure VI-12 Condenser Weight and Volume Versus Surface Area 99

Figure VI-13 Non-Condensable Removal and Storage System 105

Figure VI-14 Condensate/Product Water/Feed System 106

Figure VI-15 Condenser Off-Design Performance 109

Figure VII-1 Two Stage Re-entry Turbine-Schematic Diagram (Crossover Duct Geometry) 115

Figure VII-2 Leakage Paths in a Multistage Axial Impulse Re-entry Turbine (3 stage) (Crossover Duct Geometry) 120

Figure VII-3 Composite N_S - Efficiency Diagram for Full Admission, Partial Admission and Re-entry Axial Turbines 124

Figure VII-4 Re-entry Turbine N_S - Efficiency Diagram for Small Numbers of Blades and Large Clearances 125

Figure VII-5 N_S - Efficiency Diagram for Re-entry Turbines with Intermediate Numbers of Blades and Medium Clearances 126

Figure VII-6 N_S - Efficiency Diagram for Re-entry Turbines-Moderately Large Clearances and Small Number of Blades 127

Figure VII-7 Reynolds Number Versus Loss Factor Ratio 141

Figure VII-8 50 kw Turbine 144

Figure VII-9 500 kw Turbine 148

Figure VII-10 Turbine Off-Design Performance 152

Figure VII-11 Stage Exit Pressure for Three Operating Conditions 154

Figure IX-1	Reactant Pump Stage	181
Figure IX-2	Pressurizing Arrangement	183
Figure X-1	Regenerator Design	187
Figure XI-1	Propulsion Plant Pressure Vessel Arrangement	196
Figure A-1	Injector Head	220
Figure A-2	Rocket Type Combustion Chamber	222
Figure B-1	Schematic Diagram of Porous Plug Burner	229
Figure B-2	Cooling Coil Geometry	251
Figure B-3	Lengthwise Temperature Distribution-Cooling Coil	252
Figure B-4	Axial Distribution of Plug Temperature	257
Figure B-5	Possible Combustion Chamber	262
Figure C-1	Cutaway Schematic Diagram of a 3-stage Re-entry Turbine with Crossover Ducts	273
Figure C-2	Cutaway Schematic Diagram of a Two Stage Re-entry Turbine with Alternate Admission	276
Figure C-3	Velocity Diagram	283
Figure C-4	Leakage Paths	288
Figure C-5	Turbine Blade Geometry	297
Figure D-1	Staggered Tube Bank with Square Pitch Rotated	310
Figure D-2	Control Volume I	311
Figure D-3	Control Volume II	315
Figure D-4	Colburn j Factor Versus Reynolds Number	318
Figure D-5	Tube Layout	319
Figure D-6	Control Volume III	321

LIST OF TABLES

Table V-1 Variable Pressure Operation of the Liquid Propellant Combustion Chamber-50 kw Plant 55

Table V-2 Liquid Rocket Combustion Chamber Dimensions, Weights and Volumes 62

Table VI-1 Skin Cooler Analysis for Coolant Passage Configuration A of Figure VI-3 76

Table VI-2 Skin Cooler Analysis for Coolant Passage Configuration B of Figure VI-3 77

Table VI-3 Skin Cooler Analysis for Coolant Passage Configuration C of Figure VI-3 78

Table VI-4 Electrical Power Required for Skin Cooler 80

Table VI-5 Additional Weight Incurred for a Skin Cooler Without Fins 81

Table VI-6 Commercial Oxygen Contaminants, Typical Analysis 82

Table VI-7 Commercial Hydrogen Contaminants, Typical Analysis 83

Table VI-8 Assumed Data for Condenser Studies 86

Table VI-9 Submerged Condenser Circulating Pump Requirements for the Deep Sea Condenser (40 kw plant) 96

Table VI-10 Comparison of Skin Cooler with Standard Condenser and Deep-Sea Condenser Designs at 20,000 feet 100

Table VI-11 Non-Condensable Removal and Storage System 104

Table VI-12 Condensate/Feed Pump 105

Table VI-13 Heat Loads for Auxiliary Cooling Water System 107

Table VII-1 Effect of Pressure Ratio on Turbine Efficiency at Constant Specific Speed 132

Table VII-2 Data on a 4 Stage Re-entry Turbine with Unequal Pressure Ratios-Wong (4) 135

Table VII-3 50 kw, 3 Disk - 8 Stage Re-entry Turbine 145

Table VII-4 500 kw, 4 Disk Turbine 149

Table VII-5 Turbine Weight, Volume and Dimensions 148

Table VIII-1 Survey of Transmission Systems 162

Table VIII-2 Auxiliary Electrical Loads for a Nominal 50 kw-1000 kwh Plant 164

Table VIII-3 Alternator and Related Components and Extraneous Electrical Equipment 167

Table VIII-4 AC Propulsion Transmission System 169

Table IX-1 Reactant Required for a 50 kw, 1000 kwh Propulsion Plant 177

Table IX-2 Cryogenic Storage Weights and Volumes for Various Storage Alternatives for 20,000 Ft. Depth HY-180 Steel Pressure Vessels 179

Table IX-3 Reactant Pumps for a Nominal 50 kw Plant 182

Table X-1 Regenerator Data 188

Table XI-1 Final Plant Conditions 50 kw - 1000 kwh Plant 192

Table XI-2 Propulsion Plant Pressure Vessel and External Equipment-Weights and Volumes 193

Table XI-3 Reactant Storage and Product Water System Weights and Volumes 194

Table XI-4 Overall Weight for 50 kw, 1000 kwh Propulsion Plant 197

Table A-1 Assumed Conditions for 50 kw Shaft Power Plant 212

Table A-2 Oxygen Injector Characteristics 221

Table A-3 50 kw Design Maximum Power Level (shaft) Combustion Chamber Characteristics (sized for 125% design maximum power level) 223

Table B-1 Summary of Design Conditions for Porous Plug 249

Table B-2 Heat Flux to Burner Versus Unburned Mixture Composition 254

Table B-3 Superheating Coil 263

Table D-1 References for Fluid Properties 330

Table D-2 Condenser Data 333

CHAPTER I

Introduction

The need for new propulsion plants to power deep diving submersibles becomes apparent when one considers the power and endurance limitations on present battery powered vehicles. The associated heavy weight of batteries, even if they are externally mounted, makes mission life short and limits available power levels to low values.

The small submersible requires tending by a larger service vessel which must transport the submersible to the operating area, place it in the water, and remove it at the end of the mission. This launching and recovery process is severly hampered in any but the best weather conditions. While it has been suggested that such a vehicle operate independently and thus eliminate the launch and recovery problem, insufficient endurance levels seem to preclude this for anything but nuclear powered deep diving submersibles. To build a vehicle capable of extreme depth (8000-20,000 ft) operation and also capable of extended endurance would require a larger than normal submersible crew (two or three) as well as a significantly larger portion of the vehicle capable of withstanding extreme pressures. In essence, this would require larger living space which, in turn, would place even more difficult requirements on pressure vessel design. The weight of a spherical vessel, the most efficient shape for extreme depths, increases in an exponential fashion as vessel diameter is increased. Thus, an independently operating submarine would probably require a series of

relatively small interconnected spheres for minimum weight.

At present, the best solution to operating at extreme depths for missions of 24-36 hours duration appears to lie with the tended submersible. This choice has led to a requirement for small, high energy density propulsion plants. While the volume of such a plant is of concern, its overall weight in air is of primary importance, since it is this weight that the service vessel must lift. This vehicle weight, of course, includes sufficient flotation material to make the vehicle neutrally buoyant in water. Thus, in the comparison of various propulsion plants for the same mission endurance and the same full power level, one should include sufficient flotation material to make the propulsion plant neutrally buoyant.

In this thesis a semi-closed, hydrogen-oxygen fueled, Rankine cycle propulsion plant is investigated as a power source for submersibles operating at extreme depths in the range of 8000-20,000 feet. The advantages of such a plant are the high energy density of the reactants and the virtual absence of non-condensable combustion products.

The proposed propulsion plant is effectively an open steam cycle with recirculation of a portion of the condensate as feed water to dilute the high temperature combustion gases. A schematic diagram of the basic cycle is shown in Figure I-1.

In order to determine the optimum operating conditions for the plant, thermodynamic studies were conducted. The results of these studies required analysis of the effect of these optimum conditions on dimensions and achievable efficiency of the individual components.

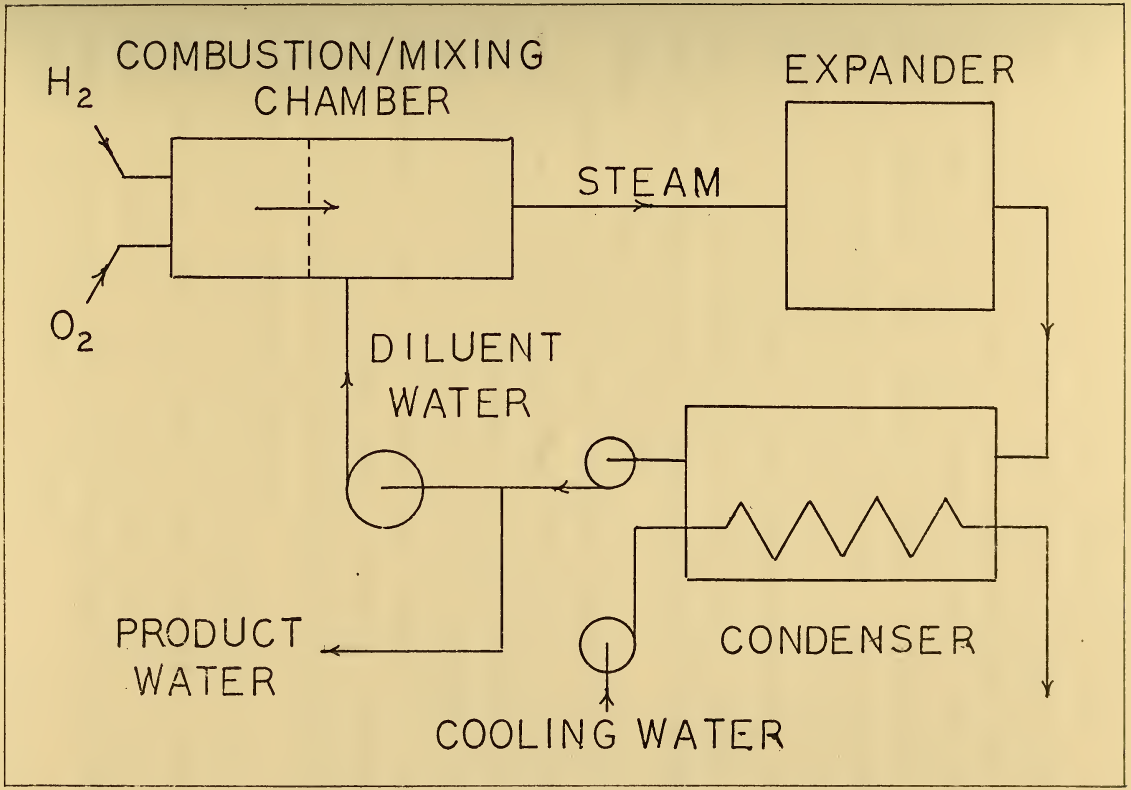

FIGURE I-1
BASIC SEMI-CLOSED RANKINE CYCLE

Analysis of such a propulsion plant requires detailed investigation of the most critical components in order to determine reliability, safety, efficiency, size and weight. In the course of the thesis, it was determined that these critical components were the combustion chamber, the turbine and the condenser. The combustion chamber was important from the aspect of reliability as well as safety and high combustion efficiency. The turbine was found to be of critical importance with respect to the overall plant thermal efficiency. The importance of the condenser lies in its size in relation to other plant components, and in the safe removal of unburned hydrogen and oxygen from the plant.

Using information from the detailed analysis of the various plant components and their efficiencies, the overall plant configuration is developed and overall weights and volumes of the power plant and associated containment vessels are presented. The overall weights are corrected for sufficient flotation material to achieve neutral buoyancy. The propulsion plant is then compared with other existing and proposed propulsion plants for comparable missions.

In contrast to the normal thesis format, lists of references and symbols are found at the end of each respective chapter or appendix. This was necessary because of the large number of engineering disciplines encompassed by the thesis and the nomenclature peculiar to each.

CHAPTER II

Previous Work

Chemical-dynamic power systems for deep submergence applications have been studied by several investigators. Reference 1, a study conducted by the Committee on Undersea Warfare, National Research Council of the National Academy of Sciences, compared various candidate propulsion plants including the fuel cell. This report recommended parallel investigation of fuel cells and chemical dynamic systems for a period of several years, followed by development of the most promising candidate. Sternlicht and Bjerklie (2) assessed a basic hydrogen and oxygen fueled open expansion cycle (discharging to ambient sea pressure) as well as other dynamic systems and determined that in the medium power, medium endurance range (about 50 kw, 1000 kwh), the closed dynamic cycle and fuel cell were comparable in an analysis of reliability, weight, serviceability, development time and development cost.

Morrison, McCartney and Blose (3) assessed the depth insensitive heat engine using hydrogen and oxygen as reactants as well as other competitive propulsion plants, but presented no details on the specific cycles considered. For a steam boiler and turbine plant below 200 HP, they estimated a basic cycle efficiency of 20%. They also stated that for power levels less than 100 HP, the reciprocating steam engine appeared to be more efficient than a steam turbine.

Catterson and Swain (4) assessed the semi-closed power

cycle for operation with various fuels, among them hydrogen and oxygen, and compared them with H_2-O_2 fuel cells, batteries and radioisotope-dynamic systems for a 30 kw power level. For a design depth of 6000 feet, the chemical-dynamic system was considerably lighter, including flotation material, than other systems in the range of 2-30 hours mission duration. They predicted an overall thermal efficiency of 20-30% for a Rankine cycle using water as the working fluid. These figures represent the results of an investigation of the semi-closed cycle of this thesis and the normal closed steam cycle with a boiler. Catterson and Swain recognized the weight penalty of encapsulation spheres for cryogenic hydrogen.

Walter (5) proposed the cycle of this thesis using cryogenic oxygen with cryogenic hydrogen or methane as fuel. The proposed power level was 400 HP. For a 1000°C (1832°F) turbine inlet temperature and a 29 lbf/in^2 condenser pressure, Walter predicted a 34% overall thermal efficiency for a plant burning stoichiometric methane and oxygen at 72.5 lbf/in^2. The proposed turbine was a 5 stage machine. As in the cycle of this thesis, diluent fluid would reduce the combustion gas temperature to a level acceptable for the turbine. The combustion products, water and carbon dioxide, would be stored on board.

Balukjian and Rackley (6) investigated the closed Brayton Cycle propulsion plant for deep submersibles for design depths of 8,000 and 20,000 feet for a 50 kw power level and at mission endurance levels of 1000 and 2000 kwh. They estimated a power cycle efficiency of 44.7% for a propulsion plant fueled by

cryogenic hydrogen and oxygen. This represents an overall thermal efficiency of about 33% (7).

A supercritical CO_2 cycle has also been proposed for deep submergence application by Karig (8) using a modified Feher cycle (9). Karig predicts an overall thermal efficiency of over 40% with this cycle. This cycle, essentially a semi-closed Brayton cycle, would operate in the same fashion as that proposed in this thesis, recirculating a diluent to reduce combustion gas temperatures to acceptable turbine inlet temperatures.

Several other chemical-dynamic propulsion plants have been investigated and some have been built. The Alton Cycle (10) is one such plant. It burned diesel oil with hydrogen peroxide as the oxidant.

The hydrogen-oxygen encapsulated fuel cell appears to be the most promising fuel cell candidate at present. It has not yet been installed on a deep submersible vehicle. The fuel cell plant has been discussed in many papers (11), (12). The estimated conversion efficiency of the hydrogen-oxygen fuel cell is in excess of 50% and may be as high as 70%.

Several other fuel cell candidates exist. Ghormley and Harrison (13) discussed a hydrazine-hydrogen peroxide system, which would not require encapsulation. This system is now under development at the Naval Ship Research and Development Laboratory. Overall weight for this system is reportedly about the same as the encapsulated hydrogen-oxygen fuel cell system. Another candidate using hydrazine and hydrogen peroxide is the Alsthom fuel cell (14).

It is apparent that the hydrogen-oxygen fueled semi-closed Rankine cycle may be expected to exhibit an overall thermal efficiency of 30% or perhaps greater. The degree of development of the major equipment associated with such an application is high. Only the combustion chamber, as noted by Morrison, McCartney and Blose (3), requires extensive development. While the achievable thermal efficiency is apparently far below that of fuel cells, it appears that the propulsion plant could be readily developed to provide reliable power for submersibles operating at extreme depths. The cost of such development could be considerably cheaper than for a comparable fuel cell plant. It is the intent of this thesis to analyze the application of a hydrogen-oxygen semi-closed Rankine cycle for the propulsion of a submersible operating at extreme depths.

REFERENCES

1. *Energy Systems of Extended Endurance in the 1-100-Kilowatt Range for Undersea Applications*, Publication 1702, Washington, D.C., National Academy of Sciences, 1968.

2. Sternlicht, B. and J.W. Bjerklie, "Comparison of Dynamic and Static Power Systems for Undersea Missions", *Journal of Engineering for Power*, Vol. 88, No. 4, October, 1966, pp 323-333.

3. Morrison, T.D., J.F. McCartney and J.F. Blose, "Power Plants for Deep Ocean Vehicles", Paper #5 presented at the Society of Naval Architects and Marine Engineers, Spring Meeting, Philadelphia, May, 1966.

4. Catterson, R.K. and J.C. Swain, "Chemical-Dynamic Systems for Undersea Power", *Battelle Technical Review*, January, 1968.

5. Walter, H., "An Undersater Propulsion System Using Cryogenic Fuel", *Marine Engineer and Naval Architect*, January 1971, p 27.

6. Balukjian, H. and R. Rackley, "A Closed Brayton Cycle Power System for Deep Submersibles", *Journal of Hydronautics*, Vol. 5, No. 1, January, 1971, pp 5-10.

7. Balukjian, H., "A Closed Brayton Cycle Power Plant for Underwater Applications and Comparison with a Fuel Cell", paper presented at the Seventh Annual Technical Symposium, Association of Senior Engineers, Naval Ship Systems Command, Washington, D.C., 1970.

8. Karig, H.E., "Proposed Supercritical Thermal Power System for Undersea Applications Using Combustion Gases for Working Fluid", Naval Underwater Center, San Diego, California, NUC TP 172, 1970.

9. Feher, E.G., "The Supercritical Thermodynamic Power Cycle", *Advances in Energy Conversion Engineering*, Intersociety Energy Conversion Engineering Conference, Miami Beach, Florida, 1967, pp 37-42.

10. Reinertson, J.H., L.E. Alsager and T.J. Morley, "Submarine Propulsion Plant", *Naval Engineer's Journal*, May, 1963, pp 349-364.

11. Thurber, W.C., "A Fuel Cell Power Plant for a Deep Diving Submarine", ASME Paper No. 67-WA/Un T-2, presented at the Winter Annual Meeting of the American Society of Mechanical Engineers, November, 1967.

12. Spadone, D.M., "Power for Deep-Submergence Vehicles", Astronautics and Aeronautics, Vol. 5, No. 7, July 1967.

13. Ghormley, D.R. and J.H. Harrison, "A Liquid Fuel Cell Power System Design for Underwater Applications", paper No. 719073, *Proceedings of the 1971 Intersociety Energy Conversion Engineering Conference*, pp 520-528.

14. Warzawski, B., B. Verger and Jean-Claude Dumas, "Alsthom Fuel Cells for Marine and Submarine Applications", *MTS Journal*, Vol. 5, No. 1, Jan-Feb, 1971, pp 28-40.

CHAPTER III

Method of Analysis

The design of a propulsion plant such as that proposed in this thesis must proceed on two paths. The first path is that of producing a feasible design. Each piece of equipment must be analyzed to determine if, in fact, it can be built to meet the constraints placed upon it, and the overall plant must be examined in the same way. The second path is that of producing an optimum design within the constraints of the mission. In this thesis, both feasibility and optimization have been considered.

Safety and reliability of the plant are primary considerations which must govern the design of individual components as well as the plant as a whole. While absolute safety would be desirable, the probability of no accidents with hydrogen and oxygen cannot be guaranteed. The example of the space program in the safe handling of these potentially lethal reactants shows that it can be done if adequate precautions are taken.

Reliability must be built into each component as well as the entire plant. The design goal for the semi-closed Rankine cycle propulsion plant is set at 4000-5000 hours time between overhauls. The common arrangement of a deep submergence propulsion plant is to house the plant and its reactants and products within several containment spheres (encapsulation) located within the hull form of the submersible. To open one or more of these pressure vessels because of an equipment

malfunction would require considerable effort and would not be normally accomplished in the field. Hence an adequate time between failures should be built into each component to meet the overall design goal. This goal may not be attainable.

The analysis of a propulsion system requires certain known factors. Some of these factors are obvious from the character of the system itself. Others must be imposed by certain assumptions. For instance, it is readily apparent that the semi-closed Rankine cycle would not be competitive at shallow depths, since at these depths a plant exhausting combustion products to the sea is more easily built and less expensive. The use of hydrogen as a fuel, moreover, incurs a great penalty in encapsulation weights over other fuels because it cannot be stored outside a pressure hull and because of its large specific volume, even as a cryogenic liquid. It is only at depths where the exhausting of combustion products to the sea requires excessive expenditure of pumping power that the depth-insensitive, combustion-product-condensing plant becomes attractive. This depth is less than 8000 feet.

A depth of 8000 feet would permit operation in the area of the continental shelves and a large percentage of the continental slopes. Furthermore, it has been shown that a 20,000 foot depth capability would permit access to about 98% of the ocean bottom. Thus two depths are of interest in this thesis, 8000 and 20,000 feet.

A second factor, one which must be imposed, is mission duration and power level. The Navy's Deep Ocean Technology Program has established a basic 1000 kwh, 50 kw mission (1), for a small submersible with a search mission. The power profile for this mission is shown in Figure III-1. This mission represents a possible application for the proposed propulsion plant and has been used for detailed analysis of the cycle. A propulsion power curve versus vehicle speed is shown in Figure III-2 for a typical deep submersible for which the 50 kw full power level is applicable (2). A speed of about 7.5 knots is about the maximum attainable for a 70% transmission efficiency and a cluttered hull for the 50 kw useful power output at rated conditions. The hull in this case would have projecting search lights, manipulator arms, etc. In the analysis, the 1000 kwh mission and 50 kw power level have been assumed to be over and above any parasitic power loads peculiar to the propulsion plant.

While the propulsion plant discussed in this thesis may be useful at other levels of power and endurance, no definite mission could be determined. In the interest of determining the behavior of the cycle at higher power levels, a 500 kw plant was also studied. For this power level, the major components are sized and component efficiencies are evaluated. The weight of reactants for such a plant is, however, unspecified. Hence detailed and overall plant weights have not been developed for the 500 kw plant.

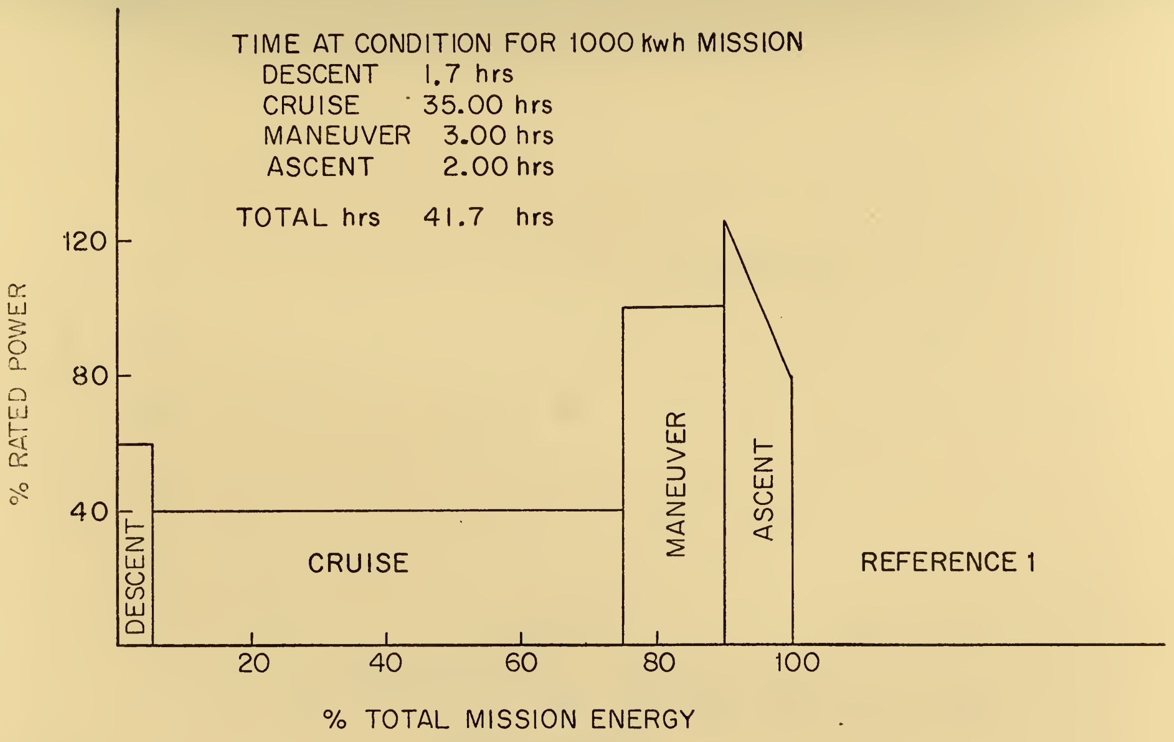

FIGURE III-1 MISSION POWER PROFILE

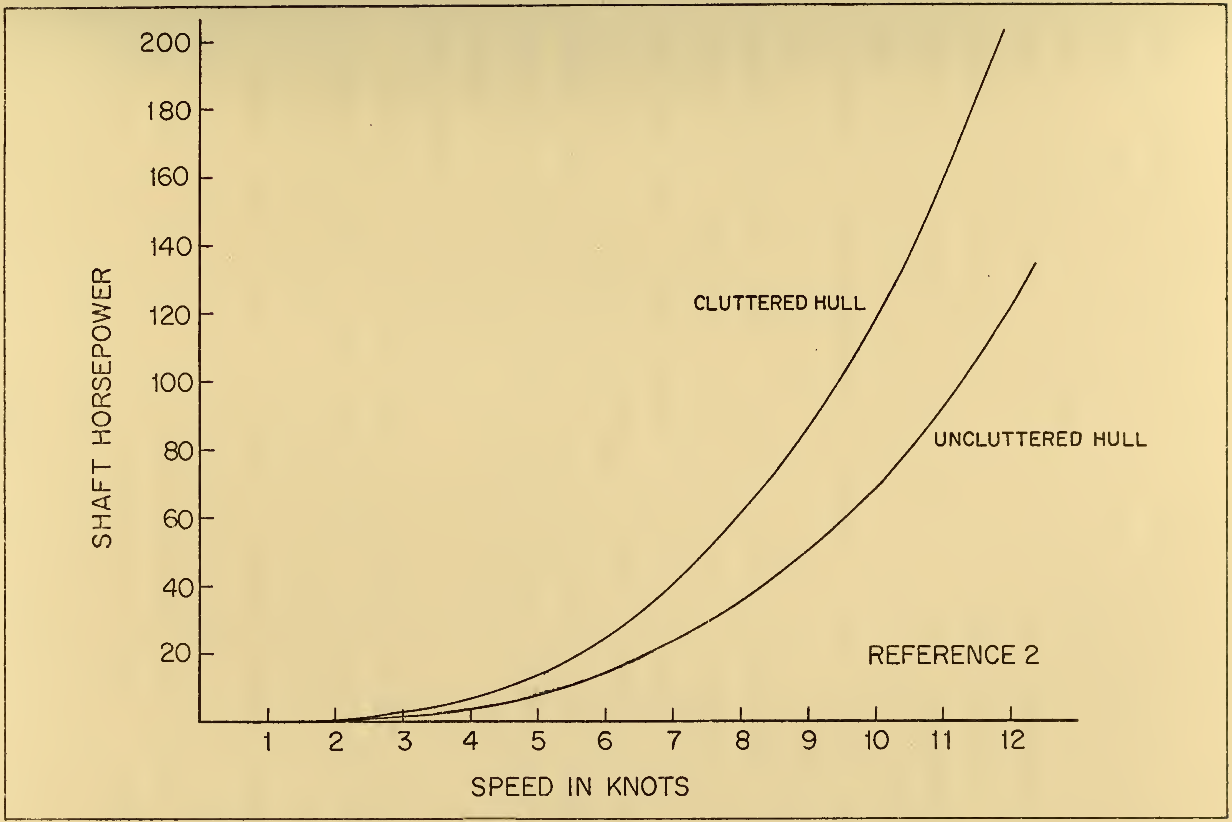

FIGURE III-2 PROPULSION POWER CURVE vs VEHICLE SPEED

With the mission power profile specified and the design depth selected, the analysis of the propulsion plant was conducted. The first step in the selection of an optimum plant was to evaluate the thermodynamic characteristics of the cycle. From the thermodynamic assessment, one could then determine the most critical components, i.e., those which would be governing with respect to plant volume and plant efficiency. These components were then analyzed in detail, and the effect of varying the thermodynamic parameters on overall plant weight could be seen. For instance, it was found that an increase of condenser volume of about 1 cubic foot would result from a reduction in condenser pressure from 2.8 to 1.0 lbf/in^2 for the 50 kw plant. This correspondingly would save about 6 cubic feet of cryogenic hydrogen in a 1000 kwh mission. Comparisons such as these led to the conclusion that the lowest attainable condenser pressure would yield the optimum plant, recognizing that condenser pressures less than 1.0 lbf/in^2 were probably not attainable.

Because of the large number of variables and the difficulty of specifying many of them analytically, no overall optimization scheme was devised. An example of such difficulty arises in turbine design where the number of possible stage pressure ratio and stage combinations becomes very large. If the turbine could be completely analyzed by computer optimization techniques this would not be so difficult, but such a scheme is difficult to devise. The approach used in the turbine analysis was to determine optimum stage characteristics by

computer optimization and then to determine stage pressure ratios and rotative speed by hand calculations. While this approach of sub-optimization of system components in order to achieve an optimimum overall system is not rigorous, it probably results in a plant which is not far from the actual optimum. The selection of the optimum thermodynamic conditions assists in this process. Assessment of optimum thermodynamic conditions is subject to computer analysis.

REFERENCES

1. *Thermal Chemical Dynamic Power Supply for Deep Submersible Vehicles*, NAVSHIPS 0907-000-6010, August 7, 1970.

2. *Deep Ocean Technology Testbed Submersible Design and Engineering Data*, Westinghouse Ocean Research and Engineering Center, January 6, 1968.

CHAPTER IV

Thermodynamic Assessment

The first step in analyzing the semi-closed Rankine cycle propulsion plant was to investigate the effect of various plant parameters of overall thermal efficiency. A schematic diagram of the cycle with regeneration is shown in Figure IV-1.

An enthalpy-entropy diagram of the semi-closed Rankine cycle is shown in Figure IV-2. The state points in this diagram correspond to the points in Figure IV-1 and are representative of the recirculated fluid.

From these diagrams one may write the first law of thermodynamics for bulk flow across the control volume of the combustion/mixing chamber:

$$\frac{dE}{dt} = 0 = i_{c,o}\,\dot{m}_c + i_{3,o}\,\dot{m}_r - i_{4,o}(\dot{m}_c+\dot{m}_r) + \cancelto{0}{\dot{Q}} - \cancelto{0}{\dot{W}_x} \qquad \text{(IV-1)}$$

where

E = internal energy within the control volume, Btu

$i_{c,o}$ = stagnation enthalpy of the reactants, including the heat of combustion, Btu/lbm

$i_{3,o}$ = stagnation enthalpy of the recirculated diluent water, Btu/lbm

$i_{4,o}$ = stagnation enthalpy of the steam leaving the combustion chamber, Btu/lbm

$\dot{m}_c$, $\dot{m}_r$ = mass flow rates of reactants (or combustion products) and recirculated water respectively, lbm/hr

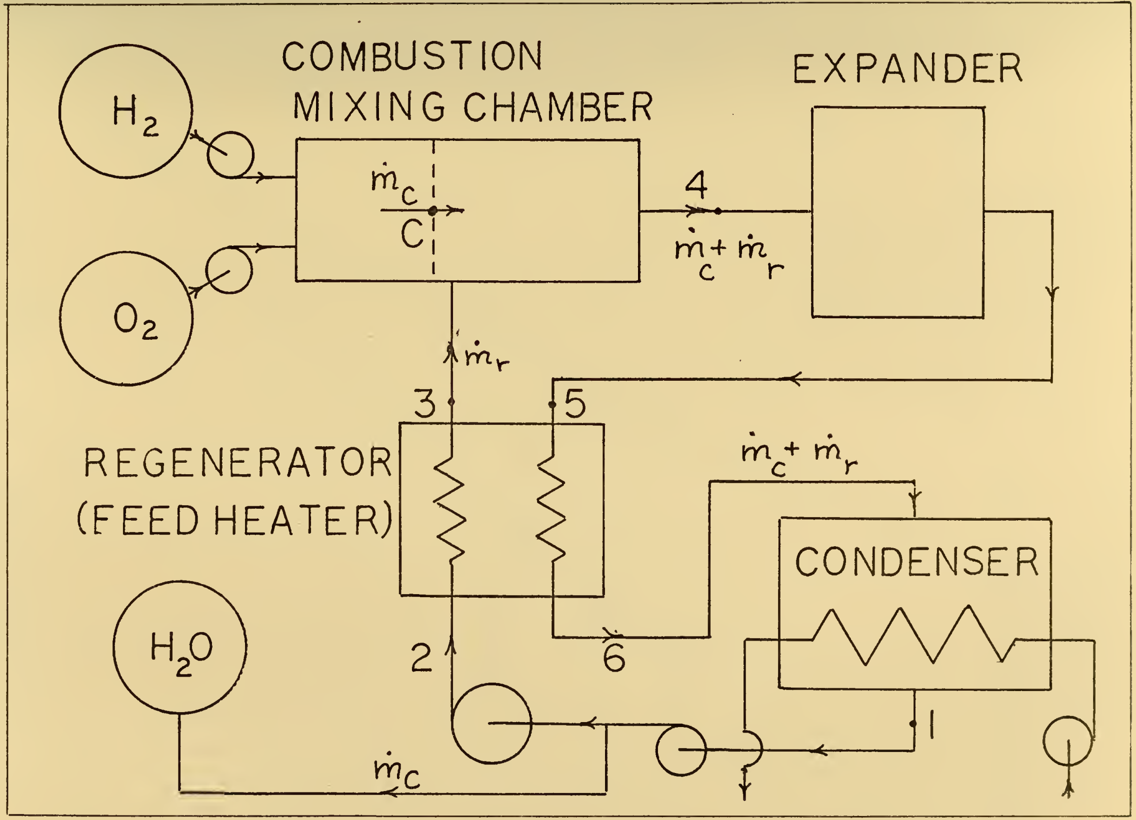

FIGURE IV-1 CYCLE WITH REGENERATION

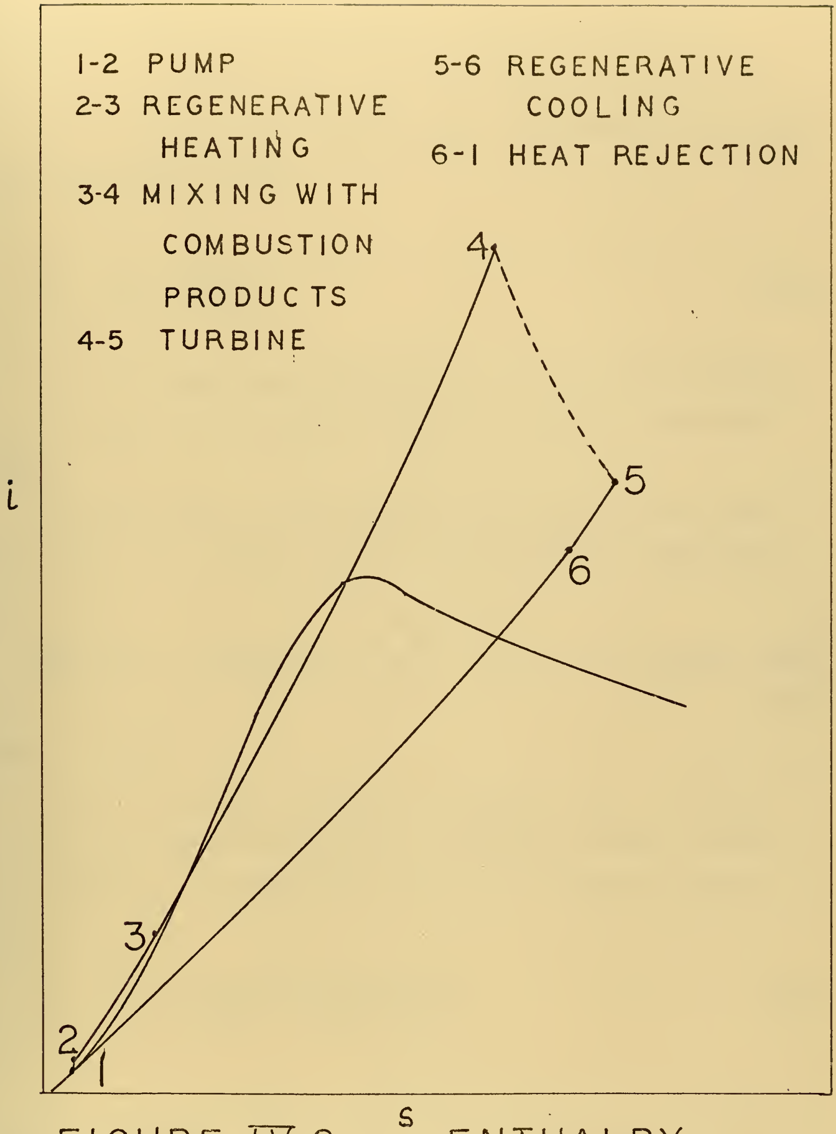

FIGURE IV-2 ENTHALPY-ENTROPY DIAGRAM FOR RECIRCULATION FLOW

$\dot{Q}$, $\dot{W}_x$ = rate of heat addition and shaft power out respectively, from the control volume, Btu/hr

By rearrangement of equation IV-1, one may then determine the recirculation ratio,

$$\frac{\dot{m}_r}{\dot{m}_c} = \frac{i_c - i_{4,o}}{i_{4,o} - i_{3,o}}. \qquad \text{(IV-2)}$$

For the case of no regeneration, one may simply replace $i_{3,o}$ by $i_{2,o}$, the stagnation enthalpy of the feed pump discharge.

The first law of thermodynamics for bulk flow may also be written for a control volume surrounding the regenerator:

$$\frac{dE}{dt} = 0 = i_{5,o}(\dot{m}_c+\dot{m}_r)+i_{2,o}\,\dot{m}_r - i_{3,o}\,\dot{m}_r - i_{6,o}(\dot{m}_c+\dot{m}_r) + \overset{0}{\cancel{\dot{Q}}} - \overset{0}{\cancel{\dot{W}}}_x \qquad \text{(IV-3)}$$

where

$i_{5,o}$ = stagnation enthalpy at expander exit, Btu/lbm

$i_{6,o}$ = stagnation enthalpy at condenser inlet, Btu/lbm

Combining equations IV-2 and IV-3, one may now write

$$\frac{\dot{m}_c}{\dot{m}_r} = \frac{(i_{c,o}-i_{4,o}) + (i_{5,o}-i_{6,o})}{(i_{4,o}-i_{2,o}) - (i_{5,o}-i_{6,o})} \qquad \text{(IV-4)}$$

As one might expect, and is now evident from equation IV-4, the recirculation ratio increases with regenerator effectiveness, since it is regenerator effectiveness which determines the

magnitude of the term $(i_{5,o}-i_{6,o})$. This results in an increase in pump work as regenerator effectiveness increases, but this is at little expense in overall thermal efficiency. The pump work is usually negligible when compared with expander work for a Rankine cycle.

Regenerator effectiveness, as defined by Kays and London (1), is as follows:

$$\eta_R = \frac{(\dot{m}_c+\dot{m}_r)\ c_{p,steam}\ (T_5-T_6)}{(\dot{m}_c+\dot{m}_r)\ c_{p,steam}\ (T_5-T_2)} \qquad \text{(IV-4)}$$

where the product, $(\dot{m}_c+\dot{m}_r)\ c_{p,steam}$ in the denominator represents the minimum product of mass flow rate and specific heat. The minimum product of $\dot{m}c_p$, for this application applies to the steam side for all cases of practical interest.

Equation IV-4 reduces to the following simple relationship:

$$\eta_R = \frac{T_5-T_6}{T_5-T_2} \qquad \text{(IV-5)}$$

Thus one may determine the regenerator steam outlet temperature, if one knows the feed pump discharge temperature and expander exit temperature.

$$T_6 = T_5(1-\eta_R) + \eta_R\ T_2 \qquad \text{(IV-6)}$$

The assumed value for the enthalpy of the combustion products, $i_{c,o}$, is dependent upon the condition of the reactants when they come in contact with the combustion

chamber. The following values were computed for $i_{c,o}$:

$i_{c,o,75}$ = 6869.8 Btu/lbm - Reactants at 75°F before contact with the combustion chamber

$i_{c,o,cry}$ = 6559.8 Btu/lbm - Reactants at saturated liquid conditions at a pressure of 1 atmosphere before contact with the combustion chamber

These enthalpy values reflect the same base enthalpy as reference 2, zero enthalpy of saturated liquid water at 32°F. The value of $i_{c,o,75}$ is associated with the higher heating value of hydrogen at standard conditions.

One observation which may be made already is the desirability of heating the reactants, if they are stored in a cryogenic state, prior to their coming into contact with the combustion chamber.

Expander total to static efficiency is defined as follows:

$$\eta_{t,t-s} = \frac{i_{4,o}-i_{5,st}}{i_{4,o}-i_{5,is,st}} \tag{IV-7}$$

where the subscript, st, denotes static conditions.

Overall cycle thermal efficiency is defined as follows:

$$\eta_{TH} = \frac{\text{net work}}{\text{heat added}} = \frac{(\dot{m}_r+\dot{m}_c)(i_{4,o}-i_{5,st})-\dot{m}_r(i_{2,o}-i_{1,o})}{\dot{m}_c \cdot i_{c,o,75°F}} \tag{IV-8}$$

For purposes of the thermodynamic assessment, one may neglect pump work, giving

$$\eta_{TH} = \frac{(\dot{m}_r+\dot{m}_c)(i_{4,o}-i_{5,st})}{\dot{m}_c \cdot i_{c,o,75}} \qquad \text{(IV-9)}$$

Of course, in the final analysis all parasitic loads must be considered when evaluating the overall thermal efficiency.

The specific reactant consumption is a somewhat better means of comparison of competitive plants. Specific reactant consumption is defined as follows:

$$\text{SRC} = \frac{\text{reactant mass flow per hour}}{\text{net work per hour}}$$

$$= \dot{m}_c \quad \frac{2545 \text{ Btu/hr HP} \cdot 1.341 \text{ HP/kw}}{(\dot{m}_r+\dot{m}_c)(i_{4,o}-i_{5,st})}$$

$$\text{SRC} = \frac{\dot{m}_c}{(\dot{m}_r+\dot{m}_c)} \quad \frac{3412.8}{(i_{4,o}-i_{5,st})}, \text{ lbm/kwh} \qquad \text{(IV-10)}$$

One may now show the effect of various plant parameters on overall thermal efficiency, bearing in mind that the efficiencies reported do not reflect parasitic losses. First, one may consider the effects of varying expander inlet temperature and pressure without regeneration for fixed condenser pressure of 1.0 lbf/in^2 and expander efficiency of 75%. This is shown in Figure IV-3.

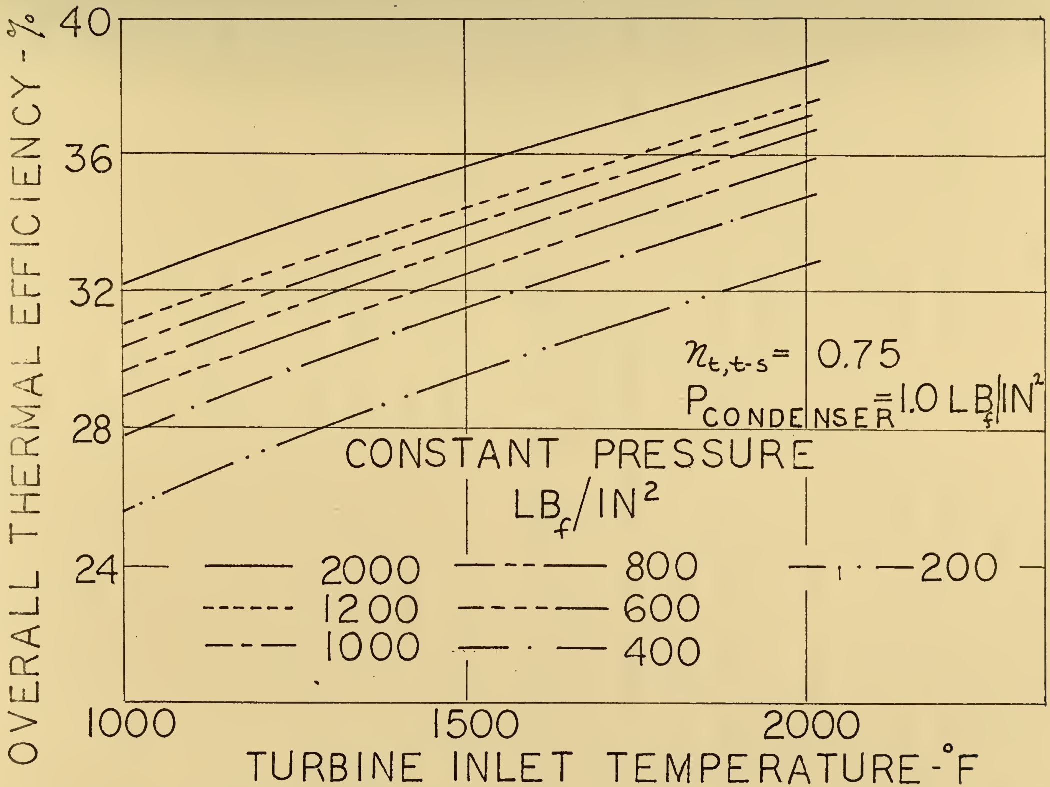

FIGURE IV-3 EFFECT OF TURBINE (EXPANDER) INLET TEMPERATURE AND PRESSURE

The beneficial effect of increasing the expander inlet temperature and pressure is evident. A considerable increase in overall thermal efficiency may be attained by increasing expander inlet temperatures above the 900-1000°F level, normal for most superheated steam plants, to 2000°F. Of course, the peak temperature attainable will be dependent upon materials and the particular expander geometry and operating conditions selected. The expander inlet pressure should also be as high as possible to attain the best overall thermal efficiency. This, too, must be tempered by constraints on the expander.

Figure IV-4 shows the effect of expander inlet pressure on expander exit temperature for constant expander inlet temperature. The result is to increase expander exit temperature with decreasing expander inlet pressure, thus making the plant a good candidate for regenerator, particularly at poor expander efficiencies.

Figure IV-5 shows the improvement of overall thermal efficiency with a constant regenerator effectiveness of 0.70 at two expander inlet temperatures. Here a constant condenser pressure of 1.0 lbf/in^2 and regenerator steam-side pressure drop of 1.0 lbf/in^2 have been assumed. Again, expander efficiency has been maintained constant at 75%. The improvement in overall thermal efficiency at a relatively poor expander efficiency is evident. At expander inlet pressures above 750 lbf/in^2 with an expander inlet temperature of 1500°F, regeneration is not effective because the expander exit temperature is too close to the saturation temperature. The same

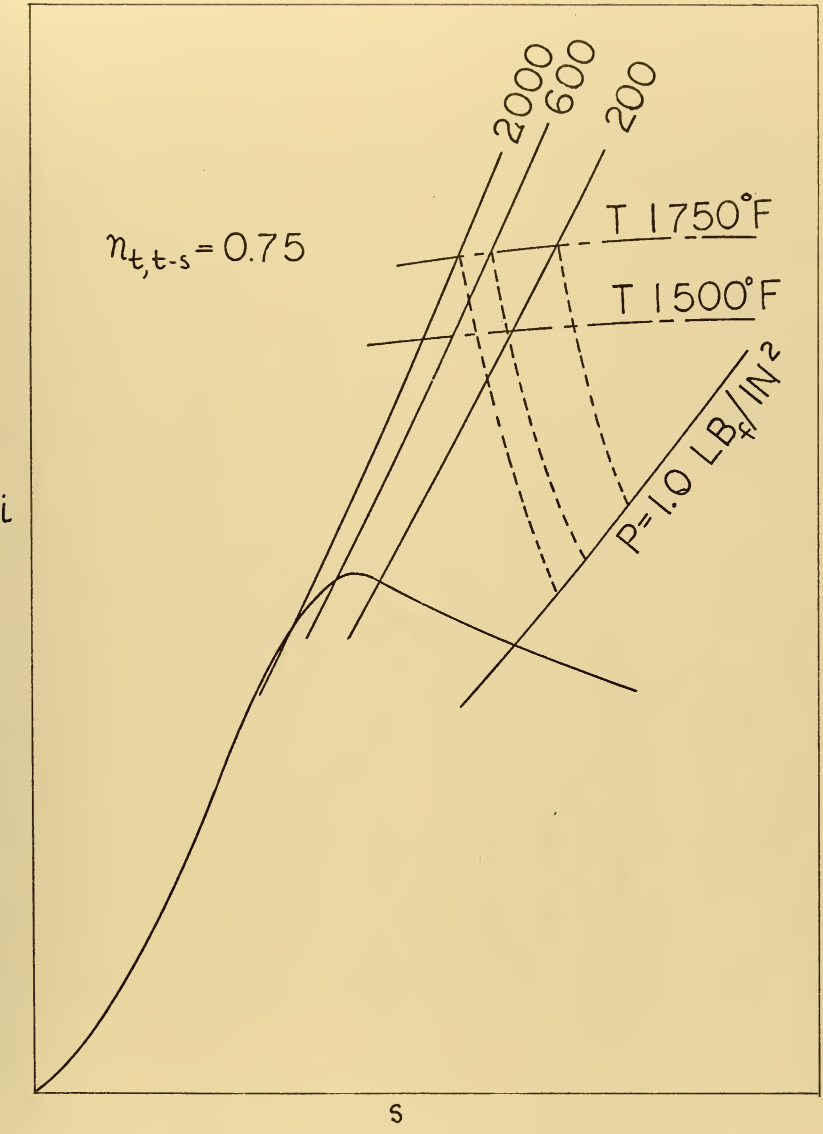

FIGURE IV-4 EFFECT OF COMBUSTION CHAMBER PRESSURE

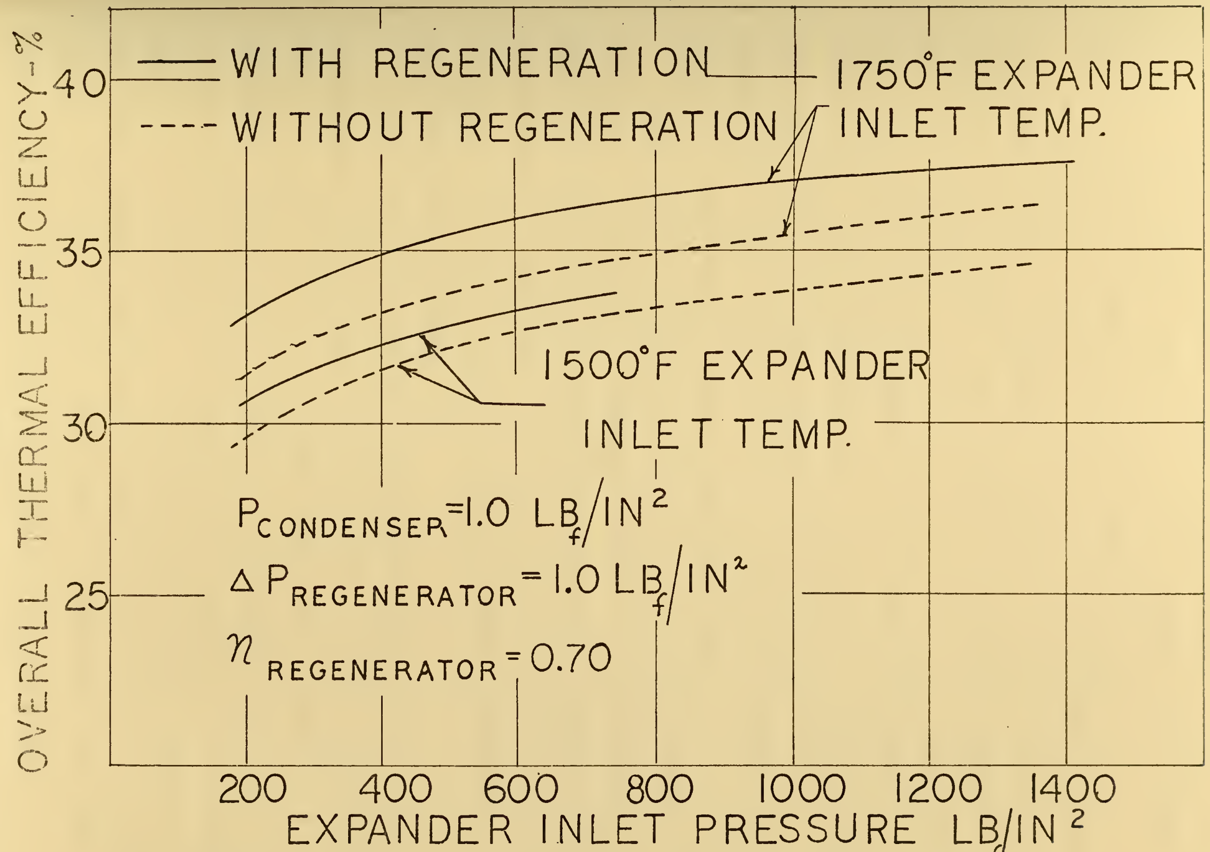

FIGURE IV-5 EFFECT OF REGENERATION

effect is noted for higher expander efficiencies. This occurs at about 80% expander efficiency for an expander inlet temperature of 1750°F and pressure of 600 lbf/in^2.

The effect of increased regenerator effectiveness is shown in Figure IV-6 for an expander efficiency of 66%, a condenser pressure of 2.8 lbf/in^2 and a constant regenerator pressure drop of 0.7 lbf/in^2. In this case, expander inlet temperature and pressure were kept constant at 1750°F and 600 lbf/in^2 respectively. The relatively small increase in overall thermal efficiency with increasing regenerator effectiveness would suggest that the regenerator is not a critical component in the semi-closed Rankine cycle propulsion plant.

Figure IV-7 illustrates the effect on overall thermal efficiency of decreased condenser pressure. Here expander efficiency has been kept constant at 75% with no regeneration. This effect is significant and points to the desirability of achieving the lowest possible condenser pressure consistent with reasonable condenser size.

The effect of increased expander efficiency is also very significant; this is shown in Figure IV-8. Here a regenerator effectiveness of 0.70 and pressure drop of 0.14 lbf/in^2, a condenser pressure of 1.0 lbf/in^2, and expander inlet pressure of 600 lbf/in^2 have been assumed at two expander inlet temperatures, 1750 and 1400°F. From Figure IV-8 one may compare the two major expander candidates, turbine and reciprocating steam engine. If a 75% turbine efficiency is achievable at a 1750°F turbine inlet temperature, a reciprocating steam engine

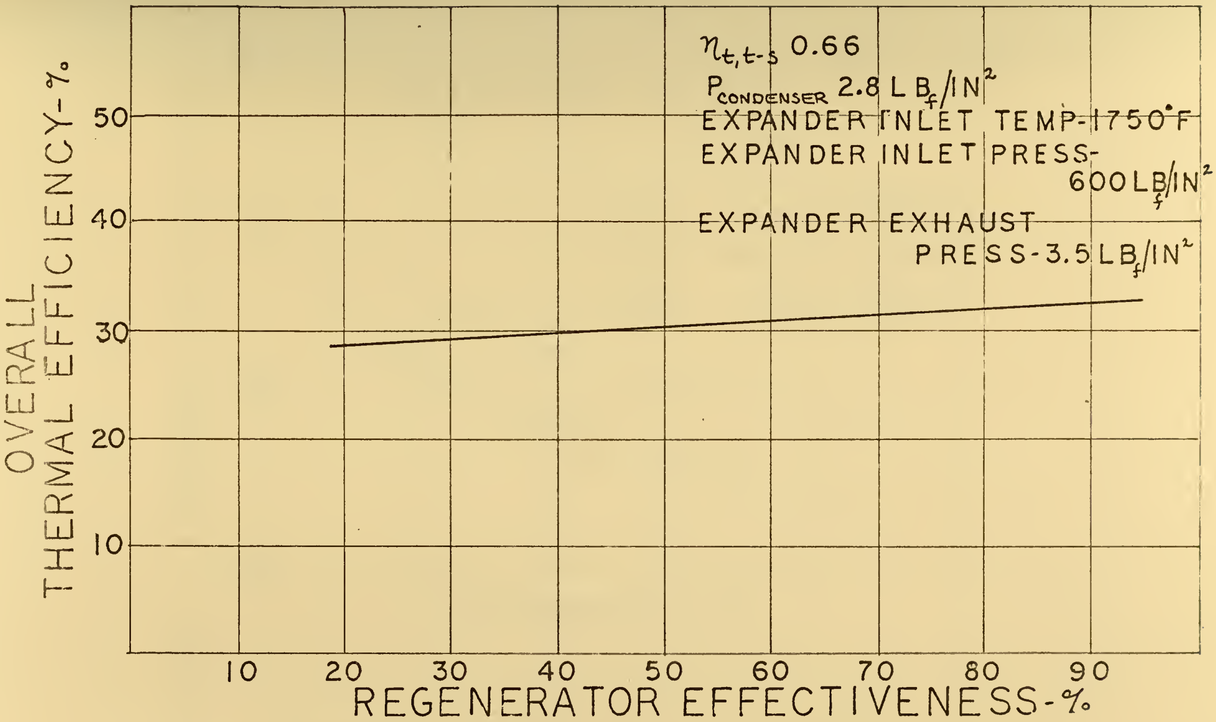

FIGURE IV-6 EFFECT OF VARYING REGENERATOR EFFECTIVENESS ON OVERALL THERMAL EFFICIENCY

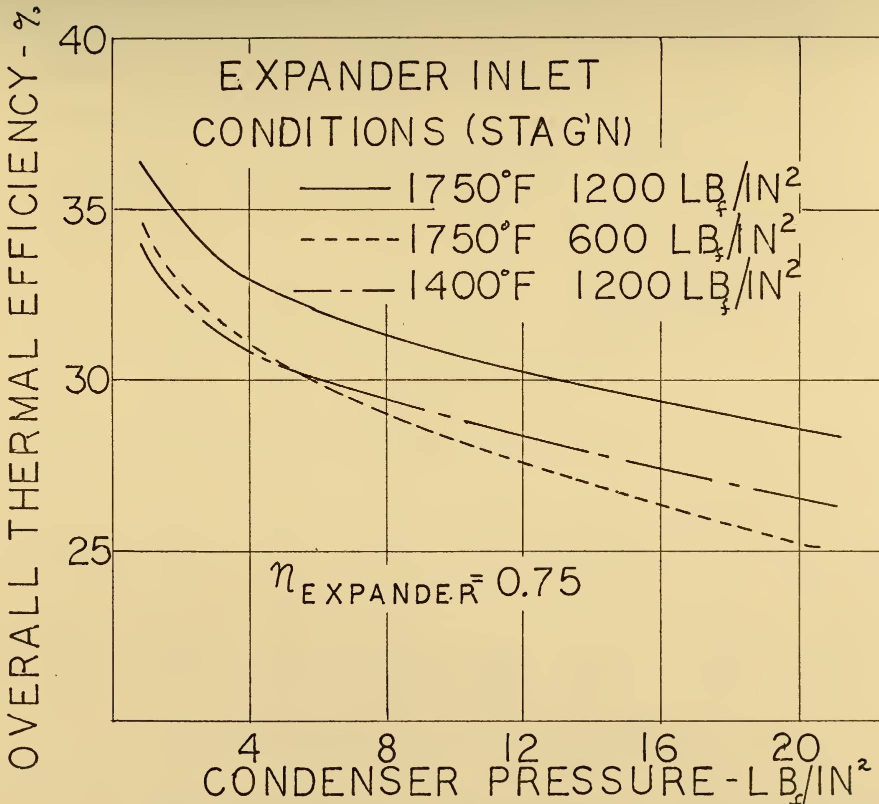

FIGURE IV-7 EFFECT OF CONDENSER PRESSURE

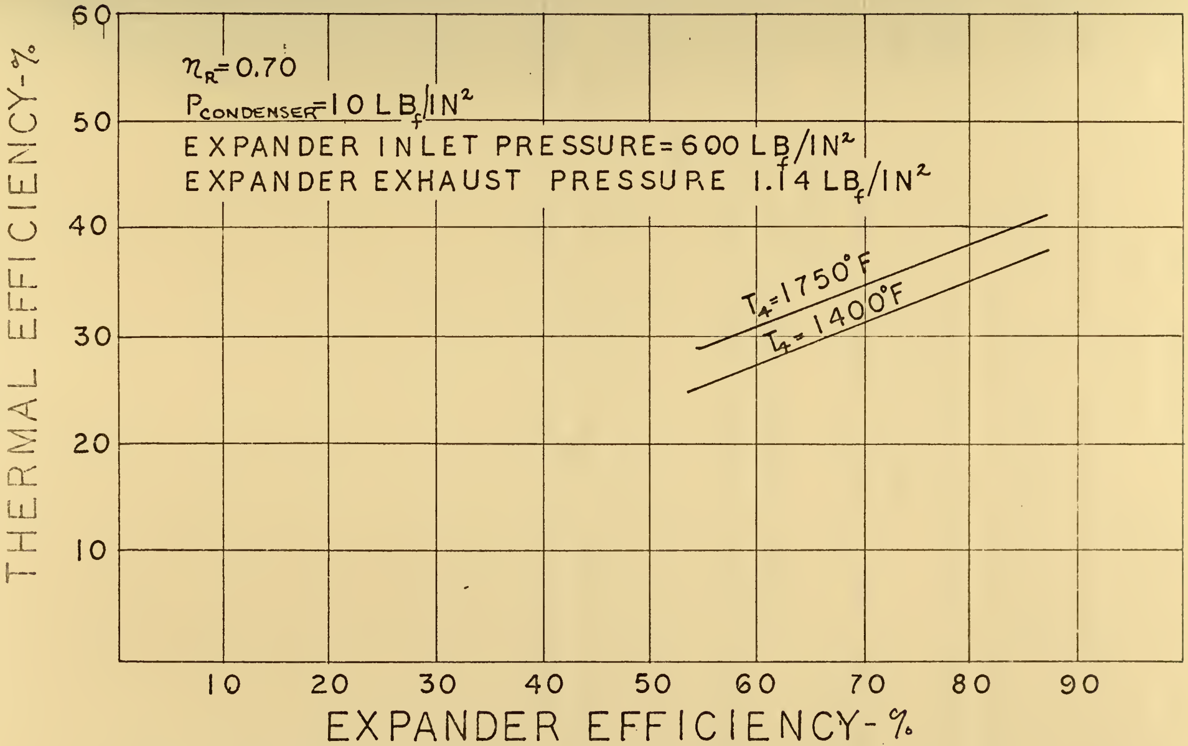

FIGURE IV-8 EFFECT OF EXPANDER EFFICIENCY ON OVERALL THERMAL EFFICIENCY

operating at an inlet temperature of 1400°F would need to have an efficiency of about 82.5% to be competitive. The figure of 1400°F for a reciprocating steam engine is probably the highest attainable at present, as is discussed in Chapter VII.

Thus it would appear that the following parameters will yield the highest overall thermal efficiencies for the semi-closed Rankine Cycle propulsion plant:

a) the highest attainable expander inlet temperature and pressure

b) the lowest possible condenser pressure

c) the lowest possible regenerator steam side pressure drop

d) the highest attainable expander efficiency

Each of these parameters must be tempered by size and material limitations of the various plant components.

REFERENCES

1. Kays, W.M. and A.L. London, *Compact Heat Exchangers*, Palo Alto, California, The National Press, 1955.

2. Keenan, J.H., F.G. Keyes, P.G. Hill and J.G. Moore, *Steam Tables*, New York, John Wiley and Sons, 1969.

LIST OF SYMBOLS

c_p - specific heat, Btu/lbm°R

E - internal energy, Btu

i - enthalpy, Btu/lbm

$\dot{m}$ - mass flow rate, lbm/hr

$\dot{Q}$ - rate of heat addition - Btu/hr

SRC - specific reactant consumption lbm/kwh

T - Temperature, - °R

$\dot{W}_x$ - rate of shaft work, Btu/hr

$\eta_{t,t-s}$ -turbine total to static efficiency

η_{TH} - overall plant thermal efficiency

η_R - regenerator effectiveness

SUBSCRIPTS

c - refers to combustion products (or reactants)

cry - refers to reactants at cryogenic temperatures (1 atmosphere, saturated liquid)

o - refers to total conditions

r - refers to recirculation flow

75 - refers to standard conditions

CHAPTER V

Combustion Chamber

General

A combustion chamber burning hydrogen and oxygen in stoichiometric mixtures must meet the following criteria:

a) Must be safe with respect to explosions or possible uncontrolled oscillations

b) Must operate at acceptable heat fluxes to combustion chamber walls and internal components

c) Must exhibit very good mixing of combustion products and diluent to avoid "hot gas streaking" or diluent droplet carryover which might prove disastrous to turbine blading.

d) Must have a reasonably long time between overhauls (4000-5000 hours is the design goal)

e) Must operate at reasonably high pressure to achieve high overall plant thermal efficiencies

f) Must be reasonably compact

g) Must operate at very high combustion efficiency (~99%) using a stoichiometric mixture of hydrogen and oxygen with diluent water

Several desirable features for such a combustion chamber may also be considered.

a) Capability to operate with varying chamber pressure to improve expander (turbine) performance at off-design conditions

b) Capability to operate on gaseous reactants to eliminate the need to heat cryogenic reactants in the combustion chamber, thereby reducing the available enthalpy of the reactants

The pressure at which a combustion chamber must operate in order to achieve high overall thermal efficiency is limited by the type of chamber selected and the reactant feed pressures available. The expenditure of power necessary to pump hydrogen and oxygen to high feed pressures with small pumps or the use of gaseous reactants, stored at high pressures, limits to some degree the pressure attainable in the combustion chamber. Gaseous storage of reactants is not possible if the combustion chamber selected requires liquid or supercritical reactants at cryogenic temperatures.

Three combustion chambers were investigated for application in the semi-closed Rankine cycle propulsion plant:

a) Liquid propellant rocket-type combustion chamber

b) Porous plug combustion chamber

c) Catalytic chamber

A 600 lbf/in^2 chamber pressure and exit temperature of 1750°F were selected because of the associated, high overall plant thermal efficiency attainable with these values and because they appeared to be achieveable.

Liquid Propellant Rocket Combustion Chamber

The liquid propellant rocket combustion chamber is discussed and analyzed in detail in Appendix A. The chamber, shown schematically in Figure V-1, burns hydrogen and oxygen

in a manner similar to that of a liquid propellant rocket. Supercritical hydrogen is admitted through a porous liner in the injector head. Liquid oxygen, pumped to supercritical pressures upstream of the head, is sprayed in through a number of swirl type injectors. The oxygen enters the chamber as a two phase mixture since at the design combustion chamber pressure selected, 600 lbf/in^2, oxygen is a liquid. The swirl injector is characterized by its ease of fabrication for small oxygen flow rates and its capability of being throttled to 50% of its design flow rate. Injectors would have to be stepped in and out for throttling down to power levels less than 50% of the maximum chamber flow rate. This corresponds to 62.5% of design power since the chamber is designed to operate continuously at 125% of the design plant power level. At the 50 kw design power level, laser fabrication of at least the smallest injector hole is necessary to permit a pilot injector to operate continuously as injector stepping is performed. Smooth stepping of injectors without flameout or pressure or temperature excursions must be shown to be satisfactory for this chamber. In all the chambers, the capability of throttling to 10% of the design mass flow was considered a requirement, even though the assumed power profile does not stipulate this.

Operation of the chamber with gaseous hydrogen and oxygen is possible but would reduce significantly the available cooling to the injector head (by the cryogenic reactants). Such cooling might be provided by spraying,in a limited amount, of diluent steam into the combustion zone, but care must be

taken to avoid quenching. Operation with gaseous hydrogen probably would result in a shorter lifetime for the combustion chamber and perhaps somewhat lower combustion efficiency than for liquid reactants, but this would have to be shown by experimental work.

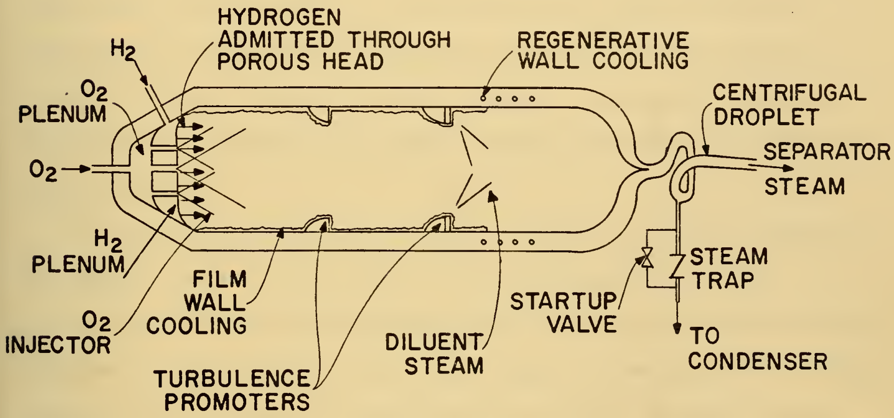

FIGURE V-1

Liquid Propellant Rocket Combustion Chamber

The heat fluxes associated with the liquid reactant chamber are very high. Adequate cooling of the walls is provided by a combination of film and regenerative cooling by the diluent feed water. Film cooling is provided in the high temperature region, where both radiative and convective heat flux are very high. Mixing of the evaporated film coolant and the bulk combustion products is enhanced by turbulence promoters at the wall, themselves protected by film cooling. After the point of wall film coolant dry out, regenerative-type coils are provided in the combustion chamber walls to evaporate the remaining diluent water which is then sprayed into the chamber from an annular plenum. Thorough mixing is necessary to eliminate hot gas streaking and must be evaluated experimentally.

Uncontrolled oscillations are a danger in liquid propellant rocket chambers and there is no indication that the possibility for such oscillations does not exist in the proposed application. For this reason, the types of reactant and diluent (feed) pumps employed in conjunction with the chamber should have a minimum of fluctuation in pressure and the frequency of any fluctuation should not be the same or a harmonic of the oscillation frequency of the chamber. Similarly, the exit nozzle of the chamber should remain choked at all operating conditions to prevent oscillations in the expander (pressure fluctuations due to turbine blade passage) from reaching the combustion chamber.

Startup of such a chamber would require a short time of hydrogen rich operation until ignition is achieved and proper film coolant flow is established. During this time, the small but quite hot flow would be directed to the condenser, bypassing the turbine. A small dilution chamber might be necessary to spray in diluent to reduce this gas temperature to one acceptable for the condenser. Shutdown would also require hydrogen rich operation, cutting out oxygen first followed by hydrogen. The only reason for hydrogen rich operation during shutdown, however, is the possibility of carryover of water into the turbine should the diluent water not be cut out early enough.

Operation of the combustion chamber at higher pressures than 600 lbf/in^2, the selected design pressure, is possible but may not be practical. At the 50 kw design power level, it is seen in Chapter VI that turbine blade height and arc of admission in the first stage are quite small. At higher design power levels, this may be of somewhat lesser importance. The other consideration is pumping power expended to pump liquid oxygen and hydrogen to suitable injection pressures. High injector pressure drops (100-250 lbf/in^2) require quite high oxygen injection pressures with even a 600 lbf/in^2 combustion chamber design pressure. Operation at variable combustion chamber pressure might be expected to improve overall plant efficiency by keeping expander (turbine) efficiency nearly constant over a wide range of power levels. With the exception of Reynolds number effects, variable pressure operation with a

constant speed turbine could produce such a constant efficiency characteristic. If 600 lbf/in^2 is the design pressure, this would mean off-design operation at lesser pressures. Table V-1 gives predicted overall plant thermal efficiencies under this mode of operation for 60% of the design power level. It appears that the efficiency gained with variable chamber pressure below 600 lbf/in^2 is not worth the increased complexity of the system. Variable pressure operation would require diluent (feed) and reactant pumps with a capability of wide discharge pressure.

Porous Plug Combustion Chamber

The porous plug combustion chamber uses a principle developed in laboratory studies of laminar flames. Siegler and Moore (1) have developed this device, explained in detail in Appendix B, for recombining radiolytically decomposed hydrogen and oxygen (off-gas) from the condenser of a boiling water reactor power plant. This device has proved to be satisfactory and reliable in a 1700 hour test under virtually operational conditions at a pressure of 1 atmosphere. For the proposed semi-closed Rankine cycle, the burner would operate at high pressures. Figure V-2 is a schematic diagram of a high pressure combustion chamber.

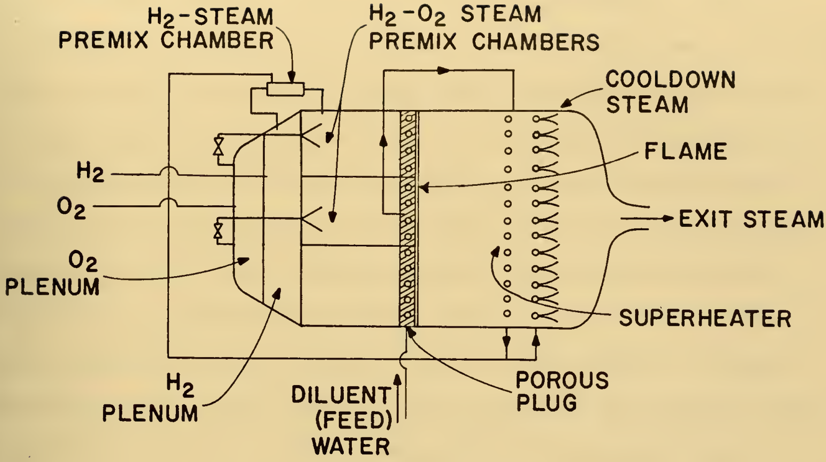

FIGURE V-2

Schematic Diagram of a High Pressure Porous Plug Combustion Chamber

Parameter	Design Point	60% power-Variable Combustion Chamber Pressure	60% power-Constant Combustion Chamber Pressure
Combustion chamber pressure, lbf/in^2	600	400	600
Turbine inlet temperature, °F	1750	1750	1750
Turbine efficiency, %	73.5	73.5	68.0
Condenser pressure, lbf/in^2	1.0	0.7	0.7
Overall Plant thermal efficiency[1], %	36.0	35.2	34.8

[1] Based on turbine power, H_2 and O_2 at 75°F, and neglecting bearing and parasitic propulsion plant losses.

TABLE V-1
Variable Pressure Operation of the Liquid Propellant Combustion Chamber-50 kw Plant

The high pressure application incurs many penalties. First is the necessity to dilute the stoichiometric mixture (pre-mixed) of hydrogen and oxygen with the only inert available, steam, in order to achieve acceptably low burning velocities and heat flux to the porous plug. This requires preheating of the stoichiometric mixture by addition of the diluent steam to temperatures in the range of 400-500°F in order to prevent condensation of the steam prior to entry into the porous plug. Evaporation of the diluent (feed) water is performed in the porous plug, where the diluent water is the coolant. Superheating is performed in a separate coil located downstream of the plug in the hot gas steam or embedded in the chamber wall. A portion of the superheated diluent is then added to the hydrogen and oxygen and the remainder is sprayed into the chamber downstream of the porous plug and superheater.

Detailed investigation of the premixing requirement has shown that the temperatures involved do not constitute a hazard as far as spontaneous ignition is concerned. This, of course, considers complete and uniform mixing of the steam, hydrogen and oxygen. The actual method of mixing and the order of mixing of the fluids as well as the velocities at which they are mixed are important. Care must obviously be taken to prevent the build-up of static charges from mixing nozzles.

The most stringent requirement on the system appears to result from the required pore size of the porous plug material when a chamber is operated at high pressures. Reduction of

pore size to prevent flashback is necessary because of reduction of quenching distance with pressure. Quenching distance, one finds, is nearly inversely proportional to pressure. Addition of the steam diluent acts to increase quenching distance and hence increase the pore size, but at a pressure of 600 lbf/in^2 this still results in a predicted quenching distance of about 37μ. If a safety factor of 10 is used to insure against flashback, this results in a pore size of about 3-4μ.

A minimum flame velocity of about 2-3 cm/sec is imposed by flammability limits. At 600 lbf/in^2 chamber pressure, it is shown in Appendix B that flame velocities greater than 4.0 cm/sec result in excessive heat flux to the porous plug, the effect of which is to heat the downstream side of the plug to temperatures in excess of that which can be tolerated for a sintered nickel material.

Reduction of pore size is detrimental, however, to gas side pressure drop across the plug if adequate effective thermal conductivity of the porous material is to be maintained to transfer the heat. Several correlations were used to estimate gas side pressure drop at the design conditions (600 lbf/in^2 chamber exit pressure, ½ inch thick porous plug), and resulted in a range of predictions from 30 to 1400 lbf/in^2. Experience with porous filtration materials of the sintered variety would indicate that the lower figure, 30 lbf/in^2 is most likely accurate, based upon experimental data in the range of interest (2). If reduction of pressure drop is necessary, it can be

achieved to some degree by decreasing plug thickness within the limitations of coolant tube diameter and required thickness downstream of the coolant tubes to achieve a uniform flow velocity. Such a design would be desirable in any case to reduce the plug exit temperature to the lowest achievable value. This is important with respect to oxidation of the nickel which could close up the pores after some period of operation. It is doubtful that a material with an oxidation resistance superior to nickel could be found which would meet the other requirements of sufficient strength and adequate thermal conductivity.

Another problem associated with the porous plug burner is the necessity to divide the burner into segments in order to throttle the chamber. This is a consequence of the previously described limitations on flame velocity of 3-4 cm/sec. This implies throttling of the chamber is not possible below 75% of its design flow rate unless the burner is split into sections and sections are "stepped out" as throttling continues. Such an arrangement would probably require some cooling steam to pass through the unused sections of the plug in order to maintain plug exit temperature in these sections considerably below the sintering temperature. This imposes an added requirement for mixing downstream of the plug of the coolant steam and the combustion gases.

In the proposed application, slightly improved overall thermal efficiency could be obtained in this device over that of the liquid propellant rocket combustion chamber. Cryogenic reactants would be heated by sea water (through an intermediate

heat transfer loop) and would enter the chamber as gases.

Catalytic Combustion Chamber

A catalytic combustion chamber was investigated as a possible alternative to the two combustion chambers previously described. This type of chamber was developed for use in the Dyna-Soar project and employed excess hydrogen to achieve acceptable temperatures. This chamber is discussed by Bailey (3). In the method of application which is of interest with respect to the semi-closed Rankine cycle, hydrogen and oxygen were mixed as gases at 540°R upstream of the catalyst bed by an injector arrangement similar to that for a liquid propellant rocket combustion chamber. A concentric injector arrangement was tested, as well as one employing impinging jets, in order to yield adequate mixing upstream of the catalyst bed in as small a volume as possible. The impinging jet arrangement produced the most satisfactory results. Flashback occurred to the injector head at high mixture ratios of oxygen to hydrogen but was non-destructive.

The 3" diameter prototype chamber developed at Sundstrand Aviation - Denver, operated at 275 lbf/in^2 and a discharge temperature of 1960°R with a mixture ratio of 0.8 pound oxygen per pound hydrogen. A packed catalyst bed 4 inches in length was used. Measured combustion efficiencies were .9911, .9730, .9455 and .9080. No explanation was given for the variation in efficiency.

Bailey (3) reported that the palladium coated aluminum oxide pellets used as the catalyst had a melting point of 3289 and 4180°R for the palladium and substrate respectively. He also reported that catalytic action was not impeded by the presence of a liquid water film on the catalyst. In another combustion application, water condensed on the catalyst bed and did not impede startup.

The literature was searched for reports of work conducted on this combustion chamber subsequent to the writing of reference 3. The most recent report found was one on the Dyna Soar APU System, apparently the last report prior to cancellation of the Dyna Soar project (4).

The catalyst described in reference 3 is a sintered aluminum oxide pellet, coated with palladium. The required life of the pellets for the Dyna Soar application was 250 hours. In reference 4 is described an evaluation program of several substrates for the palladium catalyst. Life tests which were performed invariably resulted in overtemperature of the catalyst bed, from either human error or component failure. Nevertheless, the results obtained were not encouraging. Only one catalyst met the 250 hour lifetime requirement of the Dyna Soar APU system, and its performance was somewhat degraded at the end of testing. It was, however, subjected to several temperature excursions. In one test, water was inadvertently allowed to flow into the combustor from the exhaust system. Even after vacuum drying, ignition was not possible with this catalyst bed with a stoichiometric mixture of hydrogen and oxygen.

While the catalytic combustion chamber may prove to be successful for a short lifetime (250 hours) with hydrogen rich operation, it is very doubtful that it could be utilized in the semi-closed Rankine cycle of this thesis. It is questionable if sufficiently complete combustion could be achieved in a catalyst bed of reasonable size with the amount of diluent steam necessary in this application to reduce the temperature of the catalyst bed to acceptable levels. The loss of catalytic action when the catalyst bed was exposed to water in significant amounts is also not encouraging for this application. Furthermore, because of the relatively short lifetime of the tested catalyst configurations, it is doubtful that a catalyst could be developed having a lifetime sufficiently long to permit an extended time between overhauls for the propulsion plant.

Combustion Chamber Selection

The porous plug burner has the greatest promise for extended times between overhauls and reliable operation of the three combustion chambers. However, the combination of possible oxidation problems in the porous plug, questionable porous plug pressure drop, and low effective thermal conductivity of the best available porous material would require testing to determine if these problems can be overcome. Estimated quenching distance and laminar flame velocities must also be verified since they are critical to the successful design of the burner.

The liquid rocket combustion chamber, though probably less efficient a combustor than the porous plug burner, appears to be the best short term solution to the combustion chamber problem. It is expected, however, that a design lifetime of 4000-5000 hours probably cannot be met with this chamber and that a lifetime of about 1000 hours is more realistic. This would require opening of an access to the propulsion plant pressure vessel to replace this component, which is undesirable, but possible.

A listing of weights and volumes for a 50 kw and 500 kw design power level liquid propellant rocket combustion chamber are given in Table V-2.

Parameter	Design Power Level	
	50 kw	500 kw
Inside Length, in	15.0	30.0
Inside diameter, in	4.0	8.0
Outside diameter, (including insulation) in	10.0	14.0
Overall length	18.0	36.0
Volume, ft^3	.82	3.2
Weight, lbm	50.0	300

TABLE V-2

Liquid Rocket Combustion Chamber Dimensions, Weights and Volumes

REFERENCES

1. Siegler, M. and G.E. Moore, "Flame Recombination of Oxygen and Hydrogen", *Chemical Engineering Progress Symposium Series*, Nuclear Engineering - Part XXI, Vol. 66, 1970, No. 104.

2. Stevens, D., Pall Trinity Micro Corporation, Cortland, New York, personal communication, 11 May 1972.

3. Bailey, R.N., "Development of Catalytic Hydrogen-Oxygen Reaction Chambers for Space Power Systems", *Space Power Systems*, Vol. 4 of *Progress in Astronautics and Rocketry*, N.W. Snyder, ed. New York, Academic Press, pp 183-210, 1962.

4. *Design Analysis Report, Dyna-Soar APU Thermodynamic System*, Sunstrand Aviation, Denver, Report No. 24-DER-63, 29 April 1963 (AD435892).

CHAPTER VI

Condenser and Related Equipment

Because of its anticipated large size in relation to other propulsion plant components, considerable effort was expended in the development of an acceptable condenser and condensing system. There are several vital aspects of the problem which warrant consideration:

1) The size and weight of the condenser based upon an estimated amount of non-condensables
2) Selection of the best method of heat rejection from the condenser
3) Elimination of non-condensables
4) Sensing of the amount and type of non-condensables
5) Storage of product water

Condenser Type

The selection of condenser type was predicated upon the requirement that the device be as compact as possible. Several types of condenser arrangements were considered.

1) A standard horizontal tube and shell condenser
2) A vertical tube and shell condenser
3) Condensation on the inside of vertical tubes, located outside the propulsion plant pressure vessel wall
4) Condensation on the inside wall of the propulsion plant pressure vessel
5) Spray type condensing

Condensation directly on the inner surface of the propulsion

plant pressure wall seems attractive at first glance, particularly when it is compared with heat transfer through the same wall with a standard tube and shell condenser in conjunction with an intermediate heat transfer loop. Non-vertical walls may promote improved condensation on the upper portion of the inner surface of the sphere to a certain extent. However, if the steam flow is vertically downward in the lower portion of the sphere, one may anticipate degraded performance due to condensate film thickening. Some novel ways of removing the condensate might be devised for the lower portion of the sphere or some novel arrangement of steam flow might be used over the entire surface. A set of parallel spiral passages might be used, for example, to remove the condensate and at the same time permit utilization of the major portion of the internal surface area of the sphere. Figure VI-1 shows a possible arrangement of such a pressure vessel wall condenser. Corrosion on the inner surface of the sphere, however, could not be adequately controlled in the presence of pure steam. Corrosion inhibitors could not be used here but they could be used in an intermediate heat transfer loop. Furthermore, direct contact of superheated steam with the pressure vessel wall could produce excessive thermal stresses in the vessel wall. Such stresses would have to be carefully analyzed to prove the feasibility of such an arrangement.

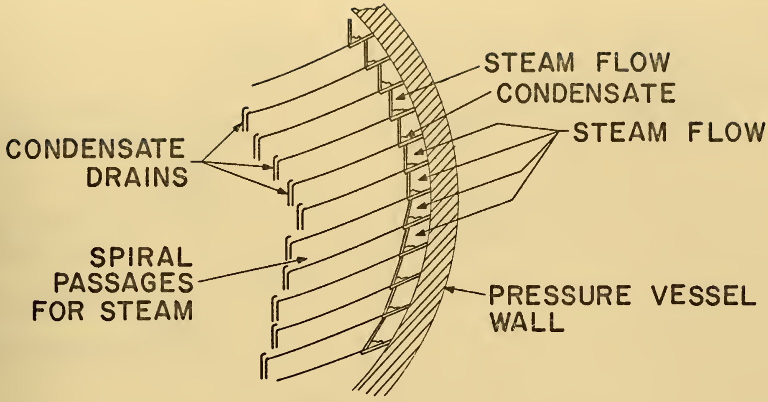

FIGURE VI-1

Possible Arrangement for Condensation Directly on the Inner Surface of the Pressure Vessel Wall

Condensation on the inside of many vertically oriented tubes located outside the pressure vessel also has certain advantages. The primary advantage of this arrangement, shown in Figure VI-2, is the reduction of required propulsion plant pressure vessel volume by that amount necessary for an internally mounted condenser. A disadvantage of this system is the size (or number) of penetrations to the pressure vessel which become necessary to duct the exhaust steam from the turbine or regenerator to the external condenser. The effect of these penetrations, of course, is to increase pressure vessel weight, probably offsetting, to some degree, the significant advantage gained by elimination of the space requirement of an internally mounted condenser.

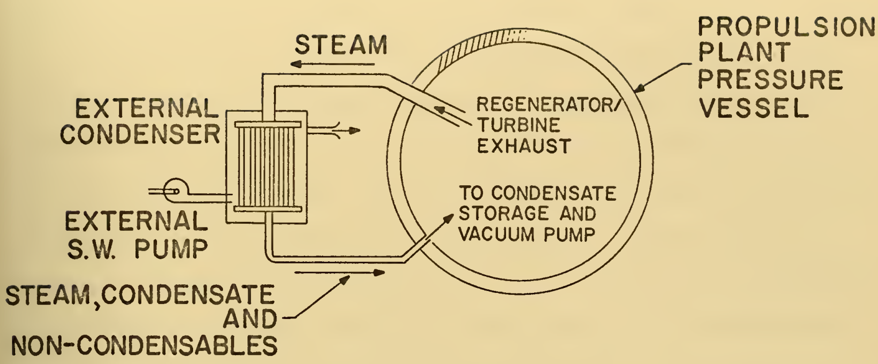

FIGURE VI-2

External Condenser Arrangement

An additional disadvantage of the external condenser is the generally larger tubes or larger number of tubes which must be employed (to accept the high volumetric flow rate of the steam inside the tubes) than for a comparable internally mounted horizontal tube and shell condenser. Unless even larger tube area is used, forced convection of seawater must be employed, requiring some sort of external shell to direct forced circulation across the vertical tube bank. Because of the compressive load to which the condenser tubes would be subjected, their thickness would be greater than for tubes of equal internal diameter subject to internal sea water pressure. Each of these items adds weight to the system. The greatest disadvantage to this system, however, is the proximity of superheated steam with the pressure vessel wall at the steam penetration. While insulation could be provided at this point,

it would have to be very carefully engineered to prevent excessive thermal stresses in the pressure vessel.

A spray-type condenser was considered primarily for desuperheating. No standard methods for analyzing this type of condenser were found. For the desuperheating process, however, it was anticipated that a droplet vaporization model similar to those described in Appendix A (for droplet vaporization in liquid propellant rockets) might be used. Subsequent analysis of the tube and shell condenser (see Appendix D) showed that desuperheating was not a significant problem. Furthermore, analysis of droplet condensation in the presence of a significant amount of non-condensable gas appeared to be particularly difficult to analyze. The spray type condenser would use a spray of subcooled condensate to produce condensation, thus adding another piece of heat transfer equipment, a condensate cooler.

The standard horizontal or vertical tube and shell condenser, mounted inside the propulsion plant pressure vessel is probably the easiest condenser to analyze. The standard method of analysis for this condenser has proved to be fairly accurate in predicting condenser performance. The advantages of the horizontal tube and shell condenser over the vertical tube and shell condenser are probably not too significant. Powell (1) has shown that the size of the two types of condensers for identical conditions of the entering steam is comparable. Kern (2) indicates that the vertical tube and shell condenser is advantageous when condensate subcooling is

desired but that the horizontal tube and shell condenser is probably somewhat smaller for equivalent entering steam conditions.

The choice of condenser type, then, is not clear cut. Several of the alternatives require detailed analysis of the effect of the condenser type on other components. For instance, while the external vertical tube condenser appears promising, the problems of the pressure vessel wall penetration for steam would require detailed stress analysis. Furthermore, the reduction of pressure vessel weight due to elimination of required internal volume for a condenser is offset by gains in tube weight and pressure vessel weight at the penetrations. Condensation on the internal wall of the pressure vessel appears dangerous in that it might result in catastrophic thermal stresses in the wall.

For the reasons outlined above, the standard tube and shell condenser was selected for the purposes of this thesis. While some other choices appeared possible and perhaps even slightly better choices as far as overall propulsion plant and encapsulation weight is concerned, this could only be proved after much detailed analysis.

Heat Rejection

The selection of a condenser located within the pressure vessel hull imposes a requirement for a means of rejection of heat to the sea water. Two alternatives were considered:

1) a skin cooler (heat rejection through the hull of the

pressure vessel) similar to that used on the U.S. Navy's deep diving submarine Dolphin

2) a conventional, but heavy, standard forced sea water arrangement (requiring penetration of the pressure vessel hull of sea water piping)

The first alternative, that of the skin cooler, appeared to be most attractive since it required no pressure vessel penetrations. Since the propulsion plant pressure vessel would be mounted inside the envelope of the streamlined body of the submersible, natural convection heat transfer for the outer surface could not be employed as in Dolphin unless unacceptably high temperatures of the intermediate heat transfer loop were permitted. Hence, forced circulation on both inside and outside of the pressure vessel wall was considered. Figure VI-3 is a schematic diagram of such an arrangement. The intermediate heat transfer loop circulates fresh water, containing a corrosion inhibitor (and perhaps ethylene glycol anti-freeze if desired), through a standard tube and shell condenser and then rejects heat by contact with the cool pressure vessel walls. Heat is then removed by the external forced circulation loop employing sea water as a fluid. A submerged sea water circulating pump, located outside the propulsion plant pressure vessel, provides the pumping power for the forced circulation.

It was estimated, for purposes of a design study, that as much as 80% of the pressure vessel wall area could be used for the skin cooler. The remaining 20% of the area would be required for access, penetrations, etc. To determine feasibility

of such an arrangement several assumptions were made, some of them slightly optimistic:

a) Outside sea water temperature was assumed constant through the external loop at 40°F, the sea water temperature at extreme depths. This assumption would result in slightly degraded plant efficiency at the surface.

b) The intermediate loop temperature was assumed to be constant throughout the loop at 75°F. This is a reasonable assumption for condenser size as will be shown later.

c) A coolant velocity of 7 ft/sec was assumed to produce an acceptable film heat transfer coefficient on both the inside and outside of the pressure vessel walls. Higher velocities, while possible, would result in significant increases in pumping power required.

d) Three possible cooling passage arrangements (A, B, and C in Figure VI-3 were considered.) Arrangement A is a 1" x $\frac{1}{4}$" passage, long dimension parallel to the pressure vessel wall. Arrangement B is a modification of the geometry of arrangement A and includes $\frac{1}{4}$" fins on both sides. 90-10 Copper Nickel was selected for the salt water side and pure copper for the fresh water side. The employment of cathodic protection could solve the corrosion problem which would exist in this arrangement. Arrangement C utilizes passages of the same size as Arrangement A, but with the long axis

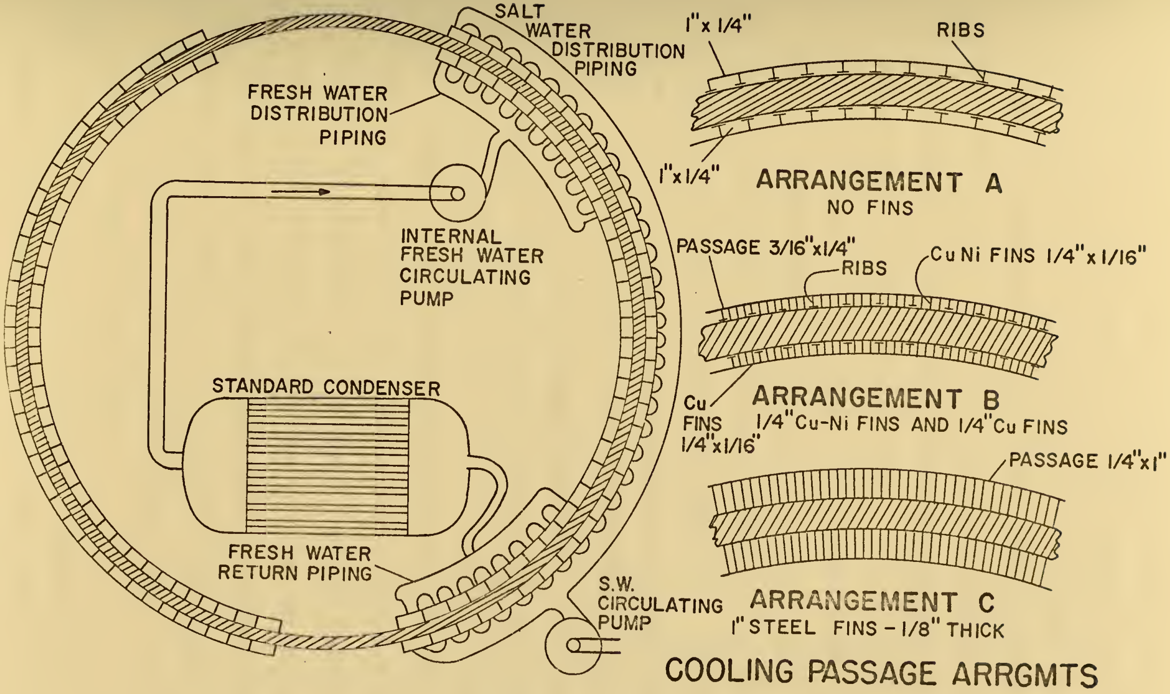

FIGURE VI-3
SCHEMATIC DIAGRAM OF SKIN COOLER

perpendicular to the pressure vessel wall, and has fins of the same material as the pressure vessel wall. For the finned arrangements, it was assumed that the method of attachment of the fins would not affect the fin efficiency. This, of course, is untrue. Welding of ferrous to non-ferrous materials (copper base materials to steel, for instance) is a possible method of attachment. Such a bond as this might not affect the fin efficiency. Certainly welding of fins of the same material as the pressure hull would be most reliable in not degrading fin efficiency. Welding to the pressure vessel walls, however, is not desirable, if it can be avoided. Certain thermally conductive epoxy materials have been successfully used for attachment of heat rejection devices to deep submergence pressure walls (3). Two such materials are STYCAST 2850 and DEVCON. The thermal conductivities of these materials are not reported by the manufacturer and must be determined. Furthermore, the thermal contact resistances associated with the application of fin attachment, are unknown. An additional requirement for this application is that the adhesive be capable of withstanding the cyclic flexing of the pressure vessel hull in compression without failure of the bond.

e) A heat load of 3 x 10^5 Btu/hr was selected for the feasibility analysis. This is representative of a 40 kw propulsion plant operating at 31.5% overall thermal efficiency.

f) A 3-4 foot I.D. propulsion plant pressure vessel is capable of housing a propulsion plant corresponding to the power plant in (e) above.

g) For all hull materials, no allowance was made for protective coatings. Aluminum, known to be subject to stress corrosion, normally employs a protective coating of several layers of plastic, and steel hulls would be painted, at least on the outside.

h) Assumed scale coefficients:

$h_{sc,sw} = 500$ Btu/hr ft^2 °R

$h_{sc,fw} = 2000$ Btu/hr ft^2 °R

Corrosion inhibitors can be employed on the fresh water side, which will permit the maintenance of a high scale coefficient on the inside surface.

i) Pressure vessel hull thermal conductivities:

Steel (HY-130 and HY-180) - k = 21 Btu/hr ft°R (HY-80 data)

Ti HY 130 - k = 4.2 Btu/hr ft°R (based upon data in reference 4 for similar alloys)

Al 7079 - T6 k = 70.2 Btu/hr ft°R (based on data in reference 4 for similar alloys)

Actually, one would anticipate a slightly lower thermal conductivity for HY-130 and HY-180 steels than that of HY-80 steel.

j) The total and usable pressure vessel areas are given below, based upon internal sphere diameter:

Sphere I.D. (ft)	Total Surface Area (ft^2)	Usable Surface Area (ft^2)
3.0	28.2	22.6
4.0	50.4	40.3

With the above assumptions, calculations of required surface area were performed for cooling passage configurations A, B, and C of Figure VI-3. These results are given in Tables VI-1 through VI-3.

From Table VI-1, the case without fins, it is evident that none of the pressure hull materials would permit transfer of the assumed heat load with a 35°R terminal temperature difference. Aluminum exhibited the best performance, but this did not include any allowance for a protective coating. Craven (5) discusses the problem of stress corrosion cracking in aluminum pressure vessels in an underseas environment, which has precluded welding of heavy pressure vessel castings. Aluminaut, which utilized a bolted 7079-T6 aluminum construction, also used several layers of a plastic coating on the exterior of the hull to guard against stress corrosion cracking.

In subsequent calculations only steel was considered for the pressure hull material. The poor thermal conductivity of titanium eliminates its use in the application of a skin cooler. The poor thermal conductivities of plastic coatings would eliminate aluminum.

Table VI-2 is an analysis of the second configuration, arrangement B of Figure VI-3. Improved performance is noted,

Design Depth ft	Pressure Vessel Internal Diameter ft	Pressure Vessel Material	Pressure Vessel Thickness in.	$h_{film,sw}$ Btu/hr ft^2°R	$h_{film,fw}$ Btu/hr ft^2°R	Overall Heat Transfer Coefficient Btu/hr ft^2°R	Required Surface Area ft^2
8000	3.0	Steel HY-130 & HY-180	0.5	1260	1530	169	50.7
		Ti HY-120	0.7	↓	↓	56.2	152.5
		Al-7079-T6	0.9	↓	↓	216	39.7
	4.0	Steel HY-130 & HY-180	0.7	↓	↓	149	57.5
		Ti HY-120	0.9	↓	↓	45.7	188.0
		Al-7079-T6	1.17	↓	↓	186	46.0
20,000	3.0	Steel HY-130	.917	1260	1530	132	64.9
		Steel HY-180	.8	↓	↓	141	60.7
		Ti-HY-120	1.1	↓	↓	40.5	212
		Al-7079-T6	2.0	↓	↓	158	54.1
	4.0	Steel HY-130	1.23	↓	↓	113.2	75.5
		Steel HY-180	1.1	↓	↓	120	71.3
		Ti-HY-120	1.45	↓	↓	29.3	293
		Al-7079-T6	2.7	↓	↓	142	60.2

Heat Load-3 x 10^5 Btu/hr

Fresh Water Temperature-75°F

Salt Water Temperature - 40°F

Passage Size-1" x ¼"

no fins

Pressure vessel thickness (safety factor of 1.5) from reference 6

TABLE VI-1

Skin Cooler Analysis for Coolant Passage Configuration A of Figure VI-3

Design Depth ft	Pressure Vessel Internal Diameter ft	Pressure Vessel Material	Pressure Vessel Thickness in.	$h_{film,sw}$ Btu/hr ft^2°R	$h_{film,fw}$ Btu/hr ft^2°R	Overall Heat Transfer Coefficient Btu/hr ft^2°R	Required Surface Area ft^2
8000	3.0	Steel HY-130& HY-180	.5	1380	1550	252	34.0
	4.0	Steel HY-130& HY-180	.7	↓	↓	210	40.8
20,000	3.0	Steel HY-130	.917	↓	↓	177	48.2
		Steel HY-180	.80	↓	↓	195	43.7
	4.0	Steel HY-130	1.23	↓	↓	146	58.5
		Steel HY-180	1.10	↓	↓	158	54.2

Heat Load - 3 x 10^5 Btu/hr

Fresh Water Temperature 75°F

Salt Water Temperature 40°F

Fins ¼" Cu-Ni Salt Water Side
¼" Cu- Fresh Water Side

Fin Thickness 1/16"

Passage Size 3/16" x 1/4"

TABLE VI-2

Skin Cooler Analysis for Coolant Passage Configuration B of Figure VI-3

Design Depth ft	Pressure Vessel Internal Diameter ft	Pressure Vessel Material	Pressure Vessel Thickness in.	$h_{film,sw}$ Btu/hr ft²°R	$h_{film,fw}$ Btu/hr ft²°R	Overall Heat Transfer Coefficient Btu/hr ft²°R	Required Surface Area ft²
8000	3.0	Steel HY-130 & HY-180	0.50	1260	1530	213.0	40.7
	4.0	Steel HY-130 & HY-180	0.70	↓	↓	182.5	47.0
20,000	3.0	Steel HY-130	0.917	↓	↓	157.0	54.5
		Steel HY-180	0.80	↓	↓	171.0	50.0
	4.0	Steel HY-130	1.23	↓	↓	130.0	65.8
		Steel HY-180	1.10	↓	↓	141.0	60.6

Heat Load 3×10^5 Btu/hr

Fresh Water Temperature 75°F

Salt Water Temperature 40°F

Fins = 1" steel

Fin thickness 1/8"

Passage Size 1/4" x 1"

TABLE VI-3

Skin Cooler Analysis for Coolant Passage Configuration C of Figure VI-3

but it is still not sufficiently increased to permit transfer of the assumed heat load at the assumed temperature difference.

Table VI-3 shows the results of using 1 inch steel fins. Such fins could be welded to the pressure vessel or might be machined from the casting. Machining would prove to be a difficult task, however, when one considers the effort expended to achieve near perfect sphericity in such a pressure vessel. Performance in this configuration is better than for arrangement A but inferior to arrangement B.

Forced circulation of the intermediate coolant (fresh water) and sea water requires the expenditure of considerable electrical power for pumping. If a 70% pump efficiency and 60% motor efficiency are assumed for both the salt water and fresh water pumps, the estimated electrical power to pump coolant through the cooling passages and associated piping for a 3 ft. I.D. sphere is as listed in Table VI-4. Power required to pump coolant through the condenser is not included here, since it is common to the alternate arrangement, forced circulation of sea water through the condenser tubes. Condenser pressure drop is small, however, in comparison to the pressure drop in the internal panels.

For any detailed analysis of the skin cooler, of course, pumping power required and its effect on plant thermal efficiency must be evaluated. A 1.3 kw drain on power produced would not represent a serious increase in reactant load for a 1000 kwh mission.

Arrangement	Electrical Power Required for Pumping (kw)
A	1.3
B	2.3
C	3.9

TABLE VI-4

Electrical Power Required for Skin Cooler Pumps (neglecting condenser pressure drop) - 3 ft I.D. sphere

The skin cooler could, of course, be employed easily if a sufficiently high terminal temperature difference is provided. For a condenser designed for a 75°F coolant temperature, this means a higher condenser pressure and reduced overall thermal efficiency. However, it can be seen that at the low condenser pressures shown in Chapter IV to give high overall thermal efficiencies, large increases in condenser volume will be necessary to provide a sufficiently high terminal temperature difference to reject the assumed heat load.

An estimate of the additional weight incurred by the inclusion of a skin cooler without fins (Arrangement A) is given in Table VI-5. Without a knowledge of the condenser geometry and required flow rates of intermediate coolant loop fresh water, one cannot yet estimate the weight and total power requirements of a fresh water circulating pump, or the weight of the intermediate coolant.

Sphere Internal Diameter (ft)	Weight (lbm)	
3.0	Panels & ribs[1]	290
	Piping	40
	External SW pump & motor[2] (308GPM)	24
	Total	354
4.0	Panels & ribs	515
	Piping	53
	External SW pump & motor (410 GPM)	43
	Total	611

[1] 1/8" steel panels & ribs

[2] 400 cycle geared, sea water compensated (oil filled) induction motor

TABLE VI-5

Additional Weight Incurred for a Skin Cooler Without Fins

The panels and ribs which form the cooling passages should be removable for cleaning and preservation of the pressure vessel surfaces. While some other lighter material than steel might be found for this application, steel was selected for a first approximation of cooler weight. The large volumetric flow rate of the sea water cooling pump results in a minimal rise in temperature of the sea water. Thus the assumption of a constant temperature of 40°F for heat rejection is reasonable for extreme depths.

Non-Condensable Gases

The amount of non-condensable gases which the condenser must accommodate is dependent upon combustion efficiency, the achievable accuracy of reactant proportioning, leakage into the condenser by the normal routes of turbine glands and condenser gaskets, and the purity of the reactants. Information obtained from oxygen suppliers indicates that the commercial grade of oxygen has a significant amount of contaminants. Table VI-6 gives a summary of commercial grade oxygen contaminants (7).

Contaminant	PPM
N_2	150
Ar	3500
Hydrocarbons	<20
CO_2	5
Moisture	6
Total Non-Condensables	3675

TABLE VI-6

Commercial Oxygen Contaminants-Typical Analysis

By far, argon is the most serious oxygen contaminant to be considered. Moisture, of course, does not present a problem in the condenser. Since argon is not condensable at normal temperatures and pressures and is non-reacting, it will represent a significant disposal problem. Only research grade oxygen gives any significant improvement in the amount of non-conden-

sables and this is at an unacceptable increase in cost. Hydrogen contaminants are given in Table VI-7

Contaminant	PPM
CO_2	1
Hydrocarbons	3
N_2	3
O_2	2
CO	1
Moisture	1
Total non-condensables	10

TABLE VI-7

Commercial Hydrogen Contaminants-Typical Analysis

Combustion efficiency is difficult to assess for a combustor which has never been built. However, the porous plug combustion chamber,described in Appendix B, is expected to have a very high combustion efficiency, on the order of 99-100% for steady operation. For this reason a 99% combustion efficiency has been selected for condenser design purposes. The accuracy of proportioning equipment at the small reactant flow rates for the 50 kw propulsion plant is unknown, but it is estimated that control of the hydrogen and oxygen flow rates without feedback could be as accurate as 1% (8). Leakage of non-condensables into the condenser through normal means is estimated to be about .05% of the steam mass flow rate (9), (10).

The selection of a design figure which takes into account all of the possible sources of contaminants is somewhat arbitrary. Clearly the effects of combustion inefficiency and non-stoichiometric proportioning are interrelated. The total effect is not simply additive. It was assumed, therefore, that unreacted hydrogen and oxygen flow rates of 2% of the design flow rate of each reactant would reach the condenser, plus an additional oxygen flow rate of .05% of the steam flow rate. This was considered to be a very conservative estimate of the non-condensables from all sources.

Comparison of the effect of hydrogen and an equal mole fraction of oxygen on condensation rates showed that condensation rates were somewhat greater in the presence of hydrogen. This might be expected from the higher diffusion coefficient for hydrogen-steam mixtures than for comparable oxygen-steam mixtures.

Computer costs for the analysis of condensation in the presence of more than one non-condensable gas (see Appendix D) were significantly higher than for just one non-condensable gas. For this reason computer analysis of condenser size and weight was conducted with oxygen only as the non-condensable. To simulate the presence of hydrogen, an equal number of moles of oxygen were substituted. An allowance was also made for an additional amount of oxygen, .05% of the steam mass flow rate by weight. Substitution of an equal molal flow rate of oxygen for hydrogen resulted in an approximate 8% increase in condenser surface area for the steam conditions tested. Thus this

assumption is conservative. The ratio of reactant to steam flow rates were based upon a representative design at 31.5% overall thermal efficiency (11). The resultant design figure for non-condensables was an oxygen flow rate of 1.39% of the steam mass flow rate.

Analysis of the Horizontal Tube and Shell Condenser

The horizontal tube and shell condenser was analyzed for the assumed non-condensable flow rate at various inlet pressures and temperatures of interest and for a wide range of mass flow rates of entering steam. Condenser weights were determined for the following cases:

1) a standard condenser to be used in conjunction with a skin cooler
2) an 8000 foot depth "deep-sea" condenser circulating sea water
3) a 20,000 foot depth "deep-sea" condenser circulating sea water

The computer program developed and described in detail in Appendix D was used to determine condenser surface area and dimensions.

Table VI-8 gives a summary of the condenser geometry assumed for the family of condensers studied in this thesis.

Tube Material (deep sea condensers only)	Inco Alloy CA719
Tube O.D., in.	.250
Tube I.D., in. (20,000 ft depth)	.190
Tube Spacing, in. (see Appendix D)	.665
Tube Arrangement	Staggered Rows, Square Pitch Rotated
Coolant (sea water) velocity, ft/sec	7.0
Coolant (sea water) inlet temperature, °F	75.0

TABLE VI-8

Assumed Data for Condenser Studies

Tube wall thickness for the 8000 ft condensers and the standard condenser were proportionately less than the .030 inch figure used for the 20,000 ft depth condenser.

Figures VI-4 and VI-5 give condenser surface areas required for a range of condenser inlet pressures from 1.0 to 10.0 lbf/in^2. Two curves are presented for each pressure, one for saturated steam and a second for superheated steam at 300° superheat. Studies of the effect of superheat indicated that the additional required surface area for superheated steam was relatively small. Calculations at 100, 200, and 300°F superheat showed no more than a 5-10% increase in required surface area over that for saturated steam at the same pressure and mass flow rate.

The standard condenser, for use in conjunction with the skin cooler was designed using the specifications of references 12 and 13 as a guide in determining shell and header weights,

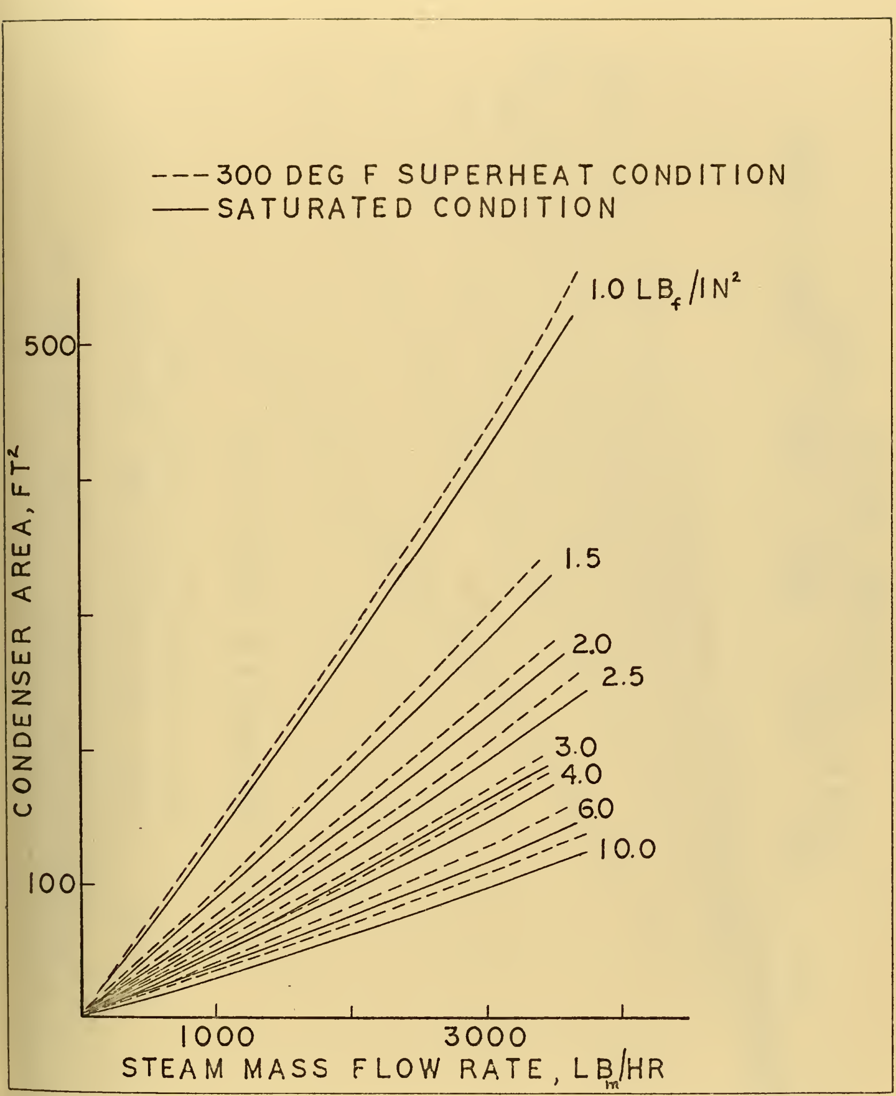

FIGURE VI 4 CONDENSER AREA VERSUS FLOW RATE

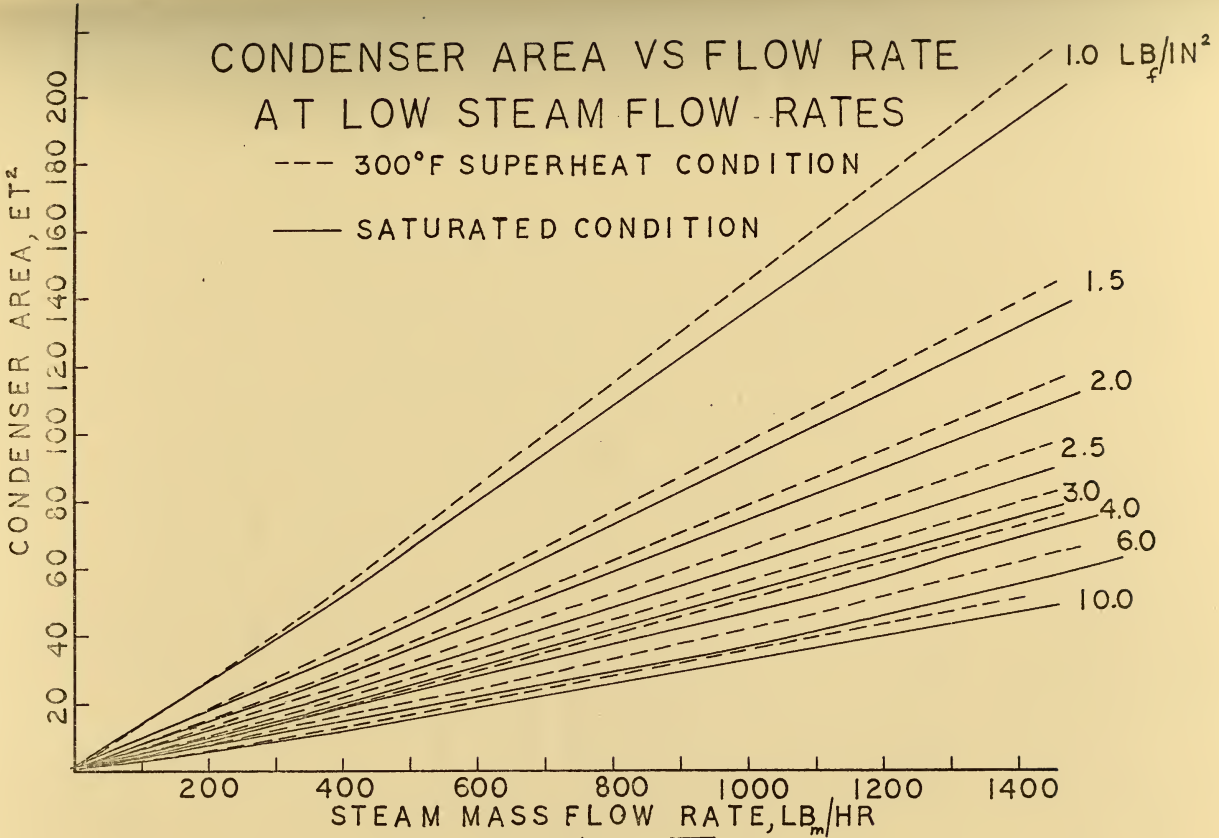
CONDENSER AREA VS FLOW RATE
AT LOW STEAM FLOW RATES
--- 300°F SUPERHEAT CONDITION
—— SATURATED CONDITION
1.0 LB$_f$/IN^2
1.5
2.0
2.5
3.0
4.0
6.0
10.0
CONDENSER AREA, FT^2
20
40
60
80
100
120
140
160
180
200
200
400
600
800
1000
1200
1400
STEAM MASS FLOW RATE, LB$_m$/HR

FIGURE VI-5

hot well volume, etc. The weights presented in Figure VI-6 represent those of a single pass condenser and include a margin of 25%. A double pass condenser might prove to be less heavy in the tradeoff of condenser weight and volume with intermediate coolant weight, but this was not investigated. Figure VI-7 is a diagram of the standard condenser.

The deep sea condenser uses a header (waterbox) design similar to that of header or steam drum design for a boiler. The cylindrical headers are kept small, usually 6" or less in internal diameter to minimize wall thickness and the weight. No detailed stress analysis was performed on the headers but a safety factor of 2 based on yield stress was applied because of the large number of penetrations. The tubes and headers are of the same material and can be joined by MIG welding techniques (14). The use of non-ferrous materials for the condenser tubes is desirable from the aspect of scale buildup and fouling. If the tube and headers materials are identical, this would then entail joining ferrous to non-ferrous materials in order to connect the piping to the pressure vessel wall. Such a joining process could be accomplished by MIG welding techniques and performed under laboratory conditions if necessary (14). If such joining proves to be unsuccessful, ferrous materials could be used throughout the condenser with a consequent increase in condenser size due to steam side and waterside corrosion. It would be wise to minimize the size of the hull piping penetration because of the effect of the size of the penetration on pressure vessel weight. Too small a penetration,

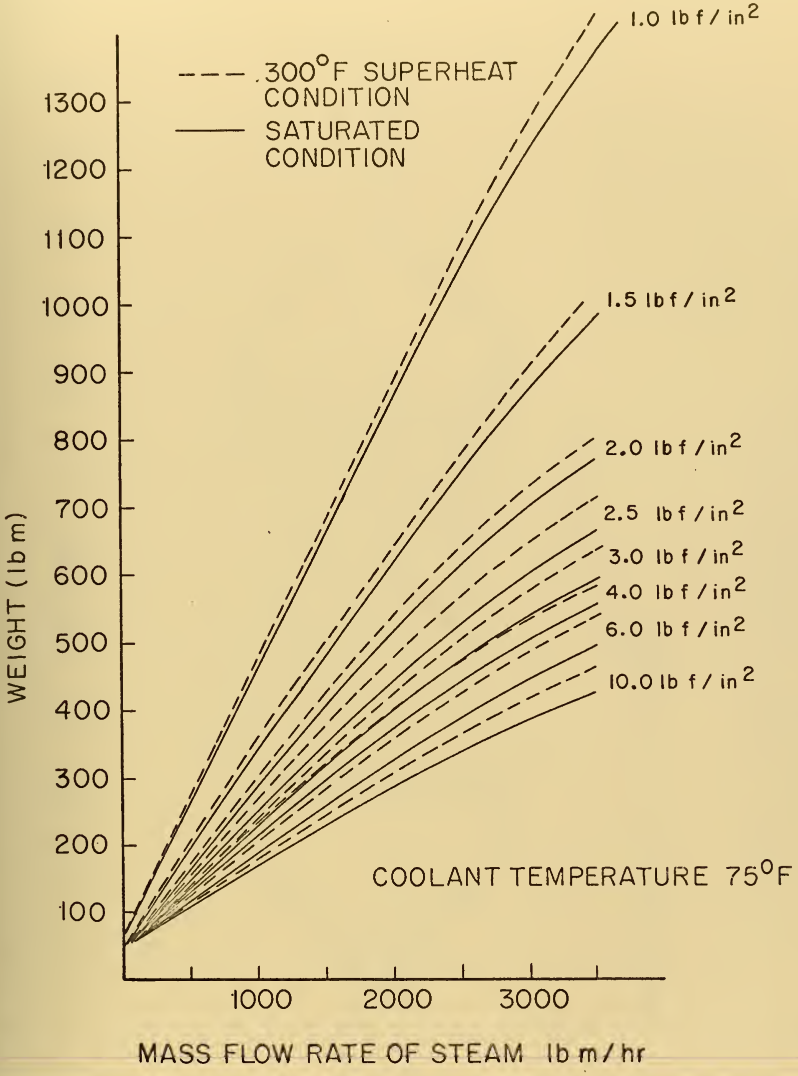

FIGURE VI-6 STANDARD CONDENSER WEIGHT vs STEAM RATE

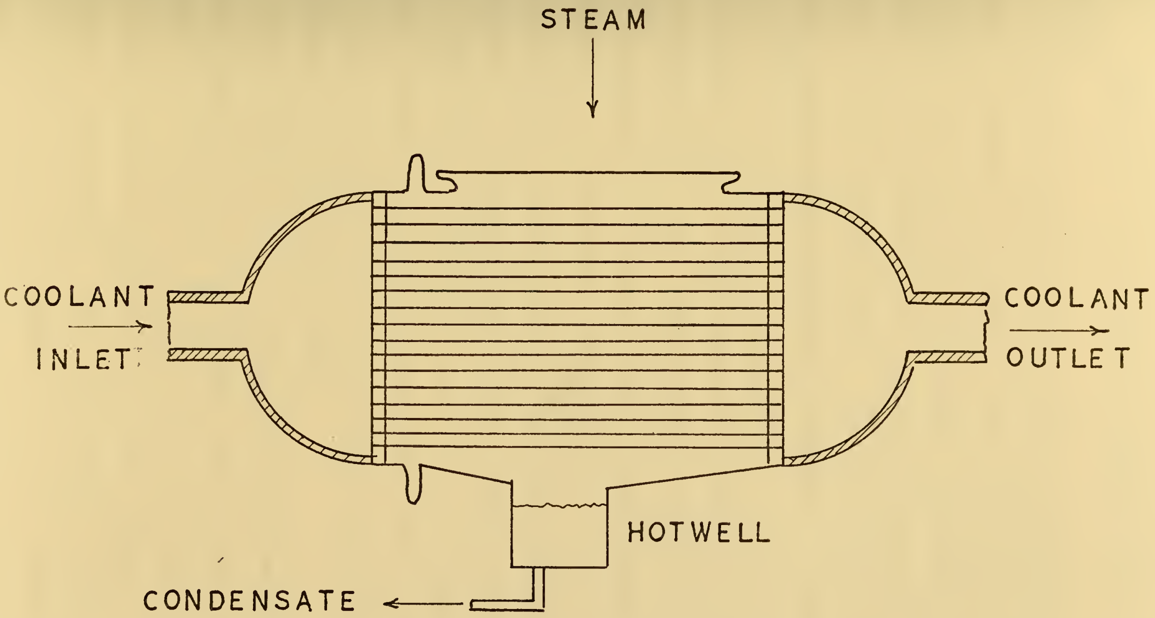

FIGURE VI-7 SCHEMATIC DIAGRAM OF STANDARD CONDENSER

however, would result in the excessive expenditure of pumping power. Figure VI-8 is a schematic diagram of the deep-sea condenser.

A detailed stress analysis must be performed on this design to determine the combined effect on piping penetrations and header joints by thermal stresses resulting from the slight heating of the condenser tubes and by stresses due to the compression of the pressure vessel. An alternative design, and probably a much simpler design to fabricate, is shown in Figure VI-8. This design is basically a two pass condenser which employs U-bend shaped tubes to provide the return pass. It is believed that this design might be somewhat better insofar as stresses are concerned than the single pass condenser. Impingement of superheated steam directly on the tubes may require detailed stress analysis for startup conditions, and insulation of the headers from direct contact with the steam may be advisable. Under normal operating conditions the tubes would be covered by a film of condensate, and the outside wall would reach a temperature no greater than the saturation temperature of the entering steam.

In the computation of overall condenser weights for the deep-sea application, an additional margin of 50% has been applied to the overall condenser weight for piping and foundations and additional pressure hull vessel weight as a result of the piping penetrations. Thus the condenser weights presented on Figure VI-9 and VI-10 represent what are believed to be very conservative preliminary design figures. Condenser volumes for

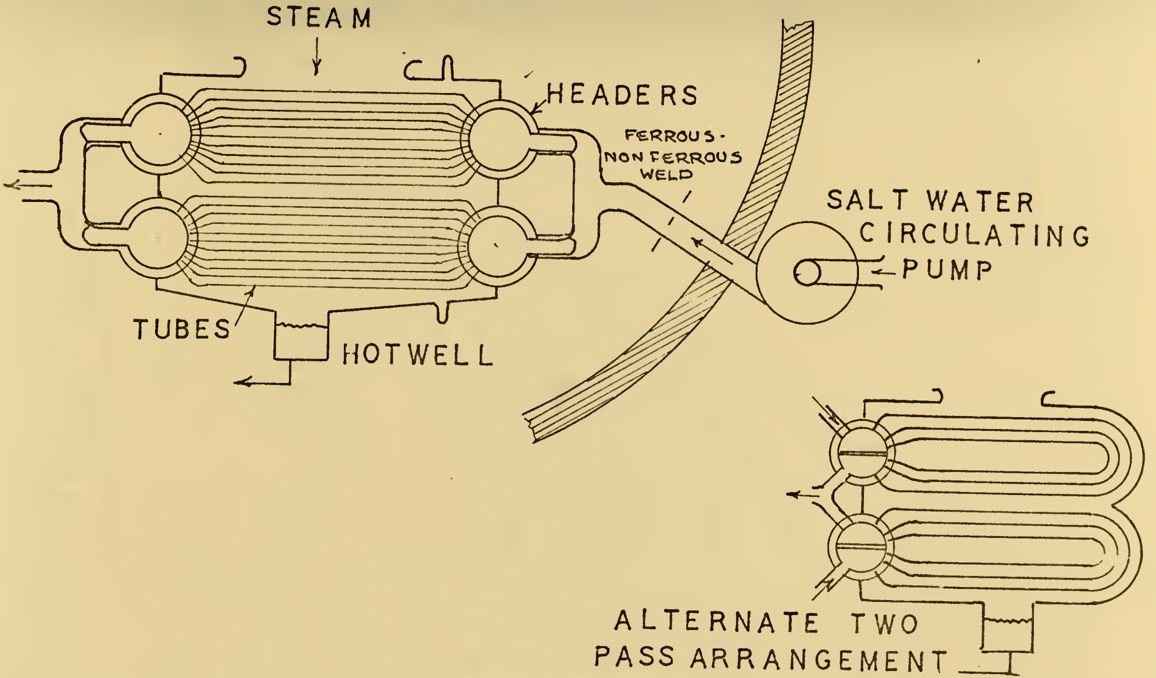

FIGURE VI-8

SCHEMATIC DIAGRAM OF DEEP SEA CONDENSER

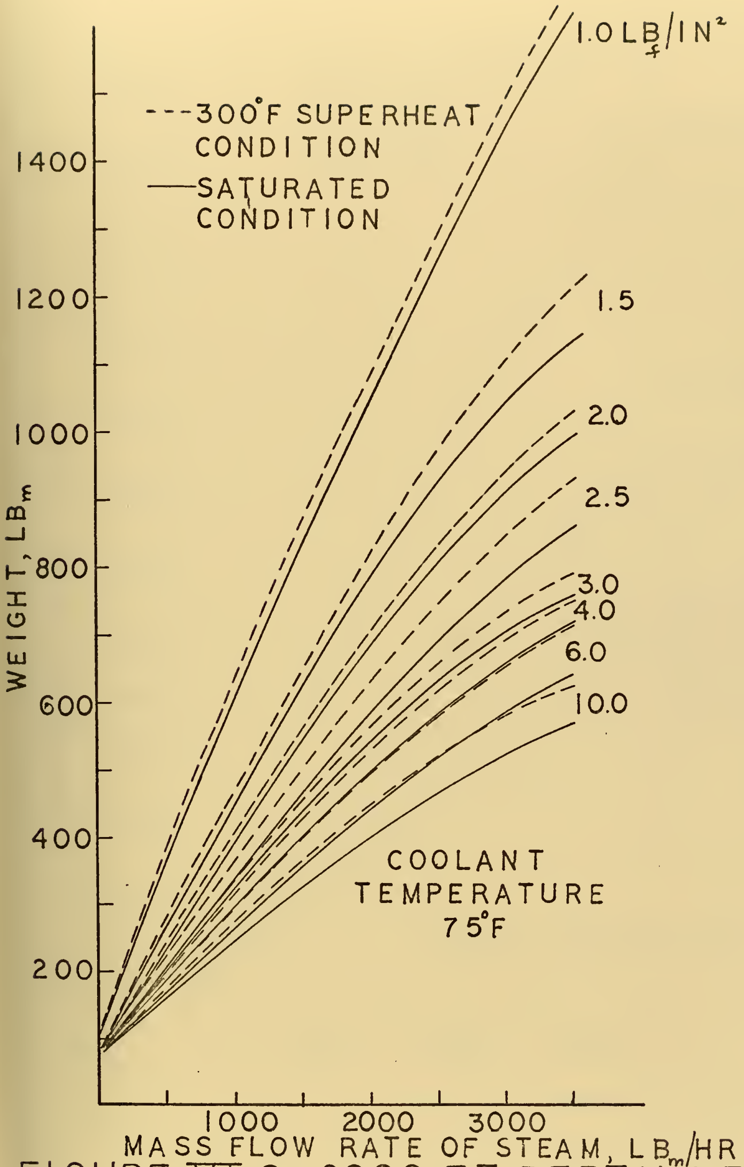

FIGURE VI-9 8000 FT DEPTH DEEP SEA CONDENSER WEIGHT VS STEAM RATE

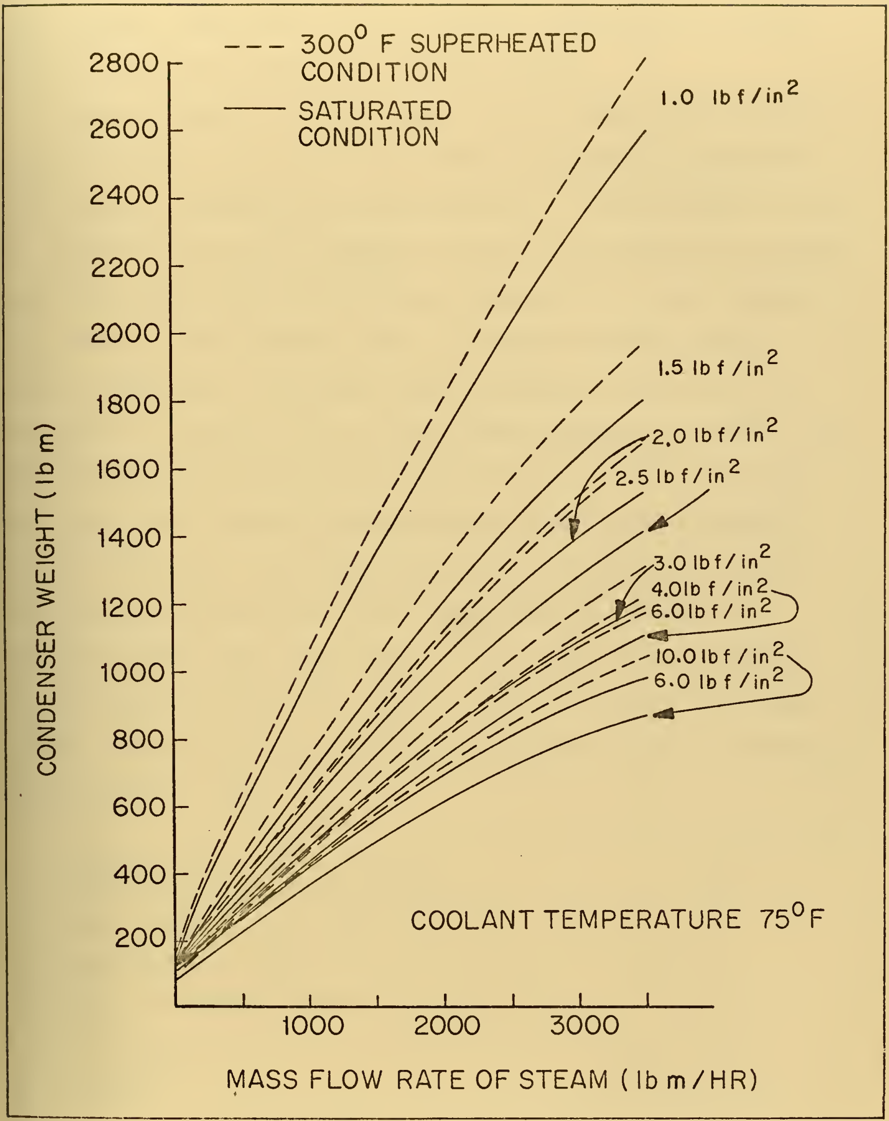

FIGURE VI-10 20,000 FT DEPTH
DEEP SEA CONDENSER WEIGHT vs STEAM RATE

the standard condenser and the deep-sea condenser are nearly equal. These are presented in Figure VI-11.

Pumping power and pump weight for the deep-sea condensers are anticipated to be relatively small but must be traded off with pressure vessel penetration weights. An estimated 2.6 kw of electrical power is required for the 40 kw propulsion plant previously mentioned. This figure represents a crude design with 2-tees, 2-90° elbows and 2 - 45 degree elbows and 2" piping throughout. Detailed weight tradeoffs might show an advantage in using a two or three pass condenser to reduce the size of the piping penetration in the hull. Such an arrangement could also reduce header weights since smaller headers could be employed, but this would be at the expense of some increase in condenser size with an attendant increase in pressure vessel size and weight. Table VI-9 gives a summary for the pump for the 40 kw plant. It is estimated that with careful piping design, the power requirement might be reduced as much as 25 - 30%.

Pump pressure rise, lbf/in^2	16.4
Electrical power required, kw	2.6
Pump & motor efficiency, %	42
Pump weight, lbm	60
Mass flow rate, lbm/sec	21.4
Power	400~AC
Condenser	Single Pass
Piping	2" throughout

TABLE VI-9
Submerged Condenser Circulating Pump Requirements
for the Deep Sea Condenser (40 kw plant)

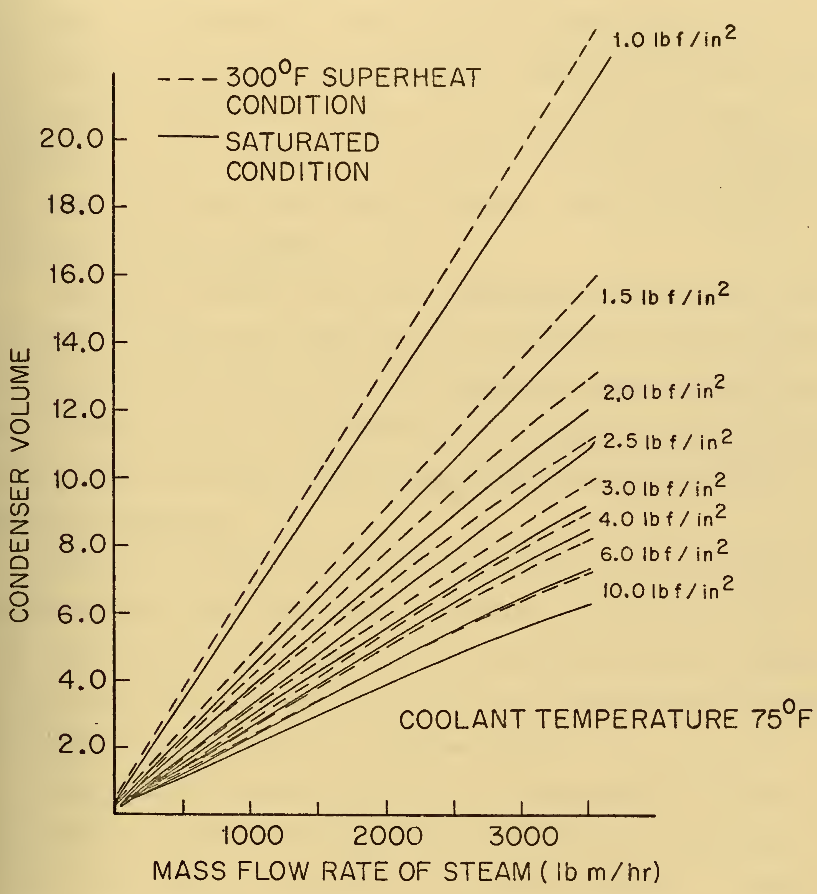

FIGURE VI-11 CONDENSER VOLUME vs STEAM RATE

Figure VI-12 is a composite graph of condenser weight and volume as a function of condensing surface area. By the use of Figure VI-12, one may compare the weights and volumes of the two types of condensers. Assuming now a design depth of 20,000 ft, condenser pressure of 1.0 lbf/in^2, and a 50 kw plant using the turbine presented in Chapter VII, one may predict the intermediate heat transfer loop minimum temperature necessary to reject the waste heat from the plant. Table VI-10 is a summary of these weights.

While the assumed sea water temperature for the deep sea condenser is 75°F, the condenser size and weight could clearly be reduced if the same sea water temperature were selected as for the skin cooler. It should be recognized that the pressure vessel size and weight may also be reduced with the smaller deep sea condenser.

While the deep-sea condenser is clearly a better choice in overall weight and volume than a comparable skin cooler, it must be recognized that the deep sea condenser will be considerably more expensive to build and is more susceptible to leaks, which would be disastrous at extreme depths.

The single greatest unknown in the skin cooler is the scale heat transfer coefficient and the effect of any preservative which might be applied to the outside surface. Experimental work will be necessary to prove the feasibility of the skin cooler for this application.

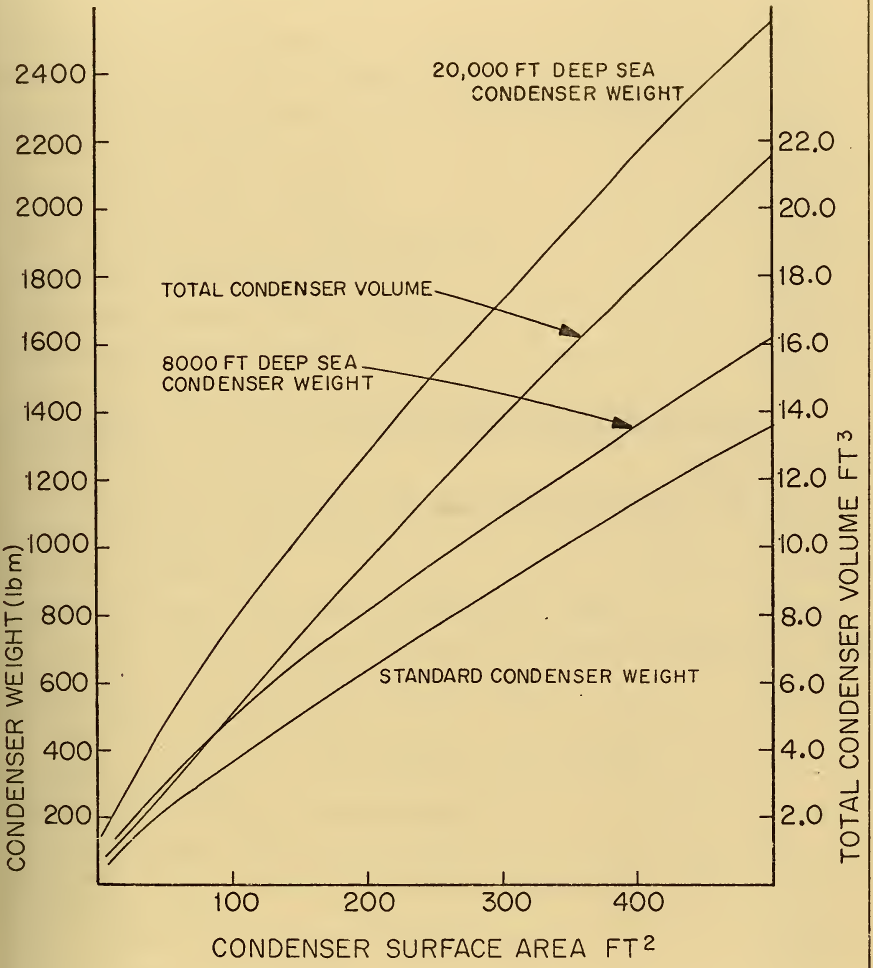

FIGURE VI-12 CONDENSER WEIGHT & VOLUME vs SURFACE AREA

ASSUMED CONDITIONS	
Sea water depth, ft	20,000
Plant nominal power level, kw	50.0
Turbine efficiency, %	73.0
Overall plant efficiency, %	36.0
Assumed pressure vessel diameter, ft	4.0
Available pressure vessel surface for heat transfer, ft^2	40.3
Sea water temperature, °F	40.0
Heat rejection rate, Btu/hr	3.31×10^5
Condenser pressure, lbf/in^2	1.0
Condenser steam inlet temperature, °F	243.5
Regenerator effectiveness, %	70.
Regenerator pressure drop, lbf/in^2	0.142
Condensation rate, lbm/hr	297.7
Oxygen flow rate, lbm/hr	4.13
Skin Cooler - $\frac{1}{4}$" Cu-Ni and $\frac{1}{4}$" Cu Fins - Arrangement B of Figure VI-3	
Pressure vessel material	HY-130 Steel
Intermediate heat transfer loop minimum temperature, °F	86.2
Condenser Surface area, ft^2	70.5
Condenser volume, ft^3	3.9
Condenser weight (including foundations), lbm	280.0
Skin cooler weight (including piping & fw and sw pumps), lbm	888.0
Total weight (less pressure vessel), lbm*	1168.0
Pumping power required, kw	2.5
*Weight of fresh water coolant not included	
Deep Sea Condenser	
Assumed design coolant temperature, °F	75.0
Condenser volume, ft^3	2.4
Condenser weight (including piping & foundations), lbm	460.0
Pump weight, lbm	66.0
Total weight (less pressure vessel), lbm	526.0
Pumping power required, kw	3.2

TABLE VI-10

Comparison of Skin Cooler with Standard Condenser and Deep-Sea Condenser Designs at 20,000 ft

Removal and Disposal of Non-Condensables

The non-condensables may be removed from the condenser by a standard vacuum pump with the expenditure of a small amount of power. For a 50 kw plant it is estimated that the steam flow rate which is uncondensed for the deep-sea condenser of Table VI-10 is 2.28 lbm/hr. With a 4.13 lbm/hr oxygen flow rate (representing the total non-condensable flow rate), a vacuum pump capable of removing 1.69 standard cubic feet per minute would be sufficient. The startup condition of large amounts of excess hydrogen must also be met. Here one must assume a time required for hydrogen rich operation until sufficient diluent steam can be admitted into the combustion chamber. If a ten second startup time is assumed, and if the pilot section of the porous plug burner (see Appendix B) is used in startup, a period of about 3.5 minutes would be required to clear the condenser of hydrogen, assuming the presence of no other non-condensables. To permit somewhat longer startup times, it is recommended that two vacuum pumps be installed, each rated for 2.0 SCFM. A single pump withdrawing 1.69 SCFM from a condenser at 1.0 lbf/in^2 pressure and discharging to 16.4 lbf/in^2 would use approximately .625 kw at a combined motor and pump efficiency of 50%. The estimated weight for the two pumps and motors is 20 lbm. A single pump would be capable of the hogging operation.

The sensing of the amount of non-condensables in the condenser would best be accomplished at the vacuum pump discharge. Instruments for detecting oxygen using the paramagnetic

principle could be used for this application (15). Equipment designed originally for flue gas analysis (and acting on the catalytic principle) could be used to detect the hydrogen concentration. This would first, however, require dilution with a predetermined amount of oxygen, since the equipment is limited to a volumetric concentration of combustible gas of about 15%. With this known amount of diluent oxygen and the oxygen concentration sensed from the paramagnetic detector, one could then determine the hydrogen concentration. Effluent from the hydrogen and oxygen detectors could then be redirected to the condenser. The two gas measurement systems are available in a single commercial instrument approximately 18" x 12" x 18" which operates on 115 VAC, 60-hertz, drawing 75 watts of power. This instrument would, however, require some modification for the proposed application. Its time response is about 30 seconds.

Elimination of the non-condensables is accomplished in two steps. The first step is a porous plug recombiner very similar to that described by Moore (16) for the recombination of radiolytically decomposed hydrogen and oxygen from the steam condenser of a boiling water reactor power plant. The device has proved to be reliable for this application. The principles of operation of the porous plug burner are discussed in Appendix B. If the plant is run very slightly oxygen rich, any excess hydrogen may be recombined at the porous plug burner. A second porous plug, downstream of the burner plug, may be used to condense water vapor from the burned mixture, which may then be routed to the condenser via a steam trap. A receiver downstream of the

condensing plug may act as a reservoir for uncondensed gases, chiefly argon with some oxygen and uncondensed water vapor. The content of this receiver might also be sensed for the presence of hydrogen and the contents could be dumped to the condenser if the hydrogen concentration becomes excessive for compression of the mixture to 5000 $\mathrm{lbf/in}^2$, the storage pressure selected for on board storage of non-condensables. For the hydrogen rich startup condition, a suitable amount of oxygen could be bled into the line downstream of the vacuum pump and upstream of the porous plug burner.

While overboard discharge of the non-condensables is a possible alternative, on board storage at high pressure has distinct advantages. The possible discharge of hydrogen at the surface could be hazardous. The amount of the non-condensables is small. It is estimated that a 7.5 inch ID sphere of HY-130 could house all the argon from a 1000 kwh mission at 36% overall thermal efficiency if the argon were compressed to 5000 $\mathrm{lbf/in}^2$. Such a sphere would weigh about 7.5 pounds. Two such spheres would probably be sufficient to house all the non-condensables. The electrical power to compress the non-condensables is estimated to be about .2kw, assuming an overall compressor and motor efficiency of 20%. Intercooling would have to be provided, necessitating some sort of auxiliary cooling water system, which could easily be provided for this component and others. A sea water/auxiliary cooling water (fresh water) heat exchanger would be necessary.

Table VI-11 is a tabulation of required equipment and estimated weights for the non-condensable removal and storage system. Figure VI-13 is a schematic diagram of the system.

Component	Estimated Wt. lbm	Estimated Vol. ft^3
Vacuum pumps (2) and motors	3.0	0.08
Porous plug burner, condenser and non-condensable gas receiver	15.0	0.30
Hydrogen-Oxygen Detector	15.0	2.25
Non-condensable gas compressor (allowance for space and weight)	20.0	.30
Non-condensable gas storage spheres (2)	14.8	.30
Total	67.8	3.23

TABLE VI-11

Non-Condensable Removal and Storage System

The condensate pump and feed water pumps have not been designed in detail, but the best solution appears to be a combined three stage condensate and feed pump. The first stage of the pump would serve a dual purpose. It would pump the product water to the product water tank as well as supply the second stage of the pump with sufficient net positive suction head. The product water mass flow rate, of course, would be nearly identical to the reactant flow rate. For the very small volumetric flow rate, 0.172 gpm discharge at design power level, a gear pump would probably prove to be

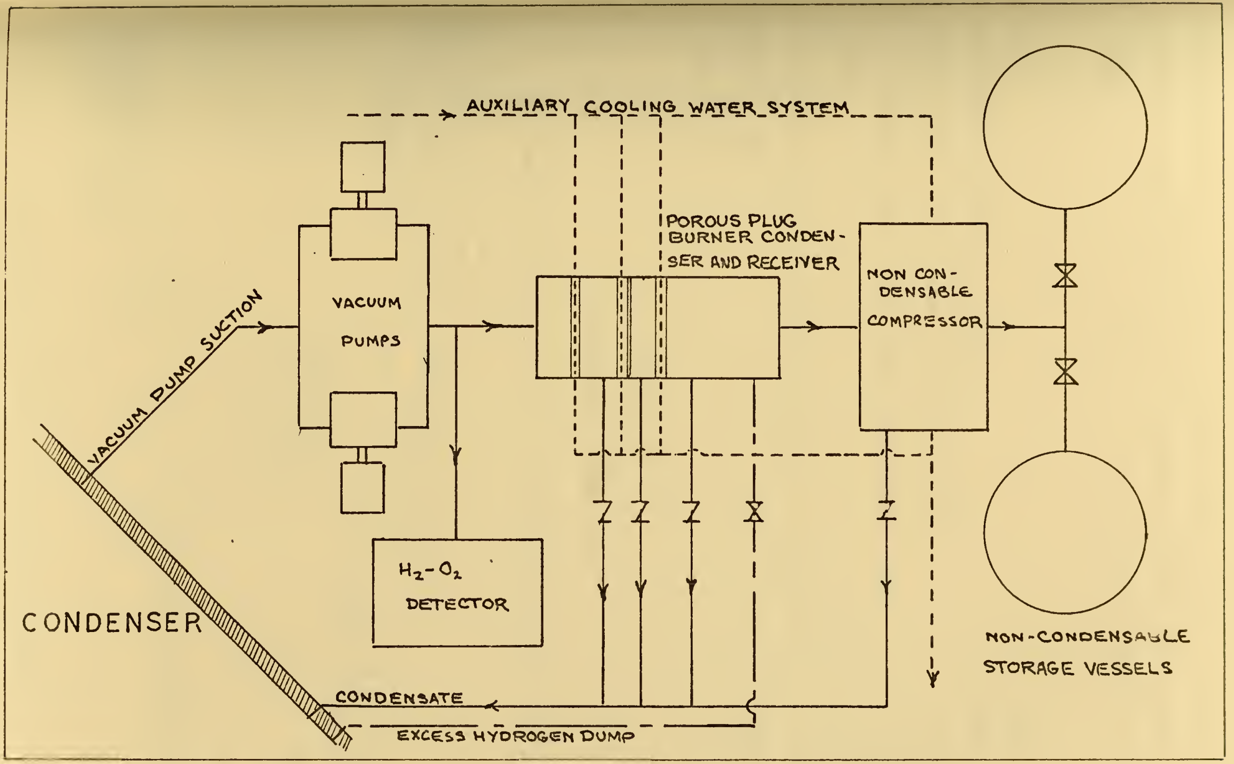

FIGURE VI-13 NON-CONDENSABLE REMOVAL AND STORAGE SYSTEM

most satisfactory for the proposed application. Table VI-12 lists the requirements and estimated weight and volume for such a pump for the 50 kw power plant described in Table VI-10.

Type	Gear -3 stage
Discharge pressure, lbf/in^2	800.
Design power flow rate (discharge) gpm	0.172
125% design power flow rate (discharge), gpm	0.214
Drive	Variable speed AC motor
Electrical power required at design flow rate, kw	0.55
Weight, lbm	20.0
Volume, ft^3	0.3

TABLE VI-12

Condensate/Feed Pump

A schematic diagram of the condensate/product water/feed system is shown below.

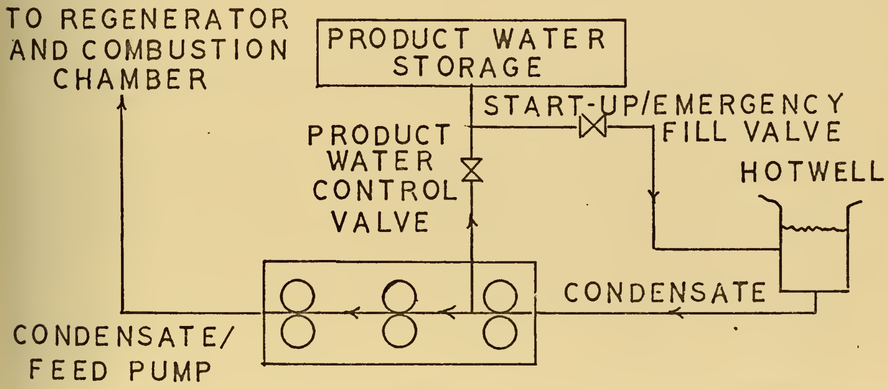

FIGURE VI-14

Condensate/Product Water/Feed System

The opening of the product water regulating valve could be coupled to the flow rates of one of the reactants, probably hydrogen, and closed if the hotwell level drops below a specified level.

An additional system is required for cooling of electronic components, motors, and other heat loads within the propulsion plant pressure vessel. A list of such equipment is given in Table VI-13.

Lube oil cooler (turbine)

Cycloconverter (if utilized for AC power transmission)

Inverters (for startup and emergency battery to AC power conversion)

Porous plug recombiner

Propulsion plant pressure vessel atmosphere cooling

Non-condensable compressor intercooling

Hydrogen and oxygen heaters (if provided)

TABLE VI-13

Heat Loads for Auxiliary Cooling Water System

No detailed study of the auxiliary cooling water system was conducted. Rather a weight/space/power allowance is provided. A weight of 150 lbm for all the heat transfer equipment and pump, including a sea water/fresh water heat exchanger, is believed to be conservative. Similarly, a volume allowance of 1 ft^3 and a power requirement of .2 kw for the system seems adequate. The atmosphere inside the pressure vessel could be

hydrogen saturated with water vapor or oxygen saturated with water vapor. Electrical components must be designed to operate in the environment selected. If a high speed generator is selected for the transmission system, which appears most promising, hydrogen would be preferable in reducing windage losses.

Condenser Off-Design Performance

Through use of Figure VI-4 or VI-5 one may construct a graph of the estimated off-design performance for a condenser of a specific design condensing rate and pressure. Such a graph is shown in Figure VI-15 for the design conditions of Table VI-10. While extrapolation of Figure VI-4 or Figure VI-5 will predict a zero condenser pressure at a zero condensation rate, a better estimate of the existing condenser pressure at zero steam flow is given in reference 10, estimating a pressure of slightly less than 0.5 $\mathrm{lbf/in^2}$ for "standard air ejection equipment" and a coolant inlet temperature of 75°F.

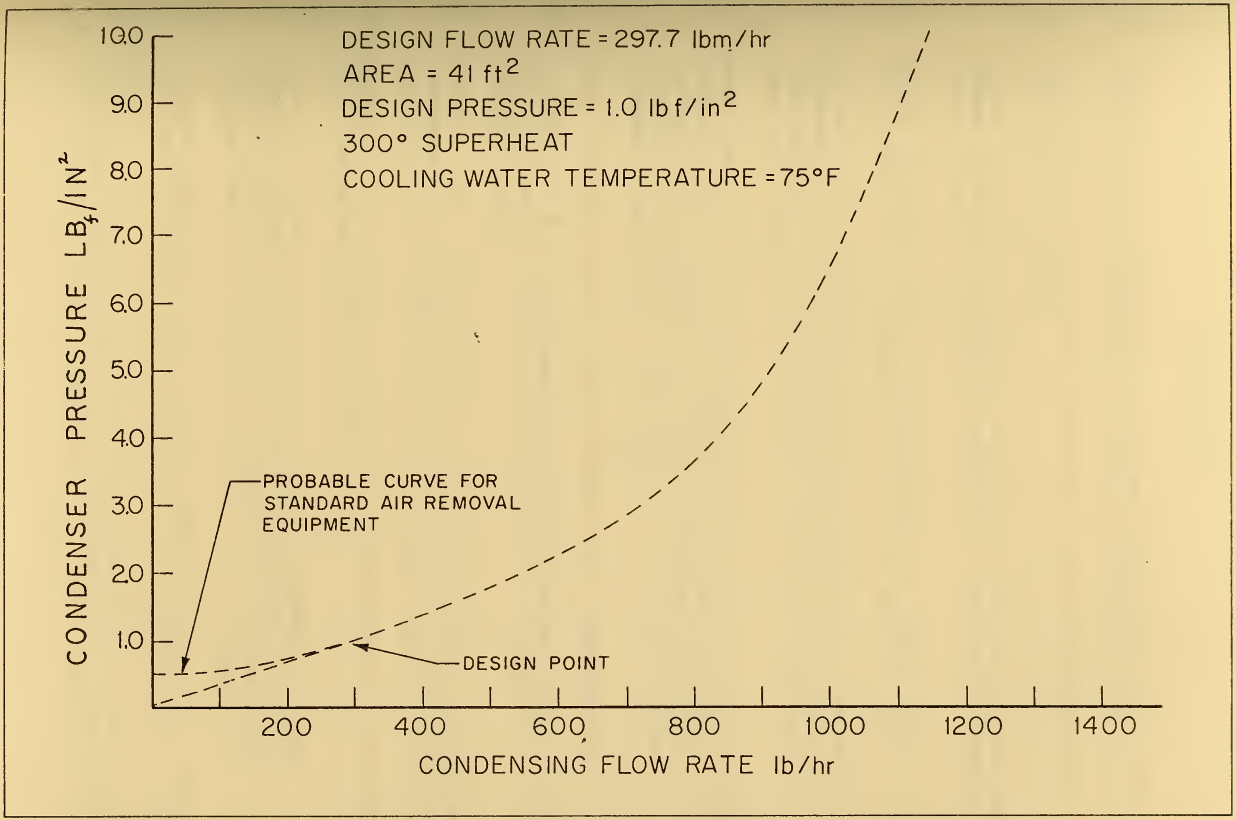

FIGURE VI - 15 CONDENSER OFF - DESIGN PERFORMANCE

REFERENCES

1. Powell, S.C., Department of Ocean Engineering, Massachusetts Institute of Technology, personal communication.

2. Kern, D.Q., *Process Heat Transfer*, New York, McGraw-Hill Book Company, 1950.

3. Walsh, E., Ocean Research and Engineering Center, Westinghouse Underseas Division, Annapolis, Maryland, personal communication, April 25, 1972.

4. *Metals Handbook*, Vol. I, 8th Edition, T. Lyman, ed., Cleveland, Ohio, American Society for Metals, 1961.

5. Craven, J.P., *The Design of Deep Submersibles*, Paper No. 9 presented at the Diamond Jubilee International Meeting of the Society of Naval Architects and Marine Engineers, New York, 1968.

6. Balukjian, H., "A Closed Brayton Cycle Power Plant for Underwater Applications and Comparison with a Fuel Cell", Paper presented at the Seventh Annual Technical Symposium, Association of Senior Engineers, Naval Ships Systems Command, Washington, D.C., 1970.

7. Union Carbide, Linde Division, personal communication.

8. Stickler, D.B., Department of Aeronautics and Astronautics, Massachusetts Institute of Technology, personal communication.

9. Silver, R.S., "An Approach to a General Theory of Surface Condensers", *Proceedings of the Institution of Mechanical Engineers*, Vol. 178, Pt. 1, No. 14, pp. 339-357, (1963-64).

10. *Standards for Surface Condensers*, Sixth Edition, New York, Heat Exchange Institute, 1970.

11. Reese, R.M. and A.D. Carmichael, "A Proposed Hydrogen-Oxygen Fueled Steam Cycle for the Propulsion of Deep Submersibles", *Proceedings of the 1971 Intersociety Energy Conversion Engineering Conference*, August 1971.

12. "Steam Condensers", *Design Data Sheet Section DDS 4601-1*, Department of the Navy, Bureau of Ships, October 15, 1953.

13. Sebald, J.F., "Main and Auxiliary Condensers", Chapter 13 of *Marine Engineering*, Roy L. Harrington, ed., New York, The Society of Naval Architects and Marine Engineers, 1971.

14. Masubuchi, K., Department of Ocean Engineering, Massachusetts Institute of Technology, personal communication.

15. Erdman, G., Project Engineer, Scott Aviation, Charlottesville, Virginia, personal communication, January 28, 1972.

16. Moore, G.E. and L.H. Tomlinson, *Requirements for and Principles of Flame Recombination of* H_2/O_2 *Mixtures*, General Electric Research and Development Center, Schenectady, New York.

CHAPTER VII

Expander Selection and Design

There are two basic choices which can be considered for the expansion of high pressure high temperature steam. These are the reciprocating engine and the turbine. Until recently very little work has been done in perfecting the reciprocating steam engine, particularly at the low power levels of interest in this thesis. With the current interest in low emission engines for automotive purposes, however, reciprocating steam engines have been reevaluated in the light of new technology. Steam engines in the past have operated on saturated steam, which in addition to a liberal supply of lubricating oil, provided sufficient lubrication. At the high superheated steam temperatures which, as shown in Chapter IV, give high overall thermal efficiencies, a different type of lubrication must be used. Syniuta (1) describes the development of an automotive reciprocating steam engine, which with the proper dry lubricant, permits operation at steam temperatures as high as 1400°F. The dry lubricant serves the purpose of replacing the condensed steam, which provides a large percentage of the lubrication in a conventional reciprocating steam engine, and eliminates the contaminating nature of lubricating oil which would foul condenser surfaces and reduce heat transfer at low condenser pressures. Detailed information on these engines is not available, but they present a promising alternative to the turbine.

A second type of reciprocating engine is one which burns the hydrogen and oxygen reactants in the cylinder. Such an engine has been built (2) which operates on excess hydrogen to reduce combustion temperatures to acceptable levels. Two significant problems were noted with this engine. The oxygen injector experienced rapid deterioration, and at the low exhaust pressures of a space environment, there was a significant loss of lubricating oil into the engine exhaust. While steam might replace the excess hydrogen as the diluent, the loss of lubricating oil could probably be rectified only through substitution of a solid lubricant. The low condenser pressures shown in Chapter IV to give high overall thermal efficiencies would again result in the collection of oil on the condenser heat transfer surfaces. It is doubtful that the problem of the oxygen injectors could be easily overcome for an engine with a design lifetime of about 5000 hours.

The turbine appeared, then, to be the best selection at present for the role of the expander. Baljé (3), in a classical paper on the optimization of turbine design, showed that at low specific speeds, the single stage axial impulse turbine is superior to the Terry turbine. He also showed that at even lower specific speeds, the partial admission axial impulse turbine and single disk, multiple-stage axial impulse re-entry turbine were superior to the full admission turbine. It is in the range of specific speeds where the re-entry turbine is most efficient, that the expander of this thesis must operate. This is particularly true of the 50 kw power level. Of course, if

large enthalpy drops are to be taken across the turbine, a single disk re-entry turbine, even though it may have as many as four stages, will not be as efficient as a multidisk machine. In normal steam turbine practice, multistage machines are the rule and partial admission is common only in the first stage. In the proposed application, however, simplicity of design requires a small machine of not more than three or four disks. Radial inflow turbines are a possible alternative to the single stage axial impulse turbine but could not be easily staged.

It is fortunate that the re-entry turbine design permits the utilization of a single disk for more than one-stage. Thus a machine of three disks could incorporate as many as twelve stages, at four stages per disk. The repeated routing of steam through the blading of a single wheel, however, requires the addition of re-entry ducting. Thus the simplicity of the rotor design is negated to a certain extent by the addition of some cumbersome re-entry ducts. The re-entry ducts may become quite large in some configurations, effectively doubling the diameter of the machine, compared to a normal machine of equivalent rotor diameter (4).

Figure VII-1 is a schematic diagram of a two stage re-entry turbine with the crossover duct geometry.

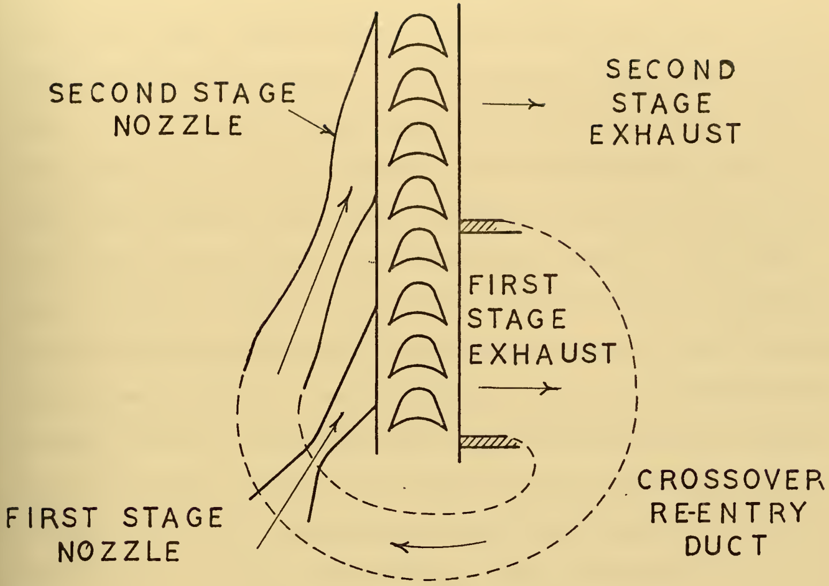

FIGURE VII-1

Two Stage Re-Entry Turbine - Schematic Diagram

(Crossover Duct Geometry)

A primary limitation of the axial impulse re-entry turbine is interstage and tip leakage. The leakage phenomenon is described in detail in Appendix C. When the ratio of axial and tip clearance to blade height is small, the machines are quite efficient, but the efficiency deteriorates rapidly with increasing clearance ratios. A clearance of .004-.005" with a tip to tip rotor diameter of 8" gives very good efficiencies, but increasing the clearances by a factor of 3 may result in a drop in efficiency by as much as 15 efficiency points at the

same pressure ratio and entering steam conditions. With the high inlet steam temperatures, thermal growth of first stage rotor blading will require careful design of component clearances. It is doubtful then that clearances less than .005" can be maintained. This becomes a problem when one investigates the required blade heights for a re-entry turbine to be used as the first disk at the 50 kw power level. If a four stage re-entry turbine is used for the application, one must sacrifice efficiency over a considerable range of the available total pressure ratio. Here multidisk staging is advantageous. By using, for the first disk, only a two stage re-entry turbine with small blade heights and large relative clearances, one may limit the low efficiency portion of the turbine to just a small portion of the total enthalpy drop available.

Another problem associated with the proposed application is material limitations. Of the many high temperature, high-strength superalloys developed, few have sufficient strength at 1600-1750°F to withstand rotative speeds in excess of 80,000 RPM. This, of course, is coupled with disk diameter, which practically could not be much less than about three inches, and blade height, which could not be less than 0.1 inches. Ideally, one might set some limitation such as 0.25" on blade height, but even for re-entry turbines this is too large for the first stage of a 50kw turbine operating with high pressure, high temperature steam.

Another advantage of the re-entry turbine is also related to materials. In the normal partial admission turbine, the

blade temperature reached in the first stage is nearly the stagnation temperature corresponding to the relative inlet conditions to the blades. In the re-entry turbine, the blading experiences this same stagnation temperature in the first stage arc of admission but the same blading experiences lower stagnation temperatures in succeeding stages on the same wheel, which cover a much wider sector of the arc of admission than the first stage. Even a two stage re-entry turbine operating at moderate stage pressure ratios is able to reduce the average stagnation temperature experienced by the rotor blades, allowing a higher rotative speed than for a comparable turbine with a simple partial admission first stage.

The speed to be selected for a small turbine is not only a function of the best speed for highest turbine efficiency, but also the best speed for the transmission system selected. It is here that the electrical transmission system is advantageous since the weight of an electrical generator decreases with rotative speed for the same power produced. With solid rotor machines, rotative speeds of 24,000, 36,000 (5) and even 93,500 RPM (6) may be reached. Of course, at these high rotative speeds and for an extended time between overhauls of 4000-5000 hours, bearing reliability may become significant. For this application, ball bearings would probably result in the lowest friction and hence the least power loss. Syniuta (7) reports bearing d_n ratings of as high as 1- 2.5 x 10^6 may now be utilized for high speed ball bearing applications, where d_n = (bore diameter in mm) x (RPM).

Of course bearing life is of vital importance, and the more conservative the bearing d_n rating, the longer the expected lifetime. Calculations of a 30 mm bore diameter, 36,000 RPM ($d_n = 1.08 \times 10^6$) design for the closed Brayton cycle engine (8) estimated a system time between overhaul of 3100 hours. This system used two angular contact (combined journal and thrust) ball bearings with gas cooling and oil-mist lubrication. Total bearing loss for this machine was about .4 kw. The operating conditions for these bearings are similar to that for the proposed cycle of this thesis with the exception of the presence of water vapor and the greater thrust which must be absorbed from a steam turbine. Subsequent models of the Brayton unit have used gas bearings with satisfactory results (9). Gas bearings using high temperature superheated steam would not be suitable for the semi-closed Rankine cycle.

While the desired transmission system speed is of importance in selecting the turbine speed, one finds in practice that in order to achieve acceptable turbine efficiencies at low power levels, (50 kw) the turbine speed is of primary importance.

It is here that the electrical transmission system is most compatible, in that it is also adaptable to high rotative speeds. Geared drives for propulsion purposes at the 50 kw power level, however, must provide gear ratios in excess of 100:1 if at all acceptable turbine efficiencies are to be realized. This high reduction ratio is at considerable expense in gear transmission efficiency. The efficiency is still high, however, but other factors, discussed in Chapter VIII, make the gear transmission unattractive.

It would then seem best to operate the turbine in its most efficient speed range, consonant with material limitations and at a speed compatible with alternator frequencies which are most useful. A speed of 24,000 RPM corresponds to a 400-hertz 2-pole machine, and is a desirable speed for low power (50 kw) applications. Other possible rotational speeds are 36,000 RPM (4-pole, 1200-hertz) (5) and 48,000 RPM (4-pole,1600-hertz).

Turbine Optimization

The methods described by Baljé (3) and amplified by Linhardt and Silvern (10) and Linhardt (11), were used to develop turbine optimization computer programs for full admission, partial admission, and multistage re-entry axial impulse turbines. Baljé and Binsley (12), describe the turbine optimization technique used in this thesis, the pattern search. The particular method used is that of Hooke and Jeeves (13). The equations for the re-entry turbine are developed in detail in Appendix C. It was necessary to modify the leakage analysis of Linhardt (11) considerably. Linhardt neglected leakage on the exit side of the rotor both in the radial and tangential directions. The possible leakage paths in a re-entry turbine are shown in Figure VII-2.

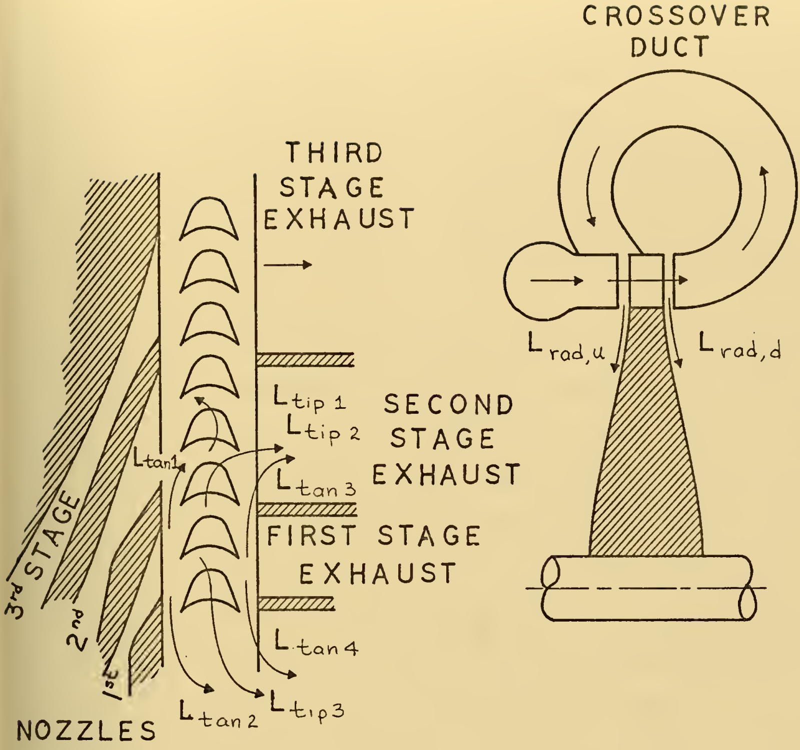

FIGURE VII-2

Leakage Paths in a Multistage Axial Impulse Re-Entry Turbine (3-stage) (crossover duct geometry)

The leakage paths are described below:

$L_{tan\ 1}$ - tangential leakage in the direction of rotor rotation from one stage to the succeeding stage, upstream of the rotor

$L_{\text{tan } 2}$ - tangential leakage in the direction opposite to rotor rotation from the first stage to the last stage, upstream at the rotor

$L_{\text{tan } 3}$ - tangential leakage downstream of the rotor in the direction of rotor rotation from the exhaust of one stage to the exhaust of the succeeding stage

$L_{\text{tan } 4}$ - tangential leakage in the direction opposite rotor rotation from the exhaust of the first stage to the exhaust of the last stage

$L_{\text{tip } 1}$ - normal tip leakage, over the end of the blade from the pressure to the suction side of the blade

$L_{\text{tip } 2}$ - leakage across the tips of the blades in the direction of rotor rotation from one stage to the exhaust of the succeeding stage

$L_{\text{tip } 3}$ - leakage across the tips of the blades in the direction opposite rotor rotation from the first stage to the exhaust of the last stage

$L_{\text{rad,u}}$ - radial leakage into the rotor cavity upstream of the rotor

$L_{\text{rad,d}}$ - radial leakage into the rotor cavity downstream of the rotor

Tip leakage for the cases of interest from paths 2 and 3 was found to be small in comparison to radial and tangential leakage and was not included in the computer optimization. An analysis of this leakage, however, is developed in Appendix C.

In addition to the leakage paths described above, there exists another possible leakage path. This leakage results from blade movement into the exhaust duct region of the succeeding stage while in the blade passage there still remains working fluid. This effectively bypasses the nozzle of the succeeding stage. This type of leakage is termed dynamic leakage (10). In the computer analysis it was assumed that no work was performed by this leakage. Baljé (14) has assumed that only half of this leakage does no work. An interesting aspect of the dynamic leakage is the fact that it is speed dependent, i.e., it increases with speed.

The modifications to the leakage analysis of Linhardt are presented in detail in Appendix C. Basically they include tangential and radial leakage downstream of the rotor, omitted by Linhardt, and assess leakage per stage as a percentage of the total steam flow rate for the multistage disk. Linhardt assessed the leakage fraction on the basis of the nozzle flow for a particular stage, which overestimates the effect of leakage. While Linhardt's assessment on the basis of stage nozzle flow rates may be adequate for small clearance ratios, it is not satisfactory for the applications of this thesis.

Reference 15 reports the experimental testing of a two stage re-entry turbine operating at a pressure ratio of 300:1. Observed efficiencies for this turbine fell short of the efficiencies predicted by methods developed by Baljé (16). The principal causes of this discrepancy were deemed to be leakage by path $L_{tan,1}$ in excess of that anticipated and

dynamic leakage, unknown prior to that time. This reportedly was experimentally substantiated by a "static" test in which the rotor was held stationary and the upstream axial leakage gap reduced to zero. The remaining leakage was nearly equivalent to the value predicted for tip leakage. The difference in the leakage observed in the static test and the total leakage which would produce the observed efficiency was evaluated as dynamic leakage, which agreed with a theoretical assessment of dynamic leakage. This assumed that no work was done by the dynamic leakage. The conclusions of this experiment are questionable, in that the conditions in the turbine change when no work is extracted from the rotor. Nevertheless, the success of this turbine is indicative of the promise of re-entry turbines for low power output and high enthalpy drop. It also indicated that the method of analysis developed by Baljé, Linhardt and Silvern can give reasonable approximations of expected turbine efficiency after further refinement.

Presentation of Data

The computer program employing the equations set forth in Appendix C was used to evaluate turbine efficiency over a wide range of conditions. The results of this study are shown in Figures VII-3, VII-4, VII-5 and VII-6. The conditions assumed are listed below:

$\alpha_2 = 16.0°$

$Pr_i = 1.97$, constant for all stages

$K_D = .003$

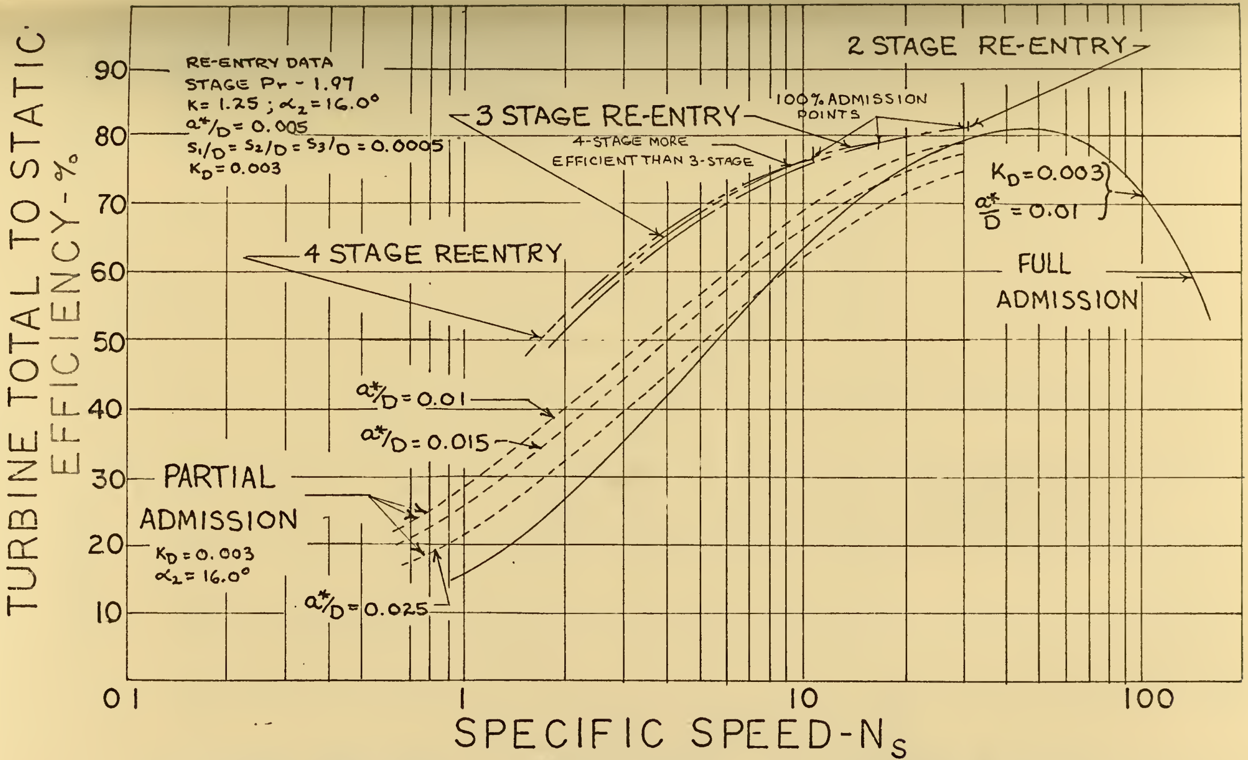

FIGURE VII-3 COMPOSITE N_S EFFICIENCY DIAGRAM FOR FULL ADMISSION, PARTIAL ADMISSION AND RE-ENTRY AXIAL TURBINES

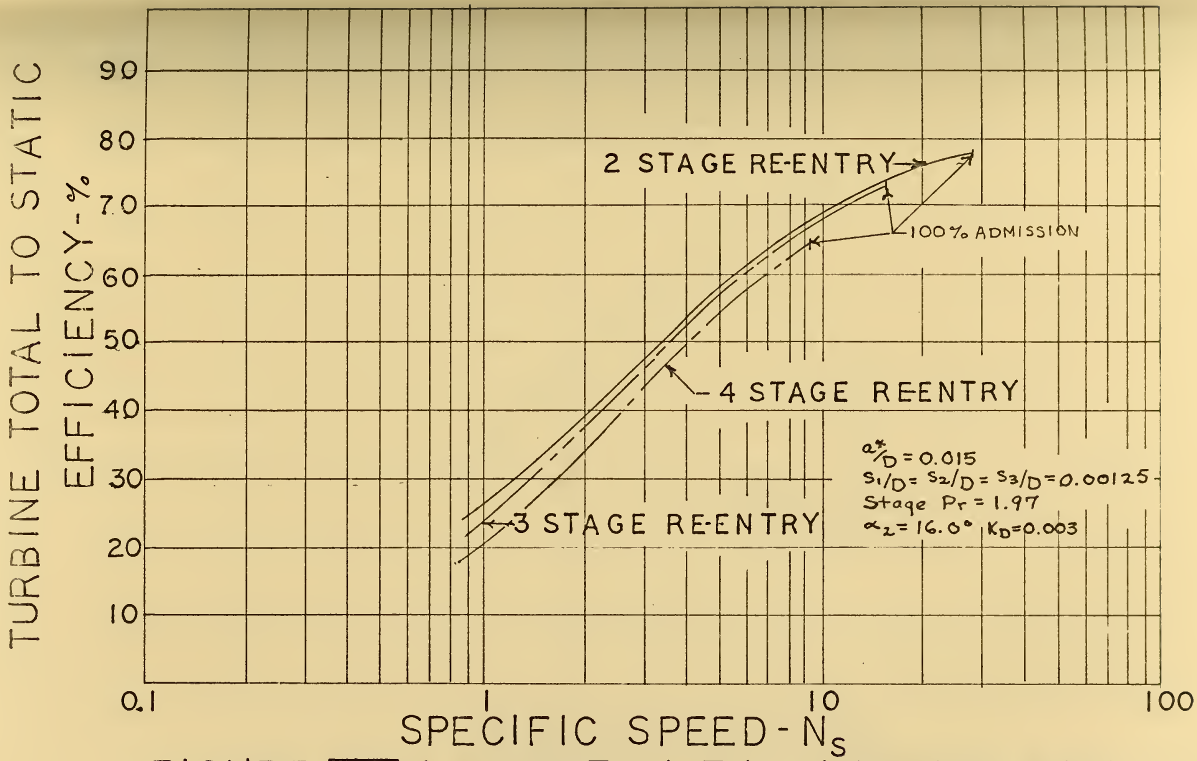

FIGURE VII-4 RE-ENTRY TURBINE N_S-EFFICIENCY DIAGRAM FOR SMALL NUMBERS OF BLADES AND LARGE CLEARANCES

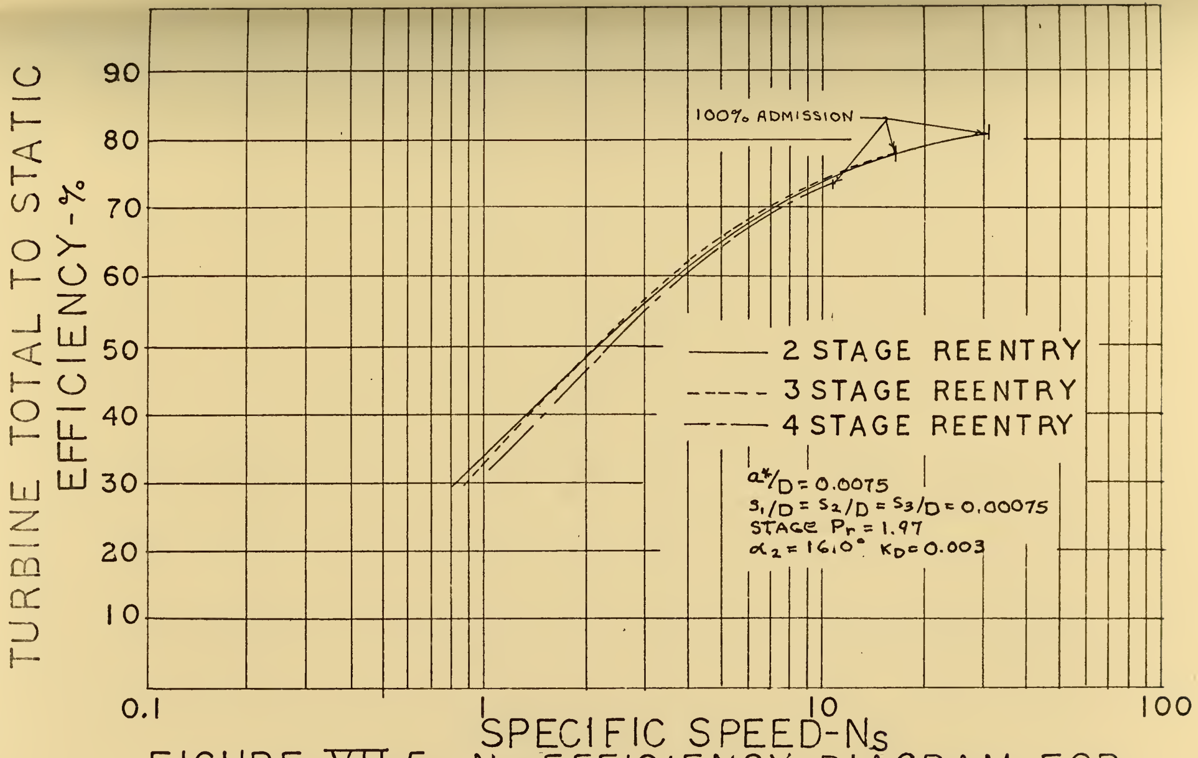

FIGURE VII-5 N_S-EFFICIENCY DIAGRAM FOR RE-ENTRY TURBINES WITH INTERMEDIATE NUMBERS OF BLADES AND MEDIUM CLEARANCES

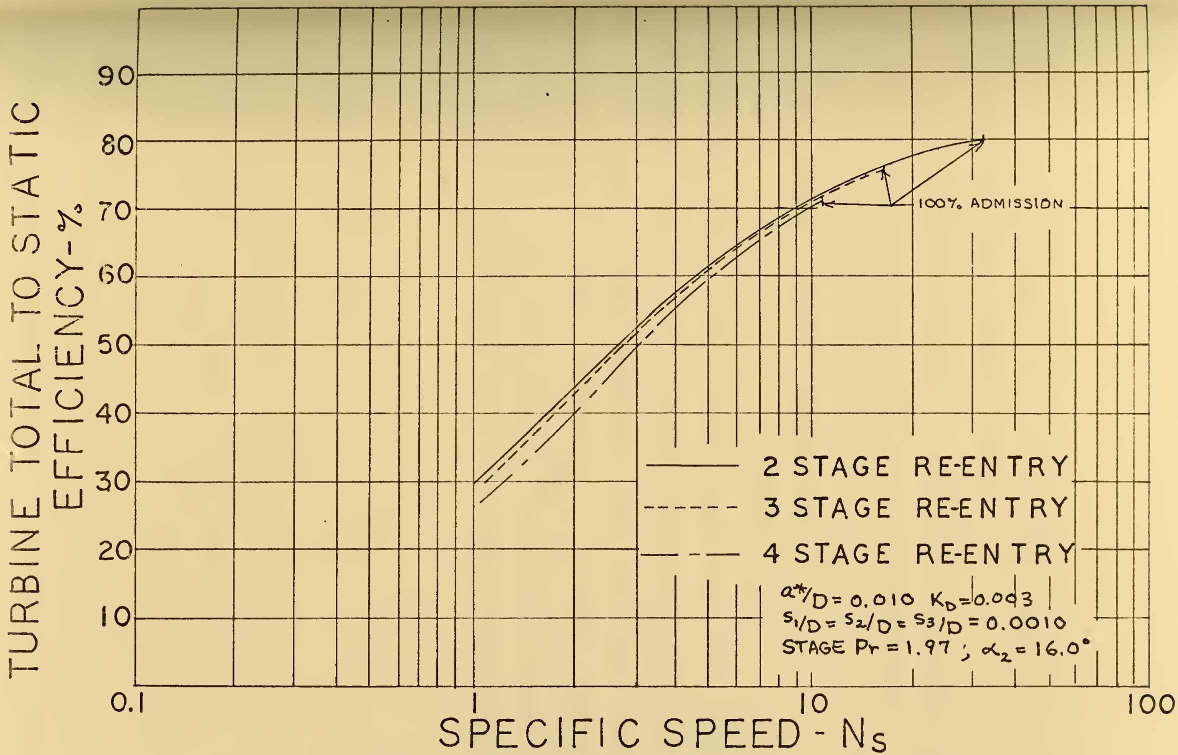

FIGURE VII-6 N_S-EFFICIENCY DIAGRAM FOR RE-ENTRY TURBINES–MODERATELY LARGE CLEARANCES AND SMALL NUMBER OF BLADES

K_P = .0014

k = 1.25

ψ_N = 0.96

where α_2 = nozzle angle measured from the tangential direction

Pr_i = the stage pressure ratio

K_D = the disk friction coefficient (see Appendix C)

K_P = pumping loss coefficient (see Appendix C)

k = ratio of specific heats

ψ_N = nozzle velocity coefficient

In the evaluation of the re-entry turbine the ratio of rotor blade throat width, a*, to rotor tip to tip diameter, D, was varied as well as the ratios of tip (s_3) and axial clearance (s_1, s_2) to rotor diameter. The significant variation of turbine total to static efficiency at constant specific speed as a*/D, s_1/D, s_2/D, and s_3/D are increased is apparent. Turbine total to static efficiency has been plotted against specific speed.

$$N_s = \frac{N\,Q_3^{\frac{1}{2}}}{H_{ad}^{\frac{3}{4}}} \qquad \text{(VII-1)}$$

N_s = specific speed in the notation of Baljé (3)

Q_3 = stage exit volumetric flow rate, ft^3/sec

H_{ad} = isentropic head, total to static, ft lbf/lbm

N = RPM

Baljé (14) in unpublished lecture notes, reports similar findings of rapid deterioration of efficiency as clearances and throat width are increased for a fixed rotor diameter.

The effect of increasing the ratio of throat width to rotor diameter is to decrease the number of blades, thus increasing the filling and emptying losses. Filling and emptying losses are common to partial admission turbines and were first identified and evaluated by Stenning (17).

Because of the emphasis on high pressure ratio turbines in references 10, 11, and 15, the effect of pressure ratio on turbine efficiency at constant specific speed was evaluated. Large pressure ratios invariably resulted in significantly lower efficiencies.

For the case of stage pressure ratios greater than the critical value, the general first stage leakage factor, ζ, may be represented by the following relationship:

$$\zeta_{L,1} = \frac{\dot{m}_{\ell,1}}{\dot{m}_1} = \frac{\dfrac{p_{1,st}A_\ell}{\sqrt{RT_{1,st}}}}{\dfrac{p_{1,0}A_{throat}}{\sqrt{RT_{1,0}}}} \qquad \text{(VII-2)}$$

where

$\dot{m}_{\ell,1}$ = a general leakage mass flow rate for the first stage, lbm/hr

$\dot{m}_1$ = the first stage nozzle mass flow rate, lbm/hr

$p_{1,st}$ = the static pressure in the first stage cavity, assumed in this case equivalent to the total pressure upstream of the leakage area, lbf/ft^2

$p_{1,0}$ = the total pressure upstream of the first stage nozzle, lbf/ft^2

A_ℓ = the leakage area, ft²

A_{throat} = the nozzle throat area, ft²

$T_{1,st}$ = the total temperature upstream of the leakage area, assumed in this case to be equal with the exit static temperature of the first stage rotor, °R

$T_{1,0}$ = the total temperature upstream of the first stage nozzle, °R

R = the gas constant for the gas in question

It may be seen that the leakage factor is inversely proportional to the stage pressure ratio. Hence, for increased pressure ratios at constant N_s one might expect the leakage factor to decrease.

For subcritical pressure ratios, in a turbine of equal pressure ratios per stage, the same relationship holds, but only because the pressure ratios for the first and second stages are equal.

$$\zeta_{L,1} = \frac{\dot{m}_{\ell,1}}{\dot{m}_1} = \frac{\dfrac{p_{1,st} A_\ell}{\sqrt{RT_{1,st}}} \sqrt{\dfrac{2k}{k-1}} \sqrt{\left(\dfrac{p_{2,st}}{p_{1,st}}\right)^{2/k} - \left(\dfrac{p_{2,st}}{p_{1,st}}\right)^{\frac{k+1}{k}}}}{\dfrac{p_{1,0} A_{throat}}{\sqrt{RT_{1,0}}} \sqrt{\dfrac{2k}{k-1}} \sqrt{\left(\dfrac{p_{1,st}}{p_{1,0}}\right)^{2/k} - \left(\dfrac{p_{1,st}}{p_{1,0}}\right)^{\frac{k+1}{k}}}}$$

where the ratios $\dfrac{p_{2,st}}{p_{1,st}}$ and $\dfrac{p_{1,st}}{p_{1,0}}$ are equal. (VII-3)

The results of the computer study show, however, that turbine efficiency, for a constant N_s, decreases with pressure ratio. This effect is small at moderate increases in pressure ratio but becomes significant at stage pressure ratios as high as 4.5.

In practice one finds that many factors combine to produce the degraded efficiency at constant specific speed as pressure ratio increases. The major effect, however, is that of reduction of the arc of admission in the first stage. This can be understood if one considers an incompressible fluid in a four stage turbine, for example. In this case the arcs of admission for all four stages are equal. With a compressible fluid, the first stage arc of admission becomes progressively smaller with respect to the other stages, increasing the filling and emptying losses in the first stage, as pressure ratio increases. Even as the total degree of admission is increased, as seen from Table VII-1, efficiency decreases. Because the effect of filling and emptying losses becomes so significant at small arcs of admission, the optimum blade height becomes smaller, resulting in a compromise between degraded efficiency due to reduced nozzle arc length and increased leakage due to increased relative clearances with respect to blade height.

The values given in Table VII-1 are computed at a constant ratio of blade throat width to rotor diameter, a*/D and axial and tip clearance ratios s_1/D, s_2/D, and s_3/D. From Table VII-1, one may see the effect of decreased first stage nozzle arc length and reduced blade height, which combine to increase

Data Common to Both Pressure Ratios

4 Stage Re-Entry Turbine

$k = 1.25$

$K_P = .0014$

$\chi = 0.6$

$s_1/D, s_2/D = .00125$

$s_3/D = .00125$

$N_s = 6.16$

$\alpha_2 = 16°$

$K_D = .003$

$a^*/D = .015$

$\psi_N = 0.96$

Pressure Ratio	40:1	80:1
D_s	4.04	3.84
β_2	23.1°	22.5°
h/D	.0331	.0276
$(c_3/\bar{c}_o)^2$	.078	.084
ψ_R	.8143	.7924
u/c_o	.1620	.1535
α_3	50.6°	46/2°
η_{T-S}	.5361	.4938
A/A^*	1.0604	1.1270
M_2/M_{w2}	1.228/0.849	1.34/0.959
ζ_{SC}	.016	0.15
ζ_D	.002	0.0016
ζ_P	0.0	0.0
a_1/D	0.128	.1019
% admission	83.7	99.5
$t/2a_1$	0.1487	0.1923
$\zeta_{L,tip}$	0.0668	0.0790
$\zeta_{L,rad}$	0.0738	0.0795
$\zeta_{L,tan}$	0.0418	0.0495
$\zeta_{L,dyn}$	0.0424	0.0462

TABLE VII-1

Effect of Pressure Ratio on Turbine Efficiency at Constant Specific Speed

leakage as pressure ratio is increased. Further increases in pressure ratios would result in additional losses when the relative Mach number of the fluid entering rotor, M_{w2}, exceeds unity. It is interesting to note the increase in the ratio of blade pitch to twice the first stage nozzle arc length, $t/2a_1$, as pressure ratio increases. This is the parameter which increases filling and emptying losses.

It is noteworthy that, with increased leakage, one cannot express analytically the function for the optimum ratio of blade height to rotor diameter, h/D, which is necessary in the computer optimization, and is of interest in the effect of pressure ratio on leakage. Baljé (3) and Linhardt (11) obtained approximate relations for h/D by partial differentiation of the expression for total to static efficiency. One finds for large clearance ratios, however, that this requires the solution of a fifth order algebraic equation and that reduction of this equation to a lesser order is not possible by simplifying assumptions. For this reason, the quantity h/D was selected as the optimization variable in the pattern search optimization. Thus the dependence of the blade height on pressure ratio cannot be seen directly.

It should be noted here that the efficiencies presented in Figures VII-3 through VII-6 are based on an equal pressure ratio split between stages. This assumption is based upon the investigation of Linhardt and Silvern (10), (15), which compared the cases of equal pressure ratio and equal isentropic head per stage for a two stage re-entry turbine with an overall

pressure ratio of 300:1. It was shown that over a wide range of specific speeds, equal pressure ratio staging was clearly preferable to equal isentropic heads in each stage. In the upper range of specific speed the advantage was as much as ten efficiency points. This does not imply that the equal pressure ratio split is the best choice in all combinations of number of stages and overall pressure ratio, and it probably is not. It does, however, result in an estimate of achievable turbine efficiency. An advantage of the assumption of equal pressure ratios is the relative ease with which the turbine performance may be evaluated. The equations for equal pressure ratio are themselves quite complicated (see Appendix C). The inclusion of the element of varying stage pressure ratios renders evaluation considerably more difficult, especially when considering a family of turbines over a wide range of specific speeds.

Wong(4), however, used the concept of unequal pressure ratios in each stage, probably to reduce the leakage from the first stage rotor cavity to the second stage and thereby to reduce overall leakage. This may be seen from the leakage equations derived in Appendix C. Leakage from the first stage rotor cavity to the second stage in a turbine with stage pressure ratios greater than the critical is truly determined by the total pressure ahead of the leakage gap and not the interstage pressure ratio, as might be inferred from equation VII-2. Wong's turbine is of considerable interest in that it is the only four stage re-entry found in the literature to have actually been built and tested. The specifications for Wong's turbine are given in Table VII-2.

Number of Stages	4
Rotor tip to tip diameter, D, in	4.125
Blade height, h, in	0.125
Average nozzle angle, α_2	22.14°
Blade angle, β_2	35.0°
Overall pressure ratio	55.56
Design speed, RPM	24,000
Flow rate (air), lb/sec	0.0044
Blade pitch, t, in	0.10
Stage pressure ratios:	
Stage 1	4.332
Stage 2	2.045
Stage 3	2.305
Stage 4	2.726
Inlet conditions,	
Pressure, lbf/in^2	200.0
Temperature, °F	120.0
Tip and axial clearance, in	.0045
N_s	2.66
H_{ad}, ft lbf/lbm	4.52×10^3
Q, ft^3/sec	0.252
Predicted total to static efficiency (Wong)	0.519
Observed total to static efficiency	0.432

TABLE VII-2

Data on a 4 Stage Re-Entry Turbine with Unequal Pressure Ratios

Wong (4)

Using the computer program developed for re-entry turbine analysis and the overall pressure ratio, clearance ratios, and nozzle angle for Wong's turbine, a total to static efficiency of .341 was predicted for a turbine with equal pressure ratios. The observed total to static efficiency of Wong's turbine was 0.432. Several conclusions may be drawn from this analysis. The first is that the computer program, based on the design method of Baljé, Linhardt and Silvern and modified by the leakage equations in Appendix C, is conservative. A possible second conclusion is that a re-entry turbine with unequal pressure ratios may very well be superior to one with equal pressure ratios. Since Reynolds number effects were not included in the equations of reference C, it is concluded that Reynolds number effects in Wong's turbine, for which he allowed in his analysis, were overshadowed by leakage effects. Although Wong showed an appreciation of interstage leakage, it is apparent that he did not consider dynamic leakage and that he was probably unaware, at the time, of the parallel work of Baljé. The small blade height, 0.125" and blade pitch, 0.010", used in Wong's turbine are important in that they show that a turbine with very small blades and blade passages can, in fact, be built and give reasonable efficiencies.

Reynolds Number Effects

The effect of Reynolds numbers on turbine efficiency has been investigated by Baljé (18), Bullock (19), Holeski and Stewart (20) and many others. A rapid deterioration of turbine efficiency occurs with separation from the back of the rotor

blades. Before separation occurs there are increasing viscous losses below some critical Reynolds number, that of the transition from turbulent to laminar flow. The difficulty is to predict the flow conditions at which this will occur. One may use a common method described by Horlock (23) involving loss factors to predict the effect of Reynolds numbers. If one considers that all the losses are Reynolds number dependent, the loss factor, ξ, may be replaced by $1-\eta_{T-S}$.

$$\frac{\xi'}{\xi} = \left(\frac{10^5}{Re'}\right)^{\frac{1}{4}} = \frac{1-\eta'_{T-S}}{1-\eta_{T-S}} \qquad \text{(VII-4)}$$

where the primed values indicate the condition of interest. Here it is implied that at Reynolds numbers above some value, 10^5, based upon the hydraulic diameter of the blade passage and blade inlet relative velocity, viscous losses are constant. The exponent, $\frac{1}{4}$, in equation VII-4 varies, depending upon the investigator (19). Another common value for the exponent is $\frac{1}{5}$.

Baljé based his rotor Reynolds number on blade chord length and relative inlet velocity to the rotor blade and distinguished between rotor and stator losses. He also established a machine Reynolds number based on blade tip speed and tip to tip rotor diameter for correlating Reynolds number effects at various specific speeds and pressure ratios. Baljé found that the critical Reynolds number, based upon chord length, at which the transition from turbulent to laminar flow occurs, varies with specific speed. The critical Reynolds number did fall, however, in the range of 10^5 to 10^6.

Bullock (19) discussed the various attempts at analyzing Reynolds number effects on turbomachinery and noted the wide variance of opinion which exists in predicting Reynolds number losses. Bullock also discusses the causes of the transition from turbulent to laminar flow peculiar to turbomachines. Some of these are the thickness of the trailing edge of the blade, the smoothness of the blade finish, and the existence of time unsteady effects which promote turbulence and delay transition and separation.

Holeski and Stewart (20) studied a large sample of full admission axial flow turbines for Reynolds numbers which varied from 10^4 to 2×10^6. Again the Reynolds number was based on a different characteristic length, in this case blade height. The velocity used by Holeski and Stewart is different from others, in that they used the axial velocity, assuming that the variance in nozzle angles and blade angles is small. Viscosity was based on stage inlet conditions.

$$Re_{\text{Holeski and Stewart}} = \frac{\dot{m}}{\mu r_m} \qquad \text{(VII-5)}$$

where r_m = rotor radius at mean blade height, ft.

Holeski and Stewart attempted many different methods to correlate Reynolds number losses and reported that a plot of stator throat area against loss parameter was most successful. The loss parameter defined by Holeski and Stewart is quite complicated and is given in reference 21. It is evident, however, that Holeski and Stewart's evaluation does not cover the case of off-design performance.

Stewart does, however, give data on the variation of loss factor with Reynolds number. The data for Reynolds numbers in the region of interest for the 50 kw application of this thesis are that of Wong and Nusbaum (22). Wong and Nusbaum evaluated the performance of a full admission turbine using the rotor of the 4-stage re-entry turbine of reference 4. Again a different definition of Reynolds number was used, based on blade height, relative velocity to the rotor and stator blades, and a viscosity based on mean static conditions.

In the interest of comparison of the various reported loss correlations with the data of Wong and Nusbaum, Figure VII-3 was plotted against the loss factor ratio of equation VII-4. Equation VII-4 was also plotted as well as a similar relation with an exponent of $\frac{1}{5}$. It is of interest that in the Reynolds number range from 10^4 to 10^5, (in the notation of Holeski and Stewart), Wong's data consists of three curves. At low Reynolds numbers, Wong and Nusbaum's turbine operated with three distinct operating curves, attributed to varying degrees of boundary layer separation in the rotor. Furthermore, the data for Wong's turbine was based on a blade to jet speed ratio (u/c_2) of .225, far from the normal ratio of about 0.5 for axial impulse turbine. In the lower range of Reynolds numbers, efficiencies at higher ratios of blade to jet speed were significantly poorer.

It is now possible to define a comparable Reynolds number for partial admission using Holeski and Stewart's notation.

$$Re_{\substack{\text{partial}\\ \text{admission}}} = \frac{\dot{m}}{a_m/2\pi\ \mu} \qquad \text{(VII-6)}$$

where a_m = the nozzle arc length of the m^{th} stage.

Here it is noted that Holeski and Stewart's notation, in addition to ignoring the effect of nozzle and blade angle, also omits a constant factor of 2π in the definition of Reynolds number (21).

To base the turbine design of this thesis on the data of Wong and Nusbaum is probably somewhat overoptimistic, primarily because of the degree of reaction on which their data is based. Wong and Nusbaum's data does, however, give an indication of Reynolds number effects in the region of interest for this thesis. It was therefore decided to utilize a compromise of the $\frac{1}{4}$ and $\frac{1}{5}$ power curves with a critical Reynolds number of 1×10^5. With proper design, it is evident from reference 20 that turbine efficiency is not significantly affected above this Reynolds number.

Turbine Design

Using the design curve for Reynolds number from Figure VII-7, and the design curves of Figures VII-3 through VII-6, several 50 kw turbine designs were attempted. The number of possible designs using full admission, partial admission, and re-entry turbines of various pressure ratio and number of stages is very large and not easily subjected to computerized optimization. The thermodynamic studies, discussed in Chapter IV, determined that as high a turbine inlet temperature and

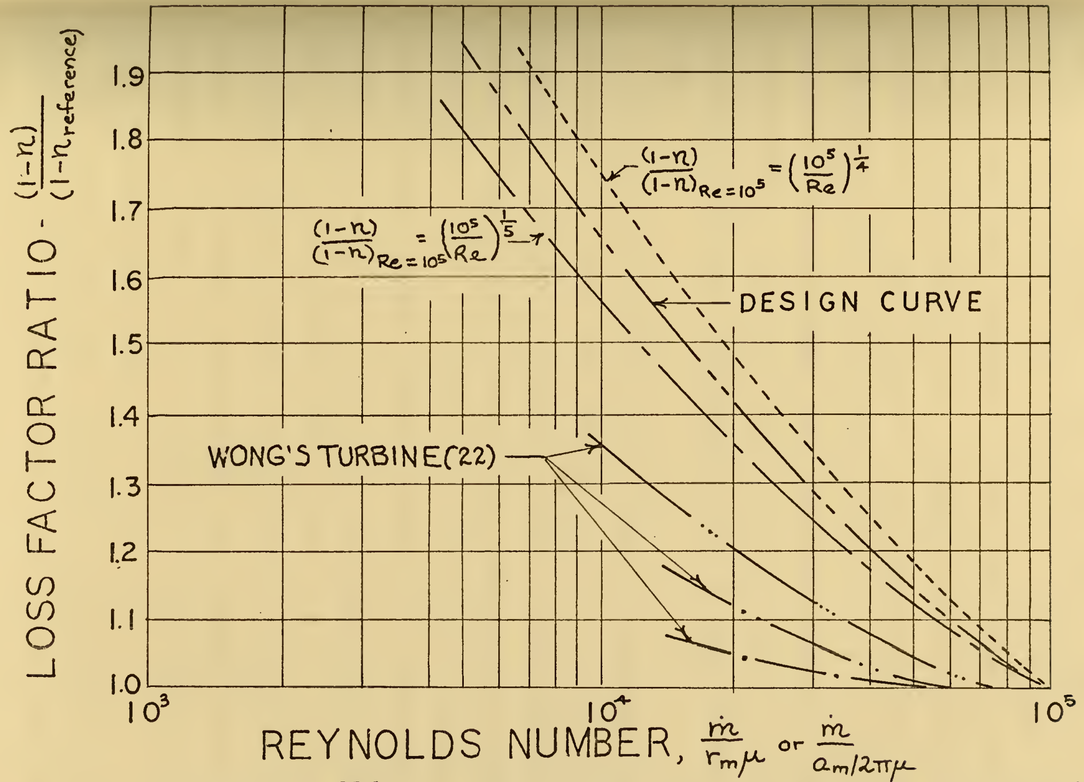

FIGURE VII-7 REYNOLDS NUMBER VERSUS LOSS FACTOR RATIO

pressure as possible would produce the highest overall thermal efficiency. Limitations on the porous plug burner restricted turbine inlet pressure to about 600 lbf/in^2. Based upon studies of available turbine blade materials, a turbine inlet temperature of 1750°F was selected. It was also shown in the thermodynamic studies that as low a condenser pressure as possible would be best. With 1.0 lbf/in^2 as a practical lower limit of condenser pressure, disregarding for the time its effect on condenser size and volume, the turbine exit pressure was established as 1.14 lbf/in^2 allowing for a 0.14 lbf/in^2 pressure drop across a regenerator with an effectiveness of 0.70.

For the design of the 50 kw turbine, a re-entry turbine was selected for the first disk because of the effect on blade stagnation temperature described earlier in this chapter. Two and four stage re-entry turbines were compared at a stage pressure ratio of 1.97,slightly greater than the critical value. The four stage re-entry turbine yielded poor efficiency over a considerable range of the available pressure ratio of the turbine, and for the limiting blade height of 0.10", resulted in a rotative speed in excess of 90,000 RPM. A two stage re-entry turbine was therefore selected for the first disk, at an overall pressure ratio of 3.88, an RPM of 24,000, and a total to static efficiency of 0.364.

The second disk stage also used a stage pressure ratio of 1.97, but because now larger disks could be used, this disk was designed as a 4 stage re-entry turbine. The final disk, a two

stage re-entry turbine, was designed for an overall pressure of 9.05. This higher pressure ratio in the last two stages (third disk) was selected on the basis of a desire to minimize Reynolds number losses in this disk due to the high specific volume of steam at low pressures. As will be shown later, this choice was fortuitous in that it permitted the turbine to operate with all nozzles choked down to power levels below 40% of the design power level. In each of the stages it was assumed that the entire dynamic head was lost in the re-entry ducts and from disk to disk. It was found that a full admission stage or stages in place of the third disk would have to operate at significantly higher rotative speeds and a consequently smaller diameter and blade height to be at all efficient.

An overload nozzle for the 125% design power level was not included in this design but could be easily added. If the turbine should be used with a geared drive, it would be necessary to provide an additional re-entry disk of at least two stages for backing purposes. The windage and blade pumping losses of this disk would detract slightly from the efficiency predicted under ahead operation.

Figure VII-8 is a diagram of the rotor of the proposed turbine, and Table VII-3 lists the detailed characteristics of the 3 disks. The predicted overall turbine efficiency, neglecting bearing losses and labyrinth leakage, for this turbine is slightly greater than 0.73. This value is believed to be conservative, particularly in view of the Reynolds number correlation used.

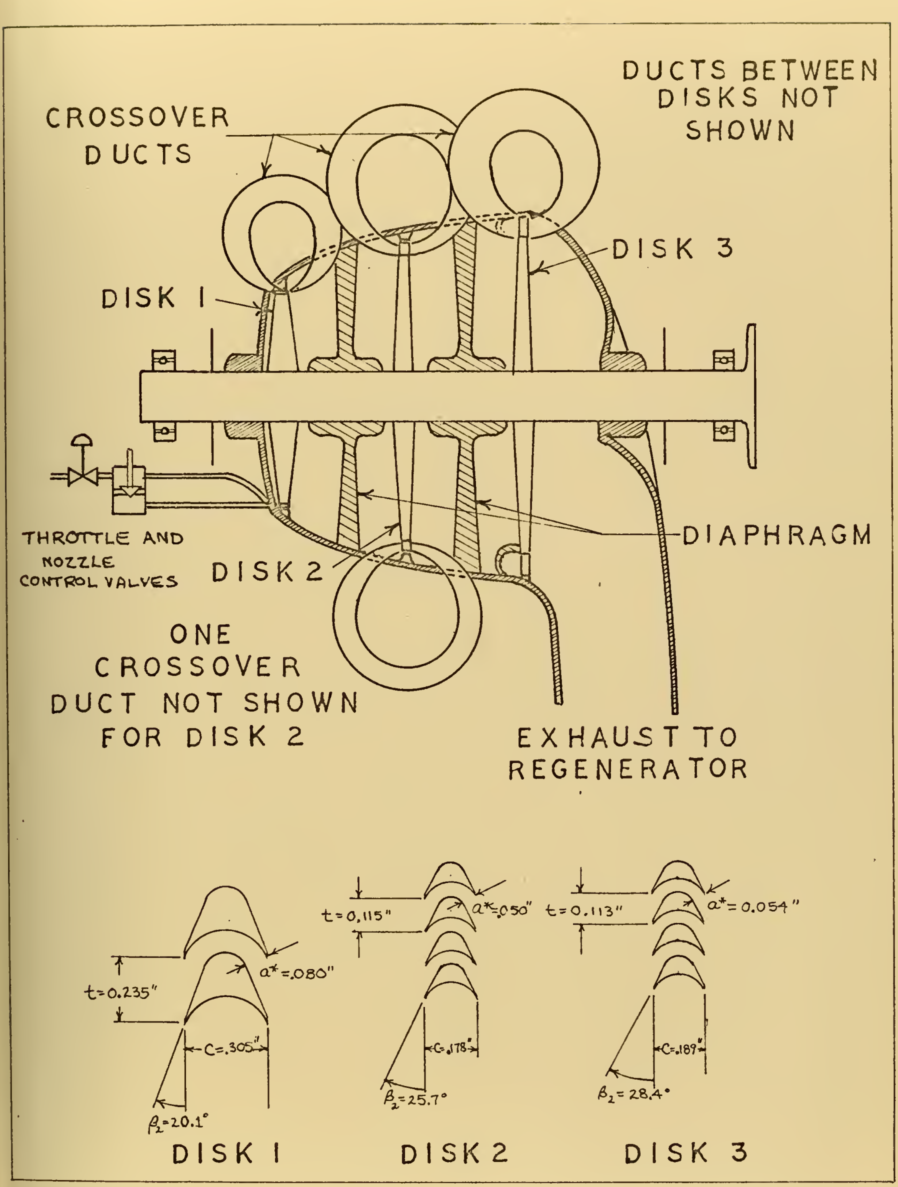

FIGURE VII-8 50 KW TURBINE

Overall Turbine and Cycle Data

Turbine inlet pressure, lbf/in^2	600.	Turbine exit temperature, °F	569.
Turbine inlet temperature, °F	1750.	Regenerator exit temperature (steam)	243.5°F
Turbine exit pressure, lbf/in^2	1.14	Nozzle angle, α_2, (all stages)	16 °
Condenser pressure, lbf/in^2	1.00	Total number of stages	8
Turbine mass flow rate, lbm/hr	297.7	Total number of disks	3
Overall turbine pressure ratio	526.0	RPM (Disk and Blade Material- IN 713LC)	24,000
Overall total to static efficiency (neglecting labyrinth seal and bearing losses)	0.734	Nozzle velocity coefficient, ψ_N	0.96

Actual turbine power developed-kw-53.5 (neglecting bearing and labyrinth seal losses)

Data on Individual Disks	Disk 1	Disk 2	Disk 3
Type of disk	Re-entry	Re-entry	Re-entry
Number of stages	2	4	2
Total pressure ratio, Pr_o	3.88	15.0	9.05
Stage pressure ratio, Pr_i	1.97	1.97	3.02
Rotor diameter (tip to tip), D, in	5.375	8.97	10.75
Blade height, h, in	0.104	0.250	0.625
Axial clearance, s_1/s_2, in	.00672/.00672	.0045/.0045	.0054/.0054
Tip clearance, s_3, in	.00672	.0045	.0054
Stage admission, %	3.93/7.34	3.57/6.39/11.47/20.57	15.5/39.2
Total admission, %	11.27	42.00	54.7
Rotor blade pitch, t, in	0.235	0.115	0.189
Rotor blade chord length, C, in	0.305	0.178	0.189
Rotor blade angle, β_2	20.1°	25.7°	28.4°
Stage Reynolds number, $\frac{2\pi\dot{m}}{a_m\mu}$ (after Holeski and Stewart)	$3.3\times10^5/1.8\times10^5$	$2.4\times10^5/1.4\times10^5/$ $8.8\times10^4/5.3\times10^4$	$6.2\times10^4/4.0\times10^4$
M_2/M_{w2}	1.035/0.882	1.035/0.652	1.345/0.774
Nozzle area ratio, A/A*	1.005	1.005	1.127
Length of first stage arc of admission, a_1, in	0.762	1.04	5.29
η_{T-S}	.364	.654	0.764
Maximum blade stress, lbf/in^2	1,290.	5,250	15,300
Maximum disk stress, (tapered disk) lbf/in^2	10,000	24,000	33,400

TABLE VII-3

50 kw, 3 Disk - 8 - Stage Re-Entry Turbine

The design of the turbine casing and crossover (re-entry) ducts was not attempted in this thesis and will require some innovation. The re-entry ducts should be as small as possible to reduce casing weight and size, yet a desire to recover the leaving loss from a previous stage would suggest large ducts. Clearly, some compromise solution considering these tradeoffs and the three disk geometry must be reached. In the estimation of turbine weight and volume, a conservative estimate of casing weight and size has been used.

The 500 kw turbine was designed in much the same manner as the 50 kw turbine. In the case of the 500 kw turbine, however, a four stage re-entry turbine could be used on the first disk. The same rotative speed, 24,000 RPM was selected in order to keep the size of the machine small and because of its compatibility with a 400 hertz, 2-pole alternator. It is of interest that aside from having one additional disk, the 500 kw turbine size is nearly identical to that of the 50 kw turbine. The second disk is a two stage re-entry turbine and the third and fourth disks are full admission disks. Dynamic head between all stages, including full admission stages, was considered lost. The overall predicted turbine efficiency was 84.3%, neglecting diaphragm labyrinth seal and bearing losses. It is estimated that a 1 kw bearing loss for this machine and a .66 kw bearing loss for the 50 kw machine is reasonable for two combined thrust-radial ball bearings based on reference 8. It must be shown, however, that such bearings are capable of maintaining the small axial clearances required by this machine.

Figures VII-9 and Table VII-4 give a detailed description of the 500 kw turbine. A regenerator was not utilized with the 500 kw turbine, since its high turbine efficiency results in a reasonably low turbine exit temperature. Estimates of weight and volume and dimensions for both the 50 and 500 kw turbine are given in Table VII-5.

The small blade throat widths associated with the re-entry portions of the turbines are a consequence of the optimum blade angle and improved performance gained from maximizing the number of blades. This reduces the filling and emptying losses of Stenning (17), common to all partial admission turbines. While these throat widths are quite small, Wong's turbine (4) is an indication that they can be fabricated. The small blade and blade passages will require very close attention to such items as trailing edge thickness and surface finish. The disks have been designed with a central hole and would be keyed to the shaft. A taper of 2:1 from hub to disk periphery has been assumed in the disk stress calculations. Blade and disk stresses are well within the present state-of-the-art of high temperature alloys. The blades and disk would be manufactured from a single casting. Electrochemical machining methods would probably be best for forming the blades. Critical speed calculations were not performed on either turbine. Rather, a shaft size of approximately 1.5" was assumed for disk stress calculations and bearing loss approximations.

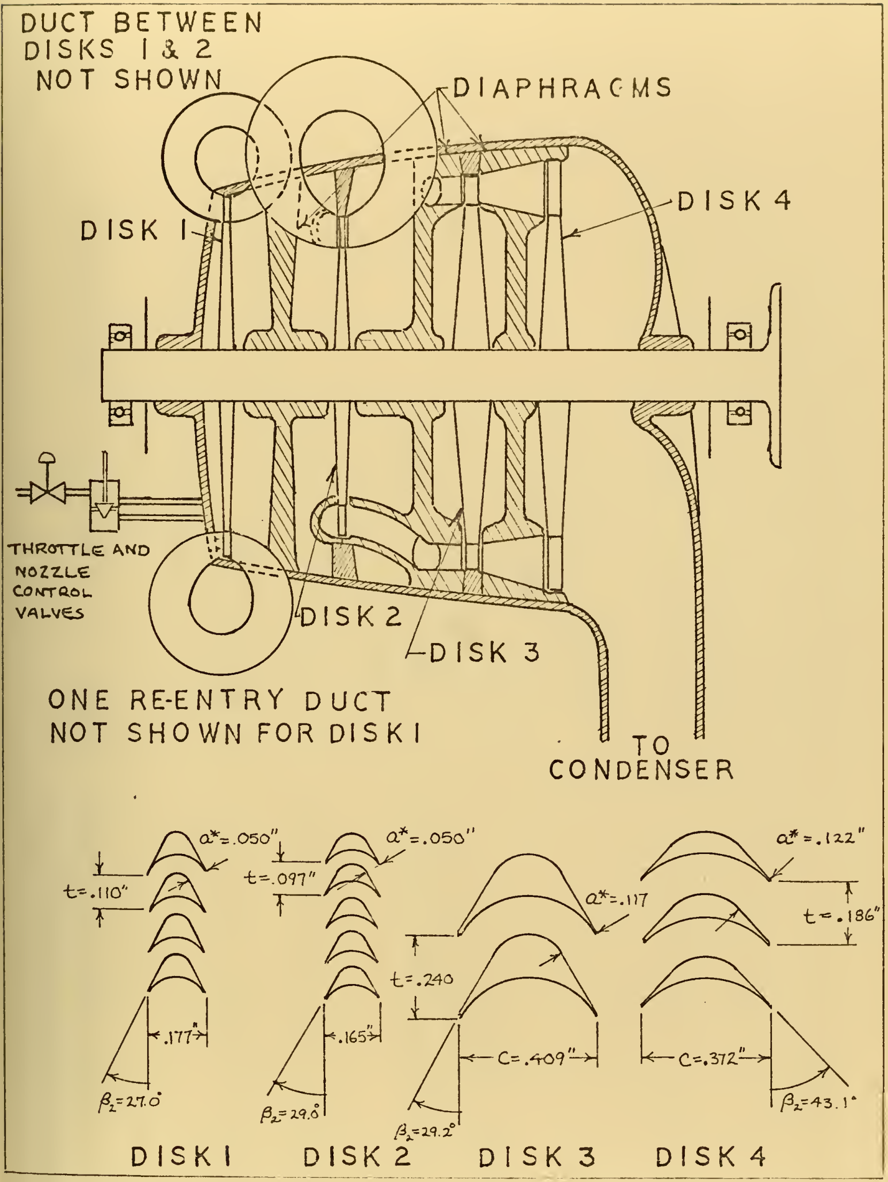

FIGURE VII-9 500 KW TURBINE

Overall Turbine and Cycle Data

Turbine inlet pressure, lbf/in^2	600.	Turbine exit temperature, °F	360.
Turbine inlet temperature, °F	1750.	Total number of disks	4
Turbine exit pressure, lbf/in^2	1.0	Total number of stages	8
Condenser pressure, lbf/in^2	1.0	RPM	24,000
Turbine mass flow rate lbm/hr	2550.	Actual turbine power developed (neglecting bearing and labyrinth seal losses)	535.0
Overall turbine pressure ratio	600.		
No regenerator		Disk and blade material	IN713LC
Overall total to static efficiency (neglecting labyrinth seal and bearing losses)	.843		

Data on Individual Disks	Disk 1	Disk 2	Disk 3	Disk 4
Type of Disk	Re-entry	Re-entry	Full	Full
Number of stages	4	2	1	1
Total pressure ratio, Pr_o	15.0	3.88	3.02	3.42
Stage pressure ratio, Pr_i	1.97	1.97	3.02	3.42
Rotor diameter (tip to tip), D, in	9.95	9.41	11.70	12.7
Blade height, h, in	.386	.888	.775	1.66
Axial clearance, s_1/s_2	.005/.005	.0047/.0047	--	--
Tip clearance, s_3	.005	.0047	--	--
Stage admission %	4.97 8.87 15.81 28.19	25.16 47.11	100.	100.
Total admission %	57.84	72.27	100.	100.
Rotor blade pitch, t, in	.110	.097	.240	.186
Rotor blade chord length, C, in	.177	0.165	.409	.372
Rotor blade angle, β_2	27.0°	29.0°	29.2°	43.1°
Nozzle angle, α_2	16.0°	16.0°	16.1°	23.4°
Stage Reynolds number $\frac{2\pi\dot{m}}{a_m\mu}$ or $\frac{\dot{m}}{r_m\mu}$ (after Holeski and Stewart)	$1.2x10^6$ $7.2x10^5$ $4.4x10^5$ $2.6x10^5$	$3.8x10^5$ $2.3x10^5$	$1.0x10^5$	$1.4x10^5$
M_2/M_{w2}	1.035/.625	1.035/.616	1.345/.800	1.43/.825
Nozzle area ratio	1.005	1.005	1.127	1.20
Length of first stage arc of admission, in	1.56	7.43	--	--
η_{T-S}	.723	.804	.805	.725
Maximum blade stress, lbf/in^2	8,800	17,750	20,000	41,900
Maximum disk stress (tapered disk), lbf/in^2	31,400	23,200	23,600	29,600

TABLE VII-4

500 kw - 4 Disk Turbine

<u>50 kw turbine</u>	
Casing diameter without return ducts, in	12.0
Maximum diameter, in	18.0
Overall length, in	18.0
Casing length, in	13.0
Turbine weight, lbm	105.0
Foundation weight, lbm	30.0
Total weight, lbm	135.0
Volume, ft^3	1.8
<u>500 kw turbine</u>	
Casing diameter without return ducts, in	14.0
Maximum diameter, in	20.0
Overall length, in	20.0
Casing length, in	15.0
Turbine weight, lbm	186.5
Foundation weight, lbm	37.0
Total weight, lbm	223.5
Volume, ft^3	2.0

TABLE VII-5

Turbine Weight, Volume and Dimensions

Control, Method of Operation and Off-design Performance

With the small length of the arcs of admission of the first stage of the first disk in both the 50 and 500 kw turbines, throttle control with perhaps a single nozzle control valve seems the best method of speed regulation. The nozzle control valve would be sized to close off a portion of the arc of admission at the cruise condition, in this case assumed to be 40% of design power. In both the 50 and 500 kw turbine, sufficient unadmitted arc exists in the first disk for the inclusion of an overload nozzle to achieve the 1.25% design power specification.

Both constant speed and propeller load off-design characteristics have been considered. The constant speed application would require an electrical transmission system and a turbine governor for speed regulation. The propeller load application would require a suitable geared transmission for speed reduction to propeller RPM.

The off-design study was conducted only at 41% of the design power level and for the 50 kw turbine. At this point, a 41% power throttled condition and a condition with the single nozzle control valve being fully shut and the throttle valve fully open were considered. The results are shown in Figure VII-10. The propeller load curves were estimated from the constant speed curves modified by data on propeller load turbine characteristics at optimum nozzle openings (24).

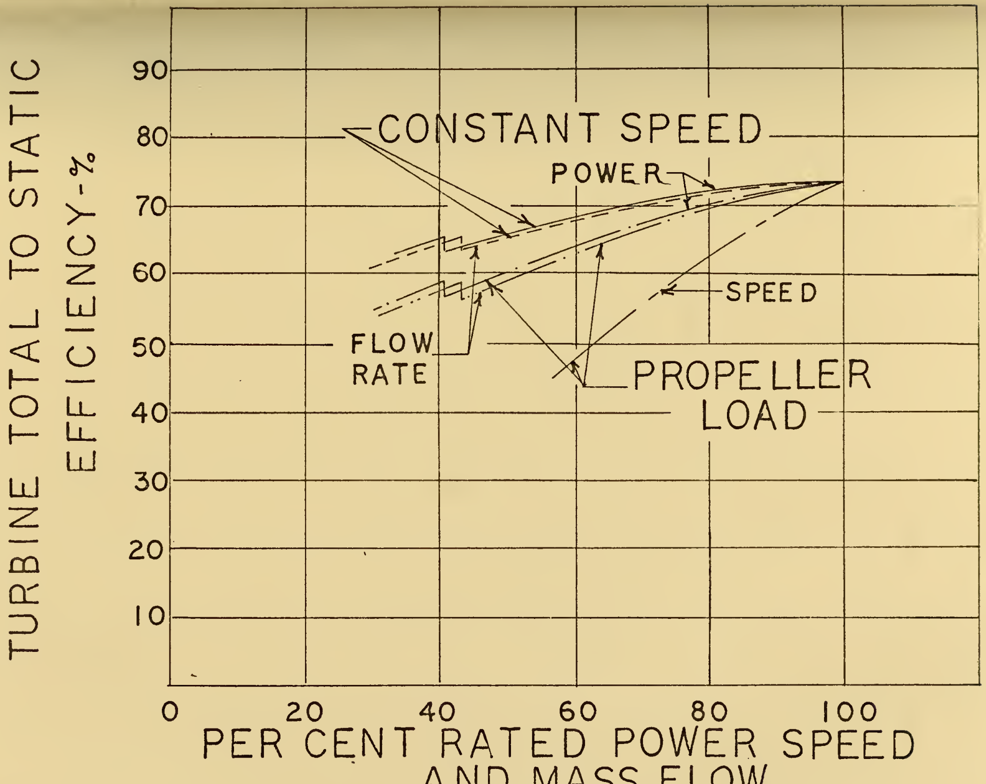

FIGURE VII-10

In the calculation of off-design performance it was noted that the last stage nozzle was still choked at the 41% power condition, which implies that all nozzles remained choked. Data from Lee (25) were used to estimate losses due to under and over expanded nozzles. In the 41% power nozzle condition, the reduction of the length of the arc of admission in the first stage negated, to a great extent, gains made by the elimination of throttling. At lower power levels, Reynolds number losses were also found to increase in importance. A graph of stage exit pressure for the design condition, the 41% power throttled condition, and the 41% power condition with the single nozzle control valve fully shut and throttle valve fully open are shown in Figure VII-11.

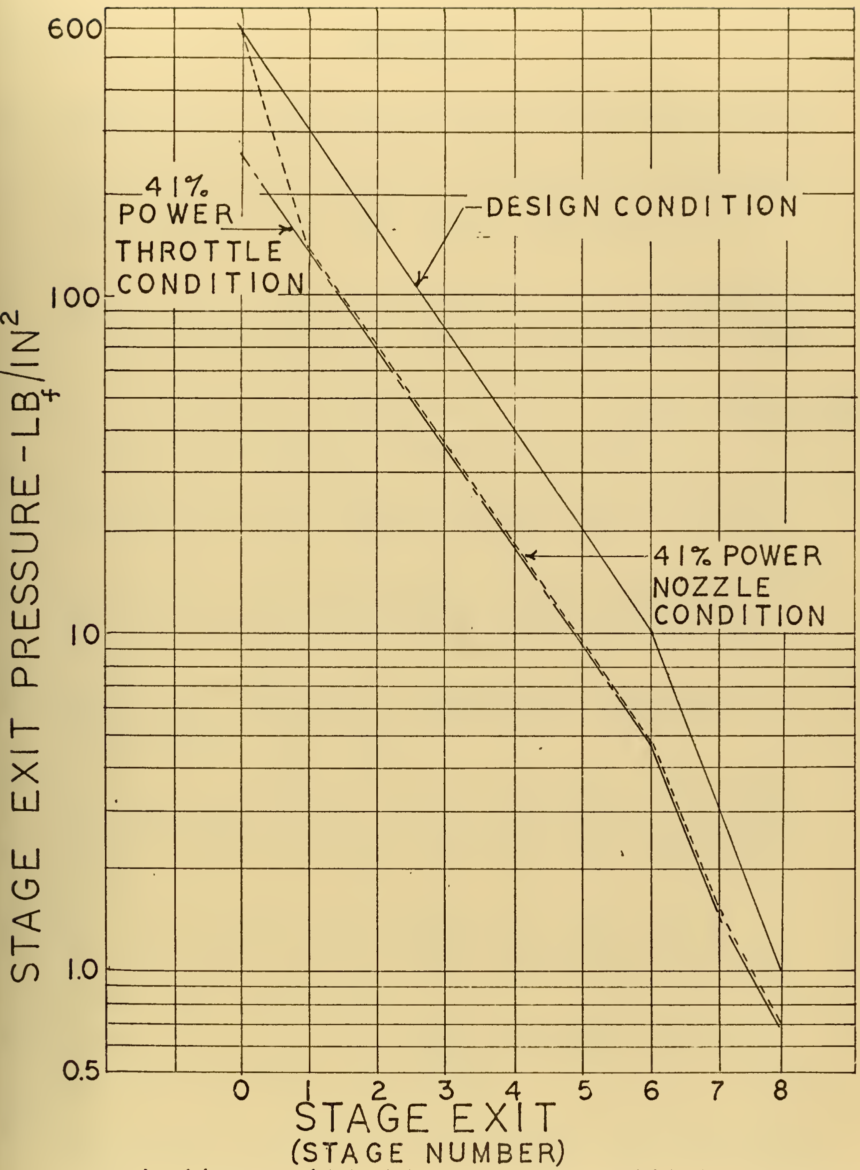

FIGURE VII-11 STAGE EXIT PRESSURE FOR 3 OPERATING CONDITIONS

REFERENCES

1. Syniuta, W.D., Steam Engine Systems Corporation, personal communication, March, 1972.

2. Morgan, N.E. and W.D. Morath, *Development of a Hydrogen-Oxygen Internal Combustion Engine Space Power System*, Vickers Corporation, NASA CR-255, Washington, D.C., July, 1965.

3. Baljé, O.E., "A Study on Design Criteria and Matching of Turbomachines, "Part A-Similarity Relations and Design Criteria of Turbines", *Journal of Engineering for Power*, Vol. 84, No. 1, January ,1962, pp 83-102.

4. Wong, R.Y. and D.L. Darmstadt, and D.E. Monroe, *Investigation of a 4.0 Inch Mean Diameter Four Stage Re-entry Turbine for Auxiliary Power Drives*, NASA TMX-152, 1960.

5. Dunn, J.H., Final Report, *1200-HZ Brayton Electrical Research Components*, AiResearch Manufacturing Company of Arizona, NASA CR-72564, March 19, 1969.

6. Richter, E., "New Developments in Very High Speed Electrical Alternators", paper 719019, *Proceedings of the 1971 Intersociety Energy Conversion Engineering Conference*, August 1971, pp 132-139.

7. Syniuta, W.D. Department of Mechanical Engineering, Massachusetts Institute of Technology, personal communication, April 1971.

8. Heath, B.B., and R.A. Luther, *Final Report, The Design and Fabrication of the Brayton Rotating Unit Operating on Roller Element Bearings (BRU-R)*, AiResearch Manufacturing Company of Arizona, NASA-CR 72642, September, 1969.

9. Dunn, J.H., "Post Test Inspection of Three Brayton Rotating Units", Paper 719030, *Proceedings of the 1971 Intersociety Energy Conversion Engineering Conference*, August, 1971, pp 220-238.

10. Linhardt, H.D. and D.H. Silvern, "Analysis of Partial Admission Axial Impulse Turbines", *ARS Journal*, Vol. 31, No. 3 (March, 1961), pp 297-308.

11. Linhardt, H.D., "Re-Entry Turbines for Space Power Systems", *ARS Journal*, Vol. 32, No. 10, (October, 1962), pp 1552-1559.

12. Baljé, O.E. and R.L. Binsley, "Axial Turbine Performance Evaluation Part B-Optimization with and without Constraints", *Journal of Engineering for Power*, October 1968, pp 349-360.

13. Hooke, R. and T.A. Jeeves, "Direct Search Solution of Numerical and Statistical Problems", *Association of Computing Machinery Journal*, Vol. 8, No. 2, (April, 1961), pp 212-219.

14. Baljé, O.E., personal communication, March 8, 1972.

15. Linhardt, H.D., *Study of Turbine and Turbo Pump Design Parameters, Final Report Volume I, A Study of High Pressure Ratio Re-entry Turbines*, Sunstrand Turbo Report S/TD No. 1735, Department of the Navy, Office of Naval Research, Contract No. NONR-2292(00), Task No. NR094-343, 30 June 1960, (AD232635).

16. Baljé, O.E., *A Study of High Energy Level, Low Power Output Turbines*, Sunstrand Turbo Report AMF/TD No. 1196, Department of the Navy, Office of Naval Research, Contract No. NONR-2292 (00), Task No. NR (094-343), 9 April 1958, (AD161323).

17. Stenning, A.H., *Design of Turbines for High Energy Fuel-Low Power Output Applications*, Massachusetts Institute of Technology Dynamic Analysis and Control Laboratory Report No. 79, September 30, 1953.

18. Baljé, O.E., "A Study on Reynolds Number Effects in Turbomachines", *Journal of Engineering for Power*, July 1964, pp 227-235.

19. Bullock, R.O., "Analysis of Reynolds Number and Scale Effects on Performance of Turbomachinery", *Journal of Engineering for Power*, July 1964, pp 247-256.

20. Holeski, D.E. and W.L. Stewart, "Study of NASA and NACA Single-Stage Axial Flow Turbine Performance as Related to Reynolds Number and Geometry", *Journal of Engineering for Power*, July 1964, pp 296-298.

21. Stewart, W.L., "A Study of Axial-Flow Turbine Efficiency Characteristics in Terms of Velocity Diagram Parameters", ASME Paper No. 61-WA-37, presented at the ASME Winter Annual Meeting, New York, N.Y., Nov. 26-Dec. 1, 1961.

22. Wong, R.Y. and W.J. Nusbaum, *Air-Performance Evaluation of a 4.0 Inch Mean Diameter Single-Stage Turbine at Various Inlet Pressures from 0.14 to 1.88 Atmospheres and Corresponding Reynolds Numbers from 2500 to 50,000*, NASA TN D-1315, Washington, D.C., August, 1962.

23. Horlock, J.H., *Axial Flow Turbines*, London, Butterworths, 1966.

24. Carmichael, A.D., Department of Ocean Engineering, Massachusetts Institute of Technology, personal communication, April 1972.

25. Lee, J.F., *Theory and Design of Steam and Gas Turbines*, New York, McGraw Hill Book Company, 1954.

LIST OF SYMBOLS

a - nozzle arc length

a^* - blade throat width

A/A^* - nozzle area ratio

c - absolute velocity

c_2 - absolute velocity leaving the stator

c_3 - absolute velocity leaving the rotor

c_o - spouting velocity, $\sqrt{2g_c\ H_{ad}}$

C - blade chord length

D - rotor tip to tip diameter, ft or in

D_s - specific diameter- $\dfrac{D\ H_{ad}^{\frac{1}{4}}}{\sqrt{Q}}$

g_c - conversion factor 32.2 ft lbm/lbf sec^2

H_{ad} - isentropic head, ft lbf/lbm

k - ratio of specific heats, assumed to be 1.25 for steam

K_D - disk friction coefficient

K_p - blade pumping loss coefficient

M - Mach number of fluid leaving the stator

M_{w2} - relative approach Mach number of fluid entering the rotor blade

$\dot{m}$ - mass flow rate, lbm/hr

N - RPM

N_s - specific speed (Baljé) $N\sqrt{Q}/H_{ad}^{\frac{3}{4}}$

p - pressure, lbf/in^2 or lbf/ft^2

Pr - pressure ratio

Q_3 - exit volumetric flow rate from a disk, ft^3/sec

Re - Reynolds number

r_m - mean rotor blade radius

s_1 - axial clearance upstream at the rotor

s_2 - axial clearance downstream of the rotor

s_3 - tip clearance

t - blade pitch

α_2 - nozzle angle measured from the tangential direction, °

β_2 - blade angle measured from the tangential direction, °

ζ_L - leakage factor

η_{T-S} - Total to static turbine efficiency

μ - dynamic viscosity, lbm/hr ft

ξ - loss factor

χ - blade density factor

ψ - velocity coefficient

SUBSCRIPTS

dyn - refers to dynamic leakage

i - refers to stage conditions

L - refers to leakage

m - refers to a general stage of a multistage re-entry turbine

N - refers to nozzle

O - refers to total conditions

rad - refers to radial leakage

SC - refers to scavenging losses

st - refers to static conditions

tan - refers to tangential leakage

tip - refers to tip leakage

CHAPTER VIII

Auxiliary/Emergency Power and Transmission System

The auxiliary/emergency power systems and the transmission system for a deep submersible power system are closely interrelated. While it is not the intention in this thesis to optimize such a system, the selection of a satisfactory system is necessary to prove feasibility of the propulsion plant. Such a transmission system must meet acceptable standards of reliability, efficiency, weight and volume.

The geared transmission and shaft seal, from the aspect of high efficiency, appears to be very promising despite the lower turbine efficiency of propeller load turbine operation compared with constant RPM turbine operation. For example, consider a 240 RPM propeller speed, which would entail a reduction of 100:1 in speed from a design turbine speed of 24,000 RPM. According to reference 1, a spur gear set with this reduction ratio would exhibit about 94% transmission efficiency. This figure would probably be somewhat reduced by the high rotational speed of the high speed pinion. If one assumes a 90% transmission efficiency for such a spur gear set for the 24,000 RPM application and neglects, for the moment, thrust bearing and sealing losses, a combined turbine/transmission efficiency of 66.1% is predicted for a 50 kw (turbine shaft) plant at design power. At the 50% design power level, this would result in a combined turbine/transmission efficiency of 53.5%. The propulsor efficiency here has not been considered.

Electrical transmission systems are penalized in power losses in the generator, the speed regulation device and the motor. Typical electrical transmission efficiencies for a 50 kw generator power supply are presented in Table VIII-1 (2) and compared with a possible reduction gear drive. The geared drive does not include thrust bearing or shaft seal losses.

The selection of a transmission system is not quite so simple as the results of Table VIII-1 would suggest. The reduction gear system, while seemingly attractive, incurs many penalties, the least of which are seal leakage and required pumping power to control it. Consider, for example, a 1 ½" shaft penetration at a 20,000 foot depth. The thrust load in such a penetration would be about 16,000 lbf. For the 8,000 foot depth, a penetration of the same size would result in a thrust load of about 6,300 lbf. A Kingsbury thrust bearing to carry this load would have a diameter of about 1 foot at the 20,000 foot depth and eight inches at the 8,000 foot depth. Considerable structural support would have to be supplied at the thrust bearing, increasing overall weight. Additional structural weight would also be necessary at the shaft penetration. Practically, the shaft should be as small as possible to reduce the thrust and buckling load and still support the torque. A proper evaluation of such a system would require determination of shaft length, diameter, torque and buckling load to minimize the thrust load. Shaft seals have not yet been developed for either the 8,000 foot depth or the 20,000 foot depth. While a shaft seal may be possible at the 8,000

System	Transmission System Efficiency 100% power/50% power	Combined Turbine and Transmission System Efficiency (50 kw plant)[3]
AC Hydraulic Propulsion[5] AC generator (3ϕ, 400-hertz, 16-24 pole AC submersible induction motors; hydraulic pumps and motors)	63.9/57.3[1]	46.9/37.8
AC Inverter Controller System[5] (AC generator, rectifier, inverter controller, AC submersible induction motor and speed reducer)	57.3/52.6[1]	42.1/34.6
AC Cycloconverter System[5] (AC generator, cycloconverter, AC submersible induction motor and speed reducer)	60.1/55.4[1]	44.1/29.1
Spur Type Reduction Gear with Shaft Seal	90/90[2]	66.1/53/5

[1] assumed generator efficiency - 94%

[2] neglects thrust bearing and sealing losses

[3] turbine efficiencies from Chapter VII

[4] electrical system data from reference 2

[5] data from reference 2

TABLE VIII-1

Survey of Transmission Systems

foot depth, it is doubtful that one can be designed for 20,000 feet with an acceptable leakage.

Another problem associated with shaft sealing is the flexing of the hull of the propulsion plant pressure vessel under compression and its effect on misalignment of the reduction gear. A second, somewhat less serious problem is the difficulty of internal arrangement posed by a relatively large condenser, a turbine, and a reduction gear and thrust bearing.

Another major problem associated with the reduction gear transmission is the need to supply auxiliary electrical power. If the turbine does not operate at constant speed, some other power conversion device must be provided for electrical power. Possible candidates are batteries, fuel cells, or a small turbine. In addition to added weight and volume, this would increase system complexity considerably. Table VIII-2 gives a summary of auxiliary electrical loads.

A significant and perhaps crucial disadvantage of the geared transmission system is the need for more than one propulsion device for the typical deep submersible. To meet the needs of hovering, reasonably exact positioning and manuverability, there is a requirement for more than one propulsor. It is here that the electrical transmission system is most versatile.

The case of the reduction gear transmission system has not been studied in detail. It is apparent, however, that associated with it are technological problems which are considerably beyond the state-of-the-art. At the 8,000 foot depth, the

Loads Propulsion Plant Related Loads	Rated Power of Equipment (kw)	Operating Load Factor	Corrected Load (kw)	Total kwh for a 41.7 hour mission (kwh)
a. Condensate/Feed Pump (variable speed)	.55	0.481	0.264	11.01
b. Salt water circulating pump	3.20	1.0	3.2	133.0
c. Vacuum pumps (2)	1.35	0.5	0.625	26.0
d. Auxiliary cooling water pump	0.20	1.0	0.20	8.3
e. Non-condensables compressor	0.20	1.0	0.20	8.3
f. H_2-O_2 detection equipment	0.075	1.0	0.075	3.1
g. Reactant Supply Pumps	1.14	0.481	0.548	22.8
h. Propulsion Plant/Reactant Supply Controls (allowance)	0.50	1.0	0.50	20.8
Subtotal	7.215		5.412	233.3[2]
Manned Sphere Power Requirements[1]	2.74	.89	2.44	101.5
External Auxiliary Equipment[1]	9.78	.32	3.28	136.5
Propulsion Motors (2)	44.70			762.0
Total	64.435			1233.3

[1] Reference 4

[2] Parasitic loads - not counted against 1000 kwh mission

TABLE VIII-2

Auxiliary Electrical Loads for a Nominal 50 kw-1000 kwh Plant

problems for a 50 kw plant could probably be overcome but limits on shaft size may rule out higher power levels. At the 20,000 foot depth, the use of such a transmission system is considered very unlikely. For this reason, an electrical transmission system has been selected for purposes of this thesis.

Electrical Transmission

At the high rotational speeds compatible with the turbine, solid rotor, brushless AC generators are the most likely candidates. Two such generators are the Lundell-Rice alternator and the homopolar inductor alternator.

The Lundell-Rice alternator has been proposed for use with the Brayton cycle for a 50 kw submersible power plant (3) with an efficiency of 94% (neglecting bearing losses) at a rotational speed of 24,000 RPM. Homopolar alternators have been built at rated speeds of 93,000 RPM and 10 kw power output (5). A description of a 4-pole, 400 hertz- 12 kw homopolar alternator operating at 12,000 RPM is given by Corcoran (6). The measured efficiency of this machine was 91.7%, neglecting bearing losses. It appears that the efficiencies, weights and volumes and associated electrical components (voltage regulator and exciter) for the two types of machines are comparable.

The Lundell-Rice rotor has been tested for windage losses (7) with rotors as large as 12" in diameter for 24,000 RPM. This rotor is about the size required for a 500 kw alternator. Thus the Rice alternator may be used at a rotational speed of 24,000 RPM for all rated power levels from 50-500 kw. The rotor diameter (6") for a 50 kw machine is given by Balukjian

and Rackley (3). The characteristics of the generator and its voltage regulator and exciter system are discussed by Corcoran (6) and given in detail by Dunn (8). Table VIII-3 gives estimated weights and volumes of two such alternators, rated at 50 and 500 kw. The use of hydrogen in the high speed alternators may reduce the windage losses and slightly improve the estimated efficiency of 94%.

The problems which have been encountered with the components of the electrical transmission systems listed in Table VIII-1 are discussed by Bloomquist (9). Based upon the experience of the Naval Ship Research and Development Laboratory, one would conclude that AC submerged motors and encapsulated power conversion systems would be the best approach at present. It is apparent that placement of inverters and other such power conditioning equipment in the sea water environment will require a considerable development effort before reliable equipment becomes available.

While the results of Table VIII-1 indicate that the AC hydraulic propulsion system is the best choice with respect to efficiency, it is apparent that the AC cycloconverter system is also very promising. The AC cycloconverter system is slightly lighter but dynamic braking would be required for this system while it would not be necessary for the electric-hydraulic system. The AC hydraulic submersible system operates at constant voltage and therefore achieves relatively good off-design performance.

	Alternator Power Level	
	50 kw	500 kw
Lundell-Rice Alternator[1]		
Rotor diameter, in	6	12
Machine diameter (frame), in	12.7	24
Machine frame length, in	12.7	12
Shaft diameter, in	1.5	2.0
Estimated volume, ft^3	0.93	3.10
Estimated weight, including foundations	230.0	720.00
Voltage Regulator-Exciter and Speed Regulator		
Weight and space allowance lbm/ft^3	20/0.5	60/1.5
Inverters, Rectifiers and Startup/Emergency Batteries		
DC-AC inverters (2), (Mounted internally) power rating kw	5	50
volume (est)	0.3	2.0
weight (est)	10	67
Startup/emergency batteries (AgZn), kwh	5	50
Weight (in air @ 47 wh/lbm)[2], lbm	106	530
Volume (@ 3.5 wh/cu in)[3], ft^3	0.83	8.3
Power conditioning equipment weight and volume allowance, lbm/ft^3	10/.5	30/1.5

[1] Weights and Volumes estimated from drawing in reference 12 and reference 7.

[2] Reference 13.

[3] Estimated from reference 14.

TABLE VIII-3

Alternator and Related Components and Extraneous Electrical Equipment

The cycloconverter system is discussed by Thomas (10) and Barnes (11). The primary advantage of the cycloconverter system is the significantly improved off-design performance of frequency control of induction motor speed over voltage control. With the assumed power profile of a 40% design power level for nearly 85% of the total mission duration, the cycloconverter appears to be an interesting and promising alternative to conventional AC induction motor speed control.

Koegel (15) reports that a cycloconverter system has been used with a 10 KVA Lundell-Rice generator operating at 100,000 RPM with frequency reduction to 400 hertz. The application is a portable power supply for the U. S. Army driven by a gas turbine. The equipment was supplied by Lear-Siegler and General Electric. It is apparent, however, that little development work has been performed in the application of cycloconverters to propulsion systems for deep submersibles.

The two systems, AC hydraulic and AC cycloconverter, cannot be adequately compared without an in-depth study involving cost, present and potential availability for deep submergence applications, weight and volume, and reliability. Such a study is beyond the scope of this thesis.

The AC submersible hydraulic system was selected because of its current availability and high efficiency. The slight weight advantage of the cycloconverter system (about 50 lbm) is considered insignificant. The AC submersible hydraulic system is listed in Table VIII-4. It includes two 400-hertz AC submerged induction motors and hydraulic pumps and motors,

Equipment	Wt (lbm)	Efficiency 100% power/50% power
Submersible Motors (2-30 HP) 16-24 poles 3ϕ, 400-hz	800	.90/.83
Hydraulic Pumps (8)	135	.88/.86
Hydraulic Motors 2-15 HP 6-10 HP	135	.86/.86
Total	1250	.68/.61

Data from reference 2

TABLE VIII-4

AC Propulsion Transmission System

which would be coupled to the propulsor(s).

Other power equipment may be necessary to provide specialized power to various vehicle equipment. Startup and emergency batteries, located outside the pressure hull, will require inhull inverters for conversion of DC to AC power.

REFERENCES

1. Dudley, D.W., ed., *Gear Handbook*, New York, McGraw Hill Book Company, 1962.

2. *Study Program Final Report, Brayton Cycle Thermo-Chemical Dynamic Power Supply for Deep-Submersible Vehicles*, NavShips No. 0907-000-6010, August 7, 1970.

3. Balukjian, H. and R. Rackley, "A Closed Brayton Cycle Power System for Deep Submersible Vehicles", *Journal of Hydronautics*, Vol. 5, No. 1, pp 5-10.

4. Deep Ocean Technology Testbed Submersible Vehicle, Conceptual Design and Engineering Data, Westinghouse Ocean Research and Engineering Center, Annapolis, Md., January, 1968.

5. Richter, E., "New Developments in Very High Speed Electrical Alternators", paper No. 719019, *Proceedings of the 1971 Intersociety Energy Conversion Engineering Conference*, pp 132-139.

6. Corcoran, C.S., "Development of Electrical Components for a 400-Hertz Brayton Cycle Energy Conversion System", *Advances in Energy Conversion in Engineering*, Intersociety Energy Conversion Engineering Conference, 1967, pp 943-950.

7. Gorland, S.H. and E.E. Kempke, Jr., "Experimental Windage Studies for High Speed Alternators", Paper No. 719056, *Proceedings of the 1971 Intersociety Energy Conversion Engineering Conference*, pp 387-393.

8. Dunn, J.H., *Final Report, 1200-HZ Brayton Cycle Electrical Research Components*, NASA CR-72564, March 19, 1969.

9. Bloomquist, D.L., "Experience with Electric Drive Systems for Deep Submergence", Paper presented at the 1971 Intersociety Energy Conversion Engineering Conference (not included in conference proceedings), August 3-6, 1971.

10. Thomas, L.R., "Designing Propulsion Motors for Undersea Craft", *Under Sea Technology*, Vol. 9, No. 2, February 1968.

11. Barnes, E.C., "Performance and Characteristics of Induction Motors for Solid State Variable Frequency Drives", *IEEE Transactions on Industry and General Applications*, Vol. IGA-7, No. 2, (March/April 1971) pp 212-217.

12. Balukjian, H., "A Closed Brayton Cycle Power Plant for Underwater Applications and Comparison with a Fuel Cell", Paper presented at 1970 Seventh Annual Technical Symposium, Association of Senior Engineers, Naval Ship Systems Command.

13. Koegel, C., Westinghouse Electric Corporation Underseas Division, Ocean Research and Engineering Center, Annapolis, Md., personal communication, April, 1972.

14. *Energy Systems of Extended Endurance in the 1-100 Kilowatt Range for Undersea Applications*, Publication 1702, National Academy of Sciences, 1968.

15. Koegel, C.S.,Supervisor Engineer, Electrical Systems, Westinghouse Electric Corporation, Undersea Division, Ocean Research and Engineering Center, Annapolis, MD, May 3, 1952.

CHAPTER IX

Reactant Supply and Storage System

The reactant supply system and storage system is the largest and heaviest system comprising the semi-closed Rankine cycle propulsion plant. In all configurations this system must be encapsulated in hard pressure vessels, with considerable penalty in weight. Hydrogen-oxygen reactant supply and storage systems for deep submergence applications have been analyzed in detail by various contractors in studies for the U.S. Navy. Reference 1 reports the results of such a study which was conducted in conjunction with an analysis of a closed Brayton cycle propulsion plant for deep submersibles.

Several reactant supply systems are possible for the semi-closed Rankine cycle propulsion plant. Four possible configurations are listed below:

(a) storage of hydrogen and oxygen as gases at high pressure with injection into a combustion chamber utilizing gaseous reactants

(b) storage of hydrogen and oxygen as subcritical cryogenic liquids, pumping them to pressures sufficiently in excess of combustion chamber pressure, and injecting them into a combustion chamber at cryogenic temperatures

(c) storage of hydrogen and oxygen as subcritical cryogenic liquids, pumping them to pressures sufficiently in excess of combustion chamber pressure, and heating them in a heat exchanger of an auxiliary cooling water

system prior to injection into the combustion chamber as gases

(d) storage of cryogenic hydrogen and oxygen at supercritical pressures, sufficiently in excess of combustion chamber pressure, and injection with or without prior heating.

The first alternative has been found to be considerably heavier than the others at a design operating depth of 20,000 feet. Reference 1 reports about a 7000 pound increase in the overall plant weight of the closed Brayton cycle propulsion plant with the high pressure gas storage system over that using a subcritical cryogenic liquid system. For lesser depths than 20,000 feet, one can expect cryogenic storage to remain preferable to high pressure gas storage (2). Two advantages of the high pressure gas storage scheme, however, are its simplicity and the elimination of the product water storage pressure vessel, in that product water can be pumped into either the hydrogen or oxygen tank or both. This, however, must be accomplished by pumping against the existing pressure in the tank, which represents a parasitic load. A considerable amount of unused reactant remains in the tanks when the tank pressure drops to the feed pressure for the combustion chamber. This is common as well to the other alternatives, particularly to the supercritical system.

The second alternative, subcritical storage, requires adequate insulation to reduce boil-off losses and is considerably more complex than the high pressure gas system. This is

true for all the cryogenic storage systems. To achieve the relatively high combustion chamber pressures necessary for good overall plant thermal efficiency requires pumping the reactants as liquids. Hydrogen and oxygen become supercritical fluids when they are pumped above about 200 and 750 lbf/in^2, respectively. This pumping is another parasitic load and requires additional reactant to accomplish it for the same mission energy requirement (e.g. 1000 kwh). Cryogenic pumps require cooldown prior to operation, and sufficient suction head to operate satisfactorily. This second alternative is particularly applicable to the liquid-propellant rocket-type combustion chamber.

The third system is identical to the second system except for heat exchangers downstream of the cryogenic pumps, which heat the cold fluid to normal temperatures. If the selected combustion chamber utilizes gaseous reactants, increased efficiency can be realized by heating the cryogenic reactants by sea water (through a suitably designed intermediate heat transfer loop) prior to their coming in contact with the combustion chamber. This increases the available enthalpy of the reactants.

The fourth alternative allows heat to be admitted to the cryogenic storage tanks, either by an electrical heating element or by returning cryogens heated by sea water to "heating coils" in the tanks. An inner pressure vessel is required in this application to contain the supercritical fluids at storage pressures from 100-250 lbf/in^2 above combustion chamber pressures,

the pressure depending upon the type of combustion chamber and chamber pressure selected. The supercritical storage method then incurs a weight penalty due to the inner pressure vessel and requires slightly less insulation than the subcritical systems. Its advantage is the elimination of the cryogenic pumps.

Using the electrical loads of Chapter VIII for a nominal 50 kw, 1000 kwh endurance plant, based upon generator electrical load over and above all parasitic loads, a comparison was made of alternatives (b), (c) and (d). First, the electrical load was used to establish a reactant load required for the assumed mission profile for the 50 kw, 1000 kwh plant. These loads are listed in Table IX-1. A 94% generator efficiency and a total of 1 kw in bearing losses for both generator and turbine (3 bearings) were assumed in computing the turbine power required for each of three conditions: full power (5 hours), 60% power (1.7 hours) and 40% power (35 hours). The period of operation at power levels above full power is included in the full power operation. The power levels apply here to all loads other than the parasitic loads, i.e., propulsion power, manned sphere power requirements, and external auxiliary equipment. The parasitic load includes reactant pumps, which of course are not necessary for the supercritical storage system. This is corrected in the reactant load necessary for the supercritical configuration. Parasitic loads actually would be slightly increased over the values in Chapter VIII, since the turbine power required is about 10% greater than that used for the 50 kw

Loads	Power Level		
Parasitic Loads	Full Power kw	60% Power kw	40% Power kw
Condensate/feed pump	0.55	0.33	0.22
SW circ pump	3.20	3.20	3.20
Vacuum pumps	0.625	0.625	0.625
Auxiliary cooling water pump	0.20	0.20	0.20
Non-condensable compressor	0.20	0.20	0.20
Reactant supply pumps	1.14	0.684	0.456
H_2-O_2 detection equipment and propulsion/reactant supply controls	0.575	0.575	0.575
Bearing losses	1.00	1.00	1.00
Total parasitic load	7.49	6.81	6.48
Propulsion Load	44.28	24.28	14.28
Manned sphere power	2.44	2.44	2.44
External Auxiliary Equipment	3.28	3.28	3.28
Total Electrical Load	57.49	36.81	26.48
Non-parasitic Load	50.00	30.00	20.00
Turbine Load	61.10	39.10	28.20

	Alternative		
	(b) Subcritical Storage-Pump H_2/O_2	(c) Subcritical Storage-Pump & Heat H_2/O_2	(d) Super-Critical Storage H_2/O_2
Reactant required, lbm*	227/1813	216/1726	211/1691

*assumes a 98% combustion efficiency by weight

TABLE IX-1

Reactant Required for a 50 KW, 1000 KWH Propulsion Plant

turbine design and used for computing the parasitic loads in Chapter VIII. This was ignored for the purposes of this analysis.

For alternatives (b), (c), and (d), the amount of unused reactants at the end of the mission was determined by assuming a 100 lbf/in^2 gas pressure at the end of the mission for alternatives (b) and (c), and a 400°R, 700 lbf/in^2 residual gas condition for alternative (d). It was also assumed that filling the cryogenic storage tanks to greater than a 95% capacity would not be possible since some space must be left to permit boil-off without inordinate pressure increases. Table IX-2 gives a summary of the required reactant volume, pressure vessel sphere inner diameters, and pressure vessel weights for the cryogenic containment spheres.

It was not considered necessary to calculate detailed weights for containment spheres. Balukjian (3) gives curves of pressure vessel thickness and weight for spherical pressure vessels of various materials for 8000 and 20,000 foot depths, but these are found to be considerably overconservative when compared with detailed pressure vessel design figures in reference 4, a more thorough investigation of the Brayton cycle propulsion plant for deep submersibles. In the computation of Table IX-2, HY-180 Steel was used for purposes of comparison of the three reactant storage alternatives, despite the fact that it has not yet been proved acceptable for welding in heavy sections (5). The pressure vessel weights, then, were derived from data in reference 4 for various spheres of similar size

	Alternative		
	(b)	(c)	(d)
	Subcritical Storage-Pump H_2/O_2	Subcritical Storage-Pump & Heat H_2/O_2	Supercritical Storage H_2/O_2
Total reactant required (including unused reactant), lbm	264/1829	252/1740	229/1848
Required storage volume for 95% fill[1], ft^3	63.0/27.0	60.0/25.6	54.6/27.2
Pressure Vessel ID, in	63.0/48.5[2]	62.0/48.2[2]	59.0/48.0[3]
Vessel thickness, in	1.3/1.0	1.3/1.0	1.22/1.0
Pressure vessel OD, in	65.6/50.5	64.6/50.2	61.44/50.0
Pressure vessel weight	6000/2200	5600/2180	4500/2160
Inner tank thickness, in	0.1/0.1	0.1/0.1	0.368/0.292
Inner tank weight	310/177	301/174	1070/537
Insulation, various internal component weight (est.), lbm	150/130	150/130	85/70
Cryogenic pumps and motors (est.)	15/15	15/15	--
Weights			
Subtotal H_2/O_2, lbm	6739/4351	6318/4239	5884/4615
Total system weight, (including reactants) lbm	11090	10547	10499

[1] density of H_2 at fill - 4.42 lbm/ft^3

density of O_2 at fill - 71.2 lbm/ft^3

[2] includes 2" thick multi-layer insulation

[3] includes vacuum annulus and vapor shield

TABLE IX-2

Cryogenic Storage Weights and Volumes for Various Storage Alternatives for 20,000 Ft. Depth-HY 180 Steel Pressure Vessels

and are only approximate. A safety factor of 1.5 based upon buckling has been used in the analysis.

The supercritical storage system may utilize a vacuum annulus and vapor cooled shield for interruption of a considerable amount of heat leakage through the pressure vessel walls. The subcritical system, storing of liquid in a subcooled state, will require multilayer insulation. Insulation techniques have been developed which permit storage of liquid hydrogen for as long as 24 hours in a space environment without venting. This can be improved by initially filling the tanks with subcooled hydrogen and oxygen.

It may be seen from Table IX-2 that the weights of the three systems are comparable. One may conclude then that other factors than weight will govern the particular system selected. At the 8000 foot depth, the subcritical systems are about 500 pounds lighter than the supercritical storage system.

Because of the choice of the liquid propellant rocket type combustion chamber as the best candidate for immediate development, reactant storage alternative (b) was selected. This system requires the development of very small reactant pumps which can operate with a minimum of fluctuation of discharge pressure. Large fluctuations in discharge pressure would not be acceptable for the combustion chamber.

Small reactant pumps of the reciprocating or diaphragm variety could probably be devised. Tyree (6) reports that a particular reciprocating pump he devised could operate on as much as 50% gas by volume. These two types of pumps would not,

however, fulfill the requirement of minimum discharge pressure fluctuation for the liquid propellant rocket combustion chamber.

A very small variable speed gear-type pump is proposed. Such a pump could be built in several stages (3-4) to very exacting specifications. Although the pumps would experience considerable leakage, this could be reduced by very small clearances. Pump cooldown could be conducted by bleeding the cryogens through the pump and burning the gases in the recombiner of the non-condensable removal system (see Chapter VI). A diagram of this pump is shown in Figure IX-1. Table IX-3 gives a description of the pumps.

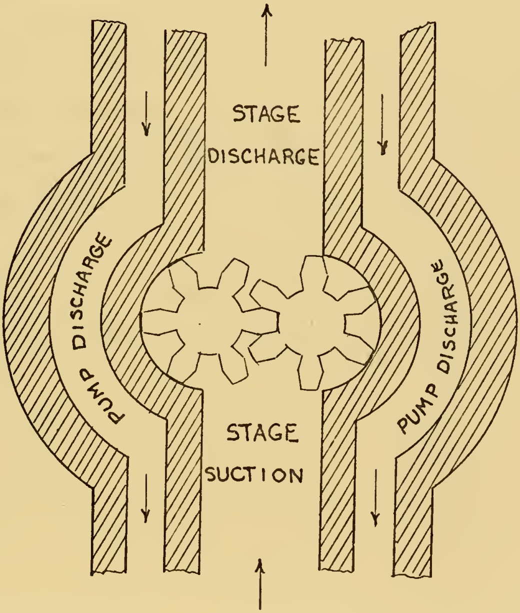

FIGURE IX-1

Reactant Pump Stage

Parameter	Oxygen	Hydrogen
Assumed reactant flow rate, lbm/hr	66.5	8.3
Reactant density, lbm/ft^3	71.25	4.42
Volumetric flow rate, ft^3/min	0.0156	0.0314
Gear OD, in	0.5	0.5
Tooth length, in	0.125	0.125
Tooth width, in	0.125	0.125
Gear length, in	0.50	0.50
Pump, rpm	308	636
Number of stages	3-4	3-4
Assumed pump efficiency	0.20	0.20
Assumed motor efficiency	0.60	0.60
Discharge pressure, lbf/in^2	885.	700.
Electrical power required, kw	0.565	0.57
Estimated pump and motor weight, lbm	15	15
Estimated pump volume, ft^3	0.2	0.2

TABLE IX-3

Reactant Pumps for a Nominal 50 KW Plant

It would be necessary to provide these pumps with sufficient net positive suction head to prevent cavitation at the inlet of the first stage. This could be accomplished by pressurizing the cryogenic storage tank to a sufficient pressure, perhaps 100 lbf/in^2, thus subcooling the reactant. An arrangement to provide such subcooling is shown in Figure IX-2. A small volume of the cryogen is kept in a very small but separate dewar located inside the main cryogen storage tank. A small amount of gas boils off when an electrical heating coil is energized in the pressurizing dewar. This gas is sufficient to raise the pressure of the gas above the main cryogen liquid storage while the bulk cryogen temperature remains essentially constant.

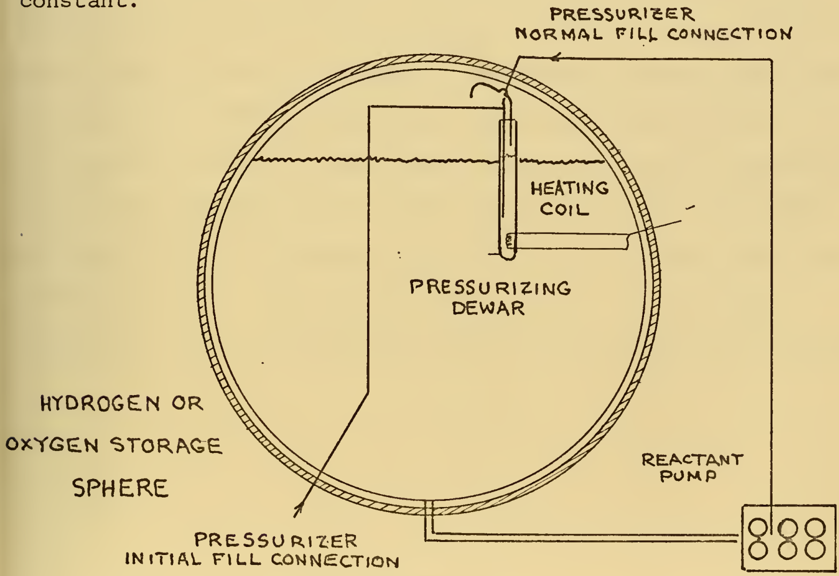

FIGURE IX-2

Pressurizing Arrangement

The power drain of the pressurizer heaters was determined to be less than 2.5 kwh in a 1000 kwh mission. It may be necessary to devise some means of emergency fill of the pressurizer dewar should all the cryogen evaporate from the pressurizer dewar because of delayed plant startup. In this regard, it may be necessary to locate the pressurizing dewar deep in the tank, rather than at the top as shown in Figure IX-2.

Assessment

The problems of cryogenic storage of hydrogen and oxygen for deep submergence applications are by no means completely solved. It appears, however, that with some developmental work in the area of transfer couplings and other areas, the system can be made safe and reliable. No detailed analysis of pump leakage rates for minimum anticipated clearances has been performed, but the assumed pump efficiencies are very low. If the reactant pumps for some reason should not prove satisfactory, it will be necessary to use the supercritical storage system and burn effectively gaseous reactants in the rocket type combustion chamber. The possible operation of a rocket type combustion chamber on gaseous reactants is discussed in Chapter V.

REFERENCES

1. Balujkian, H. and R. Rackley, "A Closed Brayton Cycle Power System for Deep Submersible Vehicles", *Journal of Hydronautics*, Vol. 5, No. 1, pp 5-10.

2. *Energy Systems of Extended Endurance in the 1-100 Kilowatt Range for Undersea Applications*, Publication 1702, National Academy of Sciences, Washington, D.C., 1968.

3. Balujkian, H., "A Closed Brayton Cycle Power Plant for Underwater Applications and Comparison with a Fuel Cell", paper presented at the Seventh Annual-Technical Symposium, Association of Senior Engineers, Naval Ship Systems Command, Washington, D.C., 1970.

4. *Thermal-Chemical Dynamic Power Supply for Deep Submergence Vehicles*, NAVSHIPS no. 0907-000-6010, August 7, 1970.

5. Masubuchi, K., Department of Ocean Engineering, Massachusetts Institute of Technology, personal communication, March, 1972.

6. Tyree, L. Jr., "A New High-Pressure Reciprocating Pump", *Advances in Cryogenic Engineering*, Vol. 8, K.D. Timmerhaus, ed., New York, Plenum Press, 1963.

7. Roder, H.M., and R.D. Goodwin, *Provisional Thermodynamic Functions for Para-Hydrogen*, NBS Technical Note 130, December, 1961.

8. Stewart, R.B., *The Thermodynamic Properties of Oxygen*, Ph.D. Thesis, Department of Mechanical Engineering, University of Iowa, June, 1966.

CHAPTER X

Regenerator

The regenerator is a relatively small piece of equipment which may be designed using standard techniques. The methods of Kays and London (1) have been used for the regenerator design. Regenerator effectiveness has been shown in Chapter IV to have only a small increase on overall plant efficiency compared to increases in turbine efficiency. Nevertheless, it was decided that if regenerator size could be kept within reason, perhaps less than one cubic foot in volume for the 50 kw plant, the maximum regenerator effectiveness attainable should be utilized. Regenerator effectiveness, according to Kays and London, is defined as

$$\eta_R = \frac{\dot{m}_{hot}\ c_{p,hot}(T_{h,in}-T_{h,out})}{(\dot{m}_{cp})_{min}(T_{h,in}-T_{c,in})} = \frac{\dot{m}_{c}\ c_{p,c}(T_{c,out}-T_{c,in})}{(\dot{m}_{cp})_{min}(T_{h,in}-T_{c,in})} \qquad (X-1)$$

where

$\dot{m}_{hot}$ = mass flow rate of the fluid on the hot side of the heat exchanger, lbm/hr

$\dot{m}_c$ = mass flow rate of the fluid on the cold side of the heat exchanger, lbm/hr

$(\dot{m}_{cp})_{min}$ = minimum product of mass flow rate and specific heat, hot or cold side

c_p = specific heat, Btu/lbm°R

T_h = hot side temperature, °R

T_c = cold side temperature, °R

Using a finned tube heat exchanger (core geometry figure 100 of reference 1), a regenerator was designed for approximately half the pressure drop of 0.14 lbf/in^2 between turbine exhaust and condenser at a regenerator effectiveness of 0.90. This resulted in a regenerator of dimensions 8" x 8" frontal dimensions, one foot in length.

The regenerator could be placed in the exhaust ducting of the turbine, between the turbine and condenser or directly above the condenser. It has been assumed that about 1½ feet of 8" diameter exhaust ducting would be adequate.

A drawing of the regenerator is shown in Figure X-1 below. Specifications for the regenerator are given in Table X-1.

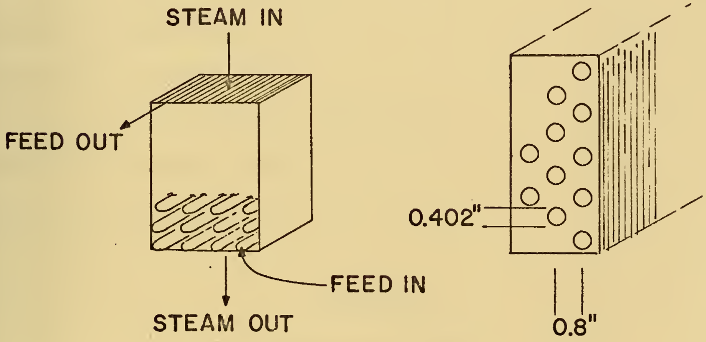

FIGURE X-1

Regenerator Design

Mass flow rate, lbm/hr	351
Frontal area, ft^2	0.450
Tubing, OD, in	0.402
Tubing, ID, in	0.382
Tube material	IN CA 719
Fin material	Cu
Fin thickness, in	0.013
Fin spacing (# per inch)	8.0
Core length, ft	1.0
Regenerator steam, lbf/in^2 side pressure drop	0.070
Regenerator Exhaust Pressure, lbf/in^2	1.0
Steam inlet temperature, °F	449
Steam exit temperature, °F	145.6
Feed inlet temperature, °F	101.7
Feed exit temperature, °F	365.5
Regenerator volume, ft^3	0.5
Turbine exhaust ducting volume, ft^3	0.52
Regenerator weight, lbm	84.6
Exhaust ducting weight, lbm	32.0

TABLE X-1

Regenerator Data

REFERENCES

1. Kays, W.M., and A.L. London, *Compact Heat Exchangers*, Palo Alto, California, The National Press, 1955.

CHAPTER XI

Encapsulation and Weight and Volume Summary

The preceding chapters of this thesis have established information on weight and volume of the components of the proposed propulsion plant. The propulsor (propeller, Kort nozzle, ducted thruster, pump jet, etc) has not been specified since the propulsor is dependent on the detailed mission and body form of the submersible.

One may then, at this point, select power plant conditions and determine overall weights and volumes. These figures may then be compared with comparable power plants for the deep submergence mission. From the weight and volume data developed, one may add or subtract components for a more direct comparison with other propulsion plants.

One item of importance is the selection of a suitable encapsulation material. Several materials are possible candidates: aluminum, titanium, and ultra high yield strength steels. It is not considered of great importance in this thesis to justify a selection of an encapsulation material. Rather it was considered necessary only to select a good candidate which would facilitate comparison with other proposed propulsion plants. The same is true, to some degree, with respect to the selection of a transmission system. Each proposed propulsion plant, whether it be fuel cells, Brayton cycle, Stirling cycle or the cycle proposed in this thesis has certain equipment in common. Certainly all encapsulated plants would utilize the

best material available, or which will probably become available in the near future. For this thesis, spheres have been selected for the shape of the encapsulating vessels. HY-180 steel was selected for the encapsulation material. It is realized that HY-180 steel could not be used for this application at present because of fabrication difficulties (1). As in Chapter X, a safety factor of 1.5, based upon buckling load, has been assumed.

The power plant conditions selected were those shown to effect the highest overall thermal efficiencies attainable. These conditions are shown in Table XI-1. A 98% combustion efficiency has been assumed with a 75°F sea water temperature. The efficiency of 27.1% for full power is based upon a turbine power of 62.4 kw to carry 50 kw electrical load other than propulsion related auxiliaries. The mission is as specified in Chapter III, 1000 kwh.

The weights and volumes for a 500 kw plant have not been included because of the lack of a specified mission, without which one cannot determine reactant weights. From previous chapters, one may, if desired, estimate weights and volumes of components for a 500 kw system or some intermediate power level between 50 and 500 kw.

Tables XI-2 and XI-3 give a summary of weights and volumes for two power plants. The first plant utilizes subcritical storage of the reactants and reactant pumps to deliver them at pressures sufficiently in excess of the 600 $\mathrm{lbf/in^2}$ combustion chamber pressure for the liquid propellant rocket combustion

<table>
<tr><th></th><th>Subcritical Reactant Storage System with Liquid Propellant Rocket Combustion Chamber</th><th>Supercritical Reactant Storage System with Porous Plug Combustion Chamber</th></tr>
<tr><td>Turbine, rpm</td><td colspan="2">24,000</td></tr>
<tr><td>Turbine inlet temperature, °F</td><td colspan="2">1,750</td></tr>
<tr><td>Turbine inlet pressure, lbf/in^2</td><td colspan="2">600</td></tr>
<tr><td>Turbine efficiency, %</td><td colspan="2">74.0</td></tr>
<tr><td>Generator efficiency, %</td><td colspan="2">94.0</td></tr>
<tr><td>Condenser pressure, lbf/in^2</td><td colspan="2">1.0</td></tr>
<tr><td>Condensate/feed pump discharge pressure, lbf/in^2</td><td colspan="2">800</td></tr>
<tr><td>Regenerator effectiveness, %</td><td colspan="2">90.0</td></tr>
<tr><td>Turbine exhaust temperature, °F</td><td colspan="2">449.0</td></tr>
<tr><td>Regenerator steam exit temperature, °F</td><td colspan="2">145.6</td></tr>
<tr><td>Regenerator and exhaust ducting pressure drop, lbf/in^2</td><td colspan="2">0.14</td></tr>
<tr><td>Regenerator feed inlet temperature, °F</td><td colspan="2">101.7</td></tr>
<tr><td>Regenerator feed exit temperature, °F</td><td>365.5</td><td>360.5</td></tr>
<tr><td>Turbine mass flow rate @ full power lbm/hr</td><td>351</td><td>338</td></tr>
<tr><td>Reactant mass flow rate @ full power, lbm/hr</td><td>90.5</td><td>82.7</td></tr>
<tr><td>Turbine load @ full power, kw</td><td>62.4</td><td>61.0</td></tr>
<tr><td>Reactant required for 1000 kwh mission[1], lbm</td><td>2150</td><td>1990</td></tr>
<tr><td>Specific reactant consumption[2], lbm/kwh</td><td>1.83</td><td>1.65</td></tr>
<tr><td>Overall thermal efficiency[2], %</td><td>27.1</td><td>30.1</td></tr>
</table>

[1] 1000 kwh mission is over and above parasitic loads; assumes 98% combustion efficiency by weight.

[2] Based upon HHV of hydrogen @ standard conditions for 50 kw useful electrical power output.

TABLE XI-1

Final Plant Conditions 50 kw - 1000 kwh Plant

Component	Volume ft^3	Dimensions L/W/H, ft	Weight (lbm)
<u>Condensing System</u>			20,000 ft/8000 ft
Condenser foundations and piping	2.5	1.9/2.1/1.2[1]	467 295
SW circ pump and motor[2]	0.3	-	70
Condensate feed pump and motor	0.37	-	23
Non-condensable removal and storage system	3.3	-	80
Auxiliary cooling water system	1.0	-	150
<u>Turbine and Regenerator</u>			
Turbine and foundations	1.8	1.5/1.5/1.5	135
Regenerator	0.5	0.66/0.66/1.0	85
Exhaust ducting	0.52	-	32
<u>Combustion Chamber</u>	1.5	1.5/0.83/0.83	50
<u>Electrical System</u>			
Lundell-Rice generator	0.93	1.06/1.06/1.06	210
Inverters and rectifiers	0.3	-	10
Power conditioning equipment	0.5	-	10
Propulsion plant controls	0.5	-	15
Start-up/emergency batteries[2]	0.83	-	106
Submersible motors and hydraulic pumps and motors[2]	3.0(est)	-	1250
<u>Miscellaneous</u>			
Reactant pumps	0.5	-	30
Piping	0.5	-	50
Fluids (including sea water condenser coolant)	-	-	60
Product water tankage (empty)	10.9	-	190

	20,000 ft	8,000 ft
Total volume of Internal components	25.62	25.62
Total volume of external components	4.13	4.13
Total weight of internal components	1597	1425
Total weight of external components	1426	1426
Total buoyancy of external components @ 64 lbm/ft^2, lbf	264	264
Propulsion plant pressure		
Vessel sphere, ID, in	48.0	48.0
Sphere internal volume, ft^3	33.5	33.5
Sphere packing factor (volumetric)	0.75	0.75
Propulsion plant sphere weight, lbm	2,400	950
Propulsion plant sphere buoyancy @ 64 lbm/ft^3, lbf	2425	2265

[1] includes hotwell

[2] mounted externally

TABLE XI-2

Propulsion Plant Pressure Vessel and External Equipment - Weights and Volumes

	Subcritical Reactant Storage System with Liquid Propellant Rocket Combustion Chamber		Supercritical Reactant Storage System[1] with Porous Plug Combustion Chamber	
Reactant Storage System	H_2/O_2		H_2/O_2	
Reactant				
usable, lbm	239/1910		221/1769	
unusable, lbm	39/20		18/165	
Total, lbm	278/1930		239/1934	
Inner tank weight, H_2/O_2 tanks, lbm	320/192		1080/544	
Miscellaneous weight				
Insulation, etc., lbm	150/130		85/70	
Inner tank diameter H_2/O_2, in	60/45.4		57/45.4	
Pressure vessel, ID H_2/O_2, in	64./47.4		60.6/49.0	
	20,000 ft/8,000 ft		20,000 ft/8,000ft	
Pressure vessel thickness, H_2/O_2, in	1.37/1.02	0.65/0.48	1.30/1.05	0.60/0.50
Pressure vessel weight, H_2/O_2, lbm	6800/2220	2800/900	5200/2450	2250/1000
Total storage vessel weights				
including cryogens, H_2/O_2, lbm	7548/4472	3548/3152	6604/4998	3654/3548
Buoyancy @ 64 lbf/ft^3	5780/2340	5500/2220	4930/2620	4590/2390

	Subcritical Reactant Storage System with Liquid Propellant Rocket Combustion Chamber	Supercritical Reactant Storage System with Porous Plug Combustion Chamber
Product Water Storage		
Product water volume, total, ft^3	34.5	31.9
Product water stored in propulsion plant pressure vessel, ft^3	10.9	10.9
Product water stored in separate product water sphere, ft^3	23.6	21.0
Product water pressure vessel ID, in	42.6	41.0
	20,000 ft/8,000 ft	20,000 ft/8,000 ft
Product water pressure vessel thickness, in	0.92/0.43	0.88/0.41
Product water pressure vessel, weight, lbm	1700/650	1550/600
Buoyancy at 64 lbf/ft^3, lbf	1725/1590	1510/1415

[1] Operating supercritical pressure-700 lbf/in^2

TABLE XI-3

Reactant Storage and Product Water System Weights and Volumes

chamber. The second plant utilizes supercritical reactant storage at 700 lbf/in^2 and the porous plug combustion chamber. Both plants were analyzed for depths of 8000 and 20,000 feet. A diagram of the internal arrangement in the propulsion plant pressure vessel is shown in Figure XI-1. Lowe (2) states that volumetric packing factors of greater than 0.60 to 0.75 are difficult to achieve. A packing factor of 0.75, including product water tankage, has been selected for the propulsion plant pressure vessel. Approximately 1/3 of the product water storage volume is provided within the propulsion plant pressure vessel sphere in otherwise unused space. The remainder of the product water is stored in a separate product water sphere.

Thus four spheres comprise the propulsion plant: a propulsion plant pressure vessel, two reactant pressure vessels (one for hydrogen and one for oxygen) containing cryogenic reactants, and a product water pressure vessel. Electric propulsion and associated hydraulic pumps and motors, startup/emergency batteries, and a salt water circulating pump for propulsion plant pressure vessel cooling are mounted externally. The arrangement of the spheres within the hull form of the submersible should be such as to facilitate transfer of cryogens from their storage tanks to the propulsion plant pressure vessel sphere.

The overall weights and volumes for the propulsion plant are given in Table XI-4 as well as the required weight and volume of flotation material to achieve neutral buoyancy. The assumed density for the flotation material is 34.5 lbm/ft^3.

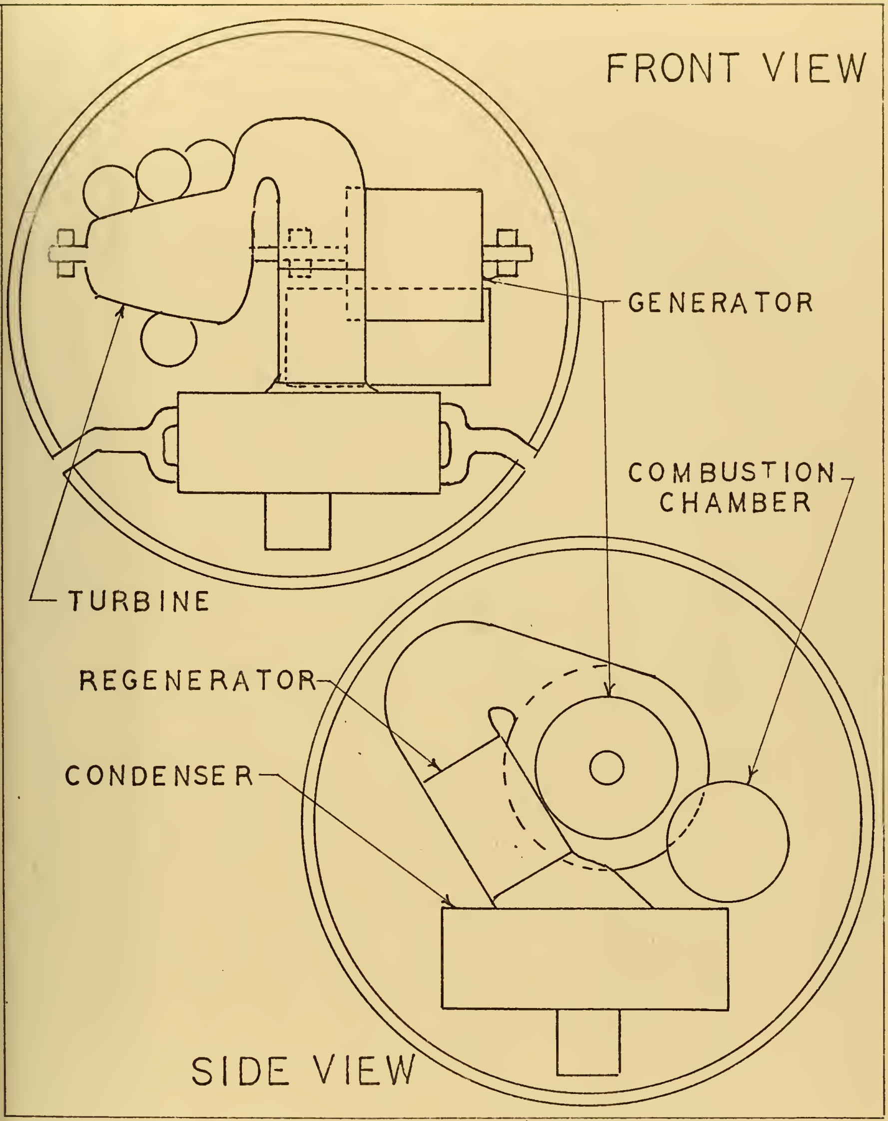

FIGURE XI-1 PROPULSION PLANT PRESSURE VESSEL ARRANGEMENT

Item	Subcritical Reactant Storage System with Liquid Propellant Rocket Combustion Chamber 20,000 ft	Subcritical Reactant Storage System with Liquid Propellant Rocket Combustion Chamber 8,000 ft	Supercritical Reactant Storage System with Porous Plug Combustion Chamber 20,000 ft	Supercritical Reactant Storage System with Porous Plug Combustion Chamber 8,000 ft
Weights				
Propulsion plant pressure vessel and internal components, weight, lbm	3997	2375	3997	2375
Hydrogen storage pressure vessel weight including fuel, lbm	7548	3548	6604	3654
Oxygen storage pressure vessel weight including oxidant, lbm	4472	3152	4998	3548
Product water storage tank	1700	650	1550	600
External components, lbm	1426	1426	1426	1426
Total weight without flotation material, lbm	19,143	11,151	18,575	11,603
Buoyancy				
Propulsion Plant pressure vessel, lbf	2425	2265	2425	2265
Hydrogen pressure vessel, lbf	5780	5500	4930	4590
Oxygen pressure vessel, lbf	2340	2220	2620	2390
Product water pressure vessel, lbf	1725	1590	1510	1415
External components, lbf	264	264	264	264
Total buoyancy without flotation material, lbf	12,634	11,839	11,749	10,924
Net buoyancy, lbf	-6,509	+688	-6,826	-679
Required flotation material for neutral buoyancy @34.5 lbm/ft^3, ft^3/lbm	220.5/7610	-	231/7990	23.0/794
Overall weight in air, lbm	26,753	11,151	26,565	12,397

TABLE XI-4

Overall Weight for 50 kw, 1000 kwh Propulsion Plant

Syntactic foam is not currently available in this light density for the 20,000 foot depth application.

It is apparent that the two systems have comparable weights in air at both the 8000 foot and 20,000 foot depths.

REFERENCES

1. Masubuchi, K., Department of Ocean Engineering, Massachusetts Institute of Technology, personal communication, April, 1972.

2. Lowe, B.J., Engineering Manager, Westinghouse Electric Corporation, Underseas Division, Ocean Research and Engineering Center, Annapolis, Maryland, personal communication, January, 1972.

CHAPTER XII

Conclusions

The hydrogen-oxygen fueled semi-closed Rankine cycle is a feasible propulsion plant for deep submersibles. With care in design of individual components, the plant can be designed for safe and reliable operation. The design goal of 4000-5000 hours time between overhauls probably cannot be met immediately, largely because of potential problems in the combustion chamber. Ball bearings for the turbine/generator unit may also shorten the time between overhauls somewhat from the design goal.

It is difficult to assess the design lifetime of a combustion chamber. The experience in space flight with rocket combustion chambers has been for relatively short design lifetimes. High heat flux and a desire to keep weights to a minimum have resulted in combustion chamber designs which would not meet the goal of long-term reliability. The availability of relatively large amounts of coolant (diluent water) and, within reason, no necessity to minimize the weight of the combustion chamber should permit a more conservative and reliable combustion chamber design to be developed. The porous plug combustion chamber appears to have the greatest promise for essentially complete combustion and for reliability if problems of oxidation of the porous metal can be kept within limits and if the device behaves as predicted. This can only be proved through experimental work. The porous plug chamber would also allow the reactant pumps to be eliminated.

The porous plug chamber permits the use of gaseous reactants at a saving of about 5% in reactant load over that for the plant with the liquid propellant rocket-type combustion chamber. The weight of the porous plug combustion chamber plant could be reduced slightly if reactant pumps were used instead of the supercritical storage system. It is believed, however, that the supercritical storage system is more reliable. An anticipated better combustion efficiency for the porous plug chamber could also reduce the estimated reactant load, based upon a 98% combustion efficiency by weight.

Overall thermal efficiency (or alternately specific reactant consumption), reflected by overall plant weight in air, is not as good as was anticipated, largely because of parasitic loads. The largest of these loads is the condenser salt water circulating pump. The required pumping power of this pump is primarily determined by the size of the pressure hull penetration and internal piping. In the trade-off of pressure vessel weight due to buildup around penetrations with overall plant weight due to increased reactant load, it may be possible to improve the pumping power considerably. It is likely that other parasitic loads may also be reduced in magnitude by more careful component design and analysis. A conservative approach was taken in the determination of these loads.

Overall plant weights in air for the proposed plant are heavier than the closed Brayton cycle plant proposed by Balukjian and Rackley (1) and outlined in detail in reference 2. Although the proposed plant includes certain equipment not

contained in the weight summary of references 1 and 2, notably startup/emergency batteries and the propulsion motors and hydraulic system, one may conclude that the proposed plant is about 4300-7400 pounds heavier than the Brayton cycle for the 20,000 foot, 50 kw, 1000 kwh mission. The variation in weight is apparently due to elimination of the need for a hard pressure vessel to contain product water in reference 2. A better comparison between the two plants is made by noting the required reactant load for the two plants for the 20,000 foot depth, 1000 kwh mission, 1711 pounds for the Brayton cycle plant and 2149 pounds for the proposed plant. At the 8000 foot depth, the proposed cycle is about 1000 pounds heavier than the Brayton cycle system.

It is estimated that the proposed plant is about twice as heavy in air as a comparable cryogenic fueled, encapsulated hydrogen-oxygen fuel cell system. Variations in mission length and definition do not permit exact comparison. For a comparable mission it is estimated that the proposed system is about half the weight of a silver-zinc battery system.

Achievable turbine efficiency was found to be much better than anticipated for the 50 kw power level. This is a result of utilization of a combination of disks, each having several re-entry stages. This led to a relatively simple rotor design at the expense of a more complicated casing design with multiple return ducts. Good turbine off-design performance was found to be achievable if constant speed operation is employed. The detailed analysis of leakage in the re-entry

turbine permitted more accurate assessment of expected turbine efficiency than would have otherwise been possible.

The detailed condenser analysis permitted reasonably accurate sizing of the condenser. The condenser analysis, although not a major portion of the analysis of the proposed plant, required extensive detailed work and represents a new contribution to condenser design. For this reason the computer program for condenser analysis has been included in this thesis.

The proposed porous plug combustion chamber is the first known evaluation of the application of this device to high pressure combustion. It appears that the concept is feasible for hydrogen and oxygen premixed with steam and at pressures up to 600 lbf/in^2.

Although the proposed plant does not, in its present configuration, equal other proposed propulsion plants for the same mission, it is considered that a more detailed design of parasitic loads could make it comparable with the Brayton cycle plant. The relatively high anticipated turbine efficiencies would permit this if parasitic loads can be sufficiently reduced. The development of reliable, very small reactant pumps in conjunction with development with the porous burner would assist in achieving this goal. The Brayton cycle plant has been subject to a much more detailed examination and development than has the proposed plant of this thesis.

REFERENCES

1. Balukjian, H. and R. Rackley, "A Closed Brayton Cycle Power System for Deep Submersible Vehicles", *Journal of Hydronautics*, Vol. 5, No. 1, January, 1971.

2. *Thermal-Chemical Dyanmic Power Supply for Deep Submersible Vehicles*, NAVSHIPS 0907-000-6010, August 7, 1970.

Thesis 134725
R2765 Reese
v.1 Analysis of a hydrogen-oxygen semiclosed rankine cycle propulsion plant for deep submersibles.

ANALYSIS OF A HYDROGEN-OXYGEN SEMI-CLOSED RANKINE CYCLE PROPULSION PLANT FOR DEEP SUBMERSIBLES

VOLUME II

RONALD MALCOLM REESE

APPENDIX A

Liquid Propellant Rocket Combustion Chamber

General

The liquid propellant rocket combustion chamber is a proven device which, with the availability of large amounts of coolant in the form of diluent water, should provide a reliable high pressure combustion chamber for deep submergence applications.

Its disadvantages are the high temperatures achieved in stoichiometric burning of such energetic reactants as hydrogen and oxygen. An additional difficulty is the problem of injection of the reactants at sufficient velocities to permit burning at some specified distance downstream of the injector. Given the fact that in most cases the reaction will be complete within an inch or two of the injector head, a tradeoff between injection velocities and mean droplet diameter is required to prevent overheating and burnout of the head or plugging of the injectors. Another difficulty, an outcome of small reactant flow rates and high injection velocities, is the extremely small injector hole size associated with low power applications. These problems may be overcome by the selection of the proper type injector. If hole sizes become extremely small, laser "drilling" may be advantageous. While injection of both reactants in the gaseous state would be advantageous with respect to injector manufacture, it would not provide as good injection head cooling as injection in the cryogenic state.

The prevention of uncontrolled combustion chamber oscillations is of major concern in any rocket combustion chamber design. While some conditions which would lead to uncontrolled oscillations may be possibly eliminated or delayed by the injection of large amounts of diluent water spray downstream of the combustion zone, this effect is not anticipated. Large pressure fluctuations could result from such a small exiting force as the passage of turbine blades downstream of the exit nozzle. For this reason, operation with choked exit flow from the chamber is desirable under all power conditions.

The achievement of very high combustion efficiency (~99%) is essential to the overall efficiency of the plant and in minimizing condenser size, since any unburned reactants represent an increase in the amount of non-condensables in the condenser. Even a small fraction of non-condensables will significantly decrease heat transfer. Such non-condensables must also be stored at high pressure, pumped overboard, or burned and condensed. Accurate control of the reactant feed rates is essential to the maintenance of stoichiometric conditions in the chamber. Any departure from stoichiometric conditions is also reflected as an increase in non-condensables in the condenser, as are impurities in the reactants.

An additional problem posed by the selection of hydrogen and oxygen as reactants is their dissociation at temperatures above 3600°R. The dissociation reaction is temperature as well as pressure dependent. If, in the process of introduction of diluent water to the combustion gases to achieve the desired

turbine inlet temperature, cooldown is too rapid, the reassociation reaction may not reach an equilibrium state within the combustion chamber. The reverse reaction (reassociation) proceeds fastest at higher temperatures and for that reason one would prefer introduction of a cooldown spray not in a single step, but rather in several stages, of which two would probably be sufficient.

High combustion zone temperatures, while detrimental to the injection head and walls if sufficient cooling is not employed, are more effective in achieving complete combustion. Quenching at the walls must be minimized to preclude large amounts of unreacted hydrogen and oxygen. It would appear, then, that the following items are desirable for high combustion efficiency:

1) As high a combustion temperature as possible
2) Minimizing of quenching at the walls by the use of as little wall cooling as practicable (minimizing cooled wall area)
3) Provision for sufficient combustion chamber volume
4) Adequate mixing in the combustion gases

Previous Work

Several gas generators burning hydrogen and oxygen have been reported in the literature. All of these have employed hydrogen rich mixtures to keep combustion gas temperatures within reasonable values. Ball (1) reported generally satisfactory operation of a liquid oxygen, gaseous hydrogen

combustion chamber at chamber pressures from 47 to 232 lbf/in^2 with a gas exit temperature ranging from 1260° to 2030°R. The total mass flow rate for this chamber varied between .18 to 170 lbm/sec, roughly 8 times the total reactant mass flow rate of a 50 kw (shaft) hydrogen-oxygen semi-closed Rankine cycle propulsion plant at design conditions. This design utilized impinging hydrogen and oxygen injectors in the primary combustion zone. Dilution with excess fuel was accomplished by spraying radially into the cylindrical chamber 12.5" downstream from the injector head.

Acker and Fenn (2) developed a liquid hydrogen, liquid oxygen combustion chamber which operated at a pressure of 220 lbf/in^2. Combustion chamber exit temperature was 1823°R. This chamber utilized a fuel rich mixture with an oxidant to fuel weight ratio of 1.0. A shower head injector was utilized in this design for oxygen injection while hydrogen was sprayed radially inward .05" downstream of the oxygen injector head from an annular plenum. Reported combustion efficiencies ranged from 93 to 96%, with the highest efficiency for a longer chamber.

Sekas and Acker (3) reported the performance of an improved model of the device described in reference 1, in which hot streaks of gas or oxidant had been responsible in burning out thermocouples located in the exit nozzle of the chamber. Such hot gas streaks could result in disastrous turbine blading failures. The chamber developed by Sekas and Acker was to provide hot gas for a 1000 kw turbine. Several

types of injectors were compared in the development of this chamber. An efficiency of .992 was reported for a 13 inch (length), 2.0 inch (ID) cylindrical combustion chamber over the range of mass flow rate tested. This best efficiency was obtained with an annular injector design, i.e. hydrogen admitted through an annular nozzle surrounding each individual oxygen injector. This combustion chamber operated at a pressure of 240 lbf/in^2 with a hot gas temperature of 1823°R.

Reference 4 reports the satisfactory testing of a high pressure liquid hydrogen-liquid oxygen fueled XLR-129 rocket engine developing 250,000 lbf thrust with a 2740 lbf/in^2 chamber pressure. In the thrust chamber, fuel rich turbo pump exhaust gases mix with additional oxygen at a 6/1 oxidant fuel weight ratio, still fuel rich, but not far from stoichiometric conditions. This engine is designed for 300 starts and a 10 hour lifetime, and is the forerunner of models for use in the space shuttle.

It should be noted that all of the small gas generators, references 1, 2 and 3, were designed for total operating lifetimes of minutes rather than the minimum 1000 hour lifetime deemed necessary for deep submergence applications. The smallest injector holes reported were .0135 inches in diameter.

Design Requirements

The most critical areas to be considered in the design of a liquid propellant rocket type combustion chamber are as follows:

1) The achievement of very high combustion efficiency (99%) through
    a) Proper selection of injector type and arrangement
    b) Proper sizing of the combustion chamber for adequate combustion length and thorough mixing of reactants
2) Smooth operation over a wide range of reactant mass flow rates through
    a) Injector throttling and stepping
    b) Control of reactant stoichiometry, dilution ratio and chamber exit temperature and pressure
3) Adequate wall and injector head cooling to ensure safe, reliable operation over an extended lifetime ($\geq$1000 hours)
4) Reduction of combustion chamber pressure oscillations and the elimination of uncontrolled oscillations through
    a) Proper injector selection
    b) Maintenance of choked flow in the exit nozzle
    c) Reactant and diluent feed pressures free of oscillations
5) The ability to operate over a very wide range of combustion chamber pressures (~2:1 pressure ratio) which is desirable under constant turbine speed operation with varying mass flow rates (This requires

reactant and feed water pumps whose speed can be varied continuously or in multiple steps to meet the wide range of discharge pressures and flow rates required)

Proposed Combustion Chamber Design

The power levels of interest in this thesis range from 50 kw to 500 kw. Since mission power profile of the 50 kw plant is known and because it is most requiring with respect to injector size, it was selected for a preliminary design analysis. The assumed conditions for the 50 kw plant are shown in Table A-1. For variable turbine speed operation, a constant combustion chamber pressure of 600 lbf/in^2 is assumed.

Previous studies (5) showed that a specific reactant consumption (lb/kwh) of 1.68 could be expected for these conditions and a 1750°F chamber exit temperature. A regenerator effectiveness of 0.7 had been established, specifying the diluent water inlet temperature at 421°F. While these conditions do not represent the optimum cycle conditions for the 50 kw (shaft) power level, they are representative and allow use of tabulated data (7).

Table A-1

Assumed Conditions for 50 KW Shaft Power Plant

Design Maximum Shaft Power (KW)	Assumed Turbine Efficiency	Assumed Condenser Pressure lbf/in^2	Recirculation Ratio	Combustion Chamber Pressure lbf/in^2	Combustion Chamber Exit Temperature °F	Diluent Temp. °F	Specific Reactant Consumption (SRC) lbm/kwh
50	.66	2.8	3.0	600	1750	421	1.68

Oxygen injector sizes and stepping arrangements were studied considering the assumed power profile, and resulted in the selection of a swirl type injector. The wide range of throttling capability and ease of fabrication of this type of injector (larger size holes) led to its selection over the impinging and shower head types. It is estimated that a given injector may be reliably throttled to 50% of its design maximum flow rate.

From Barrère (6) one may estimate the Sauter mean diameter of the droplets for a given pressure drop. Any considerable amount of throttling will result in multiple stepping of injectors. This stepping must be accomplished rapidly and reliably to preclude any pressure or temperature excursions or extinguishing of the flame in the chamber.

While the mission power profile assumes a cruising power of 40% of the design power level, it is realized that an ability to reduce power to 10% of its design level is desired when only auxiliary power is needed. For this reason injector stepping down to 10% of the design flow rate has been investigated. Since turbine efficiency would deteriorate considerably at these off-design power levels, the off-design flow rates would probably never reach less than 20% of the design maximum flow rates.

Since liquid hydrogen is a supercritical fluid at pressures above 200 $\mathrm{lbf/in^2}$ it is much simpler to introduce it into the combustion chamber than liquid oxygen. It can be easily admitted through a porous liner in the injection head, which,

in addition to distributing the fuel evenly, will provide vital cooling to the injector head.

In order to determine the length of the combustion chamber, it is necessary to investigate the combustion process in some detail. Analysis of the combustion process in a rocket combustion chamber has been attempted by several investigators, among them Spalding (8), (9), (10), (11), Williams (12), (13), Priem (14), (15) and Salant and Toong (16). Each of these models had its advantages and disadvantages, but all represent certain oversimplifications to the combustion process, which is an extremely complex phenomenon. The assumption may be made that the controlling factor in the "burning" process of an oxygen droplet in a hydrogen atmosphere is the vaporization rate of the oxygen droplet. Salant and Toong (16) include counter diffusion of the fuel and combustion products as well. Using the simplified analysis of Spalding (10), it is possible, knowing a mean droplet diameter, to determine the distance from the injector head at which a droplet will be completely vaporized. This analysis includes droplet drag, using a Stokes Law drag term and a bulk gas velocity. Somewhat unrealistically, it assumes a constant injection velocity for all droplets as well as a single droplet diameter. Ignition delay is ignored as well, and the temperature exterior to the droplet is assumed to be everywhere the adiabatic flame temperature. The gas viscosity is that for the fully burned gas. Additionally, a full droplet spray is assumed to exist at the point of injection.

Despite all of the simplifications of Spalding's model, it does give an indication of the distance downstream of the injector head at which combustion is essentially complete. Using this as a basis, one may apply an "insurance factor" of 2 to 4 for preliminary design purposes. Since the combustion chamber is small in comparison to the overall plant, it is reasonable to permit considerable "overdesign" in size compared to rocket combustion chambers to insure reliability and high combustion efficiency. For example, Spalding's analysis of the combustion region of the proposed chamber results in a combustion distance of about 2.0" for an injection velocity of 125 ft/sec and a Sauter mean diameter of 65μ.

One may use the method of Zucrow and Graham (17) to estimate convective heat flux to the walls of the combustion chamber if the Reynolds number (based on chamber diameter) is greater than 10^3 and if the mass flux of combustion gases is sufficiently high. This method probably may also be applied to transpiration cooling. Film cooling, however, would probably result in a more reliable distribution of liquid over the surface, and has therefore been selected for the proposed chamber.

Radiative heat flux was estimated by the use of charts in reference 18. Radiation heat transfer, at first thought to be relatively insignificant, was found to require a considerable amount of film cooling. While it was originally intended to produce re-association of the combustion gases by means of injection of a droplet spray into the chamber in the downstream

direction, it was found that film cooling alone in the combustion region was sufficient to reduce the bulk temperature of the combustion gases to 3600°R. This, of course, assumes complete mixing of the evaporated wall coolant and the bulk combustion gases, which will not be the case unless sufficient turbulence exists to produce it. For this reason turbulence promoters, to be shielded by adequate film cooling, are recommended for placement downstream of the main combustion region, (about 4 inches from the injector head). Materials such as silicided molybdenum, which will withstand an oxidizing atmosphere of 3600°R, might be useful for this application.

If the remainder of the diluent is then introduced as a liquid spray, the required evaporation distance becomes significant, 9-10 inches for a 100μ droplet spray injected at 100 ft/sec. One also finds that so little diluent remains (roughly 15% of the total diluent) at the point where the bulk temperature reaches 3600°R that no injector pattern placed at the walls can be sized to produce a sufficiently uniform spray across the chamber. This becomes especially evident when the chamber is throttled to 10% of its design maximum flow rate.

For this reason the remainder of the diluent is split, roughly 30% of which will be used for wall film cooling downstream of the combustion- re-association zone, and the remainder introduced radially inward from an annular plenum as a steam spray. The exact proportions of this split as well as the distribution and sizing of the steam orifices in the annular steam plenum should be the subject of experimental

work. Wall cooling should continue, either through film cooling or a regenerative cooling to a point where the bulk gas temperature is 2000°F. Turbulence promoters downstream of the point of discontinuence of wall cooling can be placed appropriately to produce more thorough mixing prior to entry into the chamber exit nozzle. A centrifugal type separator may also be built into the chamber exit geometry to remove any remaining water droplets prior to entry into the turbine. A bypass valve to the condenser might be advisable for turbine protection during startup.

One finds that, for the smallest swirl injector, the minimum chamber diameter of the design is severly limited by the combustion distance of a droplet in the 50% throttled condition. Using the equations of Barrère (6) for this type of injector (with a .015" hole diameter at 50% flow rate) one may predict a pressure drop of 60 lbf/in^2, corresponding to an injection velocity of 62.5 ft/sec. If one may use again the data of Kling shown in reference 6 to estimate the Sauter mean diameter of the droplet spray, a 210μ droplet size is predicted with a corresponding combustion distance of 4.8". The pressure drop at maximum flow rate for the smallest injector would be 220 lbf/in^2 for a 65μ droplet injected at 125 ft/sec and with combustion distance of 2.0". When accompanied by the very wide spray cone apex angle of 107° of this nozzle, a chamber diameter of at least 9" is required with injector placement as near to the center of the head as possible. As the injector is throttled, the combustion zone will move

further and further from the injection head, from an average 1.6" at maximum flow to 3.9" at 50% injector flow.

While the 9" chamber diameter is somewhat unrealistic with respect to uniform hydrogen distribution as the injector is throttled, both the 9" chamber and a 3" diameter chamber were utilized for detailed wall cooling calculations. A smaller chamber diameter would result in less radiative heat transfer per unit length and a slightly longer combustion-re-association length. Wall cooling calculations indicate, however, that even for a 3-inch diameter chamber, the wall cooling diluent is more than sufficient to reduce the bulk gas temperature to 3600°R within a distance of 4 times the calculated combustion length. In any event, a 6-8" length for combustion and re-association seems adequate and is not strongly dependent on the chamber diameter.

The injector hole size chosen for the smallest injector, .015", was selected on the basis of ease of fabrication by conventional drilling methods. A smaller hole, which could be fabricated by laser techniques, might be possible for this application, but would be more susceptible to plugging. The maximum injector flow rate for the smallest single injector is the governing parameter.

It would then seem advisable to limit the throttling of the combustion chamber to 20% of the design flow rate in order to achieve acceptable overall chamber performance. Under these conditions a .015" hole size injector would operate at maximum or nearly maximum flow rate. Four other injectors of varying

hole diameters can therefore be sized at acceptable cone apex angles to cover the remainder of the desired combustion chamber flow rates. The maximum throttling of any injector then is roughly 63.5% of the maximum injector flow rate. Figure A-1 shows the proposed injector arrangement, and Table A-2 gives details of the injector geometry and specifications. While it would be desirable to have the smallest injector operating continuously to prevent extinguishing of the flame during injector stepping, this is not possible if both operating injectors experience the same pressure drop. When the larger injector is throttled, the smallest injector should remain at maximum flow rate, a situation which would require elaborate controls. An alternative, of course, is to use laser fabricated holes for the smallest injector. If the smaller holes prove to operate adequately without plugging, a continuously operating "pilot" injector would then be possible.

Unlike a rocket combustion chamber, where axial gas velocity is high, carrying evaporating fuel or oxidant droplets rapidly downstream, the proposed rocket type combustion chamber exhibits very low axial velocities. Thus the oxygen is effectively sprayed into a stationary gas. For this reason, increase in the chamber diameter is not particularly effective in reducing chamber length. Figure A-2 shows a recommended design with a 4-inch diameter. The specifications for the chamber are given in Table A-3.

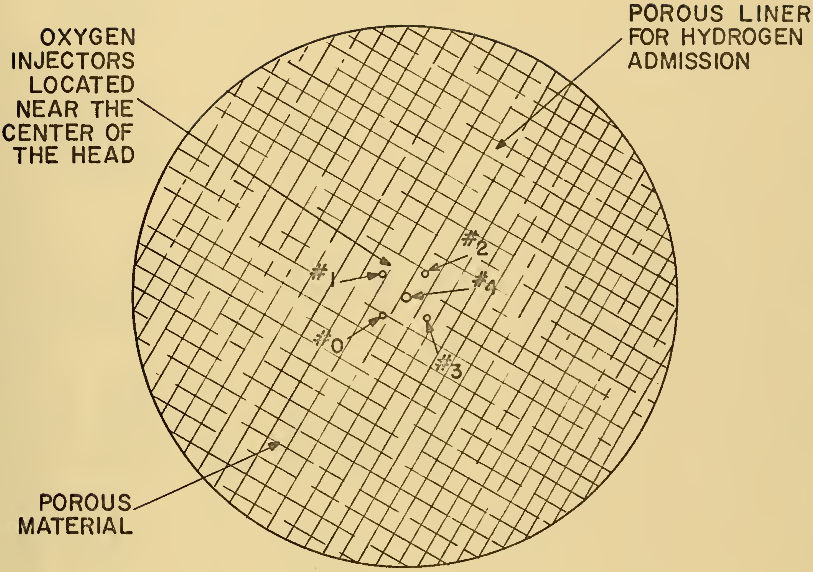

FIGURE A-1
INJECTOR HEAD

TABLE A-2

Oxygen Injector Characteristics

Injector No.	Exit Hole Size (in.)	Flow Rate Range lbm/hr	Swirl Chamber Diameter (in.)	Pressure Drop Maximum/ Minimum (lbf/in^2)	Spray Cone Apex Angle (Degrees)	Injection Velocity Maximum/ Minimum (ft/sec)	Sauter Mean Diameter Minimum/ Maximum	Tangential Hole Diameter for 4 holes (in.)
0	.015	15.1 and slightly below	.2	223/	107°	125/	65/	.018
1	.015	23.9-15.1	.2	240/95	79°	150/95	60/100	.0264
2	.018	37.6-23.9	.2	219/79	76°	150/95	65/100	.0274
3	.023	59.5-37.6	.3	205/82	74°	150/95	70/100	.0445
4	.029	94.2-59.5	.4	205/82	74°	150/95	70/100	.0582

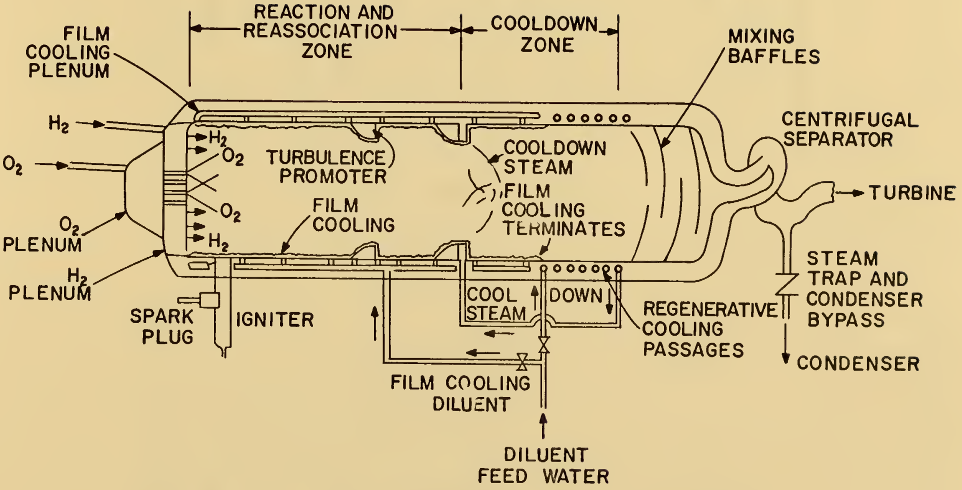

FIGURE A-2-ROCKET TYPE COMBUSTION CHAMBER

TABLE A-3

50 KW Design Maximum Power Level (shaft) Combustion Chamber Characteristics (sized for 125% design maximum power level)

Length of Combustion - Re-Association Zone, in.	8.0
Calculated Combustion Lengths, in.	1.5-1.8
Total Exit Steam Mass Flow Rate, lbm/hr	427
Total Reactant Mass Flow Rate, lbm/hr	106
H_2	11.8
O_2	94.2
Total Diluent Mass Flow Rate lbm/hr	321.
Number of Injectors	5
Combustion - Re-Association Zone Film Coolant Evaporation Rate lbm/hr	161.0
Cooldown Zone Film Coolant Mass Flow Rate, lbm/hr	48.
Cooldown Steam Mass Flow Rate, lbm/hr	112.0
Chamber Internal Diameter, in.	4
Chamber Total Length, in.	15
Chamber Exit Pressure, lbf/in^2	600
Chamber Exit Temperature, °F	1750

Ignition is best performed by a small gaseous hydrogen-gaseous oxygen igniter located adjacent to the main injector head and initiated by a spark plug. Reference 1 reports satisfactory operation of this device. If some film cooling is provided during chamber operation, burnout of the igniter should be preventable.

As indicated in reference 1, startup and shutdown may be accomplished by admission of hydrogen followed by oxygen in the startup procedure with the reverse order during shutdown. Extremely fuel rich mixtures would be advisable during startup to preclude combustion chamber burnout when diluent spray has not yet been introduced.

In order that a constant combustion chamber pressure and exit temperature may be achieved over a range of mass flow rates, it will be best to select one of the reactants, either hydrogen or oxygen as the controlling parameter to be varied with changes in chamber pressure. Selecting oxygen flow rate as the base variable, the relative amounts of hydrogen and oxygen may be sensed at the non-condensable gas exit from the condenser. The hydrogen flow rate may be adjusted to keep the hydrogen-oxygen ratio at the condenser exit at zero or at a stoichiometric value, representing other than 100% combustion efficiency. A thermocouple in the combustion chamber exit nozzle may be used to detect stagnation chamber exit temperature and this value used to regulate diluent spray to the reassociation and cool-down nozzles by maintaining a specified base ratio between oxygen flow rate and diluent flow rate adjusted by chamber exit temperature.

Variable chamber pressure may be desired over a certain range of mass flow rates. For example, chamber pressure might increase from 600 lbf/in^2 at 40% design power level (shaft) and below to 1200 lbf/in^2 at 80% design power level and above. Under these conditions, sensing of steam mass flow rate from the chamber could be accomplished over this range and chamber pressure compared with a series of preset signals for various specified mass flow rates. Hence chamber pressure could be varied in discrete steps over this range. The other controls would remain essentially the same as before.

Reactant pump and diluent water pump sizing and control are not considered in this appendix, since they are common to any high pressure hydrogen-oxygen combustion chamber.

Assessment

The rocket type combustion chamber appears to be a possible alternative for inclusion in the proposed propulsion plant. Its major advantage is its capability for variable pressure operation. Its main disadvantages are its extremely high temperatures and resultant heat fluxes to the chamber walls, the ever present possibility of catastrophic chamber pressure oscillation as in any rocket combustion chamber, and the difficulty of insuring against hot gas streaking in the exiting steam. An additional difficulty is the problem in achieving smooth operation during injector stepping.

REFERENCES

1. Ball, Calvin L., "The Performance Evaluation of a Gaseous Hydrogen-Liquid Oxygen Gas Generator for Driving Hot-Gas Research Turbines", ASME Paper 61-WA-295.

2. Acker, Loren W., David B. Fenn, and Marshall W. Dietrich, *Performance of a Small Gas Generator Using Liquid Hydrogen and Liquid Oxygen*, NASA TMX-417, Lewis Research Center, February 1961.

3. Sekas, Nick J. and Loren W. Acker, *Design and Performance of a Liquid-Hydrogen, Liquid-Oxygen Gas Generator for Driving a 1000-Horsepower Turbine*, NASA TND-1317, Lewis Research Center, July 1962.

4. "Reusable Rocket Motor Unveiled", *Aviation Week and Space Technology*, August 31, 1970.

5. Reese, R.M. and A.D. Carmichael, "A Proposed Hydrogen-Oxygen Fueled Steam Cycle for the Propulsion of Deep Submersibles", *Proceedings of the 1971 Intersociety Energy Conversion Engineering Conference*, pp 563-576, August 3-5, 1971.

6. Barrere, Marcel, A. Jaumotte, B.F. Veubeke, and J. Vandenkerckhove, *Rocket Propulsion*, New York, Elsevier Publishing Company, 1960.

7. Gordon, Sanford, and Bonnie J. McBride, *Theoretical Performance of Liquid Hydrogen with Liquid Oxygen as a Rocket Propellant*, NASA Memo 5-21-59 E, June 1959.

8. Spalding, D.B., "Combustion in Liquid Fuel Rocket Motors", *The Aeronautical Quarterly*, Vol. X, February, 1959.

9. Spalding, D.B. and V.K. Jain, *Theory of the Burning of Monopropellant Droplets*, A.R.C. 20, 176, May 19, 1958.

10. Spalding, D.B., *A One-Dimensional Theory of Liquid - Fuel Rocket Combustion*, A.R.C. 20, 175, May 19, 1958.

11. Adler, J., *A One-Dimensional Theory of Liquid Fuel Rocket Combustion II: The Influence of Chemical Reaction*, A.R.C. 20, 189, May 28, 1958.

12. Williams, F.A., *Combustion Theory*, Reading, Massachusetts, Addison-Wesley, 1965.

13. Williams, F.A., "Monodisperse Spray Deflagration", *Liquid Rockets and Propellants*, Volume 2 of *Progress in Astronautics and Rocketry*, ed. by Loren E. Bollinger, M. Goldsmith, and A.W. Lemmon, Jr., New York, Academic Press, 1960.

14. Priem, R.J., *Propellant Vaporization as a Criterion for Rocket-Engine Design; Calculations of Chamber Length to Vaporize a Single N-Heptane Drop*, NACA Technical Note 3985, July 1957.

15. Priem, R.J., *Propellant Vaporization as a Criterion for Rocket Engine Design; Calculations Using Various Log-Probability Distributions of Heptane Drops*, NACA Technical Note 4098, October 1957.

16. Salant, R.F. and T. Toong, 2.282 (combustion) class notes, Massachusetts Institute of Technology, Spring, 1971.

17. Zucrow, M.J. and A.R. Graham, "Some Considerations of Film Cooling for Rocket Motors", *Jet Propulsion*, Vol. 27, No. 6, June 1957.

18. Hottel, H.C. and A.F. Sarofim, *Radiative Transfer*, New York, McGraw-Hill Book Company, 1967.

19. Burrows, Marshall C., *Radiation Processes Related to Oxygen-Hydrogen Combustion at High Pressures*, NASA-TN D 2541, December, 1964.

APPENDIX B

Porous Plug Burner Combustion Chamber

General

A cooled porous plug burner has been used as a laboratory tool in the studies of laminar flames. The characteristics of laminar flames have been studied extensively through the use of a cooled porous plug burner. Kaskan (1) and Botha and Spalding (2) have shown that the velocity of propogation of a flame into an unburned gas mixture may be slowed if heat is extracted from the flame. Indeed this is the phenomenon which allows flame stabilization to occur. Prior to Kaskan's work, however, such stabilization was accomplished by extraction of heat at the edges of the flame, rather than uniformly throughout a flat flame front. This device has permitted the study of laminar flames in premixed, highly explosive gases even if they normally exhibit very high flame velocities. Figure B-1 is a schematic diagram of the porous plug burner.

Siegler and Moore (3) have developed the porous plug burner from its laboratory use to a reliable engineering device for safely burning essentially undiluted stoichiometric mixtures of hydrogen and oxygen at atmospheric pressures. The particular industrial application for which the device was designed is the recombination of radiolytically decomposed hydrogen and oxygen removed from the condenser of a boiling water reactor plant. For this purpose, the device appears to be well suited and reliable. The burner, however, is not limited to burning hydrogen. To the contrary, undiluted stoichiometric hydrogen

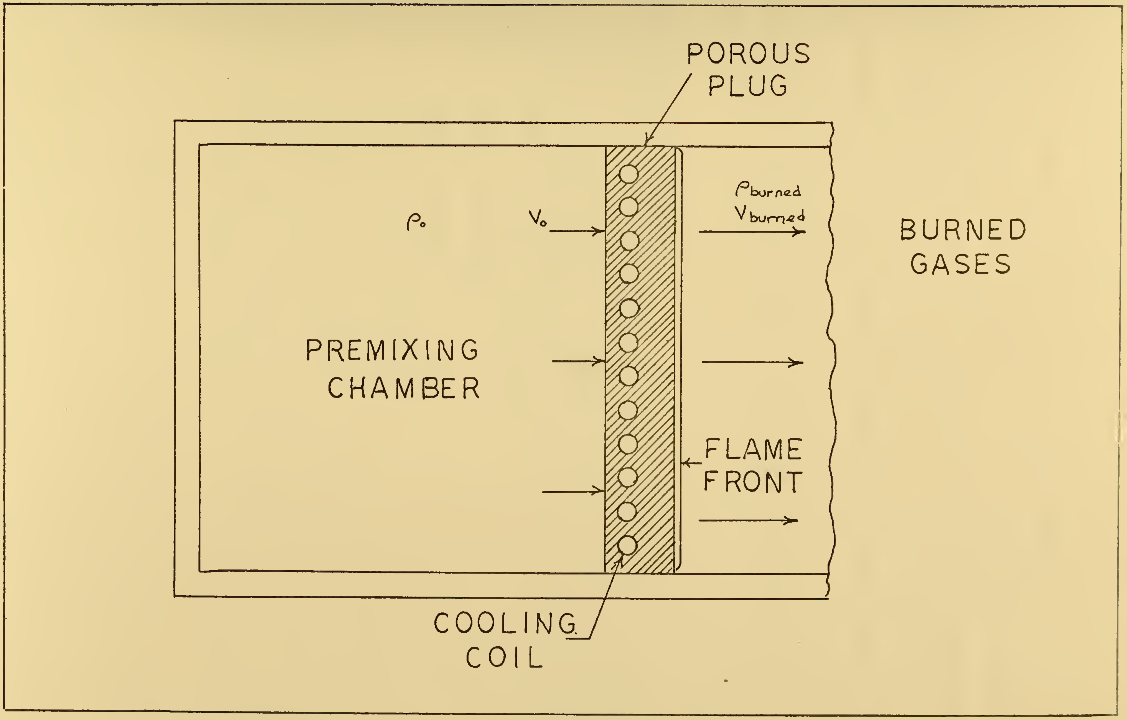

FIGURE B-1
SCHEMATIC DIAGRAM OF POROUS PLUG BURNER

and oxygen, with their very high adiabatic flame velocity (~1000 cm/sec at 25°C and 1 atm), represent an extreme case which the burner can safely and reliably meet.

The particular application in a boiling water reactor power plant requires that the device operate for long periods of time (essentially years) with little or no attention. These elements of safety and reliability, coupled with relatively low temperature combustion, make this device an interesting candidate for the semi-closed Rankine cycle proposed in this thesis.

Principles of Operation

The porous plug, fabricated from some porous material of high thermal conductivity, adequate porosity and sufficient strength, acts in three capacities:

1) a flame stabilizer
2) a flame arrestor
3) a compact heat exchanger

Its function as a flame arrestor is achieved by making the pore size sufficiently small to prevent flashback into the unburned premixed gases. The quenching distance for an undiluted stoichiometric oxyhydrogen mixture at 25°C and atmospheric pressure is about 190μ (4). By making the pore size a small fraction of this value, perhaps one-tenth, Siegler and Moore have satisfactorily prevented flashback from occurring. High values of open porosity of the plug material, while desirable from the standpoint of reducing pressure drop of the premixed

gases from the plug inlet to exit, reduce the effective thermal conductivity of the porous plug material, $\overline{k}_s$. This effective thermal conductivity has been investigated by Grootenhuis, Powell and Tye (5).

Hence for a given heat flux to the porous plug, coolant temperature, plug thickness and material, the temperature of the flame side of the plug will increase with increasing total porosity of the plug. Maintaining this temperature at a minimum is important for two reasons. First, quenching distance decreases with increasing temperature making it possible for the flame to "march" into the porous plug. This would result in destruction of the porous nature of the plug, but probably not in an explosion of the premixed gases if the coolant flow through the plug is maintained. Secondly, if the porous nature of the plug is obtained by sintering, there is some temperature within 200-300°F of the sintering temperature at which the pores would begin to close up after periods of operation as short as several hundred hours (6). Thus a high sintering temperature for sintered porous materials would probably be desirable with as low a maximum operating temperature as possible, never exceeding a temperature 300 degrees F below the sintering temperature.

Several porous materials of high conductivity may be used. Siegler and Moore (3) first used a commercial porous bronze plate but found that this had inadequate thermal conductivity. Finally several generations of sintered copper porous plugs were constructed from cut copper wire 180-250μ in diameter.

In a 1700 hour "life test" of the final generation burner of reference 3, a 5μ oxide thickness was noted on the copper particles upon metallographic examination. With a pore size of about 30μ (7), this did not adversely affect the operation of the burner. Only a slight increase in plug temperature and gas pressure drop was noted. While this did not prove to be a major problem in the burner constructed by Siegler and Moore, it does restrict the use of sintered copper to applications where the downstream face of the porous plug can be kept at low values, somewhere in the range of 130-150°C. Porous sintered nickel can be made with average pore sizes as small as 0.5μ with surprisingly good uniformity (6). The significantly higher thermal conductivity of copper and copper alloys would seemingly make sintered copper a more desirable choice than nickel, but this neglects the oxidizing atmosphere and the problems of reduction of pore size by oxide buildup.

Minimizing the thickness of the plug on the flame side of the cooling passages is an obvious solution to keeping the maximum plug temperature within satisfactory limits, but this distance must be sufficiently great to achieve a uniform velocity distribution of the premixed gases at the exit (flame side) of the plug. Pressure drop across the plug and maximum plug temperature must therefore be traded off to achieve a satisfactory design which will preclude flashback.

The relationship of heat flux to the plug in conjunction with flammability limits is another area in which a trade off is necessary. The heat flux absorbed by the plug, q''_f, may

be related to the mass flux of the premixed gases, $G = \rho_o V_o$, by the following relationship:

$$q''_f = -\rho_o V_o \bar{c}_p (T_a - T_f) = -\rho_o V_o (i_a - i_f) = \rho_o u (i_a - i_f) \qquad \text{(B-1)}$$

neglecting pressure drop across the plug and noting then that $u = -V_o$ for a stabilized flame front. The positive direction is in the direction of gas flow.

G = mass flux, lbm/hr ft²

u = flame velocity into the unburned mixture, ft/hr

V_o = the velocity of the unburned mixture upstream of the plug, ft/hr

q'' = heat flux, Btu/hr ft²

ρ_o = density of the unburned gas mixture, including diluent (if any), lbm/ft³

T_a = adiabatic flame temperature of the combustion product and diluent mixture, °R

T_f = actual flame temperature, °R

$\bar{c}_p$ = mean specific heat of burned gases and diluent between T_f and T_a, Btu/lbm°R

i_a = enthalpy of the adiabatic combustion product and diluent mixture, Btu/lbm

i_f = enthalpy of the combustion product and diluent mixture at the actual flame temperature, Btu/lbm

The actual flame velocity into the unburned mixture is related to the adiabatic flame velocity, u_a, by the following approximate relationship:

$$\frac{u}{u_a} = e^{-(E/2RT_f - E/2RT_a)} \tag{B-2}$$

where

u_a = velocity of propogation of the flame front into the unburned mixture at the adiabatic flame temperature (no heat removal)

E = an activation energy for the reaction, Btu/°R lb-mole or cal/°K g-mole

T_a, T_f in consistent units

It is obvious then that, at zero flame velocity, there will be a condition of no heat flux. A similar condition will exist when T_f equals T_a. At some intermediate temperature, Moore (8) shows that heat flux achieves a maximum value. Since flame velocity, u, is related to u_a, adiabatic flame velocity, by an exponential function, one finds that an increase in T_f when $T_f \ll T_a$ results in a very rapid increase in u, the effect of which is to increase the heat flux even though the enthalpy rejected per unit mass of the burning mixture decreases. It is necessary to keep heat flux to the burner within acceptable limits. Reference 3 states that 20 $\text{cal/cm}^2\text{sec}$ (2.7×10^5 Btu/hr ft^2), roughly one third of the heat flux to the liner of a typical rocket combustion chamber, is a reasonable design figure. Operation of a porous plug burner at a flame temperature near the adiabatic flame temperature yet within practical heat flux limits may be possible, but would occur with a significantly higher pressure

drop across the porous plug and with more critical material problems downstream of the plug due to the high combustion temperature.

Moore (9) states that at flame temperatures of 900-1000°C and flame velocities of 2-3 cm/sec the hydrogen-air flame becomes unstable. This imposes a lower limit on flame temperature.

Siegler and Moore (3) found that the plug tended to be self-regulating insofar as flow area is concerned. At lower than design flow rates of the stoichiometric hydrogen-oxygen mixtures, condensation formed in low flow regions, thus restricting the flow area and producing a nearly constant flame velocity. This effect was apparently achieved with a constant mass flow rate of coolant, which would produce such a phenomenon. Another self-regulating feature was the ability of the porous plug to maintain a uniform heat flux and thereby a stable flat flame. This can be explained by an increase in kinematic viscosity of the premixed gases in areas of high velocity (and consequently higher heat flux), which in turn reduces the velocity.

The method of flame stabilization in a porous plug burner is briefly described below. The independent variable in the combustion/heat transfer problem is the mass flux of the unburned gas, $\rho_o V_o$. The self-regulating feature of the flame is such as to exactly match the premixed gas velocity, V_o, with a flame velocity, u, into the unburned mixture, thus producing a stable flame in space at the exit of the porous

plug. This occurs because there is a heat sink available (the porous plug).

In the high velocity regime, at velocities greater than the velocity for maximum heat flux, the stabilization process can be explained as follows: first assume that the flame is stabilized at a given distance, y, from the exit of the plug. Next, consider a small perturbation to the distance, y, moving the flame front closer to the plug to some position $y' < y$. This in turn increases heat transfer to the plug, decreasing the flame temperature as shown by equation B-1. Since flame temperature and flame velocity are related through equation B-2, the flame velocity will decrease. This, in conjunction with a predetermined velocity of the unburned mixture, V_o, will blow the flame front downstream to some point $y'' > y$, where the heat transfer to the plug will be sharply reduced, again increasing the flame temperature and flame velocity.

In the low velocity regime, that of operation of the porous plug burner, the stabilizing process is somewhat different as explained by Wohl (10). There exists a minimum distance from the burner at which the flame can exist. At a lesser distance quenching will occur. As the velocity of the unburned mixture, V_o, is decreased below its value corresponding to this distance, the flame then marches away from the burner to a new equilibrium point at a distance greater than the minimum value. Thus a flame can actually exist at a given distance above the minimum distance from the burner at two different flame velocities. The minimum distance actually

corresponds to a velocity slightly greater than that for maximum heat flux (7).

Thus the laminar flame speed, u, is set by the approach velocity, V_o, since the flame velocity, u, will equal V_o as long as there is sufficient cooling available to remove the heat from the flame front. This will occur theoretically at any coolant exit temperature below the flame temperature corresponding to u. Practically speaking, however, the coolant temperature, the porous plug geometry, particularly the thickness and its effective thermal conductivity (based on plug material and porosity), and the heat transfer coefficient to the coolant in conjunction with the heat flux absorbed by the plug, q''_f, establish some fixed plug exit temperature. Clearly these are design parameters which must be tailored to achieve an acceptable plug exit temperature.

Application to the Semi-Closed Rankine Cycle Propulsion Plant

Premixing of the reactants in a gaseous state would be advantageous for a combustion chamber for the hydrogen-oxygen fueled semi-closed Rankine cycle propulsion plant. Of course, it would be necessary to demonstrate that such premixing could be accomplished without any significant danger of explosion. Premixing of the fuel and oxidant in a gaseous state rather than injection as liquids will improve the combustion efficiency of a combustion device. This will occur because of improved homogeneity of the fuel-oxidant mixture in the chamber. An additional reason for premixing in the gaseous state is the

ease with which such a burner can be throttled to lower reactant feed rates. The injection pattern is not so critical to combustor performance here as it is in a liquid propellant rocket type combustor. Therefore, reactant feed rates may be throttled with reasonable ease without the danger of producing combustor instabilities and associated excessive heat fluxes to combustor walls.

Another advantage of the porous plug burner is its lower combustion temperatures, which preclude dissociation and require less or perhaps no wall cooling. In general, it is advantageous to lower the combustion temperatures as far as possible, since this reduces material problems and improves reliability.

The application of the porous plug burner to stoichiometric oxyhydrogen mixtures at high pressures requires investigation of several factors. First, very little investigative work in the field of oxyhydrogen combustion at pressures in excess of one atmosphere has been done. However, it can be readily seen that such factors as quenching distance, adiabatic laminar flame velocity and ignition delay combine to produce a more stringent design than at atmospheric pressure. One way of reducing the deleterious effect of pressure on these parameters is to add inerts to the premixed gases. This, however, is only possible for the proposed application if steam is used as the diluent. Saturated steam at high pressures has associated high temperatures (400-500°F), and, if added to premixed gaseous oxygen and hydrogen, will preheat the mixture.

This effect will negate to some degree the effect of adding an inert.

The effect of high pressures on adiabatic laminar flame velocity was investigated by Edse (11), who measured these velocities using a bunsen burner-like apparatus at pressures up to 14.6 atmospheres. His is the only work found which reported results at high pressures. Edse, however, was forced to make estimates of laminar flame speed from turbulent flames, since at higher pressures, the flame speeds were such as to produce turbulent flames. In order to estimate laminar flame velocity, Edse measured the angle which the flame front made with the rim of the burner tube at the supposed intersection of the laminar sublayer with the turbulent core. Such estimates cannot be considered to be highly accurate, but probably do reveal trends. Edse found that, in an undiluted stoichiometric oxyhydrogen mixture, laminar flame velocity increased from about 1000 cm/sec to about 3400 cm/sec when pressure was increased from 1 to 14.6 atmospheres. With undiluted richer or leaner mixtures, the effect of pressure became less significant. The effect of pressure on flame velocity on very rich and very lean mixtures was not investigated but appeared to be negligible for rich mixtures (>85% H_2) and appeared to increase by a factor of 2 from 1 to 14.6 atmospheres for lean mixtures (<30% H_2).

More accurate work was performed by Manton and Milliken (12), who used the spherical bomb method for determining laminar flame velocity. Their work, however, was conducted at

pressures of less than 1.5 atmospheres. It showed, however, that adiabatic laminar flame velocities of all the gases tested, which included propane, ethelene, acyetylene, methane and hydrogen with various amounts of diluent argon, helium or nitrogen could be correlated by use of a pressure exponent, x, by the following equation:

$$\frac{u'_a}{u_a} = \left(\frac{p'}{p}\right)^x \qquad \text{(B-3)}$$

The unprimed quantities indicate the values at some reference pressure, p, and the primed quantities at some other pressure.

Manton and Milliken's work showed that at adiabatic flame velocities between about 50 and 100 cm/sec, there was no pressure effect whatsoever. At higher flame velocities, the pressure effect became more significant, predicting a laminar flame speed of about 2440 cm/sec for undiluted stoichiometric hydrogen and oxygen at 14.6 atmospheres, as opposed to the 3400 cm/sec velocity estimated by Edse at this pressure.

Flame theory (13) predicts that laminar flame velocity is related to pressure and temperature by the following expression:

$$u_a \sim p^{n/2-1} \, e^{-E/2RT_a} \qquad \text{(B-4)}$$

where n = the order of the reaction (the number of molecules which react in a chemical reaction)

The hydrogen-oxygen reaction, although somewhat complex, is probably the best understood of all multistep reactions. This should not imply, however, that the reaction is sufficiently well understood that one may always make reliable predictions as to its behavior. Basically, the hydrogen-oxygen reaction is a two body process, which should make it independent of pressure.

This apparently is not the case. Edse explains this by the effect of pressure on the dissociation phenomenon at high temperatures. It is known that dissociation is not significant for this reaction at temperatures below 1800°K. When the gas temperature is reduced to this value or less by means of dilution, at one atmosphere adiabatic flame speeds on the order of 300 cm/sec result, with a less significant pressure effect.

A further effect of lowering flame speed is produced by dilution itself and may be approximated by

$$\frac{u'_a}{u_a} = \frac{\{[H_2]'\ [O_2]'\}^{\frac{1}{2}}}{\{[H_2]\ [O_2]\}^{\frac{1}{2}}} \tag{B-5}$$

where the brackets, [], represent molal or molecular concentrations of the reactants at a given pressure and temperature and the primed quantities indicate values with dilution.

Equation B-5 is a consequence of the dependence of flame velocity on the square root of reaction rate. The reaction rate constant is in turn proportional to the product of the concentrations of the reactants (the collision frequency term).

Again, since the hydrogen-oxygen reaction is not a simple reaction involving only H_2 and O_2, but also many intermediate species, this expression is only approximate.

A comparison of equation B-5 and observed laminar flame velocities at standard conditions for undiluted stoichiometric hydrogen and oxygen and for stoichiometric hydrogen in air under the same conditions would predict a laminar flame speed for air of 147 cm/sec, correcting for the change in adiabatic flame temperature and dilution. The observed laminar flame velocity for stoichiometric hydrogen in air ranges from 193 to 232 cm/sec with an average of 215 cm/sec (14). Thus equation B-5 predicts a laminar flame velocity of about 70% of the observed value.

If equation B-5 is used in conjunction with a constant correction factor of 1.46 (based upon the ratio of the observed versus the predicted laminar flame speed for air) one can probably predict the effect of dilution with steam with some reliability. Then

$$\frac{u'_a}{u_a} \cong 1.46 = \frac{\{[H_2]' \ [O_2]'\}^{\frac{1}{2}}}{\{[H_2] \ [O_2]\}^{\frac{1}{2}}} \qquad \text{(B-6)}$$

is an approximation of the dilution effect by decreased collision probability on adiabatic laminar flame velocity. The other effect of dilution, of course, occurs through its effect on adiabatic flame temperature, as seen in equation B-4.

So there are actually four corrections to make to the adiabatic flame velocity of undiluted hydrogen and oxygen at standard conditions to arrive at a predition of adiabatic flame velocity at elevated pressures with steam dilution.

a) the dilution effect due to decreased collision probability

b) the effect of a change in adiabatic flame temperature due to dilution

c) the effect of preheating

d) the effect of increased pressure

The effect of pressure on quenching distance is primarily a function of its effect on the term, $\rho_o u_a$, since according to Williams (13)

$$d \cong \frac{a \bar{k}_g}{\bar{c}_p \rho_o u_a} \qquad \text{(B-7)}$$

where d = quenching distance, ft (orμ)

a = a Peclet number based upon quenching distance and adiabatic flame velocity, about 40

$\bar{k}_g$ = average thermal conductivity of the premixed gases between the initial temperature and adiabatic flame temperature, Btu/hr ft°R

$\bar{c}_p$ = average specific heat of the premixed gases between the initial temperature and the adiabatic flame temperature, Btu/lbm°R

It is found that $\bar{k}_g$ and $\bar{c}_p$ are nearly independent of pressure.

Thus, as a first approximation, one may expect quenching distance to vary inversely with pressure. This effect becomes

more pronounced if in turn the pressure exponent, x, in equation B-3 is positive. Preheating the mixture, of course, may increase $\bar{k}_g$ and $\bar{c}_p$ slightly and will decrease ρ_o, but at the same time, u_a will increase. For reasonably small increases in temperature (preheat temperature <500°F) significant changes in quenching distance are not expected.

No data was found on the effect of large amounts of steam diluent in oxyhydrogen flames, but it is expected that steam will act in a way similar to nitrogen or carbon dioxide. Reference 14 states that, insofar as flammability limits are concerned, water vapor behaves approximately like carbon dioxide. Hence one may use charts of flammability limits of References 14 and 15, and, for nearly all mixtures of interest, it appears that there is no problem of flammability. Reference 14 indicates that the pressure effect on flammability limits should not be significant.

Mixing superheated steam at temperatures in excess of 600°F with stoichiometric hydrogen and oxygen at elevated pressures might be cause for concern with respect to spontaneous ignition. Although the rate equations are somewhat complicated for the hydrogen-oxygen reaction, if one ignores reactions at the wall, reference 14 predicts the following equation for ignition lag

$$\tau = c \, \frac{1}{e^{-E/RT} p^{2}} \left(1 - \frac{2k_2}{k_6 [M]}\right) \qquad \text{(B-8)}$$

where

τ = ignition lag, milliseconds

p = pressure in appropriate units

k_2, k_6 = reaction rate constants in the notation of Lewis and Von Elbe (16)

c = constant

[M] = concentration of all components of the mixture (molecules/cc)

The associated chemical reactions are as follows:

$$H + O_2 \xrightarrow{k_2} OH + O$$

$$H + O_2 + M \xrightarrow{k_6} HO_2 + M$$

Ignition lag has been found to depend upon the mole fraction of hydrogen in a mixture and not on the relative amounts of oxygen and inerts. Charts of ignition lag versus mole percent hydrogen at atmospheric pressure and a temperature of 649°C (Anagnostou's data shown in Reference 14), were used in conjunction with Lewis and Von Elbe's method (16) for calculating k_6 and k_2 to determine the constant, c, in equation B-8 for an air-hydrogen mixture. Subsequently, equation B-8 was used to calculate the ignition lag at a lower temperature of interest (440°F) and at 600 lbf/in^2 total pressure with a mixture of the following composition (mole fractions): hydrogen - .25, oxygen - .125, steam - .625. An ignition lag in excess of 50 hours was predicted. Reference 14 substantiates this finding. The data of Zabetakis on H_2 - water vapor-air mixture explosion hazards reports spontaneous ignition temperatures of 580°C for 30% water vapor at a pressure of 7.8

atmospheres. Hence it appears that spontaneous ignition should not be a problem.

The method of mixing the steam with the hydrogen and oxygen will be important and should be the subject of experimental work. Because of reported ignition of hydrogen in air by static electricity discharges, the steam should first be added at low velocities to only one of the two reactants, followed by the other reactant after sufficiently uniform mixing has occurred.

Design of a Selected Combustion Chamber

It is noteworthy that several basic differences exist in the operating conditions of the porous plug burners of Siegler and Moore and the high pressure combustion chamber investigated in this thesis. First, Siegler and Moore's burners operated with effectively unlimited coolant supply. In the proposed chamber, the coolant available is limited by the ratio of the mass flow rates of diluent (feed) water and the combustion products. This ratio is established by the desired turbine inlet temperature. While more diluent water at a cooler temperature could, of course, be provided, it would represent wasted energy with a consequent reduction of overall thermal efficiency of the power plant. Furthermore, under reduced power conditions, a plant with a regenerator will exhibit increased coolant inlet temperatures because of decreasing turbine efficiency, a condition common to gas turbine power plants. With a coolant inlet condition already near that of

the saturated liquid state at design conditions, it is probable that nucleate boiling will occur very near the entrance of the porous plug cooling coil under reduced power conditions. This situation virtually eliminates the possibility of any self-throttling feature as experienced in the burners of Siegler and Moore. Of course, with higher power level plants with high expander efficiencies, the coolant inlet temperature will be much lower since a regenerator will not be necessary.

Secondly, if the proposed combustion chamber requires dilution with steam, the effluent of the porous plug cooling coil must be superheated prior to mixing with the unburned hydrogen and oxygen, assumed to be at 75°F. This superheating would be necessary in order to produce steam which is at least saturated at its partial pressure in the premixed gases. Superheating the steam creates material problems with a superheating coil in a high temperature environment downstream of the porous plug combustion zone. Even the best high temperature nickel-based superalloys are operating at their limits at temperatures much in excess of 2000°F.

Another problem in the proposed combustion chamber is the tolerable heat flux established by Siegler and Moore (20 cal/cm^2 sec) and its corresponding flame velocity. For the effectively undiluted stoichiometric hydrogen-oxygen burners, operating at near atmospheric pressures, the flame velocity corresponding to this heat flux is about 20 cm/sec. As shown in subsequent paragraphs, the flame velocity in the high pressure burner is about 3-4 cm/sec. Thus the proposed

chamber operates very near the unstable flame speed limit previously mentioned (2-3 cm/sec). All of these factors, coupled with temperature limits on the porous plug material, combine to produce a more stringent design situation than that existing at normal pressures.

To determine the feasibility of a combustion chamber, certain assumptions must first be made. The chamber pressure selected was 600 $\mathrm{lbf/in^2}$, and an exit temperature of 1750°F was chosen on the basis of previous studies which had shown these values to be suitable for a high overall thermal efficiency.

A 50 kw design shaft power was selected with a capability, insofar as the combustion chamber is concerned, to operate indefinitely at power levels 25% in excess of design power. Table B-1 gives a summary of plant parameters for the combustion chamber feasibility design.

Several methods of burning the hydrogen and oxygen are available, from burning with no diluent steam to burning with all of the diluent water available in the premixed gases. Calculations showed that burning with no inert at 600 $\mathrm{lbf/in^2}$ and a flame temperature of 1300°K (the probable lowest flame temperature at which the flame will be stable) results in excessive heat flux to the porous plug, on the order of 6×10^6 $\mathrm{Btu/hr\ ft^2}$ (460 $\mathrm{cal/cm^2\ sec}$).

For this reason, the effect of various amounts of diluent steam in the unburned mixture were investigated and for each mixture the heat flux to the porous plug was calculated.

TABLE B-1

Summary of Design Conditions for Porous Plug Combustion Chamber Feasibility Design Study

Chamber exit pressure, lbf/in^2	600
Chamber exit temperature, °F	1750
Plant rated shaft power, kw.	50
Combustion chamber maximum power rating, kw.	62.5
Turbine efficiency	66%
Overall plant efficiency	31.5%
Recirculation ratio, ($\dot{m}$ diluent/$\dot{m}$ reactants)	3.18
Total chamber exit mass flow rate at 125% overload, lbm/hr.	427.0
Reactant feed rate at 125% overload lb/hr.	102.0
H_2.	11.35
O_2.	90.65
Feed water pressure (diluent) lbf/in^2.	800.
Feed water inlet temperature, °F	420.6
Porous plug cooling coil inside diameter, in	0.230
Porous plug cooling coil outside diameter, in.	0.250
Chamber inside diameter, in.	11.7

Because of the desirability of maintaining uniform heat flux and consequently uniform temperature at the exit plane of the porous plug, a cooling coil geometry in the form of a spiral of Archimedes was selected. The diluent water (feed water) would enter at the periphery of the plug (near the combustion chamber wall) and exit at the center as saturated steam (see Figure B-2). The superheating, it was concluded, would probably be best accomplished by use of a separate superheating coil downstream of the porous plug burner in the path of the hot combustion gases or imbedded in the combustion chamber wall. Superheat is necessary to produce a saturated steam condition in the premixed gases when the steam is added to 75°F hydrogen and oxygen.

Except for a short section of natural convection heating, the majority of the porous plug coil would exhibit local and bulk boiling. Figure B-3 is a graph of the lengthwise temperature distribution of a coil for the design conditions selected. Using the Jens and Lottes correlation (17) for nucleate flow boiling, it is seen that a uniform wall temperature exists throughout most of the coil.

At some flow less than the maximum flow rate, it is evident that the instability limit of flame velocity will be reached. Depending upon the mixture selected, the temperature of this occurrence may vary slightly. Calculations show, however, that a reduction in flame velocity (mass flow rate) of about 25% is possible before the flame stability limit is approached. This information is based upon an initial flame

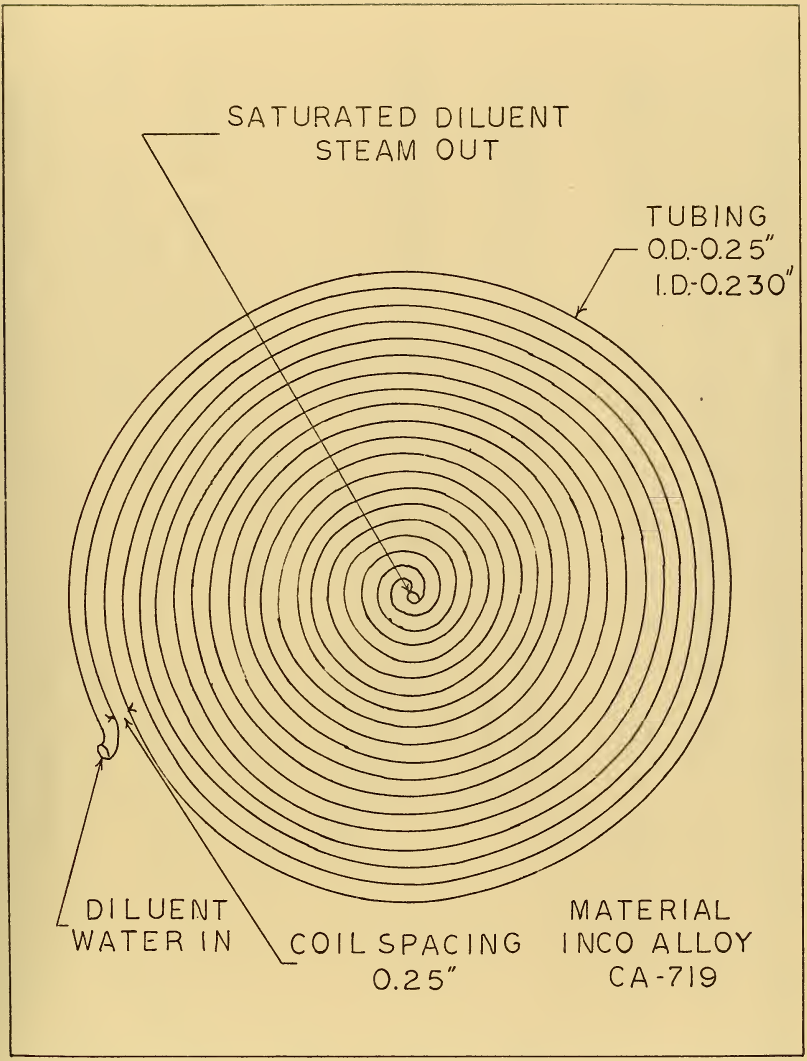

FIGURE B-2
COOLING COIL GEOMETRY

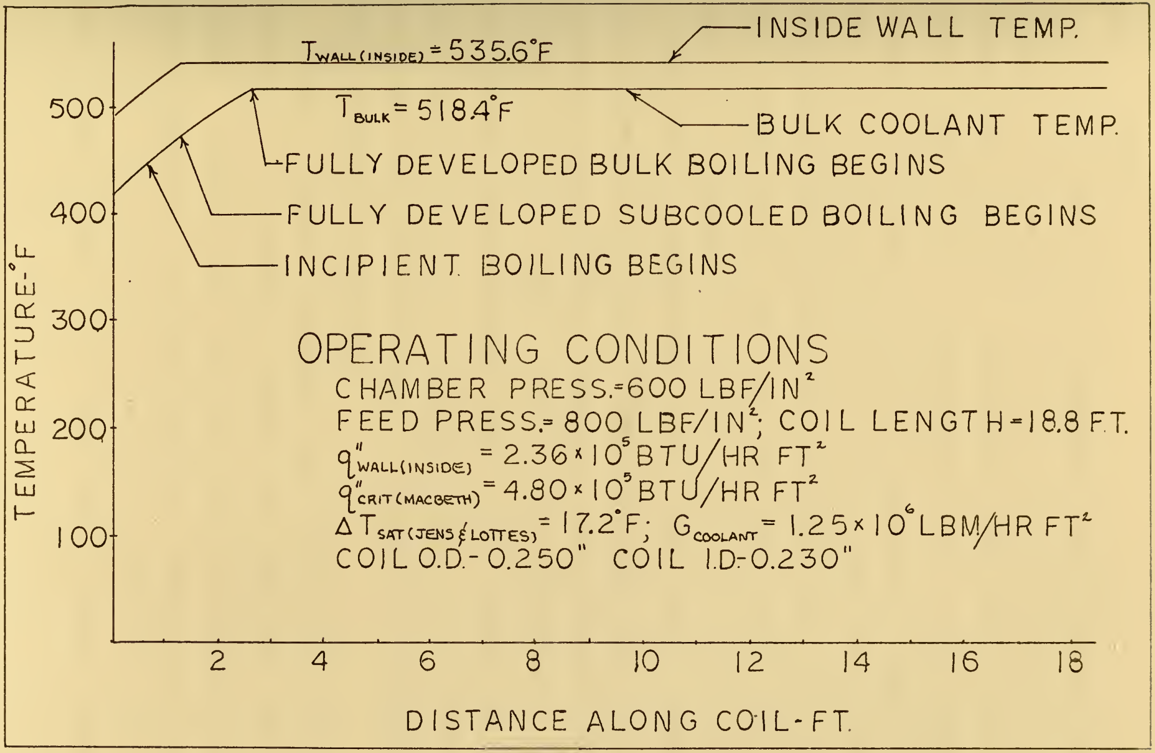

FIGURE B-3-LENGTHWISE TEMPERATURE DISTRIBUTION-COOLING COIL

temperature of 2000°F and a corresponding flame velocity of about 4.0 cm/sec.

In the calculation of temperature distributions within the plug, it was assumed, for the sake of simplicity, that uniform heat flux to the round coolant tube exists, i.e. wall thermal conductivity is sufficiently high to permit uniform heating of the coolant walls (on the upstream and downstream sides with respect to gas flow). Calculations for the design condition selected revealed that a uniform round tube heat flux is only slightly less than round tube critical heat flux predicted by MacBeth's correlation (17). Thus if the design is not carefully accomplished, partial film boiling may result with a consequent increase in tube wall temperature and a disruption of the uniform temperature distribution in the porous plug as well as an increase in plug exit temperature. Further calculations show that proper sizing of the cooling coil and proper spacing (sizing of the gap) of the spiral can adjust the operating conditions sufficiently to maintain an acceptable margin to critical heat flux.

Table B-2 shows calculated values of heat flux for several mixtures of stoichiometric hydrogen and oxygen with steam as the diluent. Laminar flame velocities have been corrected for flame temperature (including preheating) dilution and pressure. It is seen that the mixture temperature (including preheating) dilution and pressure. It is seen that the mixture temperature does not vary much from 440°F. The temperatures shown for the premixed gases correspond to saturation temperatures for the

TABLE B-2

Heat Flux to Burner Versus Unburned Mixture Composition

Mixture No.	Mole Fraction Steam Premixed	f**	Mixture Temperature °F	T_a °F/°K	T_f °F/°K	u_a cm/sec	u cm/sec	$\bar{c}_p(T_a-T_f)$ Btu/lb	q" Btu/hr ft^2 / cal/cm^2 sec	ρ_oV_o lb/hr ft^2
1*	.681	1.0	446.9	2480/1830	1840/1280	22.0	0.96	610.	$7.66\times10^4/5.76$	126.
2	.675	.975	445.9	2870/1850	1902/1310	25.8	1.79	621.	$1.44\times10^5/10.80$	235.
3	.650	.876	442.2	3035/1940	2008/1369	51.4	3.90	674.	$3.41\times10^5/25.6$	507.
4	.625	.788	439.9	3210/2040	2117/1430	82.3	6.75	726.	$6.28\times10^5/47.2$	865.
5	.600	.712	434.5	3390/2120	2250/1500	102.5	10.0	781.	$9.84\times10^5/74.0$	1272.
6	.575	.641	430.4	3552/2225	2357/1560	172.0	17.2	840.	$1.81\times10^6/136.0$	2160.
7	.550	.575	426.3	3740/2334	2412/1635	230.0	25.6	901.	$2.89\times10^6/217.0$	3210.
8	.525	.525	421.9	3872/2405	2580/1685	312.0	36.8	955.	$4.28\times10^6/323.0$	4490.
9	.500	.471	417.4	4060/2510	2722/1768	439.0	58.9	1020.	$7.28\times10^6/547.0$	7150

NOTES:

*This condition denotes all diluent water added to the unburned mixture

**Mass fraction of total diluent flow which is used for diluting the unburned gases

Assumed E = 48,000 cal/g mole

Total Pressure - 600 lbf/in^2

partial pressure of steam in the mixtures. Comparison of the laminar flame velocities predicted for these mixtures with those observed by Kaskan (1) for air and CO_2 "air" (nitrogen replaced by an equal fraction of CO_2) are favorable. A somewhat unexpected effect is the increase in heat rejected from the flame (the $\bar{c}_p$ $(T_a - T_f)$ term in equation B-1) with increasing T_f. This occurs because adiabatic flame temperature increases with decreasing amounts of diluent steam in the unburned mixture. Assuming that no flame temperature below 1300°K will maintain a stable flame and assuming that no heat fluxes in excess of 5×10^5 Btu/hr ft^2 (37.6 cal/cm^2 sec) can be absorbed, mixture 3 was selected for the feasibility design.

Calculation of the porous plug gas side pressure drop and axial temperature distribution requires an accurate assessment of quenching distance. Friedman's work (4) gives a method of predicting quenching distance but it is based on an ignition temperature, itself a somewhat fictitious quantity. His data does, however, show the effect of the addition of nitrogen to a stoichiometric hydrogen-oxygen mixture at one atmosphere. If an equivalent amount of nitrogen is calculated for hydrogen-oxygen-steam mixture 3 of Table B-2 (allowing for the preheating), one may predict a quenching distance of 1500μ at 1 atmosphere for a mole fraction of nitrogen of 0.71.

Ignoring a probable small temperature effect on quenching distance and noting that the ratio if $\bar{k}_g/\bar{c}_p$ for air and steam are not significantly different, one may conclude that the pressure effect on quenching distance alone is significant.

Hence a quenching distance of 37μ is a reasonable estimate for mixture 3. A 1.8μ pore size was selected as a conservative figure (possibly overconservative).

The temperature distribution within the plug is a function of heat flux, mass flux, porosity, plug thickness, material and coil placement. If a one-dimensional condition is assumed, the heat equation may be written in the axial direction,

$$G\, c_p \frac{dT}{dx} - \bar{k}_s \frac{d^2T}{dx^2} = 0 \qquad \text{(B-9)}$$

with the boundary conditions at the plane of the cooling coil placement.

If the plug is separated into two regions upstream of the plane of the cooling coils (I), and downstream of the cooling coils (II), the boundary conditions for region I, (see Figure B-4) become at the right hand boundary ($x = \ell_1$)

$$T(\ell_1)_I = T_1$$

$$q''(\ell_1)_I = -G\, \bar{c}_p (T(\ell_1) - T_o) = -\bar{k}_s \frac{dT}{dx} (\ell_1)_I$$

here it is assumed that the temperature of the gas and the porous plug temperature at any axial position, x, are equivalent and that axial conduction in the gas is negligible.

For region II, the boundary conditions are also known at the plane of the coolant tubes, where

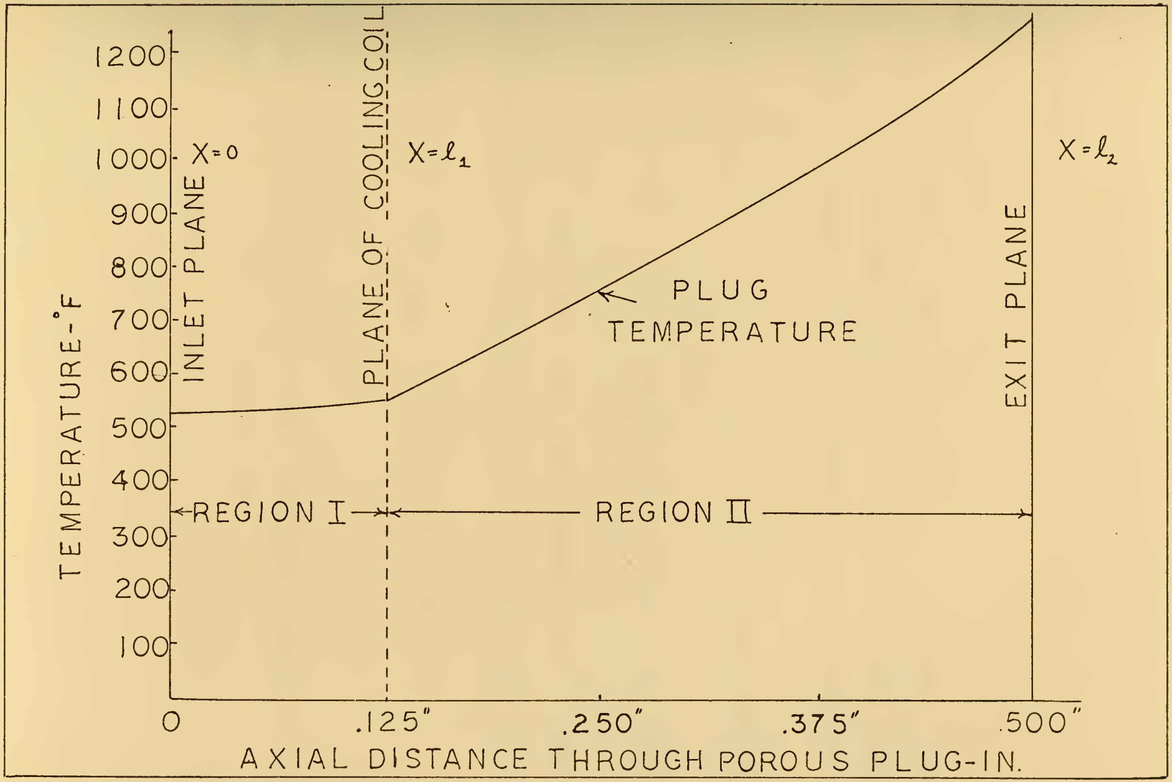

FIGURE B-4-AXIAL DISTRIBUTION OF PLUG TEMP.

$$T(\ell_1)_{II} = T(\ell_1)_I = T_1$$

$$q''(\ell_1)_{II} = q''(\ell_1)_I + q''_f$$

where

T_1 = the outside temperature of the coolant tube, assumed to be of zero thickness in the chamber axial direction

q''_f = the frontal heat flux absorbed by the porous plug, equation B-1

$\bar{c}_p$ = average gas mixture specific heat between inlet and exit for a given region

$\bar{k}_s$ = effective thermal conductivity of the porous plug

The actual heat flux at the exit plane of the burner ($x = \ell_2$) is that required to heat the premixed gases to the plug exit temperature plus the frontal heat flux, q''_f, i.e.

$$q''(\ell_2)_{II} = -G\,\bar{c}_{p,I\&II}\,(T(\ell_2)_{II} - T_o) + q''_f$$

recalling that q''_f is negative in sign.

The following conditions were assumed for the porous plug materials (data is that of Laverty (6)):

Material - carbonyl nickel power - INCO A(Typical analysis .1%C, .1% O_2, .001 S, .01 Fe)

Total porosity, % - 18.0

Open porosity, % - 15.9

Average pore size, - 1.8μ

Pore size range, ~0.5μ

Sintering temperature, °F - 1900°F (H_2 atmosphere)

Assumed thermal conductivity (fully dense), Btu/hr ft°R -
36.0

Assumed effective thermal conductivity, $\bar{k}_s$, Btu/hr ft°R -
18.0

Using this data, a plug exit temperature of 1290°F was calculated for a plug of thickness 3/8" downstream of the plane of the coolant tubes with a total thickness of 1/2".

The marked reduction of thermal conductivity of sintered materials predicted by reference 5 is corroborated by more detailed and recent work of Tye (18) and Koh and Fortini (19) for sintered stainless steel powders, "rigamesh" porous stainless steel, and sintered copper powders. This is also true for sintered porous nickel (20). For a total porosity of 20% a thermal conductivity of about 50% of the solid material is expected. Furthermore, the assumed thermal conductivity for pure nickel of the fully dense material is perhaps a little high for nickel powder. A value of 33.5 Btu/hr ft°R (20) is probably more representative of nickel powder in the temperature range of 500-1000°F.

Several pressure drop calculations were performed on the 1/2" plug, resulting in pressure drop predictions ranging from 30-1400 lbf/in^2. One pressure drop correlation used was that of Grootenhuis (21), which compared well with a correlation of Rose for packed beds of granular materials. Calculations using another correlation for packed beds (22), that of Ergun,

yielded a pressure drop about the same as by the method of Grootenhuis, about 1400 lbf/in^2. Another, more recent method (23) predicted a pressure drop of about 30 lbf/in^2, and this figure was verified as being reasonably accurate and representative of pressure drop in filtration at high pressures with filters of very small pore size for the design flow conditions (24). Certainly experimental work will be required to verify the pressure drop.

In the tradeoff of the effective thermal conductivity, pressure drop and pore size sufficiently small to prevent flashback, it may be possible to increase pore size to reduce pressure drop if necessary. Another possibility is to reduce the size of the coolant tubes, already desirable from the aspect of critical heat flux, and thereby reduce the thickness of the porous plug. This would result in a reduced plug exit temperature as well as a decreased pressure drop, dependent on plug thickness, of course, but also on exit temperature through gas viscosity. This would also benefit in reducing oxidation of the porous material. Siegler and Moore (3) used 1/8" OD, 0.020" wall thickness copper tubing for their application. Quenching distance studies must be performed with the design mixture of steam, hydrogen and oxygen to determine the maximum allowable pore size. Pressure drop studies of the sintered nickel and cooling tube compact must be performed to determine the actual pressure drop. The strength of the compact must also be determined in the proposed application.

In spite of the questionable character of the pressure

drop predictions, a preliminary design of the porous plug combustion chamber was performed. If the pressure drop can be kept at 100 lbf/in^2 or less, the burner could probably operate successfully.

The superheating arrangement of this chamber, located downstream of the porous plug, can be a very simple device, since the temperature difference between the bulk gas temperature and the maximum superheated steam temperature is over 1000°F. Table B-3 gives a complete description of the superheating coil arrangement. Several high temperature nickel-based alloys are suitable for the superheater tube material. An alternate superheating arrangement is placement of the superheating coil in the combustion chamber wall. Both arrangements are shown in Figure B-5.

After superheating, a certain fraction of the steam is mixed with the unburned hydrogen and oxygen upstream of the porous plug. The remainder of the steam is mixed with the combustion steam downstream of the superheating coil, reducing the combustion gas temperature to a final temperature of 1750°F.

Figure B-5 is a schematic diagram of the overall combustion chamber. Detailed arrangements to improve mixing in the premixed chamber and downstream burner will require experimentation. Throttling must be provided by sectioning the porous plug with one pilot section, probably centrally located, which will operate continuously. Each section of the porous plug is separated from the remaining sections by solid walls, and each section would have its own premixing chamber.

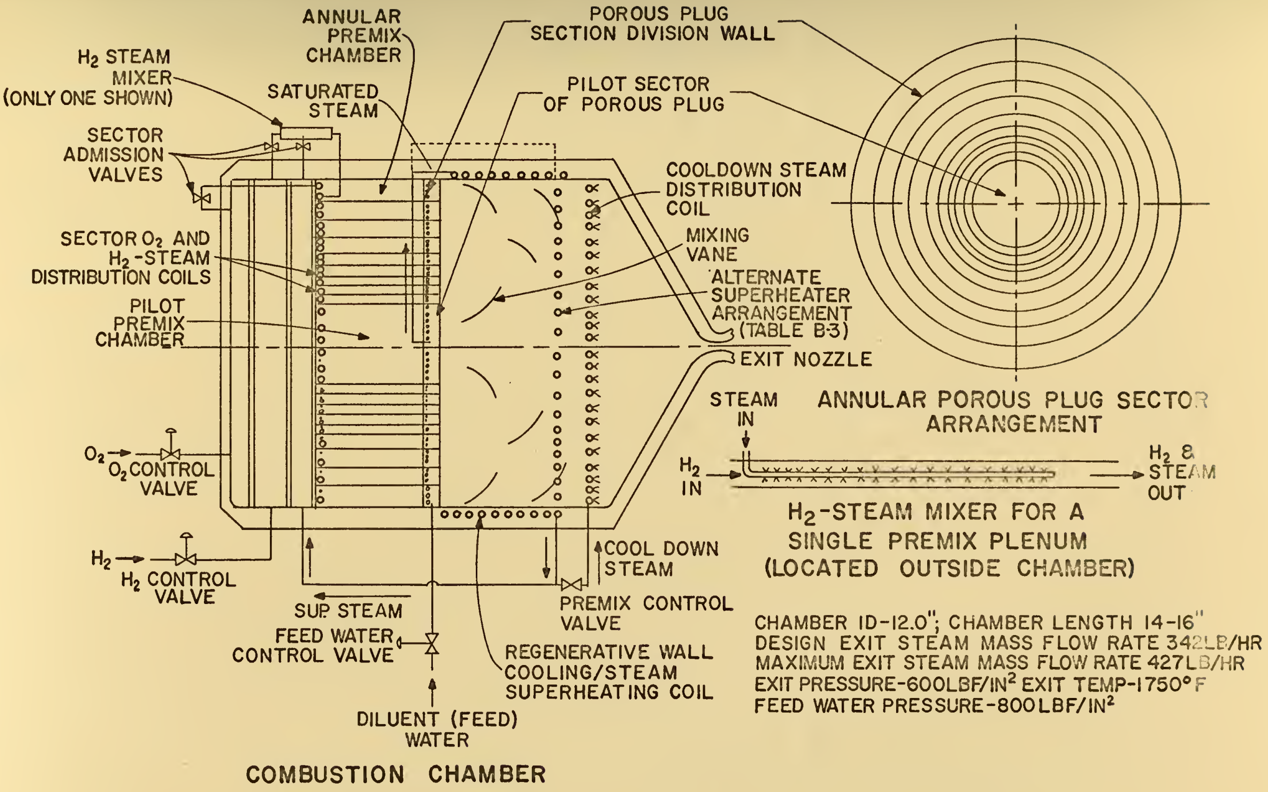

FIGURE B-5-POSSIBLE COMBUSTION CHAMBER

TABLE B-3

Superheating Coil

Arrangement	Spiral
Tube outside diameter, in.	.250
Tube inside diameter, in	.210
Tube spacing, center to center, in	.500"
Tube length, ft.	18.0
Gas side heat transfer coefficient h, Btu/hr ft^2 °F.	16.7
Gas temperature, °F.	2000°F
Steam inlet temperature, °F.	518.4
Steam outlet temperature, °F	620.0
Steam pressure	800.0

Startup of the chamber will require some diluent other than steam. If excess hydrogen is used, flammability limits will restrict flame temperature to no lower than 1940°F (24). This may limit turbine speed during the startup period, or require diluent water spray and discharge of the mixture to the condenser, bypassing the turbine during the startup sequence. Fortunately, Edse's work shows virtually no pressure effect on adiabatic laminar flame velocity with very rich mixtures of undiluted hydrogen and oxygen. The effect of pressure quenching distance then should only occur with the ρ_o term in equation B-7, and the pore size selected for the porous plug under normal operating conditions should be satisfactory in preventing flashback during the startup condition. Ignition may be provided by a spark plug or plugs suitably located or by some gas igniter such as that described for the liquid propellant rocket-type combustion chamber in Appendix A.

In the throttling process, starting at maximum flow rate, the entire burner would be throttled to 75% of its maximum mass flow rate, after which a section of the burner would be cut out as the flow to the remaining sections was increased to maximum in as smooth a transition as possible. Subsequent sections of the burner would then be cut out in the same way until the design minimum flow rate is achieved in the pilot section. It is estimated that about 9 such sections would be required to span the power range from 5 to 62.5 kw, assuming constant expander efficiency with mass flow rate. During the stepping process some incomplete combustion would probably occur.

Cooling steam to the section not in operation might be required to regulate the plug exit temperature at an acceptable value. Such cooling steam would require more thorough mixing downstream of the porous plug to produce a uniform chamber exit temperature. From a structural standpoint, the sectioning of the burner into several separate porous plugs would permit the use of thinner porous plugs than for one unsectioned plug for the entire burner.

Control of the combustion chamber exit conditions must be accomplished through sensing of several parameters:

1) Chamber pressure
2) Chamber exit temperature
3) Reactant and diluent (feed) water flow rates
4) Stoichiometry of any unreacted hydrogen and oxygen, probably best accomplished in the condenser

One may select hydrogen as a governing flow rate, adjusted by variation in combustion chamber pressure from some preset value, the design pressure. The oxygen flow rate would be coupled with the hydrogen flow rate, maintaining a stoichiometric ratio and operated with feedback from sensing devices in the condenser of the plant. Such sensing devices would determine any departure from stoichiometric conditions in the condenser, i.e., an excess of hydrogen or oxygen, allowing for other than 100% combustion efficiency. Combustion chamber exit temperature would be sensed by a thermocouple and would be compared to a preset signal providing feedback to a basic diluent water/hydrogen mass flow rate ratio. Stepping of the

burner area to produce throttling could be accomplished by coupling with the hydrogen flow rate. The maintenance of a constant dilution ratio of steam to hydrogen and oxygen in the premixed gases can be achieved by coupling premixed steam flow with the hydrogen flow rate.

Assessment

The porous plug burner with its low operating temperature, appears to be a possible alternative to undiluted stoichiometric burning in a rocket-type combustion chamber. Although the chamber outlet temperature selected for the feasibility design was fairly high, any desired lesser temperature could be achieved simply by the addition of increased amounts of diluent steam downstream of the superheating coil. This could be accomplished by an evaporating coil placed downstream of the porous plug in the stream of the combustion gases or in the chamber walls, since addition of the diluent as a water spray would unduly increase the size of the combustion chamber. The throttling problem is not simple but appears to be solvable.

The determination of quenching distance for the design hydrogen-oxygen-steam mixture is critical for the determination of pore size in the sintered material. Possible alternatives to reduce porous plug pressure drop while at the same time maintaining sufficient effective thermal conductivity should be explored. The exit temperature of the porous plug should be kept as low as possible to reduce possible plugging due to oxidization of the nickel. The use of other materials than

nickel does not seem possible since other materials do not possess a high resistance to oxidation and at the same time a reasonably satisfactory thermal conductivity. Copper would not be suitable for the proposed application because of its corrosion related temperature limitations. Silver would not be suitable for the same reason.

LIST OF SYMBOLS

d	quenching distance, ft or μ
E	activation energy for a chemical reaction Btu/lb mole or Kcal/g mole
c_p	specific heat, Btu/lbm°R
G	mass flux, lbm/hr ft^2
i	enthalpy, Btu/lbm
k_s	thermal conductivity of the porous plug material, Btu/hr ft°R
$\bar{k}_s$	effective porous plug thermal conductivity, Btu/hr ft°R
k_g	average thermal conductivity of the premixed gases, Btu/hr ft°R
k_2, k_6	reaction rate constants for the hydrogen-oxygen reaction in the notation of Lewis and Von Elbe
n	order of a chemical reaction
p	pressure, lbf/in^2
q''	heat flux, Btu/hr ft^2
q''_f	heat flux removed from the flame to lower the flame temperature from T_a to T_f (in excess of heat flux necessary to heat the incoming premixed gases)
R	Universal gas constant, 1.9860 Btu/°R lb mole or cal/°K-g mole
T	Temperature, °R or °K, as appropriate
u	flame velocity of the premixed gases
x	pressure exponent for adiabatic laminar flame velocity or axial distance through the porous plug, ft

y	distance of the flame front downstream of the porous plug, ft or cm
ρ	density, lbm/ft^3
τ	ignition lag, ms
χ	fraction of open area in a cross section of the plug material

SUBSCRIPTS

a	refers to adiabatic conditions
f	refers to actual flame conditions
o	refers to the unburned premixed condition upstream of the porous plug

REFERENCES

1. Kaskan, W.E., "The Dependence of Flame Temperature on Mass Burning Velocity", *Sixth Symposium on Combustion*, Baltimore, Md., 1957, The Williams and Wilkins Company, pp 134-143.

2. Botha, J.P. and D.B. Spalding, "The Laminar Flame Speed of Propane/Air Mixtures with Heat Extraction from the Flame", *Proceedings of the Royal Society*, A 225, 71, (1954).

3. Siegler, M. and G.E. Moore, "Flame Recombination of Oxygen and Hydrogen", *Chemical Engineering Progress Symposium Series*, Nuclear Engineering - Part XXI, Vol. 66, No. 104, 1970, pp 1-10.

4. Friedman, W.E., "The Quenching of Laminar Oxyhydrogen Flames by Solid Surfaces", *Third Symposium (International) on Combustion*, Baltimore, The Williams and Wilkins Co., 1949, pp 110-120.

5. Grootenhuis, P., R.W. Powell, and R.P. Tye, "Thermal and Electrical Conductivity of Porous Metals Made by Powder Metallurgy Methods", *The Proceedings of the Physical Society*, Vol. 65, Section B. (1952), pp 502-511.

6. Laverty, David P., Brunswick Corporation, Needham Laboratories, Needham, Massachusetts, Private Communication, November, 1971.

7. Moore, G.E., Manager Combustion Applications Projects, General Electric Research and Development Center, Schenectady, New York, personal communication, May 8, 1972.

8. Moore, George E., *Heat Flux to Porous Plug Burners*, General Electric Research and Development Center Report No. 66-C-440, Schenectady, New York, November 1966.

9. Moore, George E., *A Novel and Useful Burner for Premixed Gases*, General Electric Research and Development Center, Schenectady, New York, January 1970.

10. Wohl, K., "Quenching, Flash-back, Blow-off Theory and Experiment", *Fourth Symposium (International) on Combustion*, Baltimore, The Williams and Wilkins Company, 1953, pp 68-89.

11. Edse, Rudolph, "Studies on Bunsen Burner Flames at High Pressures with Hydrogen-Oxygen Mixtures", *Proceedings of the Second Midwestern Conference on Fluid Mechanics*, 1952, The Ohio State University, The Engineering Experiment Station, Bulletin #149, pp 441-457.

12. Manton, John and B.B. Milliken, "Study of Pressure Dependence of Burning Velocity by the Spherical Vessel Method", *Proceedings of the Gas Dynamics Symposium on Aerothermochemistry*, Northwestern University, 1956, Evanston, Illinois, pp 151-157.

13. Williams, Forman A., *Combustion Theory*, New York, Addison-Wesley Publishing Company, 1965.

14. Drell, Isadore L. and F.E. Belles, *Survey of Hydrogen Combustion Properties*, NACA Report 1383, 1958.

15. Zabetakis, Michael G., *Flammability Characteristics of Combustible Gases and Vapors*, U.S. Bureau of Mines Bulletin #627, 1965.

16. Lewis, Bernard, and G. VonElbe, Combustion, *Flames and Explosions of Gases*, New York, Academic Press, 1961.

17. Tong, L.S., *Boiling Heat Transfer and Two Phase Flow*, New York, John Wiley and Sons, Inc., 1965.

18. Tye, R.P., *Interim Report, An Experimental Investigation of the Thermal Conductivity and Electrical Resistivity of Three Porous 304 L Stainless Steel "Rigamesh" Materials to 1300°K*, Dynatech Corporation, NASA CR-72710, August 27, 1970.

19. Koh, J.C.Y. and A. Fortini, *Topical Report, Thermal Conductivity and Electrical Resistivity of Porous Material*, NASA CR-120854, October, 1971.

20. Touloukian, Y.S., *Thermophysical Properties of Matter*, Vol. 1, *Thermal Conductivity of Metals and Alloys*, Purdue Research Foundation, New York, IFI/Plenum Data Corporation, 1970.

21. Grootenhuis, P., "The Flow of Gases Through Porous Metal Compacts", *Engineering*, Vol. 167, pp 291-292 (April 1, 1949).

22. Rohsenow, W.M. and H. Choi, *Heat Mass and Momentum Transfer*, Englewood Cliffs, New Jersey, Prentice-Hall, 1961.

23. Bernicker, R.P., "An Investigation of Porous Wall Cooling", ASME Paper No. 60-WA-233, presented at the ASME Winter Annual Meeting, New York, New York, 1960.

24. Stevens, D., Pall Trinity Micro Corporation, Cortland, New York, personal communication, May 11, 1972.

25. Bailey, R.N., "Development of Catalytic Hydrogen-Oxygen Reaction Chambers for Space Power Systems", *Space Power Systems, Progress in Astronautics and Rocketry*, Vol. 4, Ed., N.W. Snyder, New York, Academic Press, pp 183-210.

APPENDIX C

Re-Entry Turbine Analysis

General

The single disk, axial impulse, multistage re-entry turbine has many of the attributes of the axial impulse partial admission turbine, but generally has higher efficiencies at lower specific speeds. Figure C-1 is a schematic diagram of such a turbine. Its inherent simplicity (a single disk) often makes it preferable to a series of partial admission stages. Its major disadvantage is interstage leakage which can at best be minimized. As might be expected, the impact of this leakage is worse for turbines with smaller blade heights, simply because the tip and axial clearances cannot be set or reliably maintained at values much less than .004-.005". The effect of leakage on efficiency is to lower the efficiency without leakage, by a multiplicative factor. This factor may be simply defined as the mass flow rate which actually does work to the total mass flow rate passing through the multistage device.

The losses, other than normal turbine nozzle and blade losses, of re-entry turbines are summarized below. Many of these losses are common to partial admission turbines. The terminology is that of Baljé, Linhardt and Silvern (1), (2), and (3).

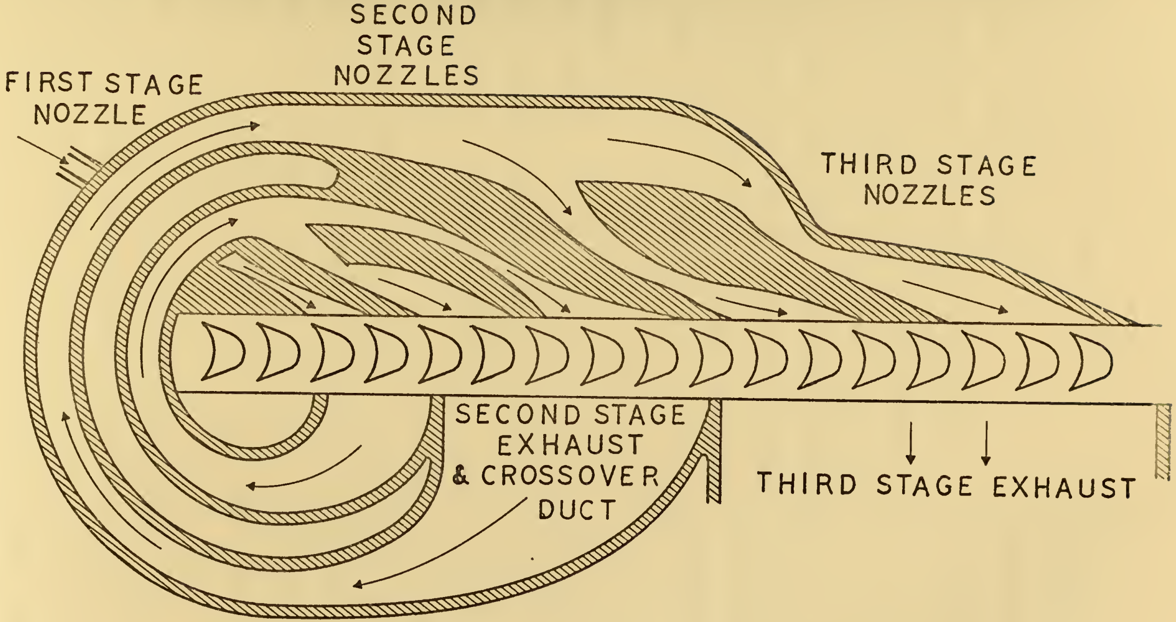

FIGURE C-I CUTAWAY SCHEMATIC DIAGRAM OF A THREE STAGE RE-ENTRY TURBINE WITH CROSSOVER DUCTS

a) Scavenging losses (the pumping and mixing loss of Stenning (4))	Common to partial admission turbines
b) Disc friction losses	
c) Blade pumping losses	
d) Tip leakage losses	
e) Effective reduction of the rotor velocity coefficient by Stenning's filling and emptying loss factor (4)	
f) A speed dependent, "dynamic", leakage	Unique to re-entry turbines
g) Interstage leakage composed of radial, tangential and tip leakage components	
h) Return duct losses	

Previous Work

Baljé and Silvern (5) published a preliminary analysis of multistage axial impulse re-entry turbines in 1958. This work was summarized in a classical paper on turbine optimization published by Baljé (1) in 1962. A two-stage, 300:1 pressure ratio, re-entry turbine was built and tested by Sundstrand Corporation (6) and the results published in the open literature by Linhardt and Silvern (3). An extension of the analysis developed in the design of the two-stage turbine was published by Linhardt (2) in 1962.

References 2 and 3 provided a good approach to the analysis of interstage leakage but neglected interstage leakage through gaps on the the downstream side of the rotor. Baljé (7) states that the leakage assessments of the earlier papers cited were

optimistic and that the leakage occurring is in fact quite complicated.

The optimum pressure ratio split for the individual stages is not easily analyzed. Linhardt (6) approached this problem by a design analysis for two cases, that of equal isentropic work per stage and that of equal pressure ratio. He found that the equal pressure ratio case afforded a significant improvement in efficiency (~ten efficiency points over a wide range of specific speed) for a two-stage re-entry turbine.

Re-entry duct losses were also analyzed in reference 6 and compared with experimental results. For the re-entry duct geometry utilized (see Figure C-2), the duct pressure loss was found to be less than is commonly assumed (1), i.e. that the dynamic head of the previous stage is completely lost in wall friction and turning.

There does not seem to be much information on re-entry turbines of more than two stages which have actually been built. Only one four-stage machine was found in the literature (8). Baljé (7) is unaware of any re-entry turbines of three or more stages which have been built using the design method developed by him and his colleagues.

Reference 8 reports a four-stage axial impulse re-entry turbine of unequal pressure ratios, with an overall pressure ratio of 55.7 and a speed of 24,000 rpm. In a probable attempt to reduce the interstage leakage from the first stage, the first stage pressure ratio was 4.51 compared to pressure ratios of 2.17, 1.83, and 3.14 for the second, third and fourth stages

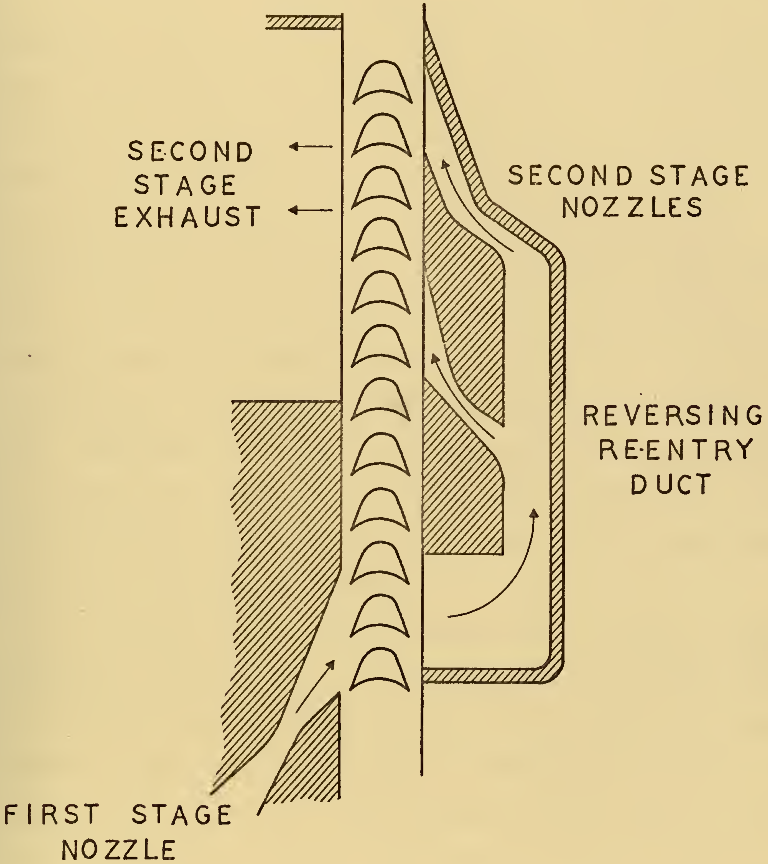

FIGURE C-2 CUTAWAY SCHEMATIC DIAGRAM OF A TWO STAGE RE-ENTRY TURBINE WITH ALTERNATE ADMISSION

respectively. The high pressure ratio fourth stage may have been an attempt to reduce Reynolds number losses in the last stage. The design point total to static efficiency achieved was 0.432 for the 1/8" blade height machine in comparison to the predicted efficiency of .52. The analysis of the design showed an appreciation for interstage leakage but apparently was done without the knowledge of Baljé's work. As might be expected from the high first stage pressure ratio, a supersonic relative inlet velocity to the rotor was experienced there, while that of the second, third, and fourth stages was subsonic. This design approach apparently was used in an attempt to reduce the static pressure in the first stage rotor cavity and hence interstage leakage into subsequent stages. However, the predicted interstage leakage as seen by the first stage analysis obviously does not take into account the significant tangential leakage on the inlet side of the rotor described first in references 5 and 6.

It is apparent from Baljé's analysis and the test results of reference 8 that there is a trade-off due to reduced efficiency because of partial admission filling and emptying losses and reduced stage flow rate because of interstage leakage. It is noted as well, that the blade design of this turbine could probably be improved, and that elimination of the supersonic first stage conditions would probably improve the overall total to static efficiency. A significant cause of the low efficiency of this machine is its small blade height and relatively large clearances resulting in large values of tip and interstage leakage.

Design Analysis

With the assumption that a turbine with equal pressure ratios for each stage represents a good design, although perhaps not the optimum pressure split, one may use the basic analysis of Linhardt (2) to design a multistage turbine. Certain of Linhardt's assumptions must, however, be reconsidered and refined, particularly those involving interstage leakage. One might simply present in this thesis only the refinements made to Linhardt's analysis. But in the interest of clarity and continuity, Linhardt's equations are included as well.

In the terminology of Baljé and Linhardt specific speed, N_s is defined as

$$N_s = \frac{N\sqrt{Q_3}}{H_{ad}^{\frac{3}{4}}} \qquad \text{(C-1)}$$

where N = speed in rpm,

Q_3 = exit volume flow rate, ft^3/sec,

and H_{ad} = isentropic total to static head, ft lbf/lbm,

and specific diameter, D_s, another similarity parameter introduced by Baljé, is defined as

$$D_s = \frac{D\ H_{ad}^{\frac{1}{4}}}{\sqrt{Q_3}} \qquad \text{(C-2)}$$

where D = overall diameter of the rotor including blades (tip to tip).

A ratio of blade speed to isentropic "spouting" velocity, c_o, may be then determined from equations C-1 and C-2 as

$$\frac{u}{c_o} = \frac{N_s D_s}{154} \tag{C-3}$$

where $c_o = \sqrt{2g_c H_{ad}}$.

The ratio of the arcs of admissions of the various stages may be obtained from the assumption of equal pressure ratios and an assumed polytropic exponent, λ, related to the polytropic efficiency, η_p, by the equation

$$\lambda = \frac{k}{1-(1-\eta_p)(k-1)} \ . \tag{C-4}$$

The polytropic efficiency is related to the isentropic efficiency by the relation

$$\eta_p \cong \frac{k}{1-k}\, \ell n \frac{\{1-\eta_{T-S}[1-(\frac{1}{Pr_o})^{\frac{k-1}{k}}]\}}{\ell n\ Pr_o} \tag{C-5}$$

where k = ratio of specific heats,

η_p = the polytropic or small stage efficiency, assumed constant for all stages,

η_{T-S} = total to static isentropic efficiency for the turbine,

and Pr_o = the overall total to static pressure ratio for the turbine.

Then the ratio of the density of the fluid entering the m^{th} stage to the density corresponding to the total pressure entering the first stage is

$$\frac{\rho_m}{\rho_{0,1}} = (\frac{p_m}{p_{0,1}})^{1/\lambda}, \qquad \text{(C-6)}$$

and the ratio lengths of the arcs of admission (a_1, a_2, etc.) become

$$\frac{a_1}{a_m} = (\frac{p_m}{p_{0,1}})^{1/\lambda} = Pr_o^{-(\frac{m-1}{n\lambda})}, \qquad \text{(C-7)}$$

neglecting interstage leakage. Another useful relationship is the area ratio for a nozzle, A/A^*,

$$\frac{A}{A^*} = [(\frac{2}{k+1})^{\frac{k+1}{k-1}} (\frac{k-1}{2})]^{\frac{1}{2}} / [Pr_o^{-\frac{2}{n\lambda}} - Pr_o^{-(\frac{k+1}{kn})}]^{\frac{1}{2}} \qquad \text{(C-8)}$$

where A = the exit area of a nozzle,

A^* = the related throat area,

and n = the number of stages.

The stage temperature ratio can be conveniently represented by the relation,

$$\frac{T_m}{T_{m-1}} = 1 - \eta_p \, [1-(\frac{1}{Pr_i})^{\frac{k-1}{k}}], \qquad \text{(C-9)}$$

where T_m = the inlet total temperature to stage m

and T_{m-1} = the inlet total temperature to stage m-1.

$$Pr_i = Pr_o^{1/n}$$

Here the exit static temperature of a stage and the exit total temperature are assumed equivalent.

The ratio of the blade speed to the mean spouting velocity, $u/\bar{c}_o$, may be evaluated by considering the relation

$$\frac{\bar{c}_o}{c_o} = \frac{1}{n} \sum_{m=1}^{n} \frac{c_{o,m}}{c_o}, \qquad \text{(C-10)}$$

where

c_o = the overall spouting velocity, corresponding to the overall pressure ratio,

$\bar{c}_o$ = the mean spouting velocity for the individual stages,

and $c_{o,m}$ = the spouting velocity for the m^{th} stage.

Two convenient definitions of terms are

$$y_o = 1 - \left(\frac{1}{Pr_o}\right)^{\frac{k-1}{k}} \qquad \text{(C-11)}$$

and

$$y_i = 1 - \left(\frac{1}{Pr_i}\right)^{\frac{k-1}{k}} \qquad \text{(C-12)}$$

Now, using equations C-9 through C-12 in conjunction with the well known isentropic flow relationship

$$c_o = \sqrt{2g_c p_o v_o \frac{k}{k-1}\left(1-\left(\frac{1}{Pr_o}\right)^{\frac{k-1}{k}}\right)} \qquad \text{(C-13)}$$

and

$$c_{o,m} = \sqrt{2g_c p_{m-1} v_{m-1} \frac{k}{k-1}\left(1-\left(\frac{1}{Pr_i}\right)^{\frac{k-1}{k}}\right)}, \qquad \text{(C-14)}$$

where p_{m-1} and v_{m-1} represent total inlet pressure and specific volume to the m^{th} stage (assumed equivalent with static exit conditions of the previous stage). Noting the following

relationship,

$$\frac{T_{m-1}}{T_{1,0}} = \left(\frac{T_m}{T_{m-1}}\right)^{m-1}, \qquad \text{(C-15)}$$

one may then derive the equation below through use of the geometric series formula:

$$\frac{\bar{c}_o}{c_o} = \frac{1}{n}\left(\frac{y_i}{y_o}\right)^{\frac{1}{2}} \sum_{m=1}^{n} \left(\frac{T_m}{T_{m-1}}\right)^{\frac{m-1}{2}} = \frac{1}{n}\left(\frac{y_i}{y_o}\right)^{\frac{1}{2}} \left[\frac{1-(1-\eta_p y_i)^{n/2}}{1-(1-\eta_p y_i)^{\frac{1}{2}}}\right] = \frac{1}{n}\,\bar{y}^{-1}, \qquad \text{(C-16)}$$

where

$$\bar{y} = \left\{\left(\frac{y_i}{y_o}\right)^{\frac{1}{2}} \left[\frac{1-(1-\eta_p y_i)^{n/2}}{1-(1-\eta_p y_i)^{\frac{1}{2}}}\right]\right\}^{-1}. \qquad \text{(C-17)}$$

Then the ratio of blade speed to average spouting velocity for a re-entry turbine with equal pressure ratio in each stage is as follows:

$$\frac{u}{\bar{c}_o} = \frac{u}{c_o} \cdot \frac{c_o}{\bar{c}_o} = n\,\frac{u}{c_o}\,\bar{y}\ . \qquad \text{(C-18)}$$

This ratio of blade speed may then be introduced into the expression for hydraulic efficiency developed by Baljé (1) for partial admission turbines, using the velocity diagram convention in Figure C-3.

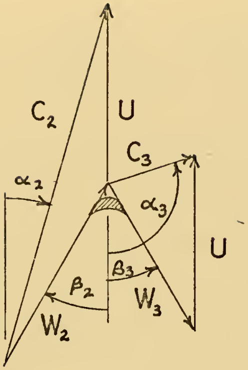

FIGURE C-3

Velocity Diagram

Hydraulic efficiency, η_h, is the total to static efficiency neglecting leakage, disk friction and partial admission losses other than Stenning's filling and emptying loss factor.

$$\eta_h = 2\frac{u}{\bar{c}_o}\left\{1+\psi_R\left(1-\frac{t}{2a_1 n}\sum_{m=1}^{n}\frac{a_1}{a_m}\right)\right\}\left\{\psi_N \cos\alpha_2 - \frac{u}{\bar{c}_o}\right\} \qquad \text{(C-19)}$$

ψ_R = rotor velocity coefficient w_3/w_2 (Figure C-3)

$\psi_R = [1-0.228(1-\beta_2/90)^3][1-0.06\ C/h][1-0.12(M_{w2} - 1.)^{1.5}]$

ψ_N = nozzle velocity coefficient, $c_2/\bar{c}_o$

M_{w2} = relative Mach number of the jet entering the rotor blading

h = blade height

C = blade chord

$\beta_2 = \mathrm{Cot}^{-1}\ [\mathrm{Cot}\alpha_2 - \frac{N_s D_s}{154\psi_N \mathrm{Sin}\alpha_2}\ n\bar{y}]$

The first term in the expression for rotor velocity coefficient is effectively a fit of the blade loss factor of Soderberg and others (Figure 3.13 of reference 9). The second factor corrects for aspect ratio and the third for Mach number losses when the inlet Mach number of the fluid relative to rotor blades exceeds unity.

The term, $(1 - \frac{t}{2a_1 n} \sum_{m=1}^{n} \frac{a_1}{a_m})$, in equation C-19 is the filling and emptying loss factor of Stenning (4) modified to include the ratio of blade pitch, t, to twice the average arc of admission for the n stage turbine. It is noteworthy that the term, (1-t/2a), is not quite in agreement with Stenning's analysis, where he predicted the factor to be (1-t/3a). Baljé (5) states that the larger loss is in agreement with test data.

Equation C-19 must now be modified by the other partial admission losses and re-entry losses. These are applied in two ways. First those which involve leakage are assumed to be mutually independent and are applied as deductions to the power developed by use of a mass flow rate deficit. Thus the hydraulic efficiency, equation C-19, is multiplied by a factor

$$(1-\bar{\zeta}_{L,rad} - \bar{\zeta}_{L,tan} - \zeta_{L,tip} - \zeta_{L,dyn}) \qquad \text{(C-20)}$$

and the ratio of actual power developed to ideal power available is

$$\eta_h \, (1- \overline{\zeta}_{L,rad} - \overline{\zeta}_{L,tan} - \zeta_{L,tip} - \zeta_{L,dyn}) \qquad \text{(C-21)}$$

This factor indicates the fraction of total mass flow rate seen by the turbine rotor which actually does work. The separate leakage factors are explained in detail in subsequent paragraphs.

The second correction factor, common to all partial admission turbines, represents the power developed in the turbine which is dissipated in doing work other than shaft work. Thus these factors represent power losses which are subtracted from the power developed to give the resultant shaft power.

The turbine total to static efficiency then becomes as follows:

$$\eta_{T-S} = \eta_h (1- \overline{\zeta}_{L,rad} - \overline{\zeta}_{L,tan} - \zeta_{L,tip} - \zeta_{L,dyn}) - \zeta_D - \zeta_P - \zeta_{SC} \qquad \text{(C-22)}$$

where ζ_D = a disk friction factor; the portion of the power developed which is dissipated in disk friction

ζ_P = a blade pumping loss, first described by Stodola (10)

ζ_{SC} = scavenging loss coefficient, due to mixing of the high velocity steam with stagnant fluid trapped in the blade passages.

The disk friction coefficient includes the effect of spacing of the disk and the surrounding walls (diaphragms) and the Reynolds number dependence due to disk diameter and local fluid conditions (5). The blade pumping coefficient

represents power dissipated by drawing of the stagnant fluid in the rotor cavity into the blade passages in the sector of the blading which is not active (unadmitted arc). The scavenging loss, analyzed by Stenning (4), is simply the fraction of work done on the rotor which must be expended to pump out stagnant fluid in a blade passage as the blade passage enters the active region.

The derivation of the equations for disk friction blade pumping, and scavenging is discussed in references (2), (4), (5), and (10). In the terminology of reference (2), they are presented below:

$$\zeta_{SC} = \frac{1.4\chi \; C/D \; (\frac{N_s D_s}{154})^3}{a_1/D \; \psi_N \; \mathrm{Sin}\alpha_2} \; (\frac{y_o}{y_i})^{\frac{3}{2}} \; [\frac{1-(1-\eta_p \; y_i)^{\frac{3}{2}}}{1-(1-\eta_p \; y_i)^{3n/2}}] \; \Pi_{\lambda,1} \qquad \text{(C-23)}$$

where

$$\Pi_{\lambda,1} = \sum_{m=1}^{n} \frac{a_m}{a_1} = \frac{1-Pr_o^{-1/\lambda}}{1-Pr_o^{-1/n\lambda}},$$

χ = blade density factor, usually about 0.6;

$$\zeta_P = 2K_p\sqrt{2g_c} \; (\frac{N_s D_s}{154})^3 (\frac{h}{D})^2 \; [1-\frac{a_1}{\pi D} \; \Pi_{\lambda,3}], \qquad \text{(C-24)}$$

where

K_p = a pumping loss coefficient, $1.4 - 2.9 \times 10^{-3}$

and $\Pi_{\lambda,3} = (Pr_o^{1/\lambda} - 1)/(Pr_o^{1/n\lambda} - 1)$;

and

$$\zeta_D = 1.25K_D\sqrt{2g_c} \quad D_s^2 \; (\frac{N_s D_s}{154})^3 , \qquad \text{(C-25)}$$

where

K_D = disk friction coefficient, a function of Reynolds number based on disk diameter and fluid conditions in the rotor cavity, given in references 1 and 5.

Leakage Losses

There are several paths which the working fluid may take in an axial impulse re-entry turbine other than through the rotor blading. Some of these paths will result in a complete loss of the working fluid. In other instances the path may be such that only one or more of the several stages will be affected by the leakage.

Tip leakage, present as well in full admission and partial admission turbines, is fairly well understood and is predictable. In the re-entry turbine, however, tip leakage may short circuit a particular stage.

A diagram of the possible leakage paths in a re-entry turbine using the cross-over duct geometry is shown in Figure C-4.

In addition to the leakage paths shown in the figure is a speed dependent, dynamic leakage. Dynamic leakage is caused by that volume of fluid which enters the blade passage yet which is prevented from leaving the blade passage in the normal manner through the re-entry duct simply because the blade moves into the sector of admission for the succeeding stage. Earlier analyses (2), (3), (6), neglect any work done by this leakage.

Baljé (7) estimates that one half of this leakage actually accomplishes work. In the analysis used in this thesis, it was assumed that no work was performed by dynamic leakage, which is conservative.

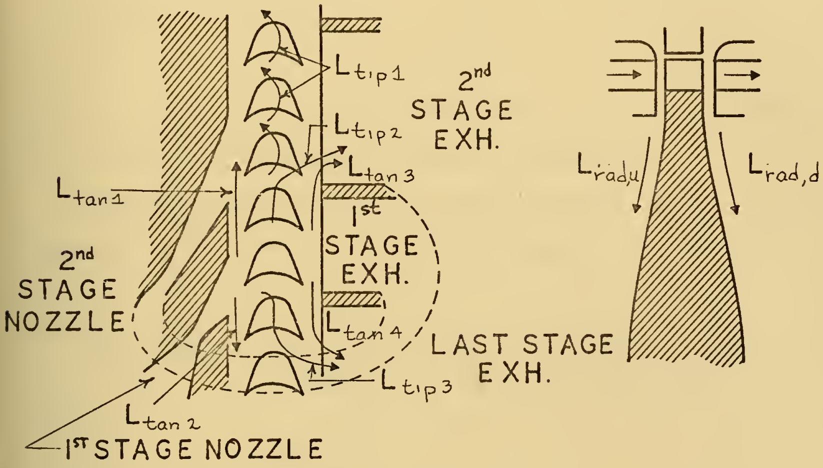

FIGURE C-4

Leakage Paths

Radial leakage may occur through the gaps on either side of the rotor. A notable discrepancy in the analyses of references 2, 3, and 6 is a failure to include leakage on the downstream side. It is evident that no accurate leakage assessment may be obtained without inclusion of leakage paths on both the inlet and exit sides of the rotor.

In assessing the radial leakage on the upstream side of the rotor, it is easiest to look first at the leakage experienced by the first stage. Assuming choked flow conditions

between stages, the ratio of the leakage flow to the inlet flow to the turbine, $\dot{m}_1$, may be expressed through use of the choked flow relation

$$\frac{\dot{m}\sqrt{RT_o}}{P_o A^*} = \text{constant} \qquad \text{(C-26)}$$

where P_o, T_o refer to total conditions and A^* is the area of the leakage gap or nozzle throat as applicable.

Using equation C-26, the radial leakage factor for leakage upstream of the rotor in the first stage is as follows:

$$\frac{\dot{m}_{\ell,rad,u,1}}{\dot{m}_1} = \frac{c_{f,r}\ s_1 p_{st,1}\ a_1}{a_{th} p_{0,1}} = \frac{c_{f,r}\ s_1 Pr_o^{-1/n}\ a_1}{h\ a_1\ \mathrm{Sin}\alpha_2\ A^*/A} =$$

$$\frac{c_{f,r}\ s_1/D\ Pr_o^{-1/n}\ A/A^*}{h/D\ \mathrm{Sin}\alpha_2} = K_1\ , \qquad \text{(C-27)}$$

where

$\dot{m}_{\ell,rad,u,1}$ = leakage mass flow rate in the radial direction, upstream of the rotor, in the 1st stage,

a_{th} = the nozzle throat area,

s_1 = the radial leakage gap upstream of the rotor,

$p_{0,1}$ = total pressure entering the first stage,

$p_{st,1}$ = static pressure in the first stage cavity,

n = number of stages,

and $c_{f,r}$ = a radial restriction factor which can be adjusted to a value of ~1/3 with proper seal geometry (2).

Here it is assumed that static pressure in the first stage rotor cavity is roughly equivalent to the total pressure in the leakage gap and that the total temperature existing in the leakage gap is equal to the total temperature at the inlet to the stage. This is contrary to the assumption of references 2, 3, and 6 which state that the stage exit static temperature exists at this point. This, however, is a small discrepancy since the interstage temperature ratio is nearly unity for reasonable stage pressure ratios.

It may be shown as well that the radial leakage on the upstream side of the rotor for the second stage is related to the mass flow through the nozzle of the second stage by the same factor, K_1. Yet when the leakage is compared to the total inlet flow rate, the ratio may be shown to be

$$\frac{\dot{m}_{\ell,rad,u,2}}{\dot{m}_1} = K_1(1-K_1). \qquad \text{(C-28)}$$

The total leakage seen by the second stage is the sum of that lost in the first stage and second stage. Thus the second stage experiences a total leakage factor of

$$\frac{\dot{m}_{\ell,rad,u,1} + \dot{m}_{\ell,rad,u,2}}{\dot{m}_1} = K_1 + K_1(1-K_1). \qquad \text{(C-29)}$$

Since there is no leakage from the n^{th} stage itself, the n^{th} and $(n-1)^{th}$ stages see a total leakage factor of

$$K_1 + K_1(1-K_1) + K_1(1-K_1)^2 + \ldots\ldots + K_1(1-K_1)^{n-2} \qquad \text{(C-30)}$$

By use of the geometric series formula, the average radial leakage factor for all n stages, for leakage upstream of the rotor, may be shown to be

$$\bar{\zeta}_{L,rad,u} = \frac{1}{n}\{n+1+\frac{1}{K_1}[(1-2K_1)(1-K_1)^{n-1} -1]\} \qquad \text{(C-31)}$$

On the downstream side of the rotor, the analysis is similar, except that a factor for stage temperature ratio must be introduced into equation C-27. Additionally, it should be noted that the leakage here occurs after it has done work in the first stage. Thus the first stage is unaffected by radial leakage at the exit side of the rotor. The last stage again experiences no radial leakage of its own but sees a mass flow rate deficit due to leakage in preceding stages.

$$\zeta_{L,rad,d,2} = \frac{\dot{m}_{\ell,rad,d,1}}{\dot{m}_1} = \frac{c_{f,r}\ s_2/D\ Pr_o^{-1/n}\ A/A^*}{h/D\ \text{Sin}\alpha_2(1-\eta_p\ y_i)^{\frac{1}{2}}} = K_2 \qquad \text{(C-32)}$$

s_2 = axial clearance at the exit of the rotor

Equation C-32 is the radial leakage factor for first stage leakage downstream of the rotor, which affects the second stage.

The third stage experiences a leakage factor which represents leakage occurring at the exit of the first and second stages,

$$\zeta_{L,rad,d,3} = \frac{\dot{m}_{\ell,rad,d,1} + \dot{m}_{\ell,rad,d,2}}{\dot{m}_1} = K_2 + K_2(1-K_2), \tag{C-33}$$

and the leakage factor for the m^{th} stage is

$$\zeta_{L,rad,d,m} = \sum_{i=2}^{m} K_2(1-K_2)^{i-2}.$$

The average radial leakage factor for all n stages for leakage at the exit side of the rotor may then be shown to be as follows:

$$\zeta_{L,rad,d} = 1 - \frac{1}{K_2 n}\,[1-(1-K_2)^n]. \tag{C-34}$$

The total radial leakage factor, combining equations C-31 and C-34, becomes

$$\bar{\zeta}_{L,rad} = \frac{n+1}{n} + \frac{1}{K_1 n}\,[(1-2K_1)(1-K_1)^{n-1} - 1] + 1 - \frac{1}{K_2 n}[1-(1-K_2)^n]. \tag{C-35}$$

Tangential leakage may also be conveniently separated into components at the inlet and exit side of the rotor. Again modeling the leakage path as a simple gap between stationary walls, one may develop equations similar to those for radial leakage. Reference 6 notes, however, that leakage at the inlet side of the rotor in the direction of rotor rotation, $L_{tan,1}$ in Figure C-4, exceeds that predicted when the assumption is made that the total pressure at the inlet to the leakage gap is the static pressure in the rotor cavity. Baljé (5) initially

assumed that this pressure exceeded the static pressure by a factor of $\sqrt{2}$. For higher pressure ratio turbines (3), (6), this assumption was found to be inadequate. Reference 6 proposes that the tangential component of the nozzle exit velocity be converted into its equivalent stagnation pressure in order to give a more realistic assessment of the total pressure conditions ahead of this gap.

This leads to the following equation for the leakage factor through path $L_{tan,1}$ for the first stage, assuming the total temperatures ahead of the nozzle and leakage gap to be equivalent:

$$\zeta_{1,tan,path\ 1,1} = \frac{\dot{m}_{\ell,tan,path\ 1,1}}{\dot{m}_1} = \frac{c_{f,tan} p_{o,1,tan}\ s_1\ h}{a_1\ Sin\alpha_2\ h\ A^*/A\ p_{o,1}} =$$

$$\frac{c_{f,tan}\ F\ s_1/D\ A/A^*}{a_1/D\ Sin\alpha_2} = R_1 \qquad (C-36)$$

where the last subscript on $\dot{m}_\ell$ and $\zeta_{L,tan}$ designates the stage affected,

$$F = \frac{p_{o,1,tan}}{p_{o,1}} = \left[\frac{1+\frac{k-1}{2}\ \psi_N^2\ M_{2,is}^2\ \ Cos^2\ \alpha_2}{1+\frac{k-1}{2}\ M_{2,is}^2}\right]^{\frac{k}{k-1}}$$

$M_{2,is}$ = the Mach number of the fluid leaving the nozzle under isentropic conditions,

and $C_{f,tan}$ = a tangential restriction factor, assumed to be about 2/3 (3), (6).

The tangential leakage through path $L_{tan,1}$ is not all lost but augments the mass flow in the second stage. If the leakage is reasonably small in comparison to the nozzle mass flow, the effect on the second stage nozzle jet may be considered minimal.

The leakage through the same gap in the second stage may be expressed as a fraction of the second stage nozzle flow using equation C-7 yielding

$$\frac{\dot{m}_{\ell,tan,path\ 1,2}}{m_2} = R_1\ Pr_o^{-1/n\lambda}, \tag{C-37}$$

which, when expressed as a fraction of the total inlet flow to the turbine, $\dot{m}_1$, becomes

$$\zeta_{L,tan,path\ 1,2} = \frac{\dot{m}_{\ell,tan,path\ 1,2}}{\dot{m}_1} = R_1\ Pr_o^{-1/n\lambda}\ (1-R_1). \tag{C-38}$$

A similar expression can be shown to exist for succeeding stages. For the m^th^ stage, the leakage factor is

$$\zeta_{L,tan,path\ 1,m} = R_1\ Pr_o^{-(\frac{m-1}{n\lambda})}\ (1-\zeta_{L,tan,path\ 1,m-1}). \tag{C-39}$$

In the first stage a tangential leakage exists upstream of the rotor in the direction opposite to rotor rotation. This leakage is lost to all stages and may be expressed as follows:

$$\zeta_{L,tan,path\ 2,1} = \frac{c_{f,tan}\ Pr_o^{-1/n}\ s_1/D\ A/A^*}{a_1/D\ Sin\alpha_2} = R_2 \tag{C-40}$$

The average tangential leakage upstream of the rotor comprising paths $L_{tan,1}$, and $L_{tan,2}$ may then be expressed as

$$\overline{\zeta}_{L,tan1,tan2} = R_2+\frac{1}{n}\{R_1+\sum_{m=2}^{n-1} R_1 \, Pr_o^{-(\frac{m-1}{n\lambda})} [1-\zeta_{L,tan,path\ 1,m-1}]\}. \tag{C-41}$$

On the downstream side of the rotor tangential leakage occurs through paths $L_{tan,3}$ and $L_{tan,4}$. The first stage is not affected by this leakage, as was the case for radial leakage at the exit side of the rotor. The leakage on the downstream side of the first stage in path $L_{tan,3}$ bypasses the second stage nozzle, and the ratio of this leakage to the mass flow rate entering the first stage is as follows:

$$\zeta_{L,tan,path\ 3,2} = \frac{\dot{m}_{\ell,path\ 3,1}}{\dot{m}_1} = \frac{c_{f,t} \; s_2/D \; Pr_o^{-1/n} \; A/A^*}{a_1/D \; Sin\alpha_2 (1-\eta_p \; y_i)^{\frac{1}{2}}} = R_3 \tag{C-42}$$

Similarly, the leakage seen by the third stage becomes

$$\zeta_{L,tan,path\ 3,3} = \frac{\dot{m}_{\ell,path3,2}}{\dot{m}_1} = R_3 \; Pr_o^{-(\frac{3-2}{n\lambda})} (1-R_3)$$

$$= R_3 \; Pr_o^{-1/n\lambda} (1-R_3), \tag{C-43}$$

and for the m^{th} stage,

$$\zeta_{L,tan,path\ 3,m} = \frac{\dot{m}_{\ell,path\ 3,m-1}}{\dot{m}_1} = R_3 \; Pr_o^{-(\frac{m-2}{n\lambda})} \cdot$$

$$(1-\zeta_{L,tan,path\ 3,m-2}). \tag{C-44}$$

Additionally, there is a tangential leakage at the exit of the rotor, in the first stage only, directed opposite to rotor rotation. This leakage, $L_{tan,path\ 4}$, reduces the mass flow rate in all the stages after the first stage and is equivalent to the leakage in the direction of rotor rotation for the first stage, equation C-42.

Thus the average tangential leakage factor for the exit side of the rotor is as follows:

$$\bar{\zeta}_{L,tan\ 3,\ tan\ 4} = \frac{1}{n}\left[(n-1)R_3 + \sum_{m=2}^{n} \zeta_{L,tan,path\ 3,m}\right], \quad \text{(C-45)}$$

where

$$\zeta_{L,tan,path\ 3,m} = R_3\, Pr_o^{-\left(\frac{m-2}{n\lambda}\right)} (1-\zeta_{L,tan,path\ 3,m-1})$$

and

$$\zeta_{L,tan,path\ 3,1} = 0.$$

Tip leakage through path $L_{tip,1}$ is the normal tip leakage from the "pressure" to the "suction side" of the blade experienced in axial turbines. Baljé (5) expresses this leakage as a fraction of the total mass flow as follows:

$$\zeta_{L,tip,path\ 1} = \frac{1.5\sqrt{C/t}}{1 + h/s_3} = \frac{1.5\sqrt{2\ \mathrm{Sin}\ 2\beta_2}}{1 + \frac{h/D}{s_3/D}} \quad \text{(C-46)}$$

where s_3 = tip clearance

and C/t = chord/pitch ratio, assumed to equal 2 Sin $2\beta_2$ (a particular geometry found by Baljé to be adequate - see Fig. C-5).

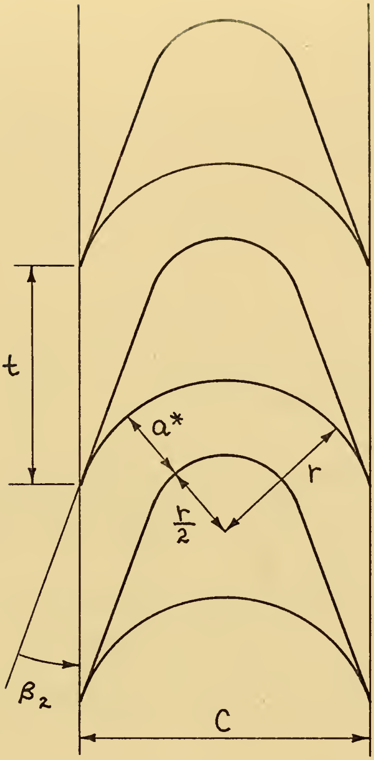

FIGURE C-5

Turbine Blade Geometry

Two other tip leakage paths exist and are unique to re-entry turbines. One of these paths, $L_{tip,3}$, exists only in the first stage, where leakage occurs over the blade tips into the exhaust of the last stage. The other path, $L_{tip,2}$ exists in all stages but the last. It, however, is not completely lost, in that it re-enters the exhaust duct of the succeeding stage

and actually does work in the second stage downstream from which it occurs.

Using an analysis similar to that for tangential leakage, the tip leakage through path 3 for the first stage may be expressed as a fraction of the inlet mass flow rate to the turbine:

$$\frac{\dot{m}_{\ell,\mathrm{tip,path}\ 3,1}}{\dot{m}_1} = \frac{c_{f,\mathrm{tip}}\ s_3\ p_{st,1}\ C_{A^*/A}}{h a_1\ \mathrm{Sin}\alpha_2 p_{o,1}} =$$

$$\frac{4c_{f,\mathrm{tip}}\ s_3/D\ Pr_o^{-1/n}\ a^*/D\ \mathrm{Cos}\beta_2 A/A^*}{h/D\ a_1/D\ \mathrm{Sin}\alpha_a} \qquad \text{(C-47)}$$

where $c_{f,\mathrm{tip}}$ = a tip restriction factor, probably about equivalent to $c_{f,\mathrm{tan}}$

and a^* = cutter diameter or rotor blade throat width (Fig. C-5).

The other leakage path for tip leakage unique to re-entry turbines $L_{\mathrm{tip},2}$ may be analyzed in the following manner. The first stage experiences a leakage out of its normal working path and into the exhaust duct of the second stage. Thus the first and second stages are affected by this leakage. The second stage also experiences leakage over the tips of the blades into the exhaust duct of the third stage. Thus any intermediate stage experiences tip leakage through path 2 in two manners, (a) bypassing of the stage nozzle by incoming tip leakage and (b) bypassing of the stage rotor by tip

leakage into the exhaust of the succeeding stage.

The leakage experienced by tip leakage by path 2 in the first stage is as follows:

$$\zeta_{1,\text{tip,path 2,1}} = \frac{\dot{m}_{\ell,\text{tip,path 2,1}}}{\dot{m}_1} =$$

$$\frac{4c_{f,\text{tip}}\ s_3/D\ F\ a^*/D\ \cos\beta_2}{h/D\ a_1/D\ \sin\alpha_2} = E_1 \qquad \text{(C-48)}$$

The second stage experiences this leakage plus its own leakage into the third stage exhaust.

$$\zeta_{1,\text{tip,path 2,2}} = E_1 + E_1\ Pr_o^{-\frac{1}{n\lambda}}\ (1-E_1) \qquad \text{(C-49)}$$

The average leakage factor for all n stages for tip leakage paths 2 and 3 becomes

$$\bar{\zeta}_{L,\text{tip,path 2, path 3}} = E_2 + \frac{1}{n}\{E_1 + \sum_{m=2}^{n-1} [\Omega_{L,\text{tip,path2,m-1}}$$

$$+ \Omega_{L,\text{tip,path 2,m}}] + \Omega_{L,\text{tip,path2,n-1}}\}, \qquad \text{(C-50)}$$

where $\Omega_{L,\text{tip,path 2,1}} = E_1$

and $\Omega_{L,\text{tip,path 2,m}} = E_1\ Pr_o^{-(\frac{m-1}{n\lambda})}\ (1 - \Omega_{m-1})$.

For the conditions of interest in this thesis, i.e. low pressure ratios, tip leakage through paths 2 and 3 did not significantly affect the efficiency and was ignored in the computer analysis.

Dynamic leakage may be represented by the following expression (2), (6), assuming that the dynamic leakage does no work:

$$\zeta_{L,dyn} = \frac{C_D \; \chi \; (C/D) \; N_s \; D_s}{\psi_N (a_1/D) \mathrm{Sin}\alpha_2 \; 154} \; \Pi_{\lambda,2} \; \overline{Y} \qquad \text{(C-51)}$$

where C_D = restriction factor, based on exhaust geometry and next stage inlet pressure, probably about 0.35 (6), and

$$\Pi_{\lambda,2} = \frac{1-Pr_o^{-\frac{(n-1)}{\lambda n}}}{1-Pr_o^{-1/\lambda n}} .$$

<u>Summary</u>

The model used to analyze leakage in this thesis is that used in references 2, 3, 5 and 6. Nowhere in the actual turbine, however, is there a leakage flow through a gap with stationary walls. The model is probably best then for radial leakage, which most closely approximates this condition. A possible alternative approach to leakage might be to model the tangential and tip leakage unique to re-entry turbines as that which occurs through a series of labyrinths comprised of blade tip, trailing or leading edge and the stationary wall. Thus the leakage would be dependent upon the total number of

labyrinths in a leakage path and the interstage or total pressure ratio (depending upon the path) rather than the static or total pressure within the rotor cavity of the stage in question. Such a model would be speed dependent, since the number of "labyrinths" in a leakage path would vary with speed. Perhaps this approach might yield a more precise agreement with experimental results. It is evident, however, that more experimentation is necessary with re-entry turbines of three and more stages before any leakage model can be shown to be much better than another.

REFERENCES

1. Baljé, O.E., "A Study on Design Criteria and Matching of Turbomachines: Part A-Similarity Relations and Design Criteria for Turbines", *Journal of Engineering for Power*, Vol. 84, No. 1, January 1962, pp 83-102.

2. Linhardt, H.D., "Re-entry Turbines for Space Power Systems", *ARS Journal*, Vol. 32, No. 10, October 1962, pp 1152-1560.

3. Linhardt, H.D. and D.H. Silvern, "Analysis of Partial Admission Axial Impulse Turbines", *ARS Journal*, Vol. 31, No. 3, March 1961, pp 297-308.

4. Stenning, A.H., *Design of Turbines for High-Energy-Fuel Low-Power-Output Applications*, Dynamic Analysis and Control Laboratory Report No. 79, Massachusetts Institute of Technology, September 30, 1953.

5. Baljé, O.E. and D.H. Silvern, *A Study of High Energy Level Low Power Output Turbines*, AMF/TD No. 1196, Department of the Navy, Office of Naval Research, Contract No. NONR - 2292 (00). Task No. NR 094-343., 9 April 1958 (AD 161323).

6. Linhardt, H.D., *Study of Turbine and Turbopump Design Parameters, Final Report-Volume I, A Study of High Pressure Ratio Re-Entry Turbines*, Department of the Navy, Office of Naval Research, Contract No. NONR-2292 (00), Task No. NR 094-343, 30 January 1960 (AD 232635).

7. Baljé, O.E., personal communication, March 8, 1972.

8. Wong, Robert Y., D.L. Darmstadt and D.E. Monroe, *Investigation of a 4.0-Inch-Mean-Diameter Four Stage Re-entry Turbine for Auxiliary Power Drives*, NASA TM X-152, 1960.

9. Horlock, J.H., *Axial Flow Turbines*, London, Butterworth and Company, 1966.

10. Stodola, A., *Steam and Gas Turbines*, New York, Peter Smith, 1945.

LIST OF SYMBOLS

a - arc of admission, ft.

a_{th} - nozzle throat area, ft^2

a^* - cutter diameter (throat width of rotor blade passage), ft

A/A^* - nozzle area ratio

C - rotor blade chord length, ft.

c - absolute velocity ft/sec

c_f - restriction factor

D - tip to tip rotor diameter

D_s - specific diameter, $D\,H_{ad}^{\frac{1}{4}}/\sqrt{Q_3}$, for the entire turbine

E - leakage factor for re-entry tip leakage for the first stage

F - ratio of total pressure in the tangential direction upstream of the rotor to total pressure ahead of the nozzle

g_c - conversion factor, 32.2 ft lbm/lbf sec^2

h - blade height, ft.

H_{ad} - isentropic head, ft lbf/lbm

k - ratio of specific heats

K - radial leakage factor for first or second stage, or loss coefficient for power dissipating losses

$\dot{m}$ - mass flow rate lbm/sec

M - Mach number

n - number of stages

N_s - specific speed, $\dfrac{N\sqrt{Q_3}}{H_{ad}^{\frac{3}{4}}}$, for the entire turbine

Pr - stage or total pressure ratio

p - pressure, lbf/in^2 or lbf/ft^2

R_1 - tangential leakage factor for first to second stage

s - clearance

s_1 - axial clearance upstream of the rotor

s_2 - axial clearance downstream of the rotor

s_3 - tip clearance

t - blade pitch, ft.

u - blade speed, ft/sec

w - velocity relative to the blade, ft/sec

y - pressure ratio function

α - angle of absolute entering or leaving velocity, measured from the tangential direction

β - relative blade angle, measured from the tangential direction

ζ - loss factor

η - efficiency

λ - polytropic exponent

ρ - density of working fluid lbm/ft^3

χ - blade density, ratio of open volume to blade volume in the rotor blading

ψ - velocity coefficient

Ω - ratio of tip leakage in the direction of rotor rotation from a particular stage to total turbine mass flow rate

SUBSCRIPTS

d - downstream of the rotor

D - disk friction

dyn - refers to dynamic leakage

h - hydraulic

i - refers to stage conditions

ℓ - refers to leakage

m - refers to general stage

o - refers to total conditions or isentropic conditions

N - refers to nozzle

p - polytropic

P - blade pumping

r,rad - refers to radial leakage

R - refers to rotor

st - refers to static conditions

SC - scavenging

t - refers to total conditions

T-S - total to static

tan - refers to tangential leakage

tip - refers to tip leakage

u - upstream of the rotor

APPENDIX D

Condenser Analysis

General

Since the condensing system of the proposed propulsion plant must allow for the presence of non-condensables in significant concentrations, the condenser was analyzed in detail. The product of this investigation is a computer program capable of predicting surface condenser area, weight, volume and fluid exit conditions for specified condenser inlet conditions and geometry. The program has the capability of analyzing cases of up to three non-condensable gases, hydrogen, oxygen and nitrogen, with superheated, saturated, or wet vapor steam.

Theory

The classical approach to condensation with the presence of significant quantities of non-condensables present is that of Colburn and Hougen (1). Colburn's approach uses the so-called Chilton-Colburn (2) analogy between heat and mass transfer. Votta (3) presented a more direct method of obtaining the condensation rate using the principles developed by Colburn and Hougen. Neither one of these approaches, however, is directly capable of analyzing condensation of superheated steam. In both methods, the solution is obtained by assuming a set of temperatures less than the temperature of the entering steam and greater than the bulk coolant inlet temperature, each temperature corresponding to a specific location in the condenser. For saturated steam conditions, this fixes the bulk (free stream)

steam partial pressure at the point in the condenser where the assumed temperature exists. At this point one may determine the condensation rate by an iterative procedure. One assumes different vapor-liquid (condensate) interface temperatures and corresponding vapor partial pressures until the energy transfer due to heat and mass transfer through the gas film matches the heat transfer to the bulk coolant. By Votta's method, the interface temperature is calculated directly. By the classical method, or by Votta's method, one may then determine the condenser area required (based upon a previously selected condenser geometry) to condense enough steam to lower the steam partial pressure to that corresponding to the assumed bulk gas-vapor temperature. Using this method with appropriately selected temperatures, one may then estimate the required condenser surface area.

Neither the previously described classical iterative method nor the method of Votta is directly applicable to mixtures of superheated steam and non-condensables. In the proposed application of this thesis it was anticipated that the state of the steam entering the condenser would be superheated in nearly every conceivable case, with between 200-300 degrees of superheat likely. For this reason a method of analyzing the superheated steam case was devised.

It was also anticipated that various mixtures of non-condensable gases could exist in the condenser at any one time. Therefore, it was determined that the method devised should permit the analysis of condensation rates for the simultaneous

presence of both hydrogen and oxygen in the condenser (the case of other than 100% combustion efficiency). Since the condenser would be placed in some sort of pressure vessel, itself having an "atmosphere", provisions were made for the additional simultaneous presence of a third gas, nitrogen. Inclusion of nitrogen in the analysis would also permit testing of the method against existing data where air is the non-condensable.

It was also determined that the method of analysis should include the most significant factors which affect the heat/mass transfer process. It is common, for instance, in the problem of condensation in the presence of a non-condensable gas, to neglect the condensate film heat transfer coefficient (4) as well as sensible heat transfer. The condensate film heat transfer coefficient becomes increasingly more important as the condensate layer is augmented by dripping from tubes above a particular row in question. Coolant film resistance to heat transfer as well as scale and tube wall resistance are also of importance and cannot be neglected.

Certain other aspects of condenser design are not easily adapted to analytical treatment and are more the subject of detailed condenser layout and design. Among these are baffle placement, steam lane location and the location of the suction for the removal of non-condensables. Each of these items has an effect on pressure drop. Condenser pressure drop is complex and is not well understood at present. Silver (5) and Griffith (6) have described the difference between the frictional pressure drop in condensers and that in normal heat transfer tube bundles.

This is essentially an effect similar to that of a diffuser, since condensation delays boundary layer separation and thereby reduces form drag. Silver estimates that under normal condensing conditions, the frictional pressure drop in a condenser may be as low as 68% of the pressure drop of a non-condensing gas of the same properties. The small pressure differences existing in a condenser make experimental determination of pressure variations difficult.

Sebald (7) gives a method of determining a mean condenser pressure which uses friction data derived apparently from non-condensing situations. This method requires iteration of steam lane and bundle arrangements for minimum pressure drop between the periphery of the condenser tube bundle and the air ejector suction.

While pressure drop is of significance in detailed condenser design, it is apparent that it is by no means as important as the effect of the presence of a significant amount of non-condensables. Reference 8 indicates that as little as 5% non-condensables by weight can result in an increase in condenser area of 300% over that of the pure vapor case. For this reason, pressure drop has been neglected in this analysis, but may be included, if desired, after the condenser surface area and basic geometry have been determined.

Method of Analysis

The best approach to the superheated steam case was determined to be a row-by-row analysis of the steam conditions in the condenser, assuming a uniform downward flow of steam

across a staggered tube bank, rectangular in layout, with a square pitch rotated. Such a bank is shown in Figure D-1. In such an analysis it would be necessary to write conservation equations for a given tube row, assuming that, except for the first and second rows, a drip of condensate would occur onto the row in question from the second row above it.

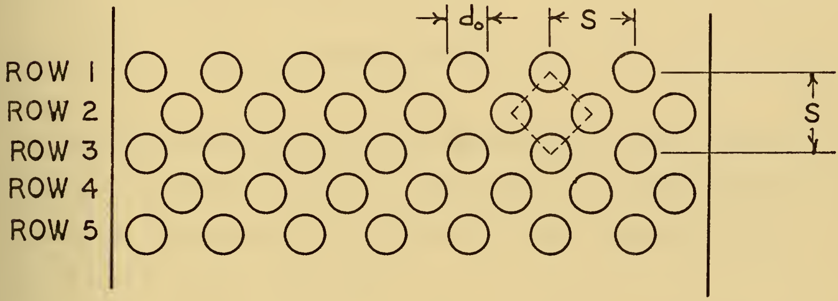

FIGURE D-1

Staggered Tube Bank with Square Pitch Rotated

A control volume for a typical tube in the first or second rows is shown below. The dotted lines indicate the boundaries of the control volume.

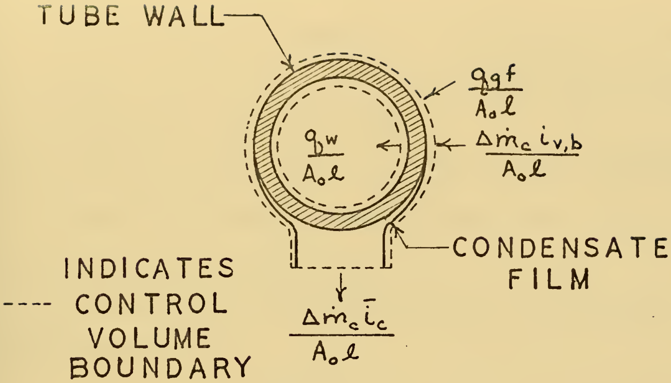

FIGURE D-2

Control Volume I

$\Delta \dot{m}_c$ = condensation rate for a particular tube, lbm/hr

A_o = outside area of the tube per unit length, ft²/ft

A_i = inside area of the tube per unit length, ft²/ft

i = enthalpy, Btu/lbm

$i_{v,b}$ = enthalpy of the bulk vapor in the free stream Btu/lbm

$\bar{i}_c$ = average enthalpy of the condensate film, Btu/lbm

q_{gf} = sensible heat per tube transferred to the condensate from the bulk vapor, Btu/hr

q_w = sensible heat per tube transferred to the bulk coolant, Btu/hr

From the basic Nusselt analysis (8) the following energy equation may be written for control volume I:

$$\Delta \dot{m}_c [i_f - \tfrac{3}{8}\bar{c}_{p,c}(T_i - T_{w,o})] + q_w - q_{gf} - \Delta \dot{m}_c \, i_{v,b} = 0 \qquad \text{(D-1)}$$

where

i_f = saturated liquid enthalpy at the gas vapor interface partial pressure, assuming no subcooling of the condensate at the interface

$\bar{c}_{p,c}$ = average condensate film specific heat, Btu/lbm°R

T_i = vapor-condensate interface temperature, °R

$T_{w,o}$ = outside wall temperature, °R

From equation D-1 one may determine the condensation rate for a single tube,

$$\Delta\dot{m}_c = \frac{q_w - q_{gf}}{i_{v,b} - i_f + \frac{3}{8}\bar{c}_{p,c}(T_i - T_{w,o})} \qquad \text{(D-2)}$$

The heat transferred to the bulk coolant, q_w, may be determined from the overall heat transfer coefficient, in this case selected on the basis of outside tube area, U_o, and the log mean temperature difference of the condensate-vapor interface and the bulk coolant.

$$q_w = U_o \;\; \Delta T_{LM} \qquad \text{(D-3)}$$

U_o = overall heat transfer coefficient based upon outside tube area, Btu/hr ft² °R

$\Delta T_{LM} = \dfrac{T_{L,\ell} - T_{L,e}}{\ell n\left(\dfrac{T_i - T_{L,e}}{T_i - T_{L,\ell}}\right)}$, the log mean temperature difference, °R

$T_{L,e}$ = bulk coolant temperature entering a tube row, °R

$T_{L,\ell}$ = bulk coolant temperature leaving a tube row, °R

T_i = condensate-vapor interface temperature, °R

The overall heat transfer coefficient, U_o, is obtained from the various resistances to heat transfer which comprise the path from interface to bulk coolant,

$$U_o = \frac{1}{\frac{d_o}{d_i h_L} + \frac{d_o}{d_i h_{sc}} + \frac{d_o \ell n\, d_o/d_i}{2k_w} + \frac{1}{h_c}} \qquad \text{(D-4)}$$

d_i = inside tube diameter, ft

d_o = outside tube diameter, ft

h_c = condensate heat transfer coefficient, Btu/hr ft² °R

h_L = coolant film heat transfer coefficient, Btu/hr ft² °R

h_{sc} = coolant side scale heat transfer coefficient, Btu/hr ft² °R

k_w = thermal conductivity of the tube wall, Btu/hr ft °R

The coolant film heat transfer is obtained from McAdams correlation:

$$\frac{h_L d_i}{k_{L,b}} = 0.023\left(\frac{G_L d_i}{\mu_{L,b}}\right)^{0.8} \left(\frac{\mu_L\, c_{p,L}}{k_L}\right)_b^{0.4} \qquad \text{(D-5)}$$

where

k_L = thermal conductivity of the coolant, Btu/hr ft°R

μ_L = coolant viscosity, lbm/hr ft

$c_{p,L}$ = coolant specific heat, Btu/lbm°R

and the subscript, b, denotes bulk properties.

The condensate film heat transfer coefficient, h_c, is obtained from Chen's correlation (8), modified to allow for superheated vapor. For Control Volume I, Chen's correlation may be approximated by

$$h_c \cong 0.728 \left[\frac{g\ \bar{\rho}_c^2\ \bar{k}_c^3\ i''_{fg}}{d_o\ \bar{\mu}_c (T_i - T_{w,o})}\right]^{\frac{1}{4}} \qquad \text{(D-6)}$$

where

g = gravitational constant, 4.17×10^8 ft/hr^2

$\bar{\rho}_c$ = average density of the condensate film, lbm/ft^3

$\bar{k}_c$ = average thermal conductivity of the condensate film, Btu/hr ft°R

$i''_{fg} = i_{fg} + \frac{3}{8}\bar{c}_{p,c}(T_i - T_{w,o}) + c_{p,v}(T_{v,b} - T_i)$ with $T_{v,b}$ the bulk vapor temperature, and $c_{p,v}$ the specific heat of the condensing vapor based upon the arithmetic average of bulk row inlet temperature and condensate-vapor interface temperature

$\bar{\mu}_c$ = the average condensate film viscosity, lbm/hr ft

For subsequent tube rows (3, 4, 5, etc.) the control volume must be modified to include dripping of the condensate from previous rows. Figure D-3, Control Volume II, gives the conservation equation and the resulting condensation rate for the third and succeeding rows:

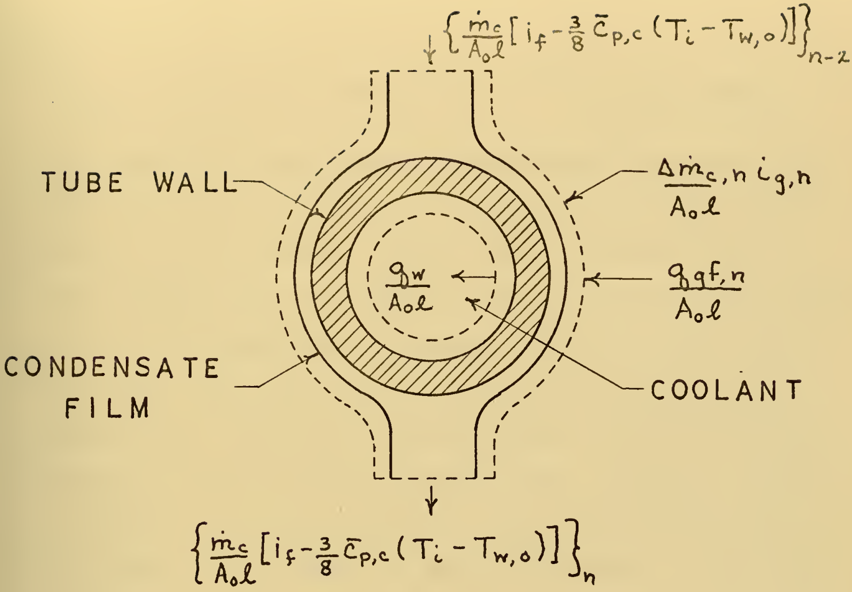

FIGURE D-3

Control Volume II

$$q_{w,n} + \{\dot{m}_c[i_f - \tfrac{3}{8}\bar{c}_{p,c}(T_i - T_{w,o})\}_n - [\dot{m}_c i_c]_{n-2} - q_{gf,n} - [\Delta\dot{m}_c i_{v,b}]_n = 0 \tag{D-7}$$

$$\Delta\dot{m}_{c,n} = \frac{1}{\{i_{v,b,n} - [i_f - \tfrac{3}{8}\bar{c}_{p,c}(T_i - T_{w,o})]_n\}} \cdot \{q_{w,n} + \dot{m}_{c,n-2}[i_f - \tfrac{3}{8}\bar{c}_{p,c}(T_i - T_{w,o})]_n - (\dot{m}_c i_c)_{n-2} - q_{gf,n}\} \tag{D-8}$$

where

$\Delta\dot{m}_{c,n}$ = condensation rate for an nth row tube, lbm/hr

The condensate heat transfer coefficient for a particular row below the second row may then be approximated from Chen's correlation, which assumes, for the row in question (row n), that all previous rows exhibited the same interface temperature as row n. This assumption, of course, is not strictly correct since the average condensate film temperature decreases with succeeding rows. Thus, this method predicts a somewhat higher condensation rate than would actually occur. However, since a real condenser would have baffles to remove condensate drip, this assumption is probably not overly optimistic. With this assumption, equation D-8 reduces to equation D-2.

Another aspect of Chen's correlation is that in its form presented in reference 8, it estimates the average heat transfer coefficient for an n-row, in-line bank of tubes. This may be applied to the nth row of a staggered bank by the approximation:

$$h_{c,n} \cong h_{c,m\text{ row bank}} \cdot m - h_{c,m-1\text{ row bank}}(m-1) \qquad \text{(D-9)}$$

where

$m = \frac{n-1}{2}$ if n odd

$m = \frac{n}{2}$ if n even

Then, substituting Chen's correlation, one may write

$$h_{c,n} = m\{0.728[\frac{1+0.2(m-1)\bar{c}_{p,c}(T_i-T_{w,o})}{i_{fg}}][\frac{g\,\bar{\rho}_c^2\,\bar{k}_c^3\,i''_{fg}}{m\,d_o\,\bar{\mu}_c(T_i-T_{w,o})}]^{\frac{1}{4}}\}$$

$$-(m-1)\{0.728[\frac{1+0.2(m-2)\bar{c}_{p,c}(T_i-T_{w,o})}{i_{fg}}][\frac{g\,\bar{\rho}_c^2\,\bar{k}_c^3\,i_{fg}''}{(m-1)d_o\,\bar{\mu}_c(T_i-T_{w,o})}]^{\frac{1}{4}}\} \tag{D-10}$$

Computation of the mass transfer coefficient requires the use of the Chilton-Colburn analogy and certain tube bank heat transfer data. Tube bank data was obtained from Colburn's 1933 data (9), based upon staggered tube banks data from as early as 1911. There was some doubt as to the number of rows in the staggered tube bank data observed by Colburn. It was evident from investigation of the American data referred to by Colburn that each of these banks were four rows deep. This is of concern since data of Kays and Lo presented in McAdams (10) shows that for succeeding rows in a staggered bank up to the 6th row, the heat transfer coefficient improves. After the 6^{th} row there is no further improvement. Applying this information to data of Colburn, assumed to apply to banks of 4 staggered rows, one may then determine the heat transfer coefficient for a given row in an n-row staggered bank. Colburn's method of data presentation is given below in Figure D-4.

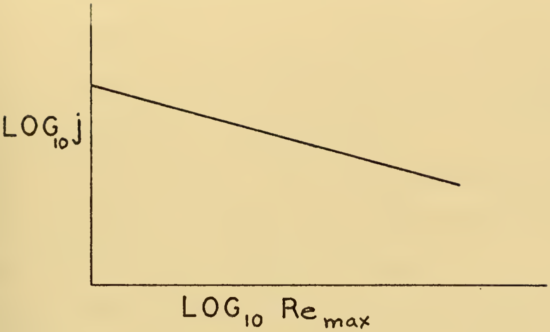

FIGURE D-4

Colburn j Factor Vs. Reynolds Number

The term, j, is Colburn's j factor

$$j = \frac{h_{gf}}{c_{p,vm}} \left(\frac{c_{p,vm}\,\mu_{vm}}{k_{vm}}\right)^{\frac{2}{3}} = \frac{K_G\,p_{gf}}{G_{max}/M_{mean}} \left(\frac{\mu_{vm}}{\rho_{vm}\mathcal{D}}\right)^{\frac{2}{3}} \qquad \text{(D-11)}$$

where

h_{gf} = gas film heat transfer coefficient Btu/hr ft^2°R

$c_{p,vm}$ = film average specific heat of the gas vapor mixture, Btu/lbm°R

G_{max} = mass flux of the gas vapor mixture based on minimum cross sectional area, lbm/hr ft^2

k_{vm} = film average thermal conductivity of the gas vapor mixture, Btu/hr ft°R

$$p_{gf} = \frac{(p-p_{v,i})-(p-p_{v,b})}{\ln\left(\frac{p-p_{v,i}}{p-p_{v,i}}\right)}$$, the log mean partial pressure difference of the non-condensing

gases across the gas film: p-total pressure, lbf/in^2; $p_{v,i}$, $p_{v,b}$ partial pressure of the condensing vapor at the condensate-vapor interface and bulk conditions respectively

K_G = mass transfer coefficient lb-mole/hr-ft^2-lbf/in^2

$\mathcal{D}$ = diffusion coefficient (mass diffusivity) ft^2/hr

ρ_{vm} = gas mixture density, lbm/ft^3

M_{mean} = mean molecular weight of the gas vapor mixture in the free stream

For heat and mass transfer, Colburn defines film average temperature as the arithmetic mean of the bulk and wall temperature.

Some confusion does exist in the definition of minimum cross sectional area, from which G_{max} is determined. Through examination of Colburn's references it was determined that the minimum area for a staggered bank is that shown in Figure D-5 for the assumed square pitch rotated configuration.

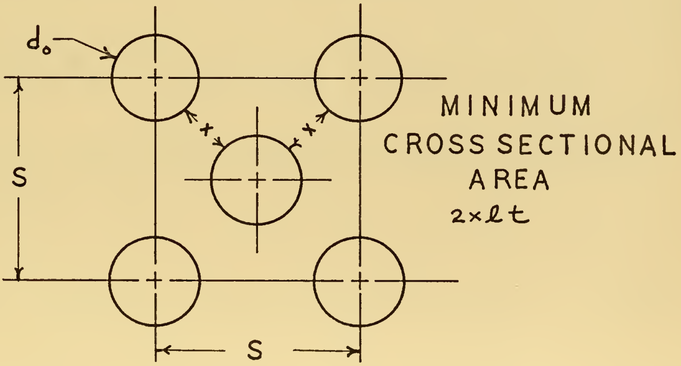

FIGURE D-5
Tube Layout

It is evident from Figure D-5 that the ratio of minimum area to frontal area is $\sqrt{2} - 2\ d_o/s$.

Using equation D-11, one may write an expression for the condensation rate $\Delta\dot{m}_c$ for a given tube,

$$\Delta\dot{m}_c = A_o \ell\ K_G\ M_v\ (p_{v,b} - p_{v,i}), \tag{D-12}$$

where M_v is the molecular weight of the condensing vapor (lbm/lb-mole), and the sensible heat transfer rate,

$$q_{gf} = A_o \ell\ h_{gf} (T_{v,b} - T_i). \tag{D-13}$$

The determination of the properties of the gas vapor mixtures is discussed in a subsequent section.

Using equations D-3, D-12, and D-13 one may then write for a single tube the condition which must be met for a solution of the heat/mass transfer problem.

$$U_o A_o \ell \Delta T_{LM} = h_{gf} A_o \ell\ (T_{v,b} - T_i) + K_G\ M_v\ A_o \ell\ i_{fg}'' (p_{v,b} - P_{v,i}) \tag{D-14}$$

One then may determine the enthalpy of the condensate leaving a particular row.

$$(\dot{m}_c i_c)_n = (\dot{m}_c i_c)_{n-2} + \{\Delta m_c [i_f - \tfrac{3}{8} \bar{c}_{p,c} (T_i - T_{w,o})]\}_n \tag{D-15}$$

The determination of bulk vapor exit conditions from a tube row requires the solution of the energy equation across still another control volume.

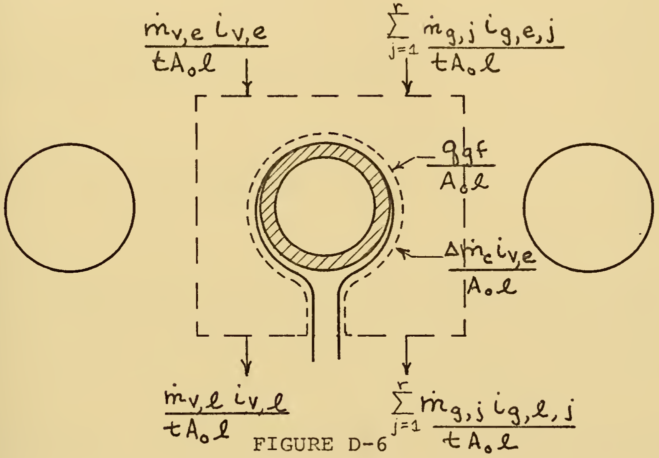

FIGURE D-6

Control Volume III

$$\dot{m}_{v,\ell}\ i_{v,\ell} + \sum_{j=1}^{r} \dot{m}_{g,j}\ i_{g,\ell,j} + t(q_{gf}+\Delta\dot{m}_c i_{v,e}) -$$

$$\sum_{j=1}^{r} \dot{m}_{g,j}\ i_{g,e,j} - \dot{m}_{v,e}\ i_{v,e} = 0 \qquad \text{(D-16)}$$

where

$\dot{m}_{v,e}$ = vapor mass flow rate entering the tube row, lb/hr

$\dot{m}_{v,\ell}$ = vapor mass flow rate leaving the tube row, lbm/hr

$\dot{m}_{g,j}$ = mass flow rate of non-condensable gas j, lbm/hr

$i_{v,e}/i_{v,\ell}$ = enthalpy of the bulk vapor entering/leaving the tube row, Btu/lbm

$i_{g,e,j}/i_{g,\ell,j}$ = enthalpy of non-condensable gas j entering/leaving the tube row, Btu/lbm

t = number of tubes in a tube row

r = number of distinct non-condensable gases present

From equation D-13, one may derive an expression for the temperature of the bulk gas vapor mixture leaving the tube row, using the familiar relationship,

$$i_{v,e} - i_{v,\ell} \cong c_{p,v}(T_{b,v,e} - T_{b,v,\ell}),$$

where

$T_{v,b,e}$ = the bulk gas-vapor temperature entering the tube row, assumed identical with $T_{b,v}$ of equation D-13.

$$(\dot{m}_{v,e} - t\Delta\dot{m}_c)[i_{g,sat,\ell} + \bar{c}_{p,v}(T_{b,v,\ell} - T_{sat})] + \sum_{j=1}^{r} \dot{m}_{j,g}\, c_{p,g,j} \cdot$$

$$(T_{b,v,\ell} - T_o) + \Delta\dot{m}_c\, t[i_g + c_{p,v}(T_{b,v,e} - T_i) + t\, q_{gf} - \dot{m}_{v,e}\, i_{v,e}$$

$$+ \sum_{j=1}^{r} \dot{m}_{g,j}\, c_{p,g,j}(T_{b,v,e} - T_o) = 0 \qquad \text{(D-17)}$$

$\bar{c}_{p,v}$ = condensing vapor specific heat based upon the arithmetic average of row bulk inlet temperature and bulk exit saturation temperature, Btu/lbm°R

$i_{g,sat,\ell}$ = enthalpy of the saturated condensing vapor at the row exit free stream partial pressure, Btu/lbm

$c_{p,g,j}$ = specific heat of the non-condensable gas j, based on row bulk inlet temperature, Btu/lbm°R

i_g = saturated vapor enthalpy of the bulk vapor at row exit conditions, Btu/lbm

T_o = the reference temperature for condensing vapor enthalpy, °R

T_{sat} = saturation temperature of the condensing vapor at the row exit partial pressure, °R

The partial pressure of the condensing vapor at the exit of the row is obtained from the molal flow rate of the condensing vapor and the total molal flow rate, knowing the inlet molal flow rates and the molal condensation rate. Thus from the exit partial pressure of the condensing vapor and equation D-17, the row exit temperature for superheated conditions may be obtained.

$$T_{b,v,\ell} = \frac{1}{[(\dot{m}_{v,e}-t\Delta\dot{m}_c)\bar{c}_{p,v}+\sum_{j=1}^{r}\dot{m}_{g,j}c_{p,g,j}]} \cdot \{\dot{m}_{v,e}i_{v,e}$$

$$+\sum_{j=1}^{r}\dot{m}_{g,j}c_{p,g,j}T_{b,v,e}-(\dot{m}_{v,e}-t\Delta\dot{m}_c)(i_{g,sat,\ell}-\bar{c}_{p,v}T_{sat})$$

$$-\Delta\dot{m}_c t[i_g+c_{p,v}(T_{b,v,e}-T_i)]-t\,q_{gf}\} \qquad \text{(D-18)}$$

In both equations D-17 and D-18 it is noted that the average non-condensable specific heat is based upon the temperature of the bulk gas-vapor mixture entering the tube row and that the sensible heat transferred to the condensate film is based upon this same temperature. Actually, the tube row experiences some average bulk temperature between inlet and

outlet conditions for the transfer of sensible heat. However, since the difference in bulk inlet and outlet temperatures is seldom much more than 10 degrees R, the effect of assuming the bulk inlet temperature for sensible heat transfer and bulk gas-vapor specific heat is negligible.

For the saturated and wet vapor conditions, of course, bulk gas-vapor exit temperature is assumed at all times to be uniquely determined by the partial pressure of the vapor leaving the tube row. A further assumption is necessary in the wet vapor case, and this involves the deposition of wet vapor droplets on condensing surfaces. If the droplets are sufficiently large, they will be deposited high in the condenser, i.e. in the first few rows. However, if they are sufficiently small, they may not be deposited until the latter few rows of the condenser are reached, and they may even pass completely through. Dalton's law of partial pressures, of course, can only be applied to the vapor portion of the two-phase mixture and even then it only approximates the actual situation in a two-phase flow. In the development of the computer program for this thesis, it was assumed that no droplets are deposited on condenser tubes, which is optimistic with respect to condensation rates yet simpler to solve. The assumption was also made in the energy equation (for the wet vapor case) that equilibrium is maintained between droplet temperature and bulk vapor temperature. Equation D-16 may now be modified to include the vapor droplet enthalpy flux,

$$\dot{m}_{v,\ell} i_{v,\ell} + \dot{m}_{d,\ell} i_{d,\ell} + \sum_{j=1}^{r} \dot{m}_{g,j} i_{g,\ell,j} + t(q_{gf} + \Delta \dot{m}_{c} i_{v,e})$$

$$- \sum_{j=1}^{r} \dot{m}_{g,j} i_{g,e,j} - \dot{m}_{v,e} i_{v,e} - \dot{m}_{d,\ell} i_{d,\ell} = 0 \qquad \text{(D-19)}$$

where

$\dot{m}_{d,\ell}/\dot{m}_{d,e}$ = the mass flow rate of the wet vapor droplets leaving/entering the tube row assuming none are deposited on the tubes of the tube row in question

$i_{d,\ell}/i_{d,e}$ = the enthalpy of the wet vapor droplets leaving/entering the tube row, assumed to exist in equilibrium with the bulk condensing vapor

Knowing the condensation rate, one may then solve equation D-19 iteratively for the bulk outlet temperature and the corresponding wet vapor droplet flow rate leaving the tube row. This, of course, assumes that the possibility exists for some evaporation of the wet vapor droplets to maintain the equilibrium condition. This assumption admittedly is somewhat unrealistic since equilibrium between droplets and the bulk gas vapor mixture will probably not exist.

Vapor-Non Condensable Gas Mixture Properties

It was necessary to determine properties of mixtures of steam, a polar gas, and the three possible non-condensable gases, hydrogen, oxygen, and nitrogen. The mixture properties were determined as follows, using methods set forth by Reid and Sherwood (11), as modified or amplified below:

1) Viscosity - by the method of Buddenburg and Wilke (12)
2) Thermal conductivity - by the method of Lindsay and Bromley (13) as modified by Bennett and Vines (14) for polar-non-polar gas mixtures
3) Density - by Amagat's Law (reference 11, pp. 321-322) since no reliable method exists for determining densities of mixtures containing polar components: $\frac{1}{\gamma_m} = \sum_i y_i \frac{1}{\gamma_i}$, where γ is the molal density and y_i the mole fraction of component i
4) Specific heat from the molal average value: $\hat{c}_{p,m} = \sum_i y_i \hat{c}_{p,i}$, where $\hat{c}_p$ is the molal specific heat, according to reference 11, pp. 323-325. Again no reliable method exists for determining the specific heat of polar mixtures.
5) Diffusion coefficient, reference 11 (pp. 523-528) and Wilke (15)

Computation of a mean diffusion coefficient for a mixture of steam and several non-condensable gases in a diffusion/momentum/temperature boundary layer is an extremely complicated situation. If it is assumed that the Lewis number and Prandtl

number are both unity, the problem is tractable. This, of course, assumes that the rates of momentum, heat and mass transfer in the boundary layer are all equal.

Wilke (15) has developed a method for determining the average diffusion coefficient for the diffusion of a single gas through a mixture of stagnant gases: Applying Wilke's method to a situation where there exists a temperature gradient,

$$\frac{d\,y_v}{d\zeta} = -\frac{N_v\ \delta_T\ \mathcal{R}T(\zeta)}{p}\left[\frac{y_a}{\mathcal{D}_{v-a}} + \frac{y_b}{\mathcal{D}_{v-b}} + \frac{y_c}{\mathcal{D}_{v-c}}\right]$$

$$\frac{d\,y_a}{d\zeta} = \frac{N_v\ \delta_T\ \mathcal{R}\ T(\zeta)\ y_a}{\mathcal{D}_{v-a}p}$$

$$\frac{d\,y_b}{d\zeta} = \frac{N_v\ \delta_T\ \mathcal{R}\ T(\zeta)\ y_b}{\mathcal{D}_{v-b}p}$$

$$\frac{d\,y_c}{d\zeta} = \frac{N_v\ \delta_T\ \mathcal{R}\ T(\zeta)\ y_c}{\mathcal{D}_{v-c}p} \qquad \text{(D-20)}$$

where

$y_v(\zeta)$ = the mole fraction of the diffusing (condensing) vapor

$y_a(\zeta)$, $y_b(\zeta)$, $y_c(\zeta)$ = mole fractions of non-condensables a, b, c

ζ = non-dimensional boundary layer thickness, zero at the free stream extremity and 1 at the condensate-vapor interface

N_v = molal flux of the diffusing (condensing) vapor, lb moles/hr ft^2

$\mathcal{R}$ = Universal gas constant

p = total pressure, lbf/ft^2

$\mathcal{D}_{v-a}$, $\mathcal{D}_{v-b}$, $\mathcal{D}_{v-c}$ = binary diffusion coefficients for the condensing vapor and each of the non-condensables a, b, c, each functions of temperature, $T(\zeta)$

T = temperature in the thermal boundary layer as a function of ζ, °R

δ_T = thickness of the temperature boundary layer, ft

The multicomponent diffusion coefficient $\overline{\mathcal{D}}_v$ is defined as follows:

$$\overline{\mathcal{D}}_v = \frac{N_v \ \delta_T \ \mathcal{R} \ T_{mean}}{p \ \ \ln \left(\frac{1-y_v(1)}{1-y_v(0)}\right)} \tag{D-21}$$

where T_{mean} is the mean temperature in the boundary layer, °R.

The solution of equation D-20 is based upon known boundary conditions at $\zeta = 0$ (the bulk conditions) and the assumed condensate vapor interface temperature, which fixes y_v at $\zeta = 1$. $y_a(1)$, $y_b(1)$, $y_c(1)$ are all unknown as is the combination of terms $N_v \ \delta_T$.

If the temperature distribution in the boundary layer is known, equation system D-20 may be solved numerically for the eigenvalue $N_v \ \delta_T \ \mathcal{R}/p$, with the condition at the condensate vapor interface, $\zeta = 1$:

$$y_v(1) + y_a(1) + y_b(1) + y_c(1) = 1 \tag{D-22}$$

For purposes of this thesis, it was assumed that Le=Pr=1. Hence a 1/7 power turbulent momentum boundary layer profile was assumed for the temperature profile in the turbulent region, and a parabolic profile in the laminar region. In the region of boundary layer detachment, of course, neither of these profiles represents the existing situation. The laminar parabolic profile, strictly applicable only in plane Poisuille flow, has been assumed because of its simplicity. Admittedly this is a somewhat crude approximation to the existing situation, which probably most closely resembles the developing boundary layer on a flat plate, at least prior to the point of separation. To use the Blasius profile, dependent upon the distance downstream of the stagnation point, would excessively complicate the solution to equation system D-20. To be sure, any assumption of a general boundary layer velocity and temperature profile for flow normal to a round tube is a crude approximation at best, and any reasonable one is almost as good as another. Any significant refinements to a general temperature/velocity profile will require detailed understanding of the angular dependence of mass/momentum/heat transfer for condensing flow normal to a round tube.

Fluid Properties

Table D-1 gives a summary of references for the properties of fluids utilized in the condenser analysis. In each case,

TABLE D-1

References for Fluid Properties

Property	Fluid	Reference	Comments
Density	Liquid Water	16, 17, 22	
	Salt Water	24, 26, 27	
	Steam	16, 17	
	Hydrogen	18	
	Oxygen	18	
	Nitrogen	18	
Viscosity	Liquid Water	22, 23, 24	
	Salt Water	23, 26	pressure dependence from fresh water data, reference 25
	Steam	20	extrapolated below 212°F
	Hydrogen	20	
	Oxygen	20	
	Nitrogen	20	
Specific Heat	Liquid Water	19	
	Salt Water	26	
	Steam	19	
	Hydrogen	19	
	Oxygen	19	
	Nitrogen	19	
Thermal Conductivity	Liquid Water	20	
	Salt Water	26	pressure dependence from reference 21
	Steam	19	
	Hydrogen	19	
	Oxygen	19	
	Nitrogen	19	

except for steam, a least squares curve fit of the best available data was performed. A computer curve fit for steam table data, based on Keenan and Keyes data (16) was obtained from the Naval Ship Engineering Center (17).

Description of the Computer Program

A computer program in FORTRAN IV was developed for the IBM System 370 to estimate condenser surface area, weight and volume for an assumed condenser geometry, inlet steam and non-condensable conditions and sea water inlet temperature and depth. The detailed input data are listed below:

a) mass flow rates of steam and non-condensable gases (hydrogen, oxygen, nitrogen)

b) bulk temperature and total pressure of the entering gas-vapor mixture

c) enthalpy of the vapor portion and quality of the entering steam

d) sea water depth, inlet temperature, and velocity through the condenser tubes

e) tube thermal conductivity, active length, inside and outside diameters, outside area per unit length, internal flow cross sectional area, and number of tubes per row

f) condenser shell (steel) thickness

g) header (waterbox) density (assumed identical with tube density), yield stress and safety factor (cylindrical tube headers)

h) an initial estimate of the overall coefficient of heat transfer, U_o.

Results of the program are listed below:

a) row by row condensation rate, fluid inlet and exit temperature and enthalpy data, if desired

b) condenser exit fluid conditions, including mass flow rate and temperature of uncondensed steam, and average condensate temperature and enthalpy

c) total number of tubes

d) surface area

e) condenser dimensions, volume and weight for deep submergence applications, if desired

The condenser exit conditions were arbitrarily set at that point where the condensation rate for a particular row became less than one thousandth of the entering steam mass flow rate.

The condenser program was tested under a variety of conditions as well as against examples in references 4 and 28. Some of the test conditions are given in Table D-2. This table shows the increase in surface area with increasing amounts of non-condensables under saturated and superheated steam conditions. While the surface area does not increase drastically with an increase of oxygen flow rate from 0.605 lbm/hr to 8.0 lbm/hr, it should be noted that there is still a significant amount of uncondensed steam in the 8.0 lbm/hr case. This is indicative of the cutoff method used in the computer program, i.e. computation ceases when the condensation rate for a row in question is less than some fraction of the inlet steam mass

Entering) Temperature, °F	138.75	138.75	138.75	138.75	138.75	138.75	138.75	138.75	138.75	138.75	138.75	138.75	138.75	138.75	335.0	335.0	335.0	335.0
) Enthalpy, Btu/lbm	1121.4	1121.4	1121.4	1121.4	1121.4	1121.4	1121.4	1121.4	1121.4	1121.4	1121.4	1121.4	1121.4	1121.4	1211.4	1211.4	1211.4	1211.4
Steam) Quality	1	1	1	1	1	1	1	1	1	1	1	1	1	1	1	1	1	1
Non-Condensable) H_2	0	0	0	0	0	0	0	0.0754	0.125	0.1875	0.250	0.315	0.375	1.00	0	0	0.0754	1.00
) O_2	.605	1.0	1.5	2.0	2.5	3.0	8.0	0	0	0	0	0	0	0	0.605	8.0	0	0
Mass Flow Rate, lbm/hr) N_2	0	0	0	0	0	0	0	0	0	0	0	0	0	0	0	0	0	0
Row Number	Condensation Rate - lbm/hr																	
1	41.1	41.1	40.8	40.9	40.5	40.5	39.4	41.0	41.1	40.8	40.6	40.4	40.3	39.3	36.1	34.9	35.7	34.1
2	40.9	40.9	40.8	40.8	40.7	40.6	39.5	41.0	41.0	40.9	40.6	40.5	40.2	39.0	36.4	35.1	36.0	34.2
3	37.2	37.2	39.1	37.0	36.9	36.9	35.9	37.1	37.1	37.0	36.9	36.8	36.6	35.4	33.4	32.2	33.2	31.7
4	37.2	37.1	36.9	36.6	36.5	36.4	35.3	37.1	37.1	36.9	36.8	36.6	36.4	34.9	34.5	32.7	34.0	32.1
5	36.6	35.3	35.1	34.8	34.6	34.4	32.6	35.6	35.6	35.3	35.0	34.8	34.6	32.3	33.8	31.4	33.4	31.0
6	35.0	34.6	34.0	33.5	33.1	32.7	30.3	35.2	34.8	34.3	33.9	33.4	33.1	30.4	34.2	30.4	34.0	30.2
7	30.6	29.0	28.4	27.7	27.2	26.8	24.5	32.0	30.9	30.1	29.4	26.7	28.2	25.6	32.9	27.3	33.1	28.0
8	12.9	14.0	14.5	15.2	15.7	15.9	17.0	11.7	12.6	13.6	14.7	15.1	15.7	17.9	24.2	21.7	27.2	23.0
9	1.35	2.25	3.54	4.24	5.01	5.59	9.26	0.98	1.65	2.38	3.10	4.13	4.81	8.9	5.83	13.4	5.02	14.3
10	0.06	0.21	0.51	0.85	1.21	1.59	4.20		0.92	0.28	0.57	0.83	1.06	3.90	0.41	6.71	0.23	7.03
11			0.08	0.14	0.25	0.35	1.78				0.08	0.13	0.22	1.56	0.02	3.01		2.82
12						0.10	0.71							0.62		1.26		1.17
13							0.32							0.24		0.50		0.45
14							0.15									0.21		
Uncondensed Steam Leaving the last row lbm/hr	0.07	0.13	0.16	0.24	0.34	0.34	0.91	0.12	0.20	0.34	0.42	0.53	0.67	1.74	0.06	0.98	0.13	1.88
Surface Area, ft²	13.1	13.1	14.4	14.4	14.4	15.7	18.3	11.8	13.1	13.1	14.4	14.4	14.4	17.1	14.4	18.3	13.1	17.1

Cooling water temp/velocity, °F/ft/sec 75/7

Total pressure - 2.8 lbf/in²

Tube length/OD/ID. in 12.0/0.25/0.19

No. of tubes per row - 20

Tube spacing, in - 0.50

Tube thermal conductivity, Btu/hr ft °F - 16.5

Steam rate, lb/hr - 272.0

Scale coefficient, Btu/hr ft² °R - 2000

TABLE D-2

Condenser Data

flow rate (0.001). An interesting observation in the superheated cases is that the second, fourth, and sometimes sixth rows exhibit slightly higher condensation rates than the first, third, and fifth rows, respectively. An explanation for this phenonmenon is the combination of reduction of sensible heat transferred in succeeding rows, tending to increase condensation rates, and an increase of condensate film resistance, tending to reduce condensation rates. Of course, when the thickening of the condensate film becomes significant (after the first few rows) and as superheat is decreased, this effect diminishes.

A test of the program against an example given in Kern's Process Heat Transfer (4) resulted in excellent correlation in the first few rows, but correlation was not possible in latter rows since Kern neglected condensate film resistance. This comparison tested the program for cases where large amounts of non-condensables are present. A test was also made for very small amounts of non-condensables (.05% by weight) by comparison with an example given in the U. S. Navy's condenser design data sheet (28). The result was very conservative, predicting a condenser area approximately 150% of that in the design data sheet example. This significant discrepancy can be explained by the fact that condensate drip, if allowed to remain on the tubes in a very large condenser (steam rate 247,000 lbm/hr), results in a serious degradation of heat transfer in the lower parts of the condenser. For the relatively small condensers

considered in this thesis, baffles to remove condensate drip will not be so important.

A considerable amount of difficulty was experienced in consistently achieving convergence in the iterative solution scheme utilized. The scheme used throughout the program is first a bracketing method which then "homes in" on the solution by repetitively bisecting the interval in which the solution is known to lie. Iteration of the following variables was required for a solution:

1) Outside tube wall temperature
2) Vapor-condensate interface temperature
3) Bulk coolant temperature
4) Condensation rate

The number of required interface temperature iterations was decreased by the assumption of an initial overall coefficient of heat transfer, U_o, and this was updated for succeeding rows after the first row, using that of the previous row. Condensation rate proved to be the most troublesome, particularly in the latter few rows. It was found here that computation of condensation rate based upon row inlet conditions invariably resulted in predicting condensation rates in excess of the entering steam mass flow rate, which is obviously impossible. It was concluded that the Chilton-Colburn analogy, if based upon tube bank data, is not applicable to a single row in the bank unless some average value of the inlet and exit steam flow rates from the tube row is used for computing the condensation rate. Iteration using the arithmetic mean of inlet and exit steam

mass flow rates was also unsuccessful. Iteration was successful, however, when condensation rate was computed using a steam mass flow rate nearly that of the exit of the tube row. While this may, at first glance, seem no more than a trial and error scheme of getting just any solution, the dependence of condensation rates on row exit conditions is defensible. One must remember that the Chilton-Colburn analogy is only accurate when no significant reduction in mass flow rate occurs across the mass transfer element in question. The mass transfer analogy is based on heat transfer data, in which there is no reduction in mass flow rate. Hence, one may not expect the analogy to give accurate results when reductions in mass flow rate as great as 50% or more occur across a given row. The Chilton-Colburn analogy may be used, however, if some average flow rate of the condensing vapor, probably one near the exit conditions, is assumed for computing mass transfer. In any event, computation of the condensation rate for a given row based upon a steam mass flow rate nearly that of the row exit conditions is conservative.

Condenser Program Input Form

The following data must be supplied to the condenser program in the FORTRAN format given below:

Card A - FORMAT 3I5

KDATA - Number of condensers to be analyzed

NOPT - Option for deep submergence weights and volumes:

NOPT = 0, weights and volumes not desired :
NOPT = 1, weights and volumes desired

KOPT - Option for row-by-row thermodynamic and condensation rate data: KOPT = 0, do not desire row-by-row information; KOPT = 1, row-by-row information desired

Card A is followed by 5 data cards for each condenser to be analyzed.

Condenser data cards

Card 1 - FORMAT 4F10.4

MDOT (1) - mass flow rate of entering steam, lbm/hr

MDOT (2) - mass flow rate of hydrogen, lbm/hr

MDOT (3) - mass flow rate of oxygen, lbm/hr

MDOT (4) - mass flow rate of nitrogen, lbm/hr

Card 2 - FORMAT 2I5, 6F 10.4

NROW - the initial tube row encountered, 1

NTUBES - the number of tubes in a row

TBIN - bulk temperature of the entering gas vapor mixture, °R

TLIN - bulk temperature of the entering sea water, °R

HVENT - enthalpy of the entering steam vapor (use saturated vapor enthalpy for wet-vapor), Btu/lbm

SPACE - the space between tube centers in a tube row (see figure D-5), ft

LENGTH - tube active length, ft

DOUT - tube O.D., ft

Card 3 - FORMAT 7F 10.4

DIN - tube I.D., ft

HSC - inside tube scale heat transfer coefficient, Btu/hr ft^2 °R

KTHWAL - tube wall thermal conductivity, Btu/hr ft °R

DEPTH - seawater depth, ft (use design depth if NOPT = 1 is desired)

AXN - tube internal flow cross sectional area, ft^2

AOUT - tube external surface area per foot of length, ft^2/ft

Card 4 - FORMAT - 3F 10.4

PTOT - total condenser inlet pressure (may be the average condenser pressure if inlet pressure is known and pressure drop can be estimated), lbf/in^2

UOVRL - initial estimate of overall heat transfer coefficient from vapor-condensate interface to bulk coolant, based upon outside tube area (500-900), Btu/hr ft^2 °R

QUAL - entering steam quality, 0 to 1.0

Card 5 - FORMAT - 4F 10.6

SHLTHK - thickness of the condenser steel shell, in

DENS - density of the tube/header material, lbm/ft^3

SF - safety factor for the tube headers (1.5, 2.0 etc.)

YS - yield stress of the tube header material (lbf/in^2)

The program requires approximately 80,000 bytes of storage. 128,000 bytes of storage are sufficient when the FORTRAN G compiler is included. The IBM Scientific Subroutine Package Subprogram HPGC (Hamming's modified predictor corrector method for the solution of a simultaneous set of linear first order differential equations) must be available for operation of the condenser analysis program.

LIST OF SYMBOLS

A_o - outside area of a condenser tube per foot of tube length, ft^2/ft

A_i - inside area of a condenser tube per foot of tube length, ft^2/ft

c_p - specific heat, Btu/lbm °R

$c_{p,v}$ - average condensing vapor specific heat, Btu/lbm °R

$\hat{c}_p$ - molal specific heat, Btu/lb mole °R

$\bar{c}_{p,c}$ - average condensate film specific heat based upon Nusselt's average film temperature, Btu/lbm °R

d_o - outside condenser tube diameter, ft

d_i - inside condenser tube diameter, ft

$\mathcal{D}$ - diffusion coefficient (mass diffusivity), ft^2/hr

G - mass flux, lbm/hr ft^2

g - gravitational constant, 4.17×10^8 ft/hr^2

h - heat transfer coefficient, Btu/hr ft^2 °R

i - enthalpy, Btu/lbm

i_{fg} - heat of vaporization of the condensing vapor at the partial pressure at the vapor-condensate interface, Btu/lbm

i_{fg}'' - heat rejected to the bulk coolant by the vapor condensed, Btu/lbm

j - Colburn j-factor

K_G - gas film mass transfer coefficient lb-mole/hr-ft^2-lbf/in^2

k - thermal conductivity, Btu/hr ft °R

ℓ - effective tube length, ft

M - molecular weight, lbm/lb-mole

$\dot{m}$ - mass flow rate lbm/hr

$\Delta\dot{m}_c$ - condensation rate per tube in a tube row, lbm/hr

N - molal velocity flux, lb moles/hr ft^2

p - pressure, lbf/in^2 or lbf/ft^2

p_{gf} - gas film log mean partial pressure of the non-condensing gases, lbf/in^2

q - heat transfer rate, Btu/hr

q_{gf} - sensible heat per condenser tube transferred through the gas film, Btu/hr

R - Universal gas constant, 1545.43 ft lbf/°R lb mole

r - total number of distinct non-condensable gases present

T - temperature, °R

ΔT_{LM} - log mean temperature difference between the condensate-vapor interface and the bulk coolant, °R

t - number of tubes in a row

U_o - overall heat transfer coefficient based upon outside tube area and condensate-vapor interface and bulk vapor temperatures, Btu/hr ft^2 °R

y - mole fraction

γ - molal density, lb-moles/ft^3

μ - viscosity, lbm/hr ft

SUBSCRIPTS

b - refers to bulk fluid conditions

c - refers to the condensate film or condensation rate

d - refers to droplets in a wet vapor condition

e - refers to conditions entering a tube row

f - refers to the saturated liquid condition

g - refers to the saturated vapor condition

gf - refers to gas film

i - refers to the vapor condensate interface

L - refers to the coolant

LM - refers to log mean conditions

m - refers to mean conditions

n - refers to a particular row

o - refers to outside conditions (tube wall) or reference conditions for enthalpy

p - refers to constant pressure conditions

sc - refers to scale on the coolant side of the condenser tube

v - refers to the condensing vapor

vm - refers to the gas vapor mixture

w - refers to tube wall

REFERENCES

1. Colburn, A.P. and O.A. Hougen, "Design of Cooler Condensers for Mixtures of Vapors with Non-Condensing Gases", *Industrial and Engineering Chemistry*, 26, No. 11, (November, 1934) pp. 1178-1182.

2. Chilton, T.H. and A.P. Colburn, "Mass Transfer (Absorption) Coefficients-Prediction from Data on Heat Transfer and Fluid Friction", *Industrial and Engineering Chemistry*, 26, No. 11, (November, 1934), pp. 1183-1187.

3. Votta, F. Jr., "Condensing from Vapor-Gas Mixtures", *Chemical Engineering*, June 8, 1964, pp. 223-228.

4. Kern, Donald Q., *Process Heat Transfer*, New York, McGraw Hill Book Company, 1950.

5. Silver, R.S., "An Approach to a General Theory of Surface Condensers", *Proceedings of the Institution of Mechanical Engineers*, Vol. 178, Pt. 1, No. 14, (1963-1964), pp. 339-357.

6. Griffith, Peter, "Condensation Heat Transfer", lecture notes from the *14th Annual Heat Transfer Conference*, College of Engineering, Oklahoma State University, Stillwater, Oklahoma, March 14-15, 1968.

7. Sebald, J.F., "Main and Auxiliary Condensers", Chapter 13 of *Marine Engineering*, Roy L. Harrington, ed., New York, The Society of Naval Architects and Marine Engineers, 1971.

8. Rohsenow, W.M. and H. Choi, *Heat Mass and Momentum Transfer*, Englewood Clifts, New Jersey, Prentice Hall, 1961.

9. Colburn, A.P., "A Method of Correlating Forced Convection Heat Transfer Data and a Comparison with Fluid Friction", *Transactions of the American Institute of Chemical Engineers*, XXIX, (1933), pp. 174-210.

10. McAdams, W.H., *Heat Transmission*, New York, McGraw Hill Book Company, 1954.

11. Reid, R.C. and T.K. Sherwood, *The Properties of Gases and Liquids-Their Estimation and Correlation*, New York, McGraw Hill, 1966.

12. Wilke, C.R., "A Viscosity Equation for Gas Mixtures", *The Journal of Chemical Physics*, 18, No. 4, (April, 1950), pp. 517-519.

13. Lindsay, A.L., and L.A. Bromley, "Thermal Conductivity of Gas Mixtures", *Industrial and Engineering Chemistry*, 42, No. 8, (August, 1950), pp. 1508-1511.

14. Bennett, L.A. and R.G. Vines, "Thermal Conductivities of Organic Vapor Mixtures", *The Journal of Chemical Physics*, 23, No. 9, (September, 1955), pp. 1587-1591.

15. Wilke, C.R., "Diffusional Properties of Multicomponent Gases", *Chemical Engineering Progress*, 46, No. 2, (February, 1950), pp. 95-104.

16. Keenan, J.H. and F.G. Keyes, *Thermodynamic Properties of Steam*, New York, John Wiley and Sons, 1936.

17. *Subroutine for the Thermodynamic Properties of Steam and Water (STMTAB)*, Ship Design Computer Program, NAVSHIPS 0900-009-5010, Naval Ship Engineering Center, Department of the Navy, Washington, D.C., April, 1968.

18. Hilsenrath, Joseph, Et.Al., *Tables of Thermal Properties of Gases*, National Bureau of Standards Circular 564, Washington, D.C., U. S. Printing Office, 1955.

19. Touloukian, Y.S., *Thermophysical Properties of Matter*, Vol. 3, *Thermal Conductivity, Non-Metallic Liquids and Gases*, Vol. 6, *Specific Heat, Non-Metallic Liquids and Gases*, Purdue Research Foundation, New York, IFI/Plenum Data Corporation, 1970.

20. Touloukian, Y.S., *Thermophysical Properties Research Center Data Book*, Vol. 2, *Non-Metallic Elements, Compounds and Mixtures*, Purdue Research Foundation, Lafayette, Indiana, 1964.

21. Washburn, E.W., ed., *International Critical Tables of Numerical Data, Physics, Chemistry and Technology*, Vol. 5, New York, McGraw Hill Book Company, 1929.

22. Forsythe, W.E., *Smithsonian Physical Tables*, Washington, D.C., The Smithsonian Institution, 1954.

23. *Heat Transfer Data Book*, the General Electric Corporation, Schenactady, New York, 1970.

24. Comstock, J.P., ed., *Principles of Naval Architecture*, New York, The Society of Naval Architects and Marine Engineers, 1964.

25. Bridgman, P.W., "The Effect of Pressure on the Viscosity of Forty-Three Pure Liquids", *Proceedings of the American Academy of Arts and Sciences*, Vol. 61, No. 3, (February, 1926), pp. 57-99.

26. Grunburg, L. "Properties of Sea Water Concentrates", *3rd International Symposium on Fresh Water from the Sea*, Vol. I, 31-39, 1970.

27. *Thermo-Chemical Dynamic Power Supply for Deep Submergence Vehicles*, NAVSHIPS 0907-000-6010, August, 1970.

28. "Steam Condensers", *Design Data Sheet Section DDS 4601-1*, Department of the Navy, Bureau of Ships, October 15, 1953.

```
C     MAIN PROGRAM FOR CONDENSER DATA                                   MAIN0001
C     NOPT-OPTION FOR CONDENSER WEIGHTS AND VOLUMES                     MAIN0002
C        NOPT=0--DO NOT DESIRE OUTPUT OF CONDENSER WEIGHTS AND VOLS     MAIN0003
C        NOPT=1--DESIRE OUTPUT OF CONDENSER WEIGHTS AND VOLUMES         MAIN0004
C     KOPT--OPTION FOR OUTPUT OF ROW BY ROW INFORMATION                 MAIN0005
C        KOPT=0--DO NOT DESIRE ROW BY ROW INFORMATION                   MAIN0006
C        KOPT=1--DESIRE ROW BY ROW INFORMATION                          MAIN0007
C     NTUBES-NUMBER OF TUBES PER ROW                                    MAIN0008
C     SPACE-HORIZONTAL OR VERTICAL DISTANCE BETWEEN ADJACENT TUBES      MAIN0009
C     CENTERS ON A  SQUARE PITCH IN STAGGERED TUBE ROWS                 MAIN0010
C     SUBPROGRAM GOOD FOR UP TO 200 TUBE ROWS                           MAIN0011
C     AOUT-OUTSIDE AREA OF A SINGLE TUBE IN SQ FT PER FOOT OF LENGTH    MAIN0012
C     AXN-INTERNAL FLOW CROSS SECTION OF A SINGLE TUBE IN SQ FT         MAIN0013
C     LENGTH-TUBE LENGTH IN FT                                          MAIN0014
C     KTHWAL-THERMAL CONDUCTIVITY OF TUBE WALL IN BTU/HR FT DEG R       MAIN0015
C     TBIN-TEMPERATURE OF THE BULK GAS-VAPOR MIXTURE ENTERING A TUBE    MAIN0016
C     ROW IN DEG R                                                      MAIN0017
C     NROW-NUMBER OF THE TUBE ROW IN THE BANK(INCREASING IN THE         MAIN0018
C     DIRECTION OF FLOW                                                 MAIN0019
C     MDOT-MASS FLOW RATE OF VAPOR(STEAM) AND GAS COMPONENTS IN LBM/HR  MAIN0020
C     MDOT(1)-MASS FLOW RATE OF HYDROGEN                                MAIN0021
C     MDOT(2)-MASS FLOW RATE OF OXYGEN                                  MAIN0022
C     MDOT(3)-MASS FLOW RATE OF OXYGEN                                  MAIN0023
C     MDOT(4)-MASS FLOW RATE OF NITROGEN                                MAIN0024
C     DOUT-TUBE OUTER DIAMETER IN FT                                    MAIN0025
C     DIN-TUBE INNER DIAMETER IN FT                                     MAIN0026
C     TLIN-TEMPERATURE OF THE BULK COOLANT LIQUID ENTERING A TUBE-DEG R MAIN0027
C     HVENT-ENTHALPY OF THE STEAM ENTERING THE TUBE ROW IN BTU/LBM      MAIN0028
C     TBOUT-TEMPERATURE OF THE BULK GAS-VAPOR MIXTURE LEAVING THE TUBE  MAIN0029
C     ROW IN DEG R                                                      MAIN0030
C     TLOUT-TEMPERATURE OF THE BULK COOLANT LEAVING THE TUBE ROW-DEG R  MAIN0031
C     HVL-ENTHALPY OF THE BULK VAPOR-GAS MIXTURE LEAVING THE TUBE ROW   MAIN0032
C     IN BTU/LBM                                                        MAIN0033
C     WATVEL-BULK VELOCITY OF COOLANT IN CONDENSER TUBES IN FT/HR       MAIN0034
C     DEPTH-DEPTH OF SEAWATER IN FT                                     MAIN0035
C     HSC-SCALE HEAT TRANSFER COEFFICIENT FOR INSIDE OF TUBES IN BTU/   MAIN0036
```

```
C     HR SQ FT DEG R                                                    MAIN0037
C     MCONDL(NROW)-MASS FLOW RATE OF CONDENSATE LEAVING A TUBE RCW IN   MAIN0038
C     LBM/HR--INCLUDES FLOW FROM TUBES DIRECTLY ABOVE(IN LINE)--FOR     MAIN0039
C     TOTAL CONDENSATE FLOW RATE FROM A STAGGERED BANK MUST ADD MCONDL  MAIN0040
C     FROM THE LAST ROW OF THE BANK TO THAT OF THE IMMEDIATELY          MAIN0041
C     PRECEDING ROW                                                     MAIN0042
C     ENFL(NROW)-ENTHALPY TRANSPORT RATE OF CONDENSATE LEAVING A TUBE   MAIN0043
C     ROW IN BTU/HR                                                     MAIN0044
C     WETVAP-MASS FLOW RATE OF DRCPLET PCRTICN OF A WET VAPOR           MAIN0045
C     COOLV-BULK VELOCITY OF COOLANT THROUGH TUBES,FT/SEC               MAIN0046
C     HTHICK-HEADER THICKNESS IN INCHES                                 MAIN0047
C     SHLTHK-THICKNESS OF CONDENSER SHELL IN INCHES                     MAIN0048
C     HOTD-HOTWELL DEPTH IN FT                                          MAIN0049
C     TOTHT-TOTAL HEIGHT OF THE CONDENSER,INCLUDING HOTWELL IN FT       MAIN0050
C     HDIAMO-HEADER DIAMETER IN FT                                      MAIN0051
C     WEIGHTS IN LBS                                                    MAIN0052
C     VOLUMES IN FT**3                                                  MAIN0053
C     DIMENSIONS IN FT                                                  MAIN0054
C     SURFACE AREA IN FT**2                                             MAIN0055
C     FRACT-THE RATIO OF OF CONDENSATION RATE FOR A PARTICULAR ROW TO   MAIN0056
C     THE MASS FLOW RATE OF THE STEAM ENTERING THE CONDENSER,SET AT .001MAIN0057
C     NERROR-ERROR MESSAGE                                              MAIN0058
C     NERROR=0--NC ERROR                                                MAIN0059
C     NERROR=1--EXCESSIVE NUMBER OF ITERATIONS                          MAIN0060
C     NERROR=3-CONDENSATION COMPLETE                                    MAIN0061
C     NERROR=4-EXCESSIVE ITERATIONS ON DELTAM-CONDENSATION RATE         MAIN0062
C     NERROR=5-ROW BULK GAS OUTLET TEMPERATURE LESS THAN OR EQUAL TO    MAIN0063
C     COOLANT INLET TEMPERATURE                                         MAIN0064
C     NERROR=6-NEGATIVE DELTAP IN THE COMPUTATION OF DELTAM-CONDENSATIONMAIN0065
C     RATE                                                              MAIN0066
      REAL MDOT,KTHWAL,MCONDL,LENGTH,MOLW                               MAIN0067
      DIMENSICN MDOT(4)                                                 MAIN0068
      CCMMCN /S1/ PRESS,TEMP,QUAL,SATLIQ(3),STEAM(3),COEFFT(237)        MAIN0069
     1/S4/PTOT/S10/MOLW(4)/S14/DOUT,DIN,HSC,WATVEL,DEPTH/S15/ENFL(200), MAIN0070
     2MCONDL(200),YDOT(4),YI(4)/S16/CLAM1,HVLMIN,HFLMIN,WALLH,ATOT,     MAIN0071
     3AXNTOT,AFRONT,DRAT,LROW,ARATIO                                    MAIN0072
```

```
      READ(5,121)KDATA,NOPT,KOPT                                        MAIN0073
  121 FORMAT(3I5)                                                       MAIN0074
      WRITE(6,131)KDATA                                                 MAIN0075
  131 FORMAT(1X,'NUMBER OF SETS OF DATA=',I5)                           MAIN0076
      DO 4 J=1,KDATA                                                    MAIN0077
      READ(5,100)(MDOT(I),I=1,4)                                        MAIN0078
  100 FORMAT(4F10.4)                                                    MAIN0079
      READ(5,101)NROW,NTUBES,TBIN,TLIN,HVENT,SPACE,LENGTH,DOUT,DIN,     MAIN0080
     1HSC,COOLV,KTHWAL,DEPTH,AXN,AOUT,PTOT,UOVRL,QUAL                   MAIN0081
  101 FORMAT(2I5,6F10.4/(7F10.4))                                       MAIN0082
      WRITE(6,113)PTOT,UOVRL,QUAL                                       MAIN0083
  113 FORMAT(1X,'PTOT=',F10.2,'UOVRL=',F10.2,'QUAL=',F10.4)             MAIN0084
      READ(5,130)SHLTHK,DENS,SF,YS                                      MAIN0085
  130 FORMAT(4F10.6)                                                    MAIN0086
      WRITE(6,106)                                                      MAIN0087
  106 FORMAT(4X,'MDOT(1)',6X,'MDOT(2)',6X,'MDOT(3)',6X,'MDOT(4)')       MAIN0088
      WRITE(6,107)(MDOT(I),I=1,4)                                       MAIN0089
  107 FORMAT(1X,4F13.6)                                                 MAIN0090
      WRITE(6,108)                                                      MAIN0091
  108 FORMAT(5X,'NROW',7X,'NTUBES',9X,'TBIN',10X,'TLIN',11X,'HVENT',7X, MAIN0092
     1'SPACE',7X,'LENGTH',8X,'DOUT')                                    MAIN0093
      WRITE(6,109)NROW,NTUBES,TBIN,TLIN,HVENT,SPACE,LENGTH,DOUT         MAIN0094
  109 FORMAT(1X,2I13,6F13.6)                                            MAIN0095
      WRITE(6,110)                                                      MAIN0096
  110 FORMAT(6X,'DIN',10X,'HSC',10X,'COOLV',10X,'KTHWAL',7X,'DEPTH',9X, MAIN0097
     1'AXN',9X,'AOUT')                                                  MAIN0098
      WRITE(6,111)DIN,HSC,COOLV,KTHWAL,DEPTH,AXN,AOUT                   MAIN0099
  111 FORMAT(1X,7F13.6)                                                 MAIN0100
      DRUM=1.414*DOUT                                                   MAIN0101
      IF(SPACE.LE.DRUM)GO TO 3                                          MAIN0102
      AFRONT=FLOAT(NTUBES)*LENGTH*SPACE                                 MAIN0103
      ARATIO=1./(1.414-2.*DOUT/SPACE)                                   MAIN0104
      DRAT=DOUT/DIN                                                     MAIN0105
      AXNTOT=FLOAT(NTUBES)*AXN                                          MAIN0106
      ATOT=FLOAT(NTUBES)*AOUT*LENGTH                                    MAIN0107
      WALLH=HWALL(KTHWAL,DOUT,DIN)                                      MAIN0108
```

```
      WETVAP=MDOT(1)*(1.-QUAL)                                          MAIN0109
      MDOT(1)=MDOT(1)-WETVAP                                            MAIN0110
      DUM=0.                                                            MAIN0111
      DO 10 I=1,4                                                       MAIN0112
      YDOT(I)=MDOT(I)/MOLW(I)                                           MAIN0113
   10 DUM=DUM+YDOT(I)                                                   MAIN0114
      PRESS=PTOT*YDOT(1)/DUM                                            MAIN0115
      CALL STMTAB(1,PRESS,0.)                                           MAIN0116
      TEMSAT=TEMP+460.                                                  MAIN0117
      IF(QUAL.EQ.1.)GO TO 12                                            MAIN0118
      GO TO 14                                                          MAIN0119
   12 CALL STMTAB(4,PRESS,0.)                                           MAIN0120
      IF(HVENT.LT.STEAM(2))GO TO 13                                     MAIN0121
      GO TO 14                                                          MAIN0122
   13 HVENT=STEAM(2)                                                    MAIN0123
      TBIN=TEMSAT                                                       MAIN0124
   14 UDT=UOVRL*(TEMSAT-TLIN)                                           MAIN0125
      WATVEL=3600.*COOLV                                                MAIN0126
      RUM=DUM-YDOT(1)                                                   MAIN0127
      TEMP=TLIN-459.90                                                  MAIN0128
      CALL STMTAB(5,TEMP,0.)                                            MAIN0129
      HVLMIN=STEAM(2)                                                   MAIN0130
      HFLMIN=SATLIQ(2)                                                  MAIN0131
      FR=PRESS/PTOT                                                     MAIN0132
      YDOTOT=RUM/(1.-FR)                                                MAIN0133
      CLAM1=YDOTOT*FR*MOLW(1)                                           MAIN0134
      TBOUT=0.                                                          MAIN0135
      TLOUT=0.                                                          MAIN0136
      HVL=0.                                                            MAIN0137
      NERROR=0                                                          MAIN0138
      WDOT=MDOT(1)                                                      MAIN0139
    7 CALL TUBROW(MDOT,NROW,TBIN,TLIN,HVENT,WETVAP,UDT,TBOUT,TLOUT,     MAIN0140
     1HVL,NERROR)                                                       MAIN0141
      KROW=NROW-1                                                       MAIN0142
      IF(NERROR.EQ.1.OR.NERROR.EQ.4)GO TO 2                             MAIN0143
      IF(NERROR.EQ.6)GO TO 11                                           MAIN0144
```

```
      IF(NERROR.EQ.3)GO TO 8                                            MAIN0145
      IF(NROW.GT.2)GO TO 5                                              MAIN0146
      DELTAM=MCONDL(NROW)                                               MAIN0147
      GO TO 6                                                           MAIN0148
    5 DELTAM=MCONDL(NROW)-MCONDL(LROW)                                  MAIN0149
      DELTAM=MCONDL(NROW)-MCONDL(LROW)                                  MAIN0150
    6 HCONDL=ENFL(NROW)/MCONDL(NROW)                                    MAIN0151
      IF(KOPT.EQ.0)GO TO 16                                             MAIN0152
      WRITE(6,115)NROW                                                  MAIN0153
  115 FORMAT(1X,'ROW NUMBER=',I3)                                       MAIN0154
      WRITE(6,114)DELTAM,HCONDL                                         MAIN0155
  114 FORMAT(1X,'CONDENSATION RATE=',F10.4,'LBM/HR',2X,'ENTHALPY OF     MAIN0156
     1CONDENSATE=',F10.4,'BTU/LBM')                                     MAIN0157
      WRITE(6,106)                                                      MAIN0158
      WRITE(6,107)(MDOT(I),I=1,4)                                       MAIN0159
      WRITE(6,103)                                                      MAIN0160
  103 FORMAT(6X,'TBIN',9X,'TBOUT',9X,'TLIN',9X,'TLOUT',9X,'HVENT',9X,   MAIN0161
     1'HVL',9X,'MCONDL')                                                MAIN0162
      WRITE(6,112)TBIN,TBOUT,TLIN,TLOUT,HVENT,HVL,MCONDL(NROW)          MAIN0163
  112 FORMAT(1X,7F13.6)                                                 MAIN0164
   16 FRACT=DELTAM/WDOT                                                 MAIN0165
      IF(FRACT.LT.0.001)GO TO 15                                        MAIN0166
      IF(NROW.GT.200)GO TO 4                                            MAIN0167
      IF(NERROR.EQ.5)GO TO 9                                            MAIN0168
      HVENT=HVL                                                         MAIN0169
      TBIN=TBOUT                                                        MAIN0170
      NROW=NROW+1                                                       MAIN0171
      HCONB4=HCONDL                                                     MAIN0172
      GO TO 7                                                           MAIN0173
    2 WRITE(6,102)                                                      MAIN0174
  102 FORMAT(1X,'EXCESSIVE NO OF TRIALS FOR TUBROW')                    MAIN0175
      GO TO 4                                                           MAIN0176
    3 WRITE(6,104)                                                      MAIN0177
  104 FORMAT(1X,'TUBE SPACING TOO SMALL')                               MAIN0178
      GO TO 4                                                           MAIN0179
    8 WRITE(6,116)                                                      MAIN0180
```

```
116 FORMAT(1X,'CONDENSATION COMPLETE')                                  MAIN0181
 15 CONDR=MCONDL(NROW)+MCONDL(KROW)                                     MAIN0182
    ENCOND=(HCONDL*MCONDL(NROW)+HCONB4*MCONDL(KROW))/CONDR              MAIN0183
    CALL STMTAB(3,ENCOND,0.)                                            MAIN0184
    CONTMP=TEMP+460.                                                    MAIN0185
    WRITE(6,119)                                                        MAIN0186
119 FORMAT(1X,'TOTAL ROWS',2X,'MDOT STM OUT',1X,'CONDENS RATE',2X,      MAIN0187
   1'ENTH COND',4X,'COND TEMP',3X,'ENTH STEAM',3X,'STEAM TEMP OUT')     MAIN0188
    WRITE(6,120)NROW,MDOT(1),CONDR,ENCOND,CONTMP,HVL,TBOUT              MAIN0189
120 FORMAT(1X,I13,6F13.6)                                               MAIN0190
    NTOT=NROW*NTUBES                                                    MAIN0191
    SURF=FLOAT(NTOT)*LENGTH*AOUT                                        MAIN0192
    IF(NOPT.EQ.0)WRITE(6,132)NTOT,SURF                                  MAIN0193
132 FORMAT(1X,'TOTAL NUMBER OF TUBES=',I10,2X,'TOTAL SURFACE AREA=',    MAIN0194
   1F10.2,'SQ FT')                                                      MAIN0195
    IF(NOPT.EQ.0)GO TO 4                                                MAIN0196
    HT=0.55*FLOAT(NROW)*SPACE                                           MAIN0197
    WIDTH=1.1*FLOAT(NTUBES)*SPACE                                       MAIN0198
    TUBSHT=HT*WIDTH                                                     MAIN0199
    ACTVOL=TUBSHT*LENGTH                                                MAIN0200
    HOTVOL=CONDR/(60.*RHOWTL(CONTMP))                                   MAIN0201
    HOTD=0.920*HOTVOL**0.333                                            MAIN0202
    HOTWT=224.*SHLTHK*HOTD**2                                           MAIN0203
    IF(HT.LE.0.5)GO TO 122                                              MAIN0204
    IF(HT.GT.0.5.AND.HT.LE.2.)GO TO 123                                 MAIN0205
    NHDRS=2*(IFIX(HT)+1)                                                MAIN0206
    HDIAMI=1.6*HT/FLOAT(NHDRS)                                          MAIN0207
    GO TO 124                                                           MAIN0208
122 NHDRS=2                                                             MAIN0209
    HDIAMI=0.8*HT                                                       MAIN0210
    GO TO 124                                                           MAIN0211
123 NHDRS=4                                                             MAIN0212
    HDIAMI=0.4*HT                                                       MAIN0213
124 PSW=PRESSW(DEPTH)                                                   MAIN0214
    HTHICK=6.*PSW*SF*HDIAMI/YS                                          MAIN0215
    IF(HTHICK.LT.0.25)HTHICK=0.25                                       MAIN0216
```

```
      HDIAMO=HDIAMI+HTHICK/6.                                           MAIN0217
      BOXDEP=HDIAMO                                                     MAIN0218
      TOTVOL=1.25*(ACTVOL+HOTVOL+2.*TUBSHT*BOXDEP)                      MAIN0219
      SHELWT=68.*SHLTHK*(WIDTH+HT)*(LENGTH+BOXDEP)                      MAIN0220
      TUBWT=0.7853*DENS*FLOAT(NTOT)*(LENGTH+BOXDEP)*(DOUT**2-DIN**2)    MAIN0221
      HDRWT=0.26179*DENS*FLOAT(NHDRS)*HTHICK*HDIAMO*(WIDTH+HDIAMO)      MAIN0222
      TOTWT=1.5*(TUBWT+SHELWT+HOTWT+HDRWT)                              MAIN0223
      TOTHT=HT+1.5*HOTD                                                 MAIN0224
      TOTWD=WIDTH+HDIAMO                                                MAIN0225
      TOTLEN=LENGTH+2.*BOXDEP                                           MAIN0226
      WRITE(6,125)                                                      MAIN0227
  125 FORMAT(2X,'TOTAL TUBES',3X,'SURF AREA',4X,'BOXDEPTH',5X,'ACTIVE   MAIN0228
     1 VOL',3X,'HOTWL VOL',3X,'TOTAL VOL',4X,'TUBE WT',5X,'SHELL WT',5X,MAIN0229
     2'HOTDEPTH')                                                       MAIN0230
      WRITE(6,126)NTOT,SURF,BOXDEP,ACTVOL,HOTVOL,TOTVOL,TUBWT,SHELWT,   MAIN0231
     1HOTD                                                              MAIN0232
  126 FORMAT(1X,I13,8F13.6)                                             MAIN0233
      WRITE(6,127)                                                      MAIN0234
  127 FORMAT(2X,'NUMBR HDRS',4X,'HOTWELL WT',3X,'HDR THICK',4X,'SHEL    MAIN0235
     1 THICK',4X,'HDR OD',7X,'HDR WT',6X,'TOTAL WT',4X,'TOTAL LENGTH',2XMAIN0236
     2,'TOTAL WIDTH')                                                   MAIN0237
      WRITE(6,126)NHDRS,HOTWT,HTHICK,SHLTHK,HDIAMO,HDRWT,TOTWT,TOTLEN,  MAIN0238
     1TOTWD                                                             MAIN0239
      WRITE(6,128)                                                      MAIN0240
  128 FORMAT(3X,'TOTAL HT',4X,'SEAWTR PRESS')                           MAIN0241
      WRITE(6,129)TOTHT,PSW                                             MAIN0242
  129 FORMAT(1X,2F13.6)                                                 MAIN0243
      GO TO 4                                                           MAIN0244
   11 WRITE(6,118)                                                      MAIN0245
  118 FORMAT(1X,'NEGATIVE DELTAP IN COMPUTATION OF DELTAM-CONDENSATION  MAIN0246
     1 RATE')                                                           MAIN0247
      GO TO 4                                                           MAIN0248
    9 WRITE(6,117)                                                      MAIN0249
  117 FORMAT(1X,'ROW BULK GAS OUTLET TEMPERATURE LESS THAN COOLANT INLETMAIN0250
     1TEMPERATURE')                                                     MAIN0251
    4 CONTINUE                                                          MAIN0252
```

```
    1 RETURN                                                            MAIN0253
      END                                                               MAIN0254
```

```
      SUBROUTINE TUBROW(MDOT,NROW,TBIN,TLIN,HVENT,WETVAP,UDT,TBOUT,     TUBR0001
     1TLOUT,HVL,NERROR)                                                 TUBR0002
C     SUBROUTINE TO DETERMINE THE RATE OF CONDENSATION OF STEAM FROM    TUBR0003
C     A STEAM-HYDROGEN-OXYGEN-NITROGEN MIXTURE WHEN PASSING THROUGH     TUBR0004
C     A SINGLE ROW OF A TUBE BANK OF MANY ROWS OF STAGGERED TUBES--     TUBR0005
C     ALSO DETERMINES THE EXIT CONDITIONS OF GAS,VAPOR,CONDENSATE, AND  TUBR0006
C     COOLING WATER FROM THE TUBE ROW                                   TUBR0007
C     TBIN-TEMPERATURE OF THE BULK GAS-VAPOR MIXTURE ENTERING A TUBE    TUBR0008
C     ROW IN DEG R                                                      TUBR0009
C     NROW-NUMBER OF THE TUBE ROW IN THE BANK(INCREASING IN THE         TUBR0010
C     DIRECTION OF FLOW                                                 TUBR0011
C     MDOT-MASS FLOW RATE OF VAPOR(STEAM) AND GAS COMPONENTS IN LBM/HR  TUBR0012
C     MDOT(1)-MASS FLOW RATE OF HYDROGEN                                TUBR0013
C     MDOT(2)-MASS FLOW RATE OF OXYGEN                                  TUBR0014
C     MDOT(3)-MASS FLOW RATE OF OXYGEN                                  TUBR0015
C     MDOT(4)-MASS FLOW RATE OF NITROGEN                                TUBR0016
C     DOUT-TUBE OUTER DIAMETER IN FT                                    TUBR0017
C     DIN-TUBE INNER DIAMETER IN FT                                     TUBR0018
C     TLIN-TEMPERATURE OF THE BULK COOLANT LIQUID ENTERING A TUBE-DEG R TUBR0019
C     HVENT-ENTHALPY OF THE STEAM ENTERING THE TUBE ROW IN BTU/LBM      TUBR0020
C     TBOUT-TEMPERATURE OF THE BULK GAS-VAPOR MIXTURE LEAVING THE TUBE  TUBR0021
C     ROW IN DEG R                                                      TUBR0022
C     TLOUT-TEMPERATURE OF THE BULK COOLANT LEAVING THE TUBE ROW-DEG R  TUBR0023
C     HVL-ENTHALPY OF THE BULK VAPOR-GAS MIXTURE LEAVING THE TUBE ROW   TUBR0024
C     IN BTU/LBM                                                        TUBR0025
C     WATVEL-BULK VELOCITY OF COOLANT IN CONDENSER TUBES IN FT/HR       TUBR0026
C     DEPTH-DEPTH OF SEAWATER IN FT                                     TUBR0027
C     HSC-SCALE HEAT TRANSFER COEFFICIENT FOR INSIDE OF TUBES IN BTU/   TUBR0028
C     HR SQ FT DEG R                                                    TUBR0029
C     MCONDL(NROW)-MASS FLOW RATE OF CONDENSATE LEAVING A TUBE ROW IN   TUBR0030
C     LBM/HR--INCLUDES FLOW FROM TUBES DIRECTLY ABOVE(IN LINE)--FOR     TUBR0031
C     TOTAL CONDENSATE FLOW RATE FROM A STAGGERED BANK MUST ADD MCONDL  TUBR0032
C     FROM THE LAST ROW OF THE BANK TO THAT OF THE IMMEDIATELY          TUBR0033
C     PRECEDING ROW                                                     TUBR0034
C     ENFL(NROW)-ENTHALPY TRANSPORT RATE OF CONDENSATE LEAVING A TUBE   TUBR0035
C     ROW IN BTU/HR                                                     TUBR0036
```

```
C     WETVAP-MASS FLOW RATE OF DROPLET PORTION OF A WET VAPOR                 TUBRO037
C     NERROR-ERROR MESSAGE                                                    TUBRO038
C     NERROR=0--NO ERROR                                                      TUBRO039
C     NERROR=1--EXCESSIVE NUMBER OF ITERATIONS                                TUBRO040
C      NERROR=3-CONDENSATION COMPLETE                                         TUBRO041
C      NERROR=4-EXCESSIVE ITERATIONS ON DELTAM-CONDENSATION RATE              TUBRO042
C     NERROR=5-ROW BULK GAS OUTLET TEMPERATURE LESS THAN OR EQUAL TO          TUBRO043
C     COOLANT INLET TEMPERATURE                                               TUBRO044
C     NERROR=6-NEGATIVE DELTAP IN THE COMPUTATION OF DELTAM-CONDENSATION      TUBRO045
C     RATE                                                                    TUBRO046
      REAL MDOT,KTHMIX,MOLW,MU,KTH,MFLOW,KGFILM,MCONDL,KTHWAL,LE,LENGTH,      TUBRO047
     1MUWTV,KTHWTV,MSTEAM,MOLWM,MTOT                                          TUBRO048
      DIMENSION MDOT(4)                                                       TUBRO049
      COMMON /S1/PRESS,TEMP,QUAL,SATLIQ(3),STEAM(3),COEFFT(237)/S2/TBULK      TUBRO050
     1,TINT,RE/S3/TMEAN/S4/PTOT/S6/YF(4)/S8/YFRACT(4),MU(4),RHO(4),CP(4)      TUBRO051
     2,KTH(4),S(4),A(4,4),SIJ(4,4)/S10/MOLW(4)/S11/TBCOOL,TWALLC,HCFILM       TUBRO052
     3/S13/YMEAN(4)/S14/DOUT,DIN,HSC,WATVEL,DEPTH/S15/ENFL(200),              TUBRO053
     4MCONDL(200),YDOT(4),YI(4) /S16/CLAM1,HVLMIN,HFLMIN,WALLH,ATOT,          TUBRO054
     5AXNTOT,AFRONT,DRAT,LROW,ARATIO                                          TUBRO055
      KID=0                                                                   TUBRO056
      LOCK=0                                                                  TUBRO057
      WENTF=0.                                                                TUBRO058
      IF(NROW.GT.2)LROW=NROW-2                                                TUBRO059
      TBAV=TBIN                                                               TUBRO060
      MSTEAM=MDOT(1)                                                          TUBRO061
      TMIN=TLIN+0.06                                                          TUBRO062
C     ITERATIONS ON CONDENSATION RATE,DELTAM                                  TUBRO063
   64 YDOT(1)=MSTEAM/MOLW(1)                                                  TUBRO064
      MFLOW=MSTEAM                                                            TUBRO065
      WET=WETVAP                                                              TUBRO066
      DO 3 I=2,4                                                              TUBRO067
    3 MFLOW=MFLOW+MDOT(I)                                                     TUBRO068
      G=MFLOW/AFRONT                                                          TUBRO069
      GMAX=G*ARATIO                                                           TUBRO070
      K=0                                                                     TUBRO071
      TBULK=TBAV                                                              TUBRO072
```

```
      DUM=YDOT(1)
      DO 1 I=2,4
      YDOT(I)=MDOT(I)/MOLW(I)
    1 DUM=DUM+YDOT(I)
      DO 2 N=1,4
    2 YI(N)=YDOT(N)/DUM
      MOLWM=MFLOW/DUM
      DO 4 I=1,4
    4 YFRACT(I)=YI(I)
      GASVIS=0.
      CALL VISMIX(TBAV,GASVIS)
      PRESS=YI(1)*PTOT
      YUM=PTOT-PRESS
      IF(ABS(YUM).LT.2.E-06)KID=1
      PFRACT=PRESS
      CALL STMTAB(1,PRESS,0.)
      TSAT=TEMP+460.
      IF(TBAV.GE.TSAT)GO TO 77
      TBAV=TSAT
      TBULK=TSAT
   77 TBCOOL=TLIN
C     INITIAL ESTIMATE OF VAPOR-LIQUID INTERFACE TEMPERATURE
      IF(KID)36,36,37
   36 REMAX=GMAX*DOUT/GASVIS
      BLAM=SPHMIX(TBAV)
      KTHMIX=0.
      CALL THCON(TBAV,KTHMIX)
      PR=BLAM*GASVIS/KTHMIX
      STORE=COLBJ(REMAX)
      TMEAN=TBAV
      DIFMIX=0.
      CALL SIMDIF(YI,DIFMIX)
      DRAM=RHCMIX(TBAV)
      LE=DRAM*BLAM*DIFMIX/KTHMIX
      CALL STMTAB(4,PRESS,0.)
      ENTHFG=STEAM(2)-SATLIQ(2)
```

```
      HGFILM=HROW(NROW)*STORE*BLAM*GMAX/PR**0.66666                     TUBRO109
      RAM=UDT*MOLWM*BLAM/(HGFILM*ENTHFG*18.016*LE**0.66666)             TUBRO110
      PINT=PTOT-(PTOT-PFRACT)*EXP(RAM)                                  TUBRO111
      IF(PINT.LE.0.)PINT=0.12                                           TUBRO112
      CALL STMTAB(1,PINT,0.)                                            TUBRO113
      TINT=TEMP+460.                                                    TUBRO114
      IF(TINT.LT.TMIN)TINT=TMIN                                         TUBRO115
      GO TO 38                                                          TUBRO116
   37 TINT=TSAT                                                         TUBRO117
   38 RE=G*DOUT/GASVIS                                                  TUBRO118
   16 COOLH=HCOOL(TBCOOL,DIN,DEPTH,WATVEL)                              TUBRO119
      IF(KID)49,49,41                                                   TUBRO120
   49 M=0                                                               TUBRO121
      KEY=0                                                             TUBRO122
C     ITERATIONS ON INTERFACE TEMPERATURE                               TUBRO123
   12 DTSAT=TSAT-TINT                                                   TUBRO124
      IF(TINT.GT.TSAT.OR.DTSAT.LT.0.05.AND.M.LE.1)GO TO 86              TUBRO125
      IF(TINT.GT.TSAT.OR.DTSAT.LT.0.05.AND.M.GT.1.AND.KEY.EQ.0)GO TO 87 TUBRO126
      IF(TINT.GT.TSAT.OR.DTSAT.LT.0.05.AND.KEY.EQ.1)GO TO 88            TUBRO127
      IF(TINT.LT.TMIN)GO TO 203                                         TUBRO128
      GO TO 89                                                          TUBRO129
  203 TINT=TMIN                                                         TUBRO130
      IF(KEY.EQ.1)TINT3=TINT                                            TUBRO131
      IF(KEY.EQ.0)TINT2=TINT                                            TUBRO132
      GO TO 89                                                          TUBRO133
   86 TINT=TSAT-0.5                                                     TUBRO134
      IF(TINT.LT.TMIN)TINT=TMIN                                         TUBRO135
      TINT2=TINT                                                        TUBRO136
      GO TO 89                                                          TUBRO137
   87 TINT=TSAT-0.05                                                    TUBRO138
      IF(TINT.LT.TMIN)TINT=TMIN                                         TUBRO139
      TINT2=TINT                                                        TUBRO140
      GO TO 89                                                          TUBRO141
   88 TINT=TSAT-0.05                                                    TUBRO142
      IF(TINT.LT.TMIN)TINT=TMIN                                         TUBRO143
      TINT3=TINT                                                        TUBRO144
```

```
C     DETERMINE HEAT AND MASS TRANSFER COEFFICIENTS                     TUBRO145
   89 CALL DIFMLT(YI,DIFMIX)                                            TUBRO146
      DO 5 I=1,4                                                        TUBRO147
    5 YFRACT(I)=YMEAN(I)                                                TUBRO148
      KTHMIX=0.                                                         TUBRO149
      CALL THCON(TMEAN,KTHMIX)                                          TUBRO150
      CALL VISMIX(TMEAN,GASVIS)                                         TUBRO151
      BLAM=SPHMIX(TMEAN)                                                TUBRO152
      DRAM=RHCMIX(TMEAN)                                                TUBRO153
      LE=DRAM*BLAM*DIFMIX/KTHMIX                                        TUBRO154
      GO TO 42                                                          TUBRO155
   41 CALL TBARV                                                        TUBRO156
      GASVIS=MUWTV(TMEAN)                                               TUBRO157
      BLAM=SPHWTV(TMEAN)                                                TUBRO158
      KTHMIX=KTHWTV(TMEAN)                                              TUBRO159
   42 PR=BLAM*GASVIS/KTHMIX                                             TUBRO160
      REMAX=GMAX*DOUT/GASVIS                                            TUBRO161
      STORE=COLBJ(REMAX)                                                TUBRO162
      HGFILM=HROW(NROW)*STORE*BLAM*GMAX/PR**0.66666                     TUBRO163
      IF(KID)39,39,40                                                   TUBRO164
   39 DELTAP=PTOT*(YI(1)-YF(1))                                         TUBRO165
      IF(DELTAP.LE.0.)GO TO 90                                          TUBRO166
      IF(KID.EQ.1)GO TO 37                                              TUBRO167
C     MASS TRANSFER COEFFICIENT                                         TUBRO168
      KGFILM=18.016*HGFILM*LE**0.66666*ALOG((1.-YF(1))/(1.-YI(1)))/(BLAM TUBRO169
     1*DELTAP*MOLWM)                                                    TUBRO170
   40 N=0                                                               TUBRO171
      IF(K.GT.0)GO TO 33                                                TUBRO172
      DELTAT=TINT-TBCOOL                                                TUBRO173
C     DETERMINE TWALL(OUTSIDE) AND OVERALL HEAT TRANSFER COEFFICIENT    TUBRO174
C     FROM CONDENSATE-VAPOR INTERFACE TO BULK COOLANT(BASED UPON AOUT)  TUBRO175
C     ITERATIONS ON OUTSIDE WALL TEMPERATURE                            TUBRO176
      TWALLO=TINT-0.4*DELTAT                                            TUBRO177
      GO TO 61                                                          TUBRO178
   33 IF(TINT-TWALLO)60,60,61                                           TUBRO179
   60 TWALLO=TINT-DTCOND                                                TUBRO180
```

```
   61 TW1=TWALLO                                                          TUBRO181
      DT=TBAV-TINT                                                        TUBRO182
      UOVRL=0.                                                            TUBRO183
    7 CALL UOUT(NROW,DT,WALLH,COOLH,DRAT,UOVRL)                           TUBRO184
      TWALLO=TINT-UOVRL*DELTAT/HCFILM                                     TUBRO185
      IF(ABS((TW1-TWALLO)/TW1).LT.0.0025)GO TO 6                          TUBRO186
      IF(N.GT.20)GO TO 22                                                 TUBRO187
      IF(TINT-TWALLO)62,62,63                                             TUBRO188
   62 DELTAT=TINT-TBCOOL                                                  TUBRO189
      TWALLO=TINT-0.4*DELTAT                                              TUBRO190
   63 TW1=TWALLO                                                          TUBRO191
      N=N+1                                                               TUBRO192
      GO TO 7                                                             TUBRO193
C     DETERMINE AVERAGE SPECIFIC HEAT OF CONDENSATE FILM                  TUBRO194
    6 CPAV=(SPHWTL(TWALLO)+SPHWTL(TINT))/2.                               TUBRO195
C     DETERMINE CONDENSATION RATE                                         TUBRO196
C     HEAT TRANSFER RATE ACROSS VAPOR-GAS FILM                            TUBRO197
      QGF=ATOT*HGFILM*DT                                                  TUBRO198
      DTCOND=TINT-TWALLO                                                  TUBRO199
      REM=0.375*CPAV*DTCOND                                               TUBRO200
      REMPRI=DT*SPHWTV(TMEAN)                                             TUBRO201
      IF(KID)43,43,44                                                     TUBRO202
C     DETERMINE CONDENSATION RATE,DELTAM                                  TUBRO203
   43 PINT=PTOT*YF(1)                                                     TUBRO204
      DELTAM=KGFILM*ATOT*DELTAP                                           TUBRO205
      CALL STMTAB(4,PINT,0.)                                              TUBRO206
      ENTHFG=STEAM(2)-SATLIQ(2)                                           TUBRO207
      GO TO 45                                                            TUBRO208
   44 CALL STMTAB(4,PTOT,0.)                                              TUBRO209
      ENTHFG=STEAM(2)-SATLIQ(2)                                           TUBRO210
      DELTAM=ATOT*(UOVRL*DELTAT-HGFILM*DT)/(ENTHFG+REM+REMPRI)            TUBRO211
   45 UDT=UOVRL*DELTAT                                                    TUBRO212
      QWALL=ATOT*UDT                                                      TUBRO213
   48 IF(NROW.GT.2)GO TO 8                                                TUBRO214
      ENFL(NROW)=DELTAM*(SATLIQ(2)-REM)                                   TUBRO215
      MCONDL(NROW)=DELTAM                                                 TUBRO216
```

```
      IF(KID)50,50,10                                                   TUBRO217
   50 QRHS=QGF+DELTAM*(ENTHFG+REM+REMPRI)                               TUBRO218
      GO TO 9                                                           TUBRO219
C     CONDENSATE MASS FLOW RATE FROM TUBE ROW                           TUBRO220
    8 MCONDL(NROW)=MCONDL(LROW)+DELTAM                                  TUBRO221
      ENFL(NROW)=DELTAM*(SATLIQ(2)-REM)+ENFL(LROW)                      TUBRO222
      IF(KID)47,47,10                                                   TUBRO223
   47 QRHS=QGF+DELTAM*(STEAM(2)+REMPRI)+ENFL(LROW)-ENFL(NROW)           TUBRO224
C     ITERATION SCHEME TO ACHIEVE CORRECT VAPOR-CONDENSATE INTERFACE    TUBRO225
C     TEMPERATURE                                                       TUBRO226
    9 RATIO=(QWALL-QRHS)/QWALL                                          TUBRO227
      IF(ABS(RATIO).LT..005)GO TO 10                                    TUBRO228
      IF(M.GT.100)GO TO 23                                              TUBRO229
      IF(KEY.EQ.1)GO TO 13                                              TUBRO230
      IF(M.GT.0)GO TO 11                                                TUBRO231
C     HAVE NOT YET BRACKETED TINT                                       TUBRO232
      M=1                                                               TUBRO233
      TINT1=TINT                                                        TUBRO234
      TINT=TINT-RATIO*(TSAT-TINT)                                       TUBRO235
      IF(TINT.LT.TMIN)TINT=TMIN                                         TUBRO236
      TINT2=TINT                                                        TUBRO237
      RAT1=RATIO                                                        TUBRO238
      GO TO 12                                                          TUBRO239
   11 RAT2=RATIO                                                        TUBRO240
      M=M+1                                                             TUBRO241
      IF(RATIO.GT.0..AND.TINT.EQ.TMIN)GO TO 10                          TUBRO242
      IF(RAT2.LT.0..AND.RAT1.LT.0..OR.RAT2.GT.0..AND.RAT1.GT.0.)GO TO 35 TUBRO243
C     TINT IS BRACKETED BY TINT1 AND TINT2                              TUBRO244
      KEY=1                                                             TUBRO245
      TINT3=(TINT1+TINT2)/2.                                            TUBRO246
      TINT=TINT3                                                        TUBRO247
      GO TO 12                                                          TUBRO248
   13 RAT3=RATIO                                                        TUBRO249
      IF(ABS(RAT3).GT.ABS(RAT1).AND.ABS(RAT3).GT.ABS(RAT2))GO TO 10     TUBRO250
      M=M+1                                                             TUBRO251
      IF(RAT3.LT.0..AND.RAT2.LT.0..OR.RAT3.GT.0..AND.RAT2.GT.0.)GO TO 14 TUBRO252
```

```
C     TINT IS BRACKETED BY TINT2 AND TINT3                              TUBRO253
      IF(ABS(TINT2-TINT3).LT.0.001)GO TC 10                             TUBRO254
      TINT=(TINT2+TINT3)/2.                                             TUBRO255
      TINT1=TINT2                                                       TUBRO256
      TINT2=TINT3                                                       TUBRO257
      TINT3=TINT                                                        TUBRO258
      RAT1=RAT2                                                         TUBRO259
      RAT2=RAT3                                                         TUBRO260
      GO TO 12                                                          TUBRO261
C     TINT IS BRACKETED BY TINT1 AND TINT3                              TUBRO262
   14 TINT=(TINT1+TINT3)/2.                                             TUBRO263
      IF(ABS(TINT1-TINT3).LT.0.001)GO TO 10                             TUBRO264
      TINT2=TINT3                                                       TUBRO265
      TINT3=TINT                                                        TUBRO266
      RAT2=RAT3                                                         TUBRO267
      GO TO 12                                                          TUBRO268
C     HAVE NOT YET BRACKETED TINT                                       TUBRO269
   35 SIGN=(TINT-TINT1)/ABS(TINT-TINT1)                                 TUBRO270
      TINT1=TINT                                                        TUBRO271
      TINT=TINT+0.1*SIGN*(TSAT-TINT)                                    TUBRO272
      IF(TINT.LT.TMIN)TINT=TMIN                                         TUBRO273
      TINT2=TINT                                                        TUBRO274
      GO TO 12                                                          TUBRO275
C     ITERATION SCHEME TO ACHIEVE CORRECT BULK COOLANT TEMPERATURE       TUBRO276
   10 TLOUT=TLIN+QWALL/(AXNTOT*WATVEL*RHOSW(TBCOOL,DEPTH)*SPHSW(TBCOOL))TUBRO277
      IF(K.EQ.2)GO TO 73                                                TUBRO278
      TBCOOL=(TLOUT+TLIN)/2.                                            TUBRO279
      IF(K.EQ.0)TBCA=TBCOOL                                             TUBRO280
      IF(K.EQ.1)TBCB=TBCOOL                                             TUBRO281
      GO TO 74                                                          TUBRO282
   73 TBCOOL=(TBCA+TBCB)/2.                                             TUBRO283
   74 TMIN=TBCOOL+0.06                                                  TUBRO284
      IF(TLOUT.EQ.TLIN)TLOUT=TLIN+0.001                                 TUBRO285
      IF(TLOUT.GE.TINT)GO TO 206                                        TUBRO286
      DELTAT=(TLOUT-TLIN)/ALOG((TINT-TLIN)/(TINT-TLOUT))                TUBRO287
      GO TO 204                                                         TUBRO288
```

```
  206 IF(TBCOOL.GE.TINT)GO TO 205                                       TUBRO289
      DELTAT=TINT-TBCOOL                                                TUBRO290
      GO TO 204                                                         TUBRO291
  205 DELTAT=TINT-TLIN                                                  TUBRO292
  204 IF(K.GT.10)GO TO 24                                               TUBRO293
      IF(K.GT.0)GO TO 15                                                TUBRO294
   18 TBC1=TBCOOL                                                       TUBRO295
      K=K+1                                                             TUBRO296
      GO TO 16                                                          TUBRO297
   16 IF(ABS(TBCOOL-TBC1).LT.0.5)GO TO 17                               TUBRO298
      GO TO 18                                                          TUBRO299
C     DETERMINATION OF VAPOR-GAS OUTLET CONDITIONS FROM TUBE ROW        TUBRO300
   17 YAM=YDOT(1)                                                       TUBRO301
      CLAM=MDOT(1)-DELTAM                                               TUBRO302
      IF(KID)81,81,84                                                   TUBRO303
C     FIX IF MASS FLOW RATE OF STEAM LEAVING IS LESS THAN THAT FOR A    TUBRO304
C     PARTIAL PRESSURE CORRESPONDING TO BULK COOLANT TEMPERATURE        TUBRO305
   81 IF(CLAM.LT.CLAM1)GO TO 82                                         TUBRO306
      GO TO 55                                                          TUBRO307
   82 CLAM=CLAM1                                                        TUBRO308
      TBOUT=TLIN                                                        TUBRO309
      HVL=HVLMIN                                                        TUBRO310
      DELTAM=MDOT(1)-CLAM                                               TUBRO311
      IF(NROW.GT.2)GO TO 202                                            TUBRO312
      MCONDL(NROW)=DELTAM                                               TUBRO313
      ENFL(NROW)=DELTAM*HFLMIN                                          TUBRO314
      GO TO 66                                                          TUBRO315
  202 MCONDL(NROW)=DELTAM+MCONDL(LROW)                                  TUBRO316
      ENFL(NROW)=ENFL(LROW)+DELTAM*HFLMIN                               TUBRO317
      GO TO 66                                                          TUBRO318
   55 YDOT(1)=CLAM/MOLW(1)                                              TUBRO319
      DUM=DUM+YDOT(1)-YAM                                               TUBRO320
      PFRACT=PTOT*YDOT(1)/DUM                                           TUBRO321
      CALL STMTAB(1,PFRACT,0.)                                          TUBRO322
      TEMSAT=TEMP+460.                                                  TUBRO323
      CALL STMTAB(4,PFRACT,0.)                                          TUBRO324
```

```
      HSATVL=STEAM(2)
      IF(YI(2).LT.2.E-06)GO TO 29
      CP(2)=SPHH2(TBIN)
   29 IF(YI(3).LT.2.E-06)GO TO 30
      CP(3)=SPHO2(TBIN)
   30 IF(YI(4).LT.2.E-06)GO TO 31
      CP(4)=SPHN2(TBIN)
C     DETERMINATION OF AVERAGE MDOT*CP FOR NON-CONDENSIBLES
   31 FUN=0.
      DO 19 I=2,4
      IF(YI(I).LT.2.E-06)GO TO 19
      FUN=FUN+MDOT(I)*CP(I)
   19 CONTINUE
C     DETERMINATION OF AVERAGE CP, BASED UPON SATURATION AND BULK INLET
C     TEMPERATURES
      CP(1)=(SPHWTV(TEMSAT)+SPHWTV(TBIN))/2.
      TEMP=TINT-460.
      CALL STMTAB(5,TEMP,0.)
      DHCON=DELTAM*(STEAM(2)+REMPRI)
      IF(WET.GT.2.E-06)GO TO 91
      GO TO 92
C     DETERMINATION OF ENTHALPY OF WET VAPOR DROPLETS ENTERING A TUBE
C     ROW, ASSUMING EQUILIBRIUM WITH BULK GAS TEMPERATURE
   91 TEMP=TBIN-460.
      CALL STMTAB(2,TEMP,0.)
      WENTE=WET*SATLIQ(2)
      GO TO 20
C     ENERGY EQUATION FOR DETERMINATION OF BULK GAS OUTLET TEMPERATURE
C     WITH SATURATED OR SUPERHEATED CONDITIONS
   92 TBOUT=(MDOT(1)*HVENT-CLAM*(HSATVL-CP(1)*TEMSAT)+FUN*
     1TBIN-QGF-DHCON)/(FUN+CLAM*CP(1))
      IF(TBOUT.LE.TEMSAT)GO TO 79
      TEMP=TBOUT-460.
      CALL STMTAB(7,PFRACT,TEMP)
      HVL=STEAM(2)
      GO TO 65
```

```
   79 HVL=HSATVL                                                          TUBR0361
      TBOUT=TEMSAT                                                        TUBR0362
      GO TO 66                                                            TUBR0363
C     CALCULATION OF ROW EXIT QUALITY,TEMPERATURE,AND DROPLET MASS FLOW   TUBR0364
C     RATE FOR WET VAPOR CONDITIONS                                       TUBR0365
   20 L=0                                                                 TUBR0366
      HBARL=MDOT(1)*HVENT+FUN*TBIN+WENTE-CGF-DHCON                        TUBR0367
      MTOT=CLAM+WET                                                       TUBR0368
      KAY=0                                                               TUBR0369
      TBOUT2=TEMSAT                                                       TUBR0370
      TBOUT1=TEMSAT                                                       TUBR0371
   93 TBOUT1=TBOUT1-0.2*(TEMSAT-TLIN)                                     TUBR0372
      IF(TBOUT1-TLIN)70,94,94                                             TUBR0373
   94 HBARL1=HBARL-FUN*TBOUT1                                             TUBR0374
      TEMP=TBOUT1-460.                                                    TUBR0375
      CALL STMTAB(5,TEMP,0.)                                              TUBR0376
      QUAL=(HBARL1-MTOT*SATLIQ(2))/(MTOT*(STEAM(2)-SATLIQ(2)))            TUBR0377
      WET=(1.-QUAL)*MTOT                                                  TUBR0378
      CLAM=QUAL*MTOT                                                      TUBR0379
      YDOT(1)=CLAM/MOLW(1)                                                TUBR0380
      PFRACT=YDOT(1)*PTOT/(YDOT(1)+RUM)                                   TUBR0381
      CALL STMTAB(4,PFRACT,0.)                                            TUBR0382
      HVL=STEAM(2)                                                        TUBR0383
      TBOUT=TEMP+460.                                                     TUBR0384
      IF(TBOUT.LT.TLIN)GO TO 70                                           TUBR0385
      IF(ABS(TBOUT-TBOUT1).LT.0.2)GO TO 66                                TUBR0386
      IF(L.GT.10)GO TO 25                                                 TUBR0387
      IF(KAY.EQ.1)GO TO 97                                                TUBR0388
      IF(TBOUT.GT.TEMSAT)GO TO 201                                        TUBR0389
      IF(TBOUT-TBOUT1)98,98,99                                            TUBR0390
   98 TBOUT3=TBOUT2                                                       TUBR0391
      TBOUT2=TBOUT1                                                       TUBR0392
      L=L+1                                                               TUBR0393
      GO TO 93                                                            TUBR0394
   97 IF(TBOUT-TBOUT1)96,96,95                                            TUBR0395
   95 TBOUT2=TBOUT1                                                       TUBR0396
```

```
      TBOUT1=(TBOUT2+TBOUT3)/2.                                         TUBR0397
      L=L+1                                                             TUBR0398
      GO TO 94                                                          TUBR0399
   96 TBOUT3=TBOUT1                                                     TUBR0400
      TBOUT1=(TBOUT2+TBOUT3)/2.                                         TUBR0401
      L=L+1                                                             TUBR0402
      GO TO 94                                                          TUBR0403
   99 KAY=1                                                             TUBR0404
      TBOUT3=TBOUT2                                                     TUBR0405
      TBOUT2=TBOUT1                                                     TUBR0406
      TBOUT1=(TBOUT2+TBOUT3)/2.                                         TUBR0407
      L=L+1                                                             TUBR0408
      GO TO 94                                                          TUBR0409
  201 TBOUT2=TEMSAT                                                     TUBR0410
      TBOUT3=TBOUT                                                      TUBR0411
      TBOUT1=(TBOUT2+TBOUT3)/2.                                         TUBR0412
      KAY=1                                                             TUBR0413
      L=L+1                                                             TUBR0414
      GO TO 94                                                          TUBR0415
   84 IF(CLAM)54,54,85                                                  TUBR0416
   85 CALL STMTAB(4,PTOT,0.)                                            TUBR0417
      HVL=(MDOT(1)*HVENT-DELTAM*(STEAM(2)+REMPRI)-QGF)/CLAM             TUBR0418
      CALL STMTAB(8,PTOT,HVL)                                           TUBR0419
      TBOUT=TEMP+460.                                                   TUBR0420
      IF(TBOUT.LT.TSAT)TBOUT=TSAT                                       TUBR0421
      CALL STMTAB(1,PTOT,0.)                                            TUBR0422
      IF(HVL.LE.SATLIQ(2))GO TO 54                                      TUBR0423
      GO TO 21                                                          TUBR0424
C     ITERATION SCHEME FOR CONDENSATION RATE                            TUBR0425
   66 IF(LOCK.EQ.0)GO TO 72                                             TUBR0426
      ERROR=(MDOT(1)-MSTEAM-0.9*DELTAM)/MDOT(1)                         TUBR0427
      IF(ABS(ERROR).LT.0.005)GO TO 21                                   TUBR0428
      IF(LOCK.EQ.1)GO TO 76                                             TUBR0429
      IF(LOCK.GT.10.AND.ABS(DELTAM-DMLAST).LT.0.05)GO TO 21             TUBR0430
      IF(LOCK.GT.20)GO TO 67                                            TUBR0431
      IF(ERROR.GT.0.)GO TO 75                                           TUBR0432
```

```
      ST2=ST1                                                           TUBR0433
      ST1=(ST2+ST3)/2.                                                  TUBR0434
      MSTEAM=ST1                                                        TUBR0435
      LOCK=LOCK+1                                                       TUBR0436
      DMLAST=DELTAM                                                     TUBR0437
      GO TO 64                                                          TUBR0438
   72 RAG=MDOT(1)-0.9*DELTAM                                            TUBR0439
      MSTEAM=RAG                                                        TUBR0440
      LOCK=LOCK+1                                                       TUBR0441
      DMLAST=DELTAM                                                     TUBR0442
      GO TO 64                                                          TUBR0443
   76 ST2=MDOT(1)                                                       TUBR0444
      ST3=RAG                                                           TUBR0445
      ST1=(ST2+ST3)/2.                                                  TUBR0446
      LOCK=LOCK+1                                                       TUBR0447
      MSTEAM=ST1                                                        TUBR0448
      DMLAST=DELTAM                                                     TUBR0449
      GO TO 64                                                          TUBR0450
   75 ST3=ST1                                                           TUBR0451
      ST1=(ST2+ST3)/2.                                                  TUBR0452
      MSTEAM=ST1                                                        TUBR0453
      LOCK=LOCK+1                                                       TUBR0454
      DMLAST=DELTAM                                                     TUBR0455
      GO TO 64                                                          TUBR0456
   22 WRITE(6,105)N                                                     TUBR0457
      GO TO 26                                                          TUBR0458
   23 WRITE(6,101)M                                                     TUBR0459
      GO TO 26                                                          TUBR0460
   24 WRITE(6,102)K                                                     TUBR0461
      GO TO 26                                                          TUBR0462
   25 WRITE(6,103)L                                                     TUBR0463
  105 FORMAT(1X,'EXCESSIVE NUMBER OF ITERATIONS ON TWALLO')             TUBR0464
  101 FORMAT(1X,'EXCESSIVE NO OF ITERATIONS ON TINT')                   TUBR0465
  102 FORMAT(1X,'EXCESSIVE NO OF ITERATIONS ON TBCOOL')                 TUBR0466
  103 FORMAT(1X,'EXCESSIVE NO OF ITERATIONS ON TBOUT')                  TUBR0467
   26 NERROR=1                                                          TUBR0468
```

```
   67 WRITE(6,137)DELTAM                                                        TUBRO469
  137 FORMAT(1X,'EXCESSIVE ITERATIONS ON DELTAM,DELTAM=',F10.2)                 TUBRO470
      GO TO 69                                                                  TUBRO471
   21 MDOT(1)=CLAM                                                              TUBRO472
      WETVAP=WET                                                                TUBRO473
      IF(TBOUT.LE.TLIN)GO TO 70                                                 TUBRO474
      GO TO 27                                                                  TUBRO475
   69 NERROR=4                                                                  TUBRO476
      GO TO 27                                                                  TUBRO477
   70 NERROR=5                                                                  TUBRO478
      GO TO 27                                                                  TUBRO479
   90 NERROR=6                                                                  TUBRO480
      GO TO 27                                                                  TUBRO481
   54 NERROR=3                                                                  TUBRO482
   27 RETURN                                                                    TUBRO483
      END                                                                       TUBRO484
```

```
      SUBROUTINE DIFMLT(YI,DIFMIX)                                      DIFM0001
C     SUB  PROGRAM TO COMPUTE THE MULTICOMPONENT GAS DIFFUSION COEFFT   DIFM0002
C     FOR WATER VAPOR DIFFUSING THROUGH A BOUNDARY LAYER CONSISTING     DIFM0003
C     OF WATER VAPOR AND A MIXTURE OF STAGNANT HYDROGEN,OXYGEN AND      DIFM0004
C     NITROGEN(STAGNANTIN THE DIRECTION NORMAL TO THE MAIN FLOW)        DIFM0005
C     RETURNS YMEAN-THE ARITHMETIC MEAN MOLE FRACTION OF EACH OF        DIFM0006
C     THE COMPONENT GASES ACROSS THE BOUNDARY LAYER -TO THE COMMON  REGN DIFM0007
C     USES SCIENTIFIC SUBROUTINE PACKAGE PROGRAM HPCG WITH SUBROUTINES  DIFM0008
C     RHS AND OUTP                                                      DIFM0009
C     REF. REID AND SHERWOOD,THE PROPERTIES OF GASES AND LIQUIDS, AND   DIFM0010
C     WILKE,C.R.,DIFFUSIONAL PROPERTIES OF MULTICOMPONENT GASES,        DIFM0011
C     CHEMICAL ENGINEERING PROGRESS,46(2),FEB. 1950,PP 95-104           DIFM0012
      EXTERNAL RHS,OUTP                                                 DIFM0013
      REAL MOLW,MU,KTH                                                  DIFM0014
      DIMENSION YI(4)                                                   DIFM0015
      COMMON /S1/PRESS,TEMP,QUAL,SATLIQ(3),STEAM(3),COEFFT(237)         DIFM0016
     1/S2/TBULK,TINT,RE/S3/TMEAN/S4/PTOT/S5/DCOE(4)/S6/YF(4)/S7/CRUM    DIFM0017
     2/S8/YFRACT(4),MU(4),RHO(4),CP(4),KTH(4),S(4),A(4,4),SIJ(4,4)      DIFM0018
     3/S9/EPSK(6),CONST(6)/S10/MOLW(4)/S12/DERY(4),PRMT(5),AUX(16,4),   DIFM0019
     4Y(4)/S13/YMEAN(4)                                                 DIFM0020
      CALL TBARV                                                        DIFM0021
      DO 1 I=2,4                                                        DIFM0022
    1 CALL DCOEAV(I)                                                    DIFM0023
      TSTEAM=TINT-460.                                                  DIFM0024
      CALL STMTAB(2,TSTEAM,0.)                                          DIFM0025
      YF(1)=PRESS/PTOT                                                  DIFM0026
      YLAST=YF(1)                                                       DIFM0027
      RUM=1.-YF(1)                                                      DIFM0028
      TUM=1.-YI(1)                                                      DIFM0029
      DO 4 N=2,4                                                        DIFM0030
    4 YF(N)=RUM*YI(N)/TUM                                               DIFM0031
      IF(YI(2).LT.2.E-06.AND.YI(3).LT.2.E-06)GO TO 26                   DIFM0032
      IF(YI(3).LT.2.E-06.AND.YI(4).LT.2.E-06)GO TO 27                   DIFM0033
      IF(YI(2).LT.2.E-06.AND.YI(4).LT.2.E-06)GO TO 28                   DIFM0034
      GO TO 29                                                          DIFM0035
   26 DIFMIX=DCOE(4)                                                    DIFM0036
```

```
      GO TO 30                                                          DIFM0037
   27 DIFMIX=DCOE(2)                                                    DIFM0038
      GO TO 30                                                          DIFM0039
   28 DIFMIX=DCOE(3)                                                    DIFM0040
      GO TO 30                                                          DIFM0041
   29 DRUM=ALOG((1.-YF(1))/(1.-YI(1)))                                  DIFM0042
      BNUM=(2.-YF(1)-YI(1))*DRUM                                        DIFM0043
      DEN=0.                                                            DIFM0044
      DO 15 I=2,4                                                       DIFM0045
   15 DEN=DEN+(YI(I)+YF(I))/DCOE(I)                                     DIFM0046
      CRUM=BNUM/(DEN*TMEAN)                                             DIFM0047
      M=0                                                               DIFM0048
      NTRIAL=0                                                          DIFM0049
      KEY=0                                                             DIFM0050
      CRUM1=CRUM                                                        DIFM0051
   10 DO 17 I=1.4                                                       DIFM0052
   17 Y(I)=YI(I)                                                        DIFM0053
      CALL HPCG(PRMT,Y.DERY,4,IHLF,RHS,CUTP,AUX)                        DIFM0054
      IF(NTRIAL.GT.20)GO TO 8                                           DIFM0055
      RATIO=(YLAST-YF(1))/YLAST                                         DIFM0056
      IF(ABS(RATIO).LT.0.01)GO TO 9                                     DIFM0057
      IF(KEY.EQ.1)GO TO 23                                              DIFM0058
      IF(NTRIAL.GT.0)GO TO 19                                           DIFM0059
      CRUM=CRUM*(1.-RATIO)                                              DIFM0060
      CRUM2=CRUM                                                        DIFM0061
      RAT1=RATIO                                                        DIFM0062
      NTRIAL=1                                                          DIFM0063
      GO TO 10                                                          DIFM0064
   19 RAT2=RATIO                                                        DIFM0065
      NTRIAL=NTRIAL+1                                                   DIFM0066
      IF(RAT2.LT.0..AND.RAT1.LT.0..OR.RAT2.GT.0..AND.RAT1.GT.0.)GO TO 20 DIFM0067
C     CRUM IS BRACKETED BY CRUM1 AND CRUM2 WITH RAT1 AND RAT2           DIFM0068
      KEY=1                                                             DIFM0069
      CRUM3=(CRUM1+CRUM2)/2.                                            DIFM0070
      CRUM=CRUM3                                                        DIFM0071
      GO TO 10                                                          DIFM0072
```

```
   23 RAT3=RATIO                                                        DIFM0073
      NTRIAL=NTRIAL+1                                                   DIFM0074
      IF(RAT3.LT.0..AND.RAT2.LT.0..OR.RAT3.GT.0..AND.RAT2.GT.0.)GO TO 24 DIFM0075
C     CRUM IS BRACKETED BY CRUM2 AND CRUM3                              DIFM0076
      CRUM=(CRUM2+CRUM3)/2.                                             DIFM0077
      CRUM1=CRUM2                                                       DIFM0078
      CRUM2=CRUM3                                                       DIFM0079
      CRUM3=CRUM                                                        DIFM0080
      RAT2=RAT3                                                         DIFM0081
      GO TO 10                                                          DIFM0082
C     CRUM IS BRACKETED BY CRUM1 AND CRUM3                              DIFM0083
   24 CRUM=(CRUM1+CRUM3)/2.                                             DIFM0084
      CRUM2=CRUM3                                                       DIFM0085
      CRUM3=CRUM                                                        DIFM0086
      RAT2=RAT3                                                         DIFM0087
      GO TO 10                                                          DIFM0088
C      CRUM IS FURTHER IN THE DIRECTION OF THE MOST RECENTLY CALCULATED DIFM0089
C     CRUM MINUS THE PREVIOUSLY CALCULATED CRUM                         DIFM0090
   20 RAT2=RAT1                                                         DIFM0091
      SIGN=(CRUM-CRUM1)/ABS(CRUM-CRUM1)                                 DIFM0092
      CRUM1=CRUM                                                        DIFM0093
      CRUM=CRUM+0.1*SIGN*CRUM                                           DIFM0094
      CRUM2=CRUM                                                        DIFM0095
      GO TO 10                                                          DIFM0096
    9 M=1                                                               DIFM0097
      GO TO 11                                                          DIFM0098
    8 WRITE(6,104)                                                      DIFM0099
  104 FORMAT(1X,'EXCESSIVE NUMBER OF TRIALS')                           DIFM0100
      WRITE(6,103)YLAST,(YF(I),I=1,4)                                   DIFM0101
  103 FORMAT(1X,'YLAST   =',F10.4,1X,'YF(1)=',F10.4,1X,'YF(2)=',F10.4,  DIFM0102
     11X,'YF(3)=',F10.4,1X,'YF(4)=',F10.4)                              DIFM0103
   11 IF(M.EQ.0)GO TO 13                                                DIFM0104
      DEN=0.                                                            DIFM0105
      DO 14 I=2,4                                                       DIFM0106
   14 DEN=DEN+0.5*(YI(I)+YF(I))/DCOE(I)                                 DIFM0107
      DIFMIX=TMEAN*CRUM/DRUM                                            DIFM0108
```

```
30 DO 25 I=1,4                                                                  DIFM0109
25 YMEAN(I)=0.5*(YI(I)+YF(I))                                                   DIFM0110
13 RETURN                                                                       DIFM0111
   END                                                                          DIFM0112
```

```
      SUBROUTINE RHS(ZETA,Y,DERY)
C     SUBROUTINE FOR DETERMINATION OF THE RIGHT HAND SIDES OF A SET OF
C     FIRST ORDER DIFFERENTIAL EQUATIONS -USED IN CONJUNCTION WITH
C     SCIENTIFIC SUBROUTINE PACKAGE SUBPROGRAM HPCG
      DIMENSION Y(4),DERY(4)
      COMMON /S5/DCOE(4)/S7/CRUM
      SUM=0.
      CALL TZETA(ZETA,TEMPR)
      ZUM=CRUM*TEMPR
      DO 1 I=2,4
      IF(Y(I).LT.2.E-06)GO TO 2
      CALL DIFFUS(TEMPR,I,DIFCOE)
      GO TO 3
    2 DERY(I)=0.
      GO TO 1
    3 A=Y(I)/DIFCOE
      SUM=SUM+A
      DERY(I)=A*ZUM
    1 CONTINUE
      DERY(1)=-ZUM*SUM
      RETURN
      END
```

```
      SUBROUTINE OUTP(ZETA,Y,DERY,IHLF,NDIM,PRMT)                       OUTP0001
C     OUTPUT SUBROUTINE USED IN CONJUNCTION WITH SCIENTIFIC SUB-        OUTP0002
C     ROUTINE PACKAGE SUBPROGRAM HPCG                                   OUTP0003
      COMMON /S6/YF(4)                                                  OUTP0004
      DIMENSION Y(4),DERY(4),PRMT(5)                                    OUTP0005
      IF(ZETA.LT.0.9999)GO TO 1                                         OUTP0006
      DO 2 I=1,4                                                        OUTP0007
    2 YF(I)=Y(I)                                                        OUTP0008
    1 RETURN                                                            OUTP0009
      END                                                               OUTP0010
```

```
      SUBROUTINE TZETA(ZETA,TEMP)
C     SUBROUTINE TO DETERMINE THE TEMPERATURE IN THE THERMAL BOUNDARY
C     LAYER WITH THE ASSUMED PROFILES FOR TURBULENT AND LAMINAR FLOW
C     EQUAL TO THE VELOCITY PROFILE IN THE MOMENTUM BOUNDARY LAYER
C     USED IN CONJUNCTION WITH SUBROUTINE RHS IN THE DETERMINATION OF
C     THE AVERAGE DIFFUSION COEFFICIENT FOR THE BOUNDARY LAYER
      COMMON /S2/TBULK,TINT,RE
      IF(RE.GT.10.)GO TO 1
      TEMP=TBULK+(TINT-TBULK)*ZETA**2
      GO TO 2
    1 TEMP=TBULK+(TINT-TBULK)*(1.-(1.-ZETA)**0.142857)
    2 RETURN
      END
```

```
      SUBROUTINE DIFFUS(TEMP,MIX,DIFCOE)                                DIFF0001
C     SUBROUTINE TO  DETERMINE THE DIFFUSION COEFFICIENT FOR THE BELOW  DIFF0002
C     LISTED GAS MIXTURES AS A FUNCTION OF TEMPERATURE IN DEG R AND     DIFF0003
C     PRESSURE(TOTAL)IN PSIA-DIFFUSION COEFF IN SQ FT/HR                DIFF0004
C     REF. REID AND SHERWOOD, THE PROPERTIES OF GASES AND LIQUIDS       DIFF0005
C     MIXTURE 1-OXYGEN AND NITROGEN                                     DIFF0006
C     MIXTURE 2-WATER VAPOR AND HYDROGEN                                DIFF0007
C     MIXTURE 3-WATER VAPOR AND OXYGEN                                  DIFF0008
C     MIXTURE 4-WATER VAPOR AND NITROGEN                                DIFF0009
C     MIXTURE 5-HYDROGEN AND OXYGEN                                     DIFF0010
C     MIXTURE 6-HYDROGEN AND NITROGEN                                   DIFF0011
      COMMON /S4/PTOT/S9/EPSK(6),CONST(6)                               DIFF0012
      TSTAR=TEMP/EPSK(MIX)                                              DIFF0013
      DIFCOE=CONST(MIX)*TEMP**1.5/(PTOT*OMEGAD(TSTAR))                  DIFF0014
      RETURN                                                            DIFF0015
      END                                                               DIFF0016
```

```
      FUNCTION OMEGAD(TSTAR)                                            OMEG0001
C     SUBROUTINE TO  GIVE THE COLLISION INTEGRAL,OMEGA SUB D, AS A      OMEG0002
C     FUNCTION OF TSTAR,WHERE TSTAR=K*T/EPSILON SUB ZERO SUB IJ         OMEG0003
C     K=BOLTZMAN CONSTANT                                               OMEG0004
C     T=TEMP IN DEG R                                                   OMEG0005
C     EPSILON SUB ZERO/K(DEG R)=1456.38  H2O                            OMEG0006
C                               107.46  H2                              OMEG0007
C                               192.06  O2                              OMEG0008
C                               128.52  N2                              OMEG0009
C     (EPSILON SUB ZERO SUB IJ)/K=SQRT((EPSILON SUB ZERO SUB I)/K*      OMEG0010
C     (EPSILON SUB ZERO SUB J)/K)                                       OMEG0011
C     TSTAR=T/(EPSILON SUB ZERO SUB IJ)/K                               OMEG0012
      IF(TSTAR.GT.2.00)GO TO 1                                          OMEG0013
      OMEGAD=EXP(0.364251-ALOG(TSTAR)*(0.491413-ALOG(TSTAR)*(0.803484   OMEG0014
     1E-01+ALOG(TSTAR)*(0.446723E-01-ALOG(TSTAR)*(0.16655E-01           OMEG0015
     2+ALOG(TSTAR)*0.775636E-02)))))                                    OMEG0016
      GO TO 2                                                           OMEG0017
    1 OMEGAD=EXP(0.390106-ALOG(TSTAR)*(0.586802-ALOG(TSTAR)*(0.220513   OMEG0018
     1-ALOG(TSTAR)*(0.553505E-01-ALOG(TSTAR)*(0.678335E-02              OMEG0019
     2-ALOG(TSTAR)*0.323991E-03)))))                                    OMEG0020
    2 IF(TSTAR.GT.400..OR.TSTAR.LT.0.30)WRITE(6,100)TSTAR               OMEG0021
  100 FORMAT(1X,'OUTSIDE THE RANGE OF OMEGAD,TSTAR=',F10.2)             OMEG0022
      RETURN                                                            OMEG0023
      END                                                               OMEG0024
```

```
      SUBROUTINE CCOEAV(MIX)                                            DCOE0001
C     SUBROUTINE TO DETERMINE THE AVERAGE DIFFUSION COEFFICIENT FOR A   DCOE0002
C     MIXTURE OF GASES AT A TEMPERATURE TMEAN IN DEGREES R              DCOE0003
C     MIXTURES SPECIFIED IN SUBROUTINE DIFFUS                           DCOE0004
      COMMON /S3/TMEAN/S5/DCOE(4)                                       DCOE0005
      CALL DIFFUS(TMEAN,MIX,DIFCOE)                                     DCOE0006
      DCOE(MIX)=DIFCOE                                                  DCOE0007
      RETURN                                                            DCOE0008
      END                                                               DCOE0009
```

```
      SUBROUTINE SIMDIF(YI,DIFMIX)                                      SIMD0001
C     SUBROUTINE TO CALCULATE THE DIFFUSION COEFFICIENT OF A MULTI-     SIMD0002
C     COMPONENT MIXTURE OF STEAM,HYDROGEN,OXYGEN,AND NITROGEN USING A   SIMD0003
C     PREDETERMINED MEAN TEMPERATURE FOR THE BOUNDARY LAYER             SIMD0004
      COMMON /S2/TBULK,TINT,RE/S3/TMEAN/S5/DCOE(4)                      SIMD0005
      DIMENSION YI(4)                                                   SIMD0006
      DEN=0.                                                            SIMD0007
      DO 1 I=2,4                                                        SIMD0008
      CALL DCOEAV(I)                                                    SIMD0009
    1 DEN=DEN+YI(I)/DCOE(I)                                             SIMD0010
      DIFMIX=(1.-YI(1))/DEN                                             SIMD0011
      RETURN                                                            SIMD0012
      END                                                               SIMD0013
```

```
      SUBROUTINE TBARV                                                  TBAR0001
C     SUBROUTINE TO DETERMINE THE AVERAGE TEMPERATURE IN THE THERMAL    TBAR0002
C     BOUNDARY LAYER,THE TEMPERATURE DISTRIBUTUON ASSUMED EQUIVALENT    TBAR0003
C     TO THE VELOCITY DISTRIBUTION IN THE MOMENTUM BOUNDARY LAYER       TBAR0004
      COMMON /S2/TBULK,TINT,RE/S3/TMEAN                                 TBAR0005
      IF(RE.GT.10.)GO TO 1                                              TBAR0006
      TMEAN=TBULK+(TINT-TBULK)/4.                                       TBAR0007
      GO TO 2                                                           TBAR0008
    1 TMEAN=TBULK+(TINT-TBULK)/2.                                       TBAR0009
    2 RETURN                                                            TBAR0010
      END                                                               TBAR0011
```

```
      SUBROUTINE UOUT(NROW,DT,WALLH,COOLH,DRAT,UOVRL)                   UOUT0001
C     SUBROUTINE TO DETERMINE THE OVERALL HEAT TRANSFER COEFFICIENT     UOUT0002
C     OF A TUBE ON WHICH CONDENSATION IS OCCURING IN A BANK CF          UOUT0003
C     STAGGERED TUBES--THIS COEFFICIENT APPLIES BETWEEN THE             UOUT0004
C     CONDENSATE-VAPOR INTERFACE AND THE BULK COOLANT FLOWING IN        UOUT0005
C     THE TUBE--THE OVERALL COEFFICIENT COMPRISES THE CONDENSATE HT XFER UOUT0006
C     COEFFICIENT FOR A TUBE IN A STAGGERED BANK BASED ON NUSSELT'S     UOUT0007
C     ANALYSIS AS MODIFIED BY CHEN,HCOND,AN EQUIVALENT HEAT             UOUT0008
C     TRANSFER COEFFICIENT FOR THE TUBE WALL BASED ON OUTER DIAMETER    UOUT0009
C     WALLH,A SCALE COEFFICIENT,HSC,AND A COOLANT FILM COEFFICIENT,     UOUT0010
C     COOLH,BASED ON MCADAM'S CORRELATION                               UOUT0011
C     UNITS-BTU/HR SQ FT DEG R                                          UOUT0012
      COMMON /S2/TBULK,TINT,RE/S11/TBCOOL,TWALLO,HCFILM/S14/DOUT,DIN,   UOUT0013
     1HSC,WATVEL,DEPTH                                                  UOUT0014
      ZAP=DOUT/DIN                                                      UOUT0015
      HCFILM=HCOND(TINT,TWALLO,DOUT,DT,NROW)                            UOUT0016
      UOVRL=1./(DRAT/COOLH+DRAT/HSC+1./WALLH+1./HCFILM)                 UOUT0017
      RETURN                                                            UOUT0018
      END                                                               UOUT0019
```

```
      FUNCTION HRCW(NROW)                                               HROW0001
C     SUBROUTINE TO DETERMINE THE MULTIPLICATIVE FACTOR FOR HEAT        HROW00C2
C     TRANSFER AND MASS TRANSFER COEFFICIENT FOR A PARTICULAR RCW IN A  HROW0003
C     STAGGERED BANK OF TUBES BASED UPON COLBURN'S FOUR ROW AVERAGE DATAHROW0004
C     AND THE DATA OF KAYS AND LO PRESENTED IN MCADAMS                  HROW0005
      GO TO (1,2,3,4,5),NROW                                            HROW0006
      HROW=1.205                                                        HROW0007
      GO TO 6                                                           HROW0008
    1 HROW=0.759                                                        HROW0009
      GO TO 6                                                           HROW0010
    2 HROW=0.916                                                        HROW0011
      GO TO 6                                                           HROW0012
    3 HROW=1.120                                                        HROW0013
      GO TO 6                                                           HROW0014
    4 HROW=1.181                                                        HROW0015
      GO TO 6                                                           HROW0016
    5 HROW=1.193                                                        HROW0017
    6 RETURN                                                            HROW0018
      END                                                               HROW0019
```

```
      FUNCTION HCOND(TINT,TWALLO,DOUT,DT,NROW)                          HCON0001
C     SUBPROGRAM TO DETERMINE THE HEAT TRAMSFER COEFFICIENT ACROSS A    HCON0002
C     CONDENSATE FILM ON THE OUTSIDE OF A TUBE IN A STAGGERED BANK      HCON0003
C     IN BTU/HR SQ FT DEG R BASED UPON NUSSELT'S ANLAYSIS AS MODIFIED   HCON0004
C     BY CHEN--A FUNCTION OF TUBE OUTSIDE DIAMETER,INTERFACT AND WALL   HCON0005
C     TEMPERATURES, AMD ROW NUMBER                                      HCON0006
      COMMON /S1/PRESS,TEMP,QUAL,SATLIQ(3),STEAM(3),COEFFT(237)/S3/TMEAN HCON0007
      REAL MUH2OL,KTHWTL                                                HCON0008
      TEMP=TINT-460.                                                    HCON0009
      CALL STMTAB(5,TEMP,0.)                                            HCON0010
      DELTAT=TINT-TWALLO                                                HCON0011
      TAV=TINT-0.375*DELTAT                                             HCON0012
      G=4.17E+08                                                        HCON0013
      XIFG=STEAM(2)-SATLIQ(2)                                           HCON0014
      XIFGPR=XIFG+0.375*SPHWTL(TAV)*DELTAT+DT*SPHWTV(TMEAN)             HCON0015
      GLUM=(G*(RHOWTL(TAV))**2*(KTHWTL(TAV))**3*XIFGPR/(DOUT*MUH2OL(TAV) HCON0016
     1*DELTAT))**0.25                                                   HCON0017
      IF(NROW.GT.2)GO TO 1                                              HCON0018
      HCOND=0.728*GLUM                                                  HCON0019
      GO TO 4                                                           HCON0020
    1 RUM=0.2*SPHWTL(TAV)*DELTAT/XIFG                                   HCON0021
      XROW=FLOAT(NROW/2)                                                HCON0022
      Z=FLOAT(NROW)/2.-XROW                                             HCON0023
      IF(ABS(Z).GT.0.001)GO TO 2                                        HCON0024
C     NROW IS EVEN                                                      HCON0025
    3 HCOND=XROW*(0.728*(1.+(XROW-1.)*RUM)*GLUM/XROW**0.25)-(XROW-1.)*  HCON0026
     1(0.728*(1.+(XROW-2.)*RUM)*GLUM/(XROW-1.)**0.25)                   HCON0027
      GO TO 4                                                           HCON0028
C     NROW IS ODD                                                       HCON0029
    2 XROW=FLOAT(NROW+1)/2.                                             HCON0030
      GO TO 3                                                           HCON0031
    4 RETURN                                                            HCON0032
      END                                                               HCON0033
```

```
      FUNCTION HCOOL(TBCOOL,DIN,DEPTH,WATVEL)                               HC000001
C     FUNCTION TO DETERMINE THE HEAT TRANSFER COEFFICIENT IN BTU/HR         HC000002
C     SQ FT DEG R OF SALT WATER IN TURBULENT PIPE FLOW AS A FUNCTION        HC000003
C     OF BULK TEMPERATURE IN DEG R,DEPTH OF WATER IN FT,AVERAGE WATER       HC000004
C     VELOCITY IN FT/HR AND PIPE INTERNAL DIAMETER IN FT ACCORDING TO       HC000005
C     MCADAM'S CORRELATION                                                  HC000006
      REAL KTHSW,MUSW                                                       HC000007
      HCOOL=0.023*(KTHSW(TBCOOL,DEPTH))**0.6*(RHOSW(TBCOOL,DEPTH)*WATVEL    HC000008
     1)**.8*(SPHSW(TBCOOL)/MUSW(TBCOOL,DEPTH))**0.4/DIN**0.2                HC000009
      RETURN                                                                HC000010
      END                                                                   HC000011
```

```
      FUNCTION HWALL(KTHWAL,DCUT,DIN)                                   HWAL0001
C     SUBPROGRAM TO DETERNINE AN EQUIVALENT WALL HEAT TRANSFER          HWAL0002
C     COEFFICIENT OF A TUBE WITH THERMAL CONDUCTIVITY,KTHWAL(BTU/HR FT  HWAL0003
C     DEG R), AND OUTER DIAMETER,DOUT(FT),INNER DIAMETER,DIN(FT),BASED  HWAL0004
C     ON TUBE OUTER DIAMETER--UNITS BTU/HR SQ FT DEG R                  HWAL0005
      REAL KTHWAL                                                       HWAL0006
      HWALL=2.*KTHWAL/(DOUT*ALOG(DOUT/DIN))                             HWAL0007
      RETURN                                                            HWAL0008
      END                                                               HWAL0009
```

```
      REAL FUNCTION KTHSW(T,D)                                          KTHS0001
C     SUBPROGRAM TO DETERMINE THE THERMAL CONDUCTIVITY OF SALT WATER    KTHS0002
C     IN BTU/HR FT DEG R AS A FUNCTION OF TEMPERATURE IN DEG R AND      KTHS0003
C     DEPTH IN FT                                                       KTHS0004
      PR=PRESSW(D)/3203.6                                               KTHS0005
      TR=T/1165.44                                                      KTHS0006
      EZERO=14.55-0.8*(TR-0.4)                                          KTHS0007
      CONFAC=1.+0.117*PR/EZERO                                          KTHS0008
      KTHSW=CONFAC*(-0.121505E+01+T*(0.904306E-02-T*(0.230692E-04-T*    KTHS0009
     1(0.32855E-07-T*(0.248241E-10-T*0.758733E-14)))))                  KTHS0010
      IF(T.GT.815.4 .OR.T.LT.491.4)WRITE(6,100)T                        KTHS0011
  100 FORMAT(1X,'OUTSIDE THE TEMP RANGE OF KTHSW,TEMP=',F10.2)          KTHS0012
      RETURN                                                            KTHS0013
      END                                                               KTHS0014
```

```
      FUNCTION PRESSW(D)
C     SUBPROGRAM TO DETERMINE THE PRESSURE IN LBF/IN**2 OF SALT WATER
C     AS A FUNCTION OF DEPTH IN FT
      IF(D.LE.300.)GO TO 1
      IF(D.LE.600.)GO TO 2
      IF(D.LE.6000.)GO TO 3
      PRESSW=0.4456*D+0.2972E-06*D**2
      GO TO 4
    1 PRESSW=0.44236*D
      GO TO 4
    2 PRESSW=0.4402*D+0.3611E-05*D**2
      GO TO 4
    3 PRESSW=C.4439*D+0.4375E-06*D**2
    4 RETURN
      END
```

```
      FUNCTION RHOSW(T,D)                                                       RHOS0001
C     FUNCTION TO DETERMINE THE DENSITY OF SALT WATER IN LBM/FT**3              RHOS0002
C     AS A FUNCTION OF TEMPERATURE IN DEG R AND DEPTH IN FT                     RHOS0003
      P=PRESSW(D)                                                               RHOS0004
    4 IF(P.LE.4410.)GO TO 5                                                     RHOS0005
      RHOSW=(1.0023+.272E-05*P)*(0.132143E+02+T*(0.263591-T*(0.43522E-03        RHOS0006
     1-T*0.223489E-06)))                                                        RHOS0007
      GO TO 6                                                                   RHOS0008
    5 RHOSW=(1.+0.310E-05*P)*(0.132143E+02+T*(0.263591-T*(0.43522E-03-T*        RHOS0009
     10.223489E-06)))                                                           RHOS0010
    6 IF(T.LT.500..OR.T.GT.545.)WRITE(6,100)T                                   RHOS0011
  100 FORMAT(1X,'OUTSIDE THE TEMP LIMITS OF RHOSW,TEMP=',F10.2)                 RHOS0012
      IF(P.GT.10300.)WRITE(6,101)P                                              RHOS0013
  101 FORMAT(1X,'OUTSIDE THE PRESS RANGE OF RHOSW, PRESS=',F10.2)               RHOS0014
      RETURN                                                                    RHOS0015
      END                                                                       RHOS0016
```

```
      REAL FUNCTION KTHWTL(T)                                           KTHW0001
C     FUNCTION TO DETERMINE THE THERMAL CONDUCTIVITY OF SATURATED       KTHW0002
C     LIQUID WATER IN BTU/HR FT DEG R AS A FUNCTION OF TEMPERATURE IN   KTHW0003
C     DEG R                                                             KTHW0004
      KTHWTL=-0.159334E+01+T*(0.115501E-01-T*(0.297468E-04-T*(0.417299  KTHW0005
     1E-07-T*(0.305779E-10-T*0.897563E-14))))                           KTHW0006
      IF(T.GT.954..OR.T.LT.486.)WRITE(6,100)T                           KTHW0007
  100 FORMAT(1X,'OUTSIDE THE TEMP RANGE OF KTHWTL,TEMP=',F10.2)         KTHW0008
      RETURN                                                            KTHW0009
      END                                                               KTHW0010
```

```
      FUNCTION RHOWTL(T)                                                RHOW0001
C     FUNCTION TO DETERMINE THE DENSITY OF SATURATED LIQUID WATER IN    RHOW0002
C     LBM/FT**3 AS A FUNCTION OF TEMPERATURE IN DEG R                   RHOW0003
      RHOWTL=-0.989888E+02+T*(0.109695E+01-T*(0.292341E-02-T*(0.386525RHOW0004
     1E-05-T*(0.256658E-08-T*0.673921E-12))))                           RHOW0005
      IF(T.GT.942..OR.T.LT.492.)WRITE(6,100)T                           RHOW0006
  100 FORMAT(1X,'OUTSIDE THE TEMP LIMITS OF RHOWTL,TEMP=',F10.2)        RHOW0007
      RETURN                                                            RHOW0008
      END                                                               RHOW0009
```

```
      REAL FUNCTION MUH2OL(T)                                           MUH20001
C     FUNCTION TO DETERMINE THE VISCOSITY OF LIQUID WATER IN LBM/HR FT  MUH20002
C     AS A FUNCTION OF TEMPERATURE IN DEG R                             MUH20003
      IF(T.LE.654.)GO TO 1                                              MUH20004
      MUH2OL=EXP(-0.228646E+03-ALOG(T)*(0.129293E+03-ALOG(T)*           MUH20005
     1(0.736894E+02-ALOG(T)*(0.719914E+01+ALOG(T)*(0.482603             MUH20006
     2-ALOG(T)*0.684196E-01)))))                                        MUH20007
      GO TO 2                                                           MUH20008
    1 MUH2OL=EXP(0.240077E+04-ALOG(T)*(0.726488E+03-ALOG(T)*(0.136497   MUH20009
     1E+02+ALOG(T)*(0.980581E+01-ALOG(T)*(0.114972+ALOG(T)*             MUH20010
     20.640635E-01)))))                                                 MUH20011
    2 IF(T.GT.897..OR.T.LT.492.)WRITE(6,100)T                           MUH20012
  100 FORMAT(1X,'OUTSIDE THE TEMP RANGE OF MUH2OL,TEMP=',F10.2)         MUH20013
      RETURN                                                            MUH20014
      END                                                               MUH20015
```

```
      FUNCTION SPHSW(T)                                                 SPHS0001
C     FUNCTION TO DETERMINE THE SPECIFIC HEAT OF SALT WATER IN BTU/     SPHS0002
C     HR FT DEG R AS A FUNCTION OF TEMPERATURE IN DEG R                 SPHS0003
      SPHSW=0.574673+T*(0.199028E-02-T*(0.353152E-05-T*0.213965E-08))   SPHS0004
      IF(T.GT.815.4 .OR.T.LT.492.)WRITE(6,100)T                         SPHS0005
  100 FORMAT(1X,'OUTSIDE THE TEMP RANGE CF SPHSW,TEMP=',F10.2)          SPHS0006
      RETURN                                                            SPHS0007
      END                                                               SPHS0008
```

```
      REAL FUNCTION MUSW(T,D)                                           MUSW0001
C     FUNCTION TO DETERMINE THE VISCOSITY OF SALT WATER IN LBM/HR FT    MUSW0002
C     AS A FUNCTION OF TEMPERATURE IN DEG R AND DEPTH IN FT             MUSW0003
      P=PRESSW(D)                                                       MUSW0004
      IF(T.LE.510.6)GO TO 1                                             MUSW0005
      IF(T.LE.546..AND.T.GT.510.6)GO TO 2                               MUSW0006
      IF(T.GT.546.)GO TO 3                                              MUSW0007
      IF(T.GT.627..OR.T.LT.492.)WRITE(6,100)T                           MUSW0008
  100 FORMAT(1X,'OUTSIDE THE TEMP RANGE OF MUSW,TEMP=',F10.2)           MUSW0009
    1 PFAC1=0.999284-P*(0.10851E-04-P*0.363151E-09)                     MUSW0010
    2 PFAC2=1.00018-P*(0.55984E-05-P*0.166028E-09)                      MUSW0011
      IF(T.LE.510.6)GO TO 4                                             MUSW0012
    3 PFAC3=0.999963+P*(0.318264E-05+P*0.404453E-10)                    MUSW0013
      IF(T.LE.546.)GO TO 5                                              MUSW0014
      PFAC4=0.999464+P*(0.534374E-05-P* 0.344093E-12)                   MUSW0015
      PFAC=PFAC3+T*(PFAC4-PFAC3)/81.                                    MUSW0016
      GO TO 6                                                           MUSW0017
    4 PFAC=PFAC2-(510.6-T)*(PFAC2-PFAC1)/18.6                           MUSW0018
      GO TO 6                                                           MUSW0019
    5 PFAC=PFAC2+(T-510.6)*(PFAC3-PFAC2)/35.4                           MUSW0020
    6 MUSW=PFAC*EXP(-0.140282E+04+ALOG(T)*(0.920506E+03-ALOG(T)*        MUSW0021
     1(0.16615E+03+ALOG(T)*(0.189294E+01-ALOG(T)*(0.291516E+01-ALOG(T)* MUSW0022
     20.193465)))))                                                     MUSW0023
      RETURN                                                            MUSW0024
      END                                                               MUSW0025
```

```
      FUNCTION SPHWTL(T)                                                SPHW0001
C     FUNCTION TO DETERMINE THE SPECIFIC HEAT OF LIQUID WATER IN        SPHW0002
C     BTU/LBM DEG R AS A FUNCTION OF TEMPERATURE IN DEG R               SPHW0003
      SPHWTL=0.213974E+01-T*(0.537854E-02-T*(0.828815E-05-T*            SPHW0004
     10.415190E-08))                                                    SPHW0005
      IF(T.GT.738..OR.T.LT.492.)WRITE(6,100)T                           SPHW0006
  100 FORMAT(1X,'OUTSIDE THE TEMP RANGE OF SPHWTL,TEMP=',F10.2)         SPHW0007
      RETURN                                                            SPHW0008
      END                                                               SPHW0009
```

```
      SUBROUTINE VISMIX(TEMPR,GASVIS)                                           VISM0001
C     SUBPROGRAM TO DETERMINE THE VISCOSITY OF A MIXTURE OF WATER VAPOR,        VISM0002
C     HYDROGEN,OXYGEN,AND NITROGEN AT LOW PRESSURES UP TO SEVERAL               VISM0003
C     ATMOSPHERES----GASVIS IN LBM/HR FT,PTOT IN LBF/SQ IN TOTAL PRESS,         VISM0004
C     TEMP IN DEG R                                                             VISM0005
      COMMON /S1/PRESS,TEMP,QUAL,SATLIQ(3),STEAM(3),COEFFT(237)/S4/PTOT         VISM0006
     1/S8/YFRACT(4),MU(4),RHO(4),CP(4),KTH(4),S(4),A(4,4),SIJ(4,4)              VISM0007
      REAL MU,MUWTV,MUH2,MUO2,MUN2,KTH                                          VISM0008
      TEMP=TEMPR-460.                                                           VISM0009
      CALL STMTAB(7,PTOT,TEMP)                                                  VISM0010
      RHO(1)=1./STEAM(1)                                                        VISM0011
      MU(1)=MUWTV(TEMPR)                                                        VISM0012
      IF(YFRACT(2).LT.2.E-06)GO TO 6                                            VISM0013
      RHO(2)=RHOH2(TEMPR,PTOT)                                                  VISM0014
      MU(2)=MUH2(TEMPR)                                                         VISM0015
    6 IF(YFRACT(3).LT.2.E-06)GO TO 7                                            VISM0016
      RHO(3)=RHOO2(TEMPR,PTOT)                                                  VISM0017
      MU(3)=MUO2(TEMPR)                                                         VISM0018
    7 IF(YFRACT(4).LT.2.E-06)GO TO 8                                            VISM0019
      RHO(4)=RHON2(TEMPR,PTOT)                                                  VISM0020
      MU(4)=MUN2(TEMPR)                                                         VISM0021
    8 DO 1 I=2,4                                                                VISM0022
      IF(YFRACT(I).LT.2.E-06)GO TO 1                                            VISM0023
      CALL DIFFUS(TEMPR,I,DIFCOE)                                               VISM0024
      A(1,I)=DIFCOE                                                             VISM0025
      A(I,1)=A(1,I)                                                             VISM0026
    1 CONTINUE                                                                  VISM0027
      IF(YFRACT(2).LT.2.E-06)GO TO 2                                            VISM0028
      CALL DIFFUS(TEMPR,5,DIFCOE)                                               VISM0029
      A(2,3)=DIFCOE                                                             VISM0030
      A(3,2)=A(2,3)                                                             VISM0031
      CALL DIFFUS(TEMPR,6,DIFCOE)                                               VISM0032
      A(2,4)=DIFCOE                                                             VISM0033
      A(4,2)=A(2,4)                                                             VISM0034
    2 IF(YFRACT(3).LT.2.E-06)GO TO 3                                            VISM0035
      CALL DIFFUS(TEMPR,1,DIFCOE)                                               VISM0036
```

```
      A(3,4)=DIFCCE                                                     VISM0037
      A(4,3)=A(3,4)                                                     VISM0038
    3 GASVIS=0.                                                         VISM0039
      DO 4 I=1,4                                                        VISM0040
      IF(YFRACT(I).LT.2.E-06)GO TO 4                                    VISM0041
      GLUM=0.                                                           VISM0042
      DO 5 J=1,4                                                        VISM0043
      IF(I.EQ.J)GO TO 5                                                 VISM0044
      IF(YFRACT(J).LT.2.E-06)GO TO 5                                    VISM0045
      GLUM=GLUM+YFRACT(J)/A(I,J)                                        VISM0046
    5 CONTINUE                                                          VISM0047
      GASVIS=GASVIS+MU(I)/(1.+1.385*MU(I)*GLUM/(YFRACT(I)*RHO(I)))      VISM0048
    4 CONTINUE                                                          VISM0049
      RETURN                                                            VISM0050
      END                                                               VISM0051
```

```
      FUNCTION RHOMIX(TEMPR)                                              RHOM0001
      COMMON /S1/PRESS,TEMP,QUAL,SATLIQ(3),STEAM(3),COEFFT(237)/S4/       RHOM0002
     1PTOT/S8/YFRACT(4),MU(4),RHO(4),CP(4),KTH(4),S(4),A(4,4),SIJ(4,4)    RHOM0003
     2/S10/MOLW(4)                                                        RHOM0004
      REAL MU,MOLW,KTH                                                    RHOM0005
C     SUBPROGRAM TO DETERMINE THE DENSITY OF A MIXTURE OF WATER VAPOR,    RHOM0006
C     HYDROGEN,OXYGEN,AND NITROGEN---RHOMIX IN LBM/CU FT                  RHOM0007
      TEMP=TEMPR-460.                                                     RHOM0008
      CALL STMTAB(7,PTOT,TEMP)                                            RHOM0009
      IF(YFRACT(2).LT.2.E-06)GO TO 1                                      RHOM0010
      RHO(2)=RHOH2(TEMPR,PTOT)                                            RHOM0011
    1 IF(YFRACT(3).LT.2.E-06)GO TO 2                                      RHOM0012
      RHO(3)=RHOO2(TEMPR,PTOT)                                            RHOM0013
    2 IF(YFRACT(4).LT.2.E-06)GO TO 3                                      RHOM0014
      RHO(4)=RHON2(TEMPR,PTOT)                                            RHOM0015
    3 SUM=YFRACT(1)*MOLW(1)                                               RHOM0016
      DEN=SUM*STEAM(1)                                                    RHOM0017
      DO 4 I=2,4                                                          RHOM0018
      IF(YFRACT(I).LT.2.E-06)GO TO 4                                      RHOM0019
      B=YFRACT(I)*MOLW(I)                                                 RHOM0020
      DEN=DEN+B/RHO(I)                                                    RHOM0021
      SUM=SUM+B                                                           RHOM0022
    4 CONTINUE                                                            RHOM0023
      RHOMIX=SUM/DEN                                                      RHOM0024
      RETURN                                                              RHOM0025
      END                                                                 RHOM0026
```

```
      FUNCTION SPHMIX(TEMPR)                                                   SPHM0001
C     FUNCTION TO DETERMINE THE SPECIFIC HEAT IN BTU/LB DEG R OF A             SPHM0002
C     GAS MIXTURE AT LOW PRESSURES OF WATER VAPOR,HYDROGEN,OXYGEN,AND          SPHM0003
C     NITROGEN AS A FUNCTION OF TEMPERATURE IN DEG R                           SPHM0004
      COMMON /S8/YFRACT(4),MU(4),RHO(4),CP(4),KTH(4),S(4),A(4,4),              SPHM0005
     1SIJ(4,4)/S10/MOLW(4)                                                     SPHM0006
      REAL MU,MOLW,KTH                                                         SPHM0007
      CP(1)=SPHWTV(TEMPR)                                                      SPHM0008
      IF(YFRACT(2).LT.2.E-06)GO TO 1                                           SPHM0009
      CP(2)=SPHH2(TEMPR)                                                       SPHM0010
    1 IF(YFRACT(3).LT.2.E-06)GO TO 2                                           SPHM0011
      CP(3)=SPHO2(TEMPR)                                                       SPHM0012
    2 IF(YFRACT(4).LT.2.E-06)GO TO 3                                           SPHM0013
      CP(4)=SPHN2(TEMPR)                                                       SPHM0014
    3 DEN=YFRACT(1)*MOLW(1)                                                    SPHM0015
      SUM=DEN*CP(1)                                                            SPHM0016
      DO 4 I=2,4                                                               SPHM0017
      IF(YFRACT(I).LT.2.E-06)GO TO 4                                           SPHM0018
      B=YFRACT(I)*MOLW(I)                                                      SPHM0019
      SUM=SUM+B*CP(I)                                                          SPHM0020
      DEN=DEN+B                                                                SPHM0021
    4 CONTINUE                                                                 SPHM0022
      SPHMIX=SUM/DEN                                                           SPHM0023
      RETURN                                                                   SPHM0024
      END                                                                      SPHM0025
```

```
      SUBROUTINE THCON(TEMPR,KTHMIX)                                    THC00001
C     PROGRAM TO DETERMINE THE THERMAL CONDUCTIVITY AT ONE ATMOSPHERE   THC00002
C      PRESSURE OF A MIXTURE OF ONE POLAR GAS(WATER VAPOR) AND /        THC00003
C     HYDROGEN,OXYGEN,AND NITROGEN                                      THC00004
C     GAS WITH SUBSCRIPT 1 IS THE POLAR GAS                            'THC00005
C     YFRACT-MOLE FRACTION OF THE VARIOUS COMPONENT GASES               THC00006
C     MOLW-MOLECULAR WEIGHT OF VARIOUS COMPONENT GASES                  THC00007
C     MOLW OF WATER=18.016,MOLW OF HYDROGEN=2.016,MOLW OF OXYGEN=32.000 THC00008
C     MOLW OF NITROGEN=28.016                                           THC00009
C     SUTHERLAND COEFFICIENTS--WATER-1008.,HYDROGEN-142.2,OXYGEN-243.51 THC00010
C     ,NITROGEN-208.8                                                   THC00011
C     TEMPR-TEMPERATURE IN DEG R                                        THC00012
C     MU-DYNAMIC VISCOSITY OF VARIOUS COMPONENT GASES                   THC00013
C     CS-SUTHERLAND COEFFICIENT MULTIPLIER FOR SIJ(SUTHERLAND COEFF)    THC00014
C        OF A BINARY MIXTURE OF A POLAR AND A NON POLAR GAS             THC00015
C     S-SUTHERLAND COEFFICIENT                                          THC00016
C     KTH-THERMAL CONDUCTIVITY OF VARIOUS COMPONENT GASES               THC00017
C     KTHMIX-THERMAL CONDUCTIVITY OF GASEOUS MIXTURE                    THC00018
C     CS FOR WATER AND A NON POLAR GAS =0.7                             THC00019
      COMMON /S8/YFRACT(4),MU(4),RHO(4),CP(4),KTH(4),S(4),A(4,4),       THC00020
     1SIJ(4,4)/S10/MOLW(4)                                              THC00021
      REAL MOLW,MU,KTH,KTHMIX,KTHWTV,KTHH2,KTHO2,KTHN2,MUWTV,MUH2,MUO2, THC00022
     1MUN2                                                              THC00023
      CS=0.7                                                            THC00024
      KTH(1)=KTHWTV(TEMPR)                                              THC00025
      MU(1)=MUWTV(TEMPR)                                                THC00026
      IF(YFRACT(2).LT.2.E-06)GO TO 9                                    THC00027
      KTH(2)=KTHH2(TEMPR)                                               THC00028
      MU(2)=MUH2(TEMPR)                                                 THC00029
    9 IF(YFRACT(3).LT.2.E-06)GO TO 10                                   THC00030
      KTH(3)=KTHO2(TEMPR)                                               THC00031
      MU(3)=MUO2(TEMPR)                                                 THC00032
   10 IF (YFRACT(4).LT.2.E-06)GO TO 11                                  THC00033
      KTH(4)=KTHN2(TEMPR)                                               THC00034
      MU(4)=MUN2(TEMPR)                                                 THC00035
   11 DO 1 J=1,4                                                        THC00036
```

```
      SIJ(1,J)=CS*SQRT(S(1)*S(J))                                       THC00037
    1 SIJ(J,1)=SIJ(1,J)                                                 THC00038
      DO 2 I=2,4                                                        THC00039
      DO 3 J=2,4                                                        THC00040
      IF(J.LE.I)GO TO 3                                                 THC00041
      SIJ(I,J)=SQRT(S(I)*S(J))                                          THC00042
      SIJ(J,I)=SIJ(I,J)                                                 THC00043
    3 CONTINUE                                                          THC00044
    2 CONTINUE                                                          THC00045
      DO 4 I=1,4                                                        THC00046
      IF(YFRACT(I).LT.2.E-06)GO TO 4                                    THC00047
      DO 5 J=1,4                                                        THC00048
      IF(YFRACT(J).LT.2.E-06)GO TO 5                                    THC00049
      IF(I.EQ.J)GO TO 5                                                 THC00050
      A(I,J)=0.25*(1.+(MU(I)/MU(J)*(MOLW(J)/MOLW(I))**0.75*(1.+S(I)/    THC00051
     1TEMPR)/(1.+S(J)/TEMPR))**0.5)**2*(1.+SIJ(I,J)/TEMPR)/(1.+S(I)/    THC00052
     2TEMPR)                                                            THC00053
    5 CONTINUE                                                          THC00054
    4 CONTINUE                                                          THC00055
      KTHMIX=0.                                                         THC00056
      DO 7 I=1,4                                                        THC00057
      IF(YFRACT(I).LT.2.E-06)GO TO 7                                    THC00058
      SUM=0.                                                            THC00059
      DO 8 J=1,4                                                        THC00060
      IF(I.EQ.J)GO TO 8                                                 THC00061
      IF(YFRACT(J).LT.2.E-06)GO TO 8                                    THC00062
      SUM=SUM+A(I,J)*YFRACT(J)                                          THC00063
      SUM=SUM/YFRACT(I)                                                 THC00064
    8 CONTINUE                                                          THC00065
      KTHMIX=KTHMIX+KTH(I)/(1.+SUM)                                     THC00066
    7 CONTINUE                                                          THC00067
      RETURN                                                            THC00068
      END                                                               THC00069
```

```
      FUNCTION SPHWTV(T)                                                SPHW0001
C     SPECIFIC HEAT IN BTU/LBM DEG R VERSUS TEMPERATURE FOR WATER VAPOR SPHW0002
C   (STEAM) AT 1 ATM AS A FUNCTION OF TEMPERATURE IN DEG R              SPHW0003
      IF(T.GT.960.)GO TO 1                                              SPHW0004
      IF(T.GT.671.4)GO TO 2                                             SPHW0005
      SPHWTV=0.452219-T*(0.71791E-04-T*(0.128706E-06-T*0.343623E-10))   SPHW0006
      GO TO 3                                                           SPHW0007
    2 SPHWTV=1.9534-T*(0.49912E-02-T*(0.555928E-05-T*0.204759E-08))     SPHW0008
      GO TO 3                                                           SPHW0009
    1 SPHWTV=0.443254-T*(0.163791E-04-T*(0.614717E-07-T*0.114103E-10))  SPHW0010
    3 IF(T.GT.2460..OR.T.LT.486.)WRITE(6,100)T                          SPHW0011
  100 FORMAT(1X,'OUTSIDE THE TEMP LIMITS OF SPHWTV,TEMP=',F10.2)        SPHW0012
      RETURN                                                            SPHW0013
      END                                                               SPHW0014
```

```
      FUNCTION SPHH2(T)                                                 SPHH0001
C     FUNCTION TO DETERMINE THE SPECIFIC HEAT OF HYDROGEN IN BTU/LBM    SPHH0002
C     DEG R AS A FUNCTION OF TEMPERATURE IN DEG R                       SPHH0003
      IF(T.GT.756.)GO TO 1                                              SPHH0004
      SPHH2=0.15395E+01+T*(0.8379E-02-T*(0.1242E-04-T*0.62336E-08))     SPHH0005
      GO TO 2                                                           SPHH0006
    1 SPHH2=0.358927E+01-T*(0.308387E-03-T*(0.21427E-06-T*0.24889E-10)) SPHH0007
    2 IF(T.GT.2700..OR.T.LT.180.)WRITE(6,100)T                          SPHH0008
  100 FORMAT(1X,'OUTSIDE THE TEMP LIMITS OF SPHH2,TEMP=',F10.2)         SPHH0009
      RETURN                                                            SPHH0010
      END                                                               SPHH0011
```

```
      FUNCTION SPHO2(T)                                                 SPHO0001
C     FUNCTION TO DETERMINE THE SPECIFIC HEAT OF OXYGEN IN BTU/LBM      SPHO0002
C     DEG R AS A FUNCTION OF TEMPERATURE IN DEG R                       SPHO0003
      IF(T.GT.1422.)GO TO 1                                             SPHO0004
      SPHO2=0.227218-T*(0.591067E-04-T*(0.102887E-06-T*0.34678E-10))    SPHO0005
      GO TO 2                                                           SPHO0006
    1 SPHO2=0.160484+T*(0.109343E-03-T*(0.396454E-07-T*0.54518E-11))    SPHO0007
    2 IF(T.GT.2700..OR.T.LT.437.4)WRITE(6,100)T                         SPHO0008
  100 FORMAT(1X,'OUTSIDE THE TEMP RANGE OF SPHO2,TEMP=',F10.2)          SPHO0009
      RETURN                                                            SPHO0010
      END                                                               SPHO0011
```

```
      FUNCTION SPHN2(T)
C     FUNCTION TO DETERMINE THE SPECIFIC HEAT OF NITROGEN IN BTU/LBM
C     DEG R AS A FUNCTION OF TEMPERATURE IN DEG R
      SPHN2=0.261365-T*(0.500574E-04-T*(0.556552E-07-T*0.121568E-10))
      IF(T.GT.1404..OR.T.LT.450.)WRITE(6,100)T
  100 FORMAT(1X,'OUTSIDE THE TEMP RANGE OF SPHN2,TEMP=',F10.2)
      RETURN
      END
```

```
      REAL FUNCTION MUWTV(T)                                                    MUWT0001
C     VISCOSITY OF STEAM AT 1 ATM IN LBM/HR FT AS A FUNCTION OF TEMP            MUWT0002
C     IN DEG R OVER THE TEMPERATURE RANGE 640-2700 DEG R-GOOD AT LOW            MUWT0003
C     PRESSURES UP TO SEVERAL ATMOSPHERES                                       MUWT0004
      MUWTV=2.3344E-03+T*(3.9441E-05+T*(6.8772E-09-T*1.7283E-12))               MUWT0005
      IF(T.GT.2700..OR.T.LT.640.)WRITE(6,100)T                                  MUWT0006
  100 FORMAT(1X,'OUTSIDE THE TEMPERATURE RANGE OF MUWTV, TEMP=',F10.2)          MUWT0007
      RETURN                                                                    MUWT0008
      END                                                                       MUWT0009
```

```
      REAL FUNCTION MUH2(T)
C     VISCOSITY FO GASEOUS HYDROGEN AT 1 ATM IN LBM/HR FT AS A FUNCTION       MUH20001
C     OF TEMP IN DEG R OVER THE TEMP RANGE 20-1740 DEG R-GOOD A LOW           MUH20002
C     PRESSURES UP TO SEVERAL ATMOSPHERES                                     MUH20003
      MUH2=5.0922E-04+T*(6.416E-05-T*(7.4502E-08-T*(6.7125E-11                MUH20004
     1-T*(2.9502E-14-T*4.8859E-18))))                                         MUH20005
      IF(T.GT.1740..OR.T.LT.20.)WRITE(6,100)T                                 MUH20006
  100 FORMAT(1X,'OUTSIDE THE TEMPERATURE LIMITS OF MUH2, TEMP=',F10.2)        MUH20007
      RETURN                                                                  MUH20008
      END                                                                     MUH20009
                                                                              MUH20010
```

```
      REAL FUNCTION MUO2(T)
C     VISCOSITY OF GASEOUS OXYGEN AT 1 ATM IN LBM/HR FT AS A FUNCTION   MUO20001
C     OF TEMP IN DEG R OVER THE TEMP RANGE 60-1840 DEG R-GOOD AT LOW    MUO20002
C     PRESSURES UP TO SEVERAL ATMOSPHERES                               MUO20003
      MUO2=-2.2361E-03+T*(1.2657E-04-T*(6.7397E-08-T*(2.454E-11-T*      MUO20004
     13.3316E-15)))                                                     MUO20005
      IF(T.GT.1840..OR.T.LT.60.)WRITE(6,100)T                           MUO20006
  100 FORMAT(1X,'OUTSIDE THE TEMPERATURE RANGE OF MUO2, TEMP=',F10.2)   MUO20007
      RETURN                                                            MUO20008
      END                                                               MUO20009
                                                                        MUO20010
```

```
      REAL FUNCTION MUN2(T)                                                     MUN20001
C     VISCOSITY OF GASEUUS NITROGEN AT 1 ATM IN LBM/HR FT AS A FUNCTION         MUN20002
C     OF TEMP IN DEC R OVER THE TEMP RANGE 410-3060 DEG R-GOOD AT LOW           MUN20003
C     PRESSURES UP TO SEVERAL ATMOSPHERES                                       MUN20004
      MUN2=1.2637E-03+T*(9.7228E-05-T*(4.3403E-08-T*(1.3343E-11-T*              MUN20005
     11.6341E-15)))                                                             MUN20006
      IF(T.GT.3060..OR.T.LT.410.)WRITE(6,100)T                                  MUN20007
  100 FORMAT(1X,'OUTSIDE THE TEMPERATURE RANGE OF MUN2, TEMP=',F10.2)           MUN20008
      RETURN                                                                    MUN20009
      END                                                                       MUN20010
```

```
      REAL FUNCTION KTHWTV(T)                                           KTHW0001
C     THERMAL CONDUCTIVITY OF STEAM AT 1 ATM IN BTU/HR FT DEG R AS A    KTHW0002
C     FUNCTION OF TEMPERATURE IN DEG R OVER THE TEMPERATURE RANGE 504-  KTHW0003
C     1620 DEG R-GOOD AT LOW PRESSURES                                  KTHW0004
      KTHWTV=0.208936E-02+T*(0.553685E-05+T*(0.211891E-07-T*            KTHW0005
     10.472519E-11))                                                    KTHW0006
      IF(T.GT.1620..OR.T.LT.504.)WRITE(6,100)T                          KTHW0007
  100 FORMAT(1X,'OUTSIDE TEMPERATURE RANGE OF KTHWTV, TEMP=',F10.2)     KTHW0008
      RETURN                                                            KTHW0009
      END                                                               KTHW0010
```

```
      REAL FUNCTION KTHH2(T)                                            KTHH0001
C     THERMAL CONDUCTIVITY OF GASEOUS HYDROGEN AT 1 ATM IN BTU/HR FT DEG KTHH0002
C     R AS A FUNCTION OF TEMP IN DEG R OVER THE TEMP RANGE 504-3600     KTHH0003
C     DEG R-GOOD AT LOW PRESSURES                                       KTHH0004
      IF(T.LE.1476.)GO TO 1                                             KTHH0005
      KTHH2=-0.125809E-01+T*(0.232309E-03-T*(0.924892E-07-T*(0.353848E  KTHH0006
     1-10-T*(0.734297E-14-T*0.69291E-18))))                             KTHH0007
      GO TO 2                                                           KTHH0008
    1 KTHH2=-0.141532+T*(0.106434E-02-T*(0.188696E-05-T*(0.184137E-08-T* KTHH0009
     1(0.884784E-12-T*0.167396E-15))))                                  KTHH0010
    2 IF(T.GT.3600..OR.T.LT.504.)WRITE(6,100)T                          KTHH0011
  100 FORMAT(1X,'OUTSIDE TEMPERATURE RANGE OF KTHH2, TEMP=',F10.2)      KTHH0012
      RETURN                                                            KTHH0013
      END                                                               KTHH0014
```

```
      REAL FUNCTION KTHO2(T)                                            KTH00001
C     THERMAL CONDUCTIVITY OF GASECUS OXYGEN AT 1 ATM IN BTU/HR FT DEG R KTH00002
C     AS A FUNCTION OF TEMP IN DEG R OVER THE TEMPERATURE RANGE 504-2700 KTH00003
C     DEG R-GOOD AT LOW PRESSURES                                       KTH00004
      KTHO2=0.659632E-03+T*(0.29935E-04-T*(0.506793E-08-T*0.591072E-12)) KTH00005
      IF(T.GT.2700..OR.T.LT.504.)WRITE(6,100)T                          KTH00006
  100 FORMAT(1X,'OUTSIDE TEMPERATURE RANGE OF KTHO2, TEMP=',F10.2)      KTH00007
      RETURN                                                            KTH00008
      END                                                               KTH00009
```

```
      REAL FUNCTION KTHN2(T)                                            KTHN0001
C     THERMAL CONDUCTIVITY OF GASEOUS NITROGEN AT 1 ATM IN BTU/HR FT DEG KTHN0002
C     R OVER THE TEMP RANGE 504-1512 DEG R-GOOD AT LOW PRESSURES        KTHN0003
      KTHN2=-0.229136E-03+T*(0.355993E-04-T*(0.173562E-07-T*(0.757675E  KTHN0004
     1-11-T*0.148916E-14)))                                             KTHN0005
      IF(T.GT.1512..OR.T.LT.504.)WRITE(6,100)T                          KTHN0006
  100 FORMAT(1X,'OUTSIDE TEMPERATURE RANGE OF KTHN2, TEMP=',F10.2)      KTHN0007
      RETURN                                                            KTHN0008
      END                                                               KTHN0009
```

```
      FUNCTION RHOH2(T,P)
C     FUNCTION TO DETERMINE THE  DENSITY OF HYDROGEN IN LBM/FT**3 AS
C     A FUNCTION OF TEMPERATURE IN DEG R AND PRESSURE IN LBF/IN**2
      RHOH2=P/14.7*( 0.140767E-01-T*(0.264654E-04-T*(0.217512E-07-T*
     10.659390E-11)))
      IF(T.GT.1080..OR.T.LT.504.)WRITE(6,100)T
  100 FORMAT(1X,'OUTSIDE THE TEMP RANGE OF RHOH2,TEMP=',F10.2)
      IF(P.GT.14.7)WRITE(6,101)P
  101 FORMAT(1X,'OUTSIDE THE PRESS RANGE OF RHOH2,PRESS=',F10.2)
      RETURN
      END
```

```
      FUNCTION RHOO2(T,P)
C     FUNCTION TO DETERMINE THE  DENSITY OF OXYGEN IN LBM/FT**3 AS
C     A FUNCTION OF TEMPERATURE IN DEG R AND PRESSURE IN LBF/IN**2
      RHOO2=P/14.7*(0.362206-T*(0.122468E-02-T*(0.2172E-05-T*
     1(0.213345E-08-T*(0.110134E-11-T*0.233601E-15)))))
      IF(T.GT.1440..OR.T.LT.504.)WRITE(6,100)T
      IF(P.GT.14.7)WRITE(6,101)P
  100 FORMAT(1X,'OUTSIDE THE TEMP RANGE OF RHOO2,TEMP=',F10.2)
  101 FORMAT(1X,'OUTSIDE THE PRESS RANGE OF RHOO2,PRESS=',F10.2)
      RETURN
      END
```

```
      FUNCTION RHON2(T,P)
C     FUNCTION TO DETERMINE THE  DENSITY OF NITROGEN IN LBM/FT**3 AS      RHON0001
C     A FUNCTION OF TEMPERATURE IN DEG R AND PRESSURE IN LBF/IN**2        RHON0002
      RHON2=P/14.7*(0.314131-T*(0.105419E-02-T*(0.185808E-05-T*(0.181589  RHON0003
     1E-08-T*(0.933661E-12-T*0.197444E-15)))))                             RHON0004
      IF(T.GT.1080..OR.T.LT.504.)WRITE(6,100)T                             RHON0005
      IF(P.GT.14.7)WRITE(6,101)P                                           RHON0006
  100 FORMAT(1X,'OUTSIDE THE TEMP RANGE OF RHON2,TEMP=',F10.2)              RHON0007
  101 FORMAT(1X,'OUTSIDE THE PRESS RANGE OF RHON2,PRESS=',F10.2)            RHON0008
      RETURN                                                               RHON0009
      END                                                                  RHON0010
                                                                           RHON0011
```

```
      FUNCTION COLBJ(R)                                                 COLB0001
C     FUNCTION TO DETERMINE THE COLBURN J-FACTOR AS A FUNCTION OF       COLB0002
C     REYNOLDS NUMBER BASED UPON MINIMUM CROSS SECTIONAL AREA           COLB0003
      COLBJ=EXP(0.152241-ALOG(R)*(0.667829-ALOG(R)*(0.153528E-01-ALOG(R)COLB0004
     1*0.116247E-03)))                                                  COLB0005
      IF(R.GT.100000..OR.R.LT.1.)WRITE(6,100)R                          COLB0006
  100 FORMAT(1X,'OUTSIDE THE REYNOLDS NO RANGE OF COLBJ,RE=',E13.6)     COLB0007
      RETURN                                                            COLB0008
      END                                                               COLB0009
```

```
      BLOCK DATA
      COMMON /S1/PRESS,TEMP,QUAL,SATLIQ(3),STEAM(3),COEFFT(237)
     1/S8/YFRACT(4),MU(4),RHO(4),CP(4),KTH(4),S(4),A(4,4),SIJ(4,4)
     2/S9/EPSK(6),CONST(6)/S10/MOLW(4)/S12/DERY(4),PRMT(5),AUX(16,4),
     3Y(4)
      REAL MOLW,MU,KTH
      DIMENSION C1(30),C2(30),C3(30),C4(30),C5(30),C6(30),C7(30),C8(27)
      EQUIVALENCE(C1,COEFFT(1)),(C2,COEFFT(31)),(C3,COEFFT(61)),
     1(C4,COEFFT(91)),(C5,COEFFT(121)),(C6,COEFFT(151)),(C7,COEFFT(181))
     2,(C8,COEFFT(211))
      DATA C1/ .2208222 E+04, .6500000 E+03
     1, .6957339 E+03, .6046426 E+01, .7000000 E+01, .1855268 E+00
     2,-.1951368 E+00,-.5227995 E+00, .9114895 E-01, .6184368 E-01
     3,-.5062585 E+00, .7259572 E+00, .1458569 E+02, .1240432 E+03
     4, .5559294 E+03, .2000000 E+01,-.7413344 E-06, .7332482 E-06
     5, .2654891 E-04, .9134931 E-04, .1567992 E-02, .2503253 E-01
     6, .3070692 E+00, .3624134 E+01, .4496062 E+02, .1792673 E+03
     7, .4500000 E+03, .5500000 E+03,-.9873689 E-22, .1930123 E-19/
      DATA C2/ .3004118 E-17,-.4211366 E-15
     1,-.3289318 E-14,-.1173447 E-11, .1124448 E-07,-.7841965 E-05
     2, .8153684 E-02, .6951926 E+01, .2500000 E+03, .2057555 E-23
     3,-.6427270 E-21, .1270437 E-18,-.9697616 E-16, .8337000 E-13
     4,-.6425156 E-10, .4479732 E-07,-.2810476 E-04, .1749054 E-01
     5, .3395990 E+01, .4301016 E+03, .5492738 E+03,-.1844478 E-19
     6, .9275654 E-17,-.9547066 E-15,-.2900468 E-12, .3535329 E-10
     7, .3993660 E-08,-.9956731 E-06,-.5915799 E-03, .7814327 E+00/
      DATA C3/ .5500000 E+03, .2184803 E+03
     1,-.1472259 E-21, .6655357 E-19, .4772560 E- 17,-.5334916 E-14
     2, .2745550 E-12,-.1833530 E-10,-.3116033 E-06,-.1195635 E-03
     3, .9351275 E+00, .2500000 E+03, .4700000 E+03, .5500000 E+03
     4, .7385718 E-22, .3322551 E-19, .3007558 E-18,-.7389865 E-15
     5,-.7067923 E-14, .9011420 E-11, .5814964 E-09, .8671298 E-07
     6, .3073420 E-04, .2176269 E-01, .2500000 E+03,-.7845913 E-25
     7,-.3360803 E-23, .8581979 E-20, .2572936 E-18,-.3159190 E-15/
      DATA C4/ .6050630 E-13, .1368459 E-10
     1, .1558777 E-07, .8126444 E-05, .1700264 E-01, .4500000 E+03
```

```
     2, .5500C00 E+03, .9474315 E-18, .2497148 E-16,-.3830259 E-14                BLKD0037
     3, .4497967 E-12,-.5133738 E-10, .4917899 E-08, .4832690 E-05                BLKD0038
     4, .1239961 E-02, .1279855 E+01, .5492738 E+03, .2500000 E+03                BLKD0039
     5, .1294537 E-21,-.6587314 E-19,-.1381757 E-17, .6252011 E-14                BLKD0040
     6, .1754300 E-12, .2320242 E-09, .3614597 E-06, .1250646 E-03                BLKD0041
     7, .1015097 E+01, .2184804 E+03, .4500000 E+03, .5500C00 E+03/               BLKD0042
      DATA C5/ -.2113443 E-20, .1532703 E-18                                      BLKD0043
     1, .6921786 E-16,-.1834582 E-14,-.6641746 E-12, .1458956 E-10                BLKD0044
     2, .5959841 E-08, .4557592 E-06, .1232510 E-02, .7496980 E+00                BLKD0045
     3, .2500000 E+03, .5008454 E-23,-.1565907 E-21,-.4609912 E-18                BLKD0046
     4, .4923963 E-17, .1625035 E-13,-.7406832 E-12, .1047990 E-08                BLKD0047
     5,-.8554650 E-06, .1428571 E-02, .367534C E+00, .1700000 E+01                BLKD0048
     6, .1900000 E+01,-.1108508 E+05,-.1599459 E+05, .9140769 E+04                BLKD0049
     7,-.1879611 E+03, .1569980 E+03,-.2021334 E+03,-.4865018 E+02/               BLKD0050
      DATA C6/ .1504045 E+03, -.1905054 E+03                                      BLKD0051
     1, .1119949 E+04, .1500000 E+01,-.1486358 E+06,-.1341482 E+06                BLKD0052
     2, .6237994 E+05, .2947450 E+05,-.1890759 E+05,-.5785888 E+03                BLKD0053
     3, .3512247 E+04,-.1234083 E+04,-.6892883 E+02, .1203684 E+04                BLKD0054
     4, .3000000 E+01, .1300000 E+04, .7084899 E+01, .1650779 E+02                BLKD0055
     5, .5212274 E+03,-.1168295 E-01,-.1200159 E+00, .2041199 E+01                BLKD0056
     6, .1234095 E-04, .1355514 E-03,-.1509932 E-03, .300000C E+01                BLKD0057
     7, .1800000 E+01, .2332209 E+02, .1877665 E+03, .330805C E+03/               BLKD0058
      DATA C7/-.3214140 E+01, .4244910 E+03                                       BLKD0059
     1, .1640084 E+04, .1874666 E+02, .6397888 E+02, .2071984 E+04                BLKD0060
     2, .1300000 E+04, .1800000 E+01,-.6436980 E-05, .9641880 E-02                BLKD0061
     3, .3887925 E+01, .1103406 E-05, .47225CC E-03T-C94113 0 E&01                BLKD0062
     4, .6941697 E-05,-.6089212 E-02, .1095192 E+01, .130000C E+04                BLKD0063
     5, .1800000 E+01,-.3310121 E-03, .2166192 E+01, .5350029 E+03                BLKD0064
     6,-.7723662 E-03, .3675365 E+00,-.2545012 E+03, .2524971 E-02                BLKD0065
     7,-.1642711 E+01, .6147777 E+03,      0.0,            0.0      /             BLKD0066
      DATA C8/  0.0,0.0,0.0,0.0,0.0                                               BLKD0067
     1, 0.0,0.0,0.0,0.0,0.0,0.0,0.0,0.0,0.0,0.0,0.0, .9000000 E+03                BLKD0068
     2, .1400000 E+01,-.1547826 E-04, .1935156 E-01, .2469891 E+01                BLKD0069
     3, .2332964 E-04, .1149379 E-02,-.1313921 E+02, .5886022 E-05                BLKD0070
     4,-.1259290 E-01, .5510116 E+01/                                             BLKD0071
      DATA EPSK/157.110,447.617,585.668,480.182,143.662,117.519/,                 BLKD0072
```

```
1CONST/0.859426E-03,0.444396E-02,0.140743E-02,0.129898E-02,                      BLKD0073
20.321267E-02,0.291187E-02/                                                      BLKD0074
 DATA MOLW/18.016,2.016,32.0,28.016/                                             BLKD0075
 DATA S/1008.,142.2,243.51,208.8/                                                BLKD0076
 DATA DERY/0.5,0.5,0.5,0.5/,PRMT/0.0,1.0,0.50,0.01,0.0/                          BLKD0077
 END                                                                             BLKD0078
```

```
      SUBROUTINE STMTAB (NI,XI,YI)                                      STMT0001
C**** ******************************************************************STMT0002
C                                                                       STMT0003
C     SUBROUTINE FOR THE THERMODYNAMIC PROPERTIES OF STEAM AND WATER    STMT0004
C       BASED ON KEENAN AND KEYES STEAM TABLES  2/23/67  M.E.AUGHEY      STMT0005
C                                                                       STMT0006
C**** ******************************************************************STMT0007
C     USE OF SUBROUTINE STMTAB (NI,XI,YI)                               STMT0008
C                                                                       STMT0009
C  1. MAINLINE PROGRAM MUST HAVE DIMENSION AND COMMON STATEMENTS        STMT0010
C     IN AGREEMENT WITH STMTAB                                          STMT0011
C      I.E.   DIMENSION SATLIQ(3),STEAM(3)                              STMT0012
C             COMMON PRESS,TEMP,QUAL,SATLIQ,STEAM                       STMT0013
C                                                                       STMT0014
C  2. TERMINOLOGY                                                       STMT0015
C      NAME        PROPERTY                   SYMBOL      UNITS         STMT0016
C      PRESS       PRESSURE                   P OR PSAT - PSIA          STMT0017
C      TEMP        TEMPERATURE                T OR TSAT - DEG.F         STMT0018
C      QUAL        QUALITY                    X         - FRACTION      STMT0019
C      SATLIQ(1)   SAT.LIQUID SPEC.VOLUME     VF        - FT3/LB        STMT0020
C      SATLIQ(2)   SAT.LIQUID ENTHALPY        HF        - BTU/LB        STMT0021
C      SATLIQ(3)   SAT.LIQUID ENTROPY         SF        - BTU/LB-DEG.F  STMT0022
C      STEAM(1)    VAPOR SPECIFIC VOLUME      V OR VG   - FT3/LB        STMT0023
C      STEAM(2)    VAPOR ENTHALPY             H OR HG   - BTU/LB        STMT0024
C      STEAM(3)    VAPOR ENTROPY              S OR SG   - BTU/LB-DEG.F  STMT0025
C                                                                       STMT0026
C  3. NI IS AN INDEX WHICH INDICATES TO THE SURROUTINE THE PROPERTIES   STMT0027
C     SUPPLIED AS ARGUMENTS AND THE PROPERTIES DESIRED AS ANSWERS       STMT0028
C                                                                       STMT0029
C      EX.  CALL STMTAB (1,X,0.) RETURNS TSAT,VF,HF AND SF              STMT0030
C                                WITH PSAT AS ARGUMENT                  STMT0031
C           CALL STMTAB (2,X,0.) RETURNS PSAT,VF,HF AND SF              STMT0032
C                                WITH TSAT AS ARGUMENT                  STMT0033
C           CALL STMTAB (3,X,0.) RETURNS PSAT,TSAT,VF AND SF            STMT0034
C                                WITH HF AS ARGUMENT                    STMT0035
C           CALL STMTAB (4,X,0.) RETURNS VF,VG,HF,HG,SF AND SG          STMT0036
```

```
C                                       WITH PSAT AS ARGUMENT                   STMT0037
C          CALL STMTAB (5,X,0.) RETURNS PSAT,VF,VG,HF,HG,SF AND SG              STMT0038
C                                       WITH TSAT AS ARGUMENT                   STMT0039
C          CALL STMTAB (6,X,0.) RETURNS PSAT,TSAT,VF,VG,HG,SF AND SG            STMT0040
C                                       WITH HF AS ARGUMENT                     STMT0041
C          CALL STMTAB (7,X,Y)  RETURNS V,H,S AND X=1.0                         STMT0042
C                                       WITH P AND T AS ARGUMENTS               STMT0043
C          CALL STMTAB (8,X,Y)  RETURNS T,V,S AND X                             STMT0044
C                                       WITH P AND H AS ARGUMENTS               STMT0045
C          CALL STMTAB (9,X,Y)  RETURNS T,V,H AND X                             STMT0046
C                                       WITH P AND S AS ARGUMENTS               STMT0047
C          CALL STMTAB (10,X,Y) RETURNS P,T,V AND X                             STMT0048
C                                       WITH H AND S AS ARGUMENTS               STMT0049
C          CALL STMTAB (11,X,Y) RETURNS V,H,S AND X=1.0                         STMT0050
C                                       WITH P AS ARGUMENT AT CONSTANT T        STMT0051
C                                                                               STMT0052
C  4. LIMITS - SATURATION LIMITED TO MAXIMUMS OF 2208 PSIA, 650 F, AND          STMT0053
C              695.7 BTU/LB                                                     STMT0054
C              SUPERHEAT LIMITED TO SPECIFIC VOLUME ABOVE .1603 FT3/LB          STMT0055
C                                                                               STMT0056
C  5. ACCURACY - WITHIN ROUNDING ERROR OF KEENAN AND KEYES VALUES               STMT0057
C                                                                               STMT0058
C  6. MEMORY SPACE REQUIRED - APPROXIMATELY 1100 WORDS TOTAL                    STMT0059
C                                                                               STMT0060
C**** *****************************************************************          STMT0061
      COMMON /S1/PRESS,TEMP,QUAL,SATLIQ(3),STEAM(3),COEFFT(237)                 STMT0062
      N=NI                                                                      STMT0063
      X=XI                                                                      STMT0064
      Y=YI                                                                      STMT0065
      I=N-3                                                                     STMT0066
      LINK=0                                                                    STMT0067
      PRESS=X                                                                   STMT0068
      DELTA1=0.0                                                                STMT0069
      ERROR1=0.0                                                                STMT0070
      ERROR2=0.0                                                                STMT0071
      IF (N-6) 1000,1000,1030                                                   STMT0072
```

```
1000 IF (I) 1020,1020,1010
1010 LINK=1
     N=I
1020 IF (X-COEFFT(N)) 1040,1040,1620
1030 N=I
1040 GO TO (1130,1060,1190,1230,1080,1090,1180,1330),N
1050 X=Z
     N=2
1060 TEMP=X
     GO TO 1190
1070 PRESS=EXP(Z)
     GO TO 1150
1080 II=2
     JJ=3
     TOLER=.005
     GO TO 1100
1090 II=3
     JJ=2
     TOLER=.000005
1100 H=Y
     LINK=2
1120 N=1
1130 X=ALOG(PRESS)
     PLOG=X
     GO TO 1190
1140 TEMP=Z
1150 X=TEMP
     J=1
     N=4
     GO TO 1190
1160 SATLIQ(J)=Z
     J=J+1
     N=N+1
     IF (J-3) 1190,1190,1170
1170 IF (LINK) 1640,1640,1300
1180 H=X
```

```
      S=Y                                                               STMT0109
      X=S                                                               STMT0110
 1190 I=23*N-19                                                         STMT0111
      K=1                                                               STMT0112
      IF (X-COEFFT(I)) 1200,1200,1210                                   STMT0113
 1200 K=12                                                              STMT0114
 1210 I=I+K                                                             STMT0115
      ARG=X-COEFFT(I)                                                   STMT0116
      Z=0.0                                                             STMT0117
      DO 1220 K=1,10                                                    STMT0118
      I=I+1                                                             STMT0119
 1220 Z=Z*ARG+COEFFT(I)                                                 STMT0120
      GO TO (1140,1070,1050,1160,1160,1160,1410),N                      STMT0121
 1230 TEMP=Y                                                            STMT0122
      GO TO 1300                                                        STMT0123
 1240 ERROR=H-STEAM(II)                                                 STMT0124
      IF (ABS(ERROR)-TOLER) 1640,1250,1250                              STMT0125
 1250 IF (ERROR1) 1260,1280,1260                                        STMT0126
 1260 ERROR1=ERROR1-ERROR                                               STMT0127
      IF (ABS(ERROR1)-TOLER) 1290,1290,1270                             STMT0128
 1270 SLOPE=DELTA1/ERROR1                                               STMT0129
 1280 DELTA1=SLOPE*ERROR                                                STMT0130
      ERROR1=ERROR                                                      STMT0131
 1290 TEMP=TEMP+DELTA1                                                  STMT0132
 1300 IF (PRESS-COEFFT(1)) 1320,1320,1310                               STMT0133
 1310 IF ((.00001178*PRESS+.09411)*PRESS+382.1-TEMP) 1320,1320,1620     STMT0134
 1320 T=.55555556*TEMP+255.38223                                        STMT0135
      TLOG=ALOG(T)                                                      STMT0136
      TAU=1.0/T                                                         STMT0137
      COEFFT(222)=TAU*TAU*.1862101E+06                                  STMT0138
      COEFFT(217)=EXP(COEFFT(222)+.7879148E+01-TLOG)                    STMT0139
      COEFFT(221)=162460.*TAU                                           STMT0140
      COEFFT(220)=126970.*TAU                                           STMT0141
      COEFFT(219)=EXP(.1492776E+03-23.*TLOG)                            STMT0142
      COEFFT(212)=1.89-COEFFT(217)                                      STMT0143
      COEFFT(211)=82.546-COEFFT(221)                                    STMT0144
```

```
      COEFFT(210)=.21828*T-COEFFT(220)                                  STMT0145
      COEFFT(209)=COEFFT(219)-.0003635*T                                STMT0146
      COEFFT(222)=(COEFFT(222)+COEFFT(222)+1.0)*COEFFT(217)             STMT0147
      COEFFT(217)=COEFFT(212)-COEFFT(222)                               STMT0148
      COEFFT(214)=COEFFT(217)/COEFFT(212)                               STMT0149
      COEFFT(216)=COEFFT(211)*COEFFT(214)+41.273-COEFFT(221)            STMT0150
      COEFFT(215)=COEFFT(210)*COEFFT(214)-.5*COEFFT(220)                STMT0151
      COEFFT(214)=COEFFT(209)*COEFFT(214)+1.8461538*COEFFT(219)         STMT0152
      COEFFT(221)=.50*COEFFT(211)-COEFFT(216)                           STMT0153
      COEFFT(220)=.25*COEFFT(210)-COEFFT(215)                           STMT0154
      COEFFT(219)=.076923077*COEFFT(209)-COEFFT(214)                    STMT0155
      COEFFT(218)=(.0037299965*T+14.531813)*T+17306.513+472.24937*TLOG  STMT0156
      COEFFT(223)=-.0074599931*T-14.531813*TLOG+2.4524439+472.24937*TAU STMT0157
 1330 P=.068046190*PRESS                                                STMT0158
      PLOG=ALOG(PRESS)                                                  STMT0159
      COEFFT(213)=COEFFT(212)*TAU                                       STMT0160
      COEFFT(226)=COEFFT(213)*P                                         STMT0161
      COEFFT(225)=COEFFT(226)*COEFFT(226)                               STMT0162
      COEFFT(224)=COEFFT(225)*COEFFT(225)                               STMT0163
      COEFFT(224)=COEFFT(224)*COEFFT(224)*COEFFT(226)                   STMT0164
      COEFFT(226)=COEFFT(226)*COEFFT(213)                               STMT0165
      COEFFT(213)=P*TAU                                                 STMT0166
      STEAM(1)=(((COEFFT(209)*COEFFT(224)+COEFFT(210))*COEFFT(225)+     STMT0167
     1COEFFT(211))*COEFFT(226)+COEFFT(212)+4.55504/COEFFT(213))         STMT0168
     1*.0160185                                                         STMT0169
      STEAM(2)=((((COEFFT(214)*COEFFT(224)+COEFFT(215))*COEFFT(225)+    STMT0170
     2COEFFT(216))*COEFFT(226)+COEFFT(217))*P+COEFFT(218))*.04355685    STMT0171
      STEAM(3)=((((COEFFT(219)*COEFFT(224)+COEFFT(220))*COEFFT(225)+    STMT0172
     3COEFFT(221))*COEFFT(226)+COEFFT(222))*COEFFT(213)+COEFFT(223)     STMT0173
     3+4.55504*PLOG)*(-.02419825)                                       STMT0174
      QUAL=1.0                                                          STMT0175
      I=LINK+1                                                          STMT0176
      GO TO (1640,1640,1340,1240,1340,1450),I                           STMT0177
 1340 X=STEAM(II)                                                       STMT0178
      IF (H-X) 1350,1640,1360                                           STMT0179
 1350 Y=SATLIQ(II)                                                      STMT0180
```

```
      QUAL=(H-Y)/(X-Y)                                                  STMT0181
      X=1.0-QUAL                                                        STMT0182
      STEAM(1)=QUAL*STEAM(1)+X*SATLIQ(1)                                STMT0183
      STEAM(JJ)=QUAL*STEAM(JJ)+X*SATLIQ(JJ)                             STMT0184
      STEAM(II)=H                                                       STMT0185
      IF (LINK-2) 1640,1640,1460                                        STMT0186
 1360 I=(II-1)*11+154                                                   STMT0187
      J=1                                                               STMT0188
      X=PLOG                                                            STMT0189
 1370 DO 1380 K=209,219                                                 STMT0190
      COEFFT(K)=COEFFT(I)                                               STMT0191
 1380 I=I+1                                                             STMT0192
      X=X-COEFFT(209)                                                   STMT0193
      Y=Y-COEFFT(210)                                                   STMT0194
      COEFFT(209)=(COEFFT(211)*X+COEFFT(212))*X+COEFFT(213)             STMT0195
      COEFFT(210)=(COEFFT(214)*X+COEFFT(215))*X+COEFFT(216)             STMT0196
      COEFFT(211)=((COEFFT(217)*X+COEFFT(218))*X+COEFFT(219))*Y         STMT0197
      Z=COEFFT(211)+COEFFT(210)                                         STMT0198
      SLOPE=COEFFT(211)+Z                                               STMT0199
      Z=Z*Y+COEFFT(209)                                                 STMT0200
      GO TO (1390,1430,1530,1540),J                                     STMT0201
 1390 LINK=3                                                            STMT0202
      IF (Z-TEMP) 1300,1300,1400                                        STMT0203
 1400 TEMP=Z                                                            STMT0204
      GO TO 1300                                                        STMT0205
 1410 J=2                                                               STMT0206
      I=227                                                             STMT0207
      X=H                                                               STMT0208
      IF (Z-H) 1420,1370,1370                                           STMT0209
 1420 I=187                                                             STMT0210
      GO TO 1370                                                        STMT0211
 1430 DPDS=SLOPE                                                        STMT0212
      PRESS=EXP(Z)                                                      STMT0213
      PLOG=Z                                                            STMT0214
      IF (I-227) 1520,1520,1440                                         STMT0215
 1440 LINK=4                                                            STMT0216
```

```
      II=2                                                              STMT0217
      JJ=3                                                              STMT0218
      GO TO 1120                                                        STMT0219
 1450 DH=H-STEAM(2)                                                     STMT0220
      STEAM(3)=STEAM(3)+DH/(TEMP+459.69)                                STMT0221
 1460 DS=S-STEAM(3)                                                     STMT0222
      DELTA1=STEAM(3)-ERROR1                                            STMT0223
      IF (ERROR1) 1470,1490,1470                                        STMT0224
 1470 IF (ABS(DELTA1)-.000005) 1500,1500,1480                           STMT0225
 1480 DPDS=(PLOG-PLOG1)/DELTA1                                          STMT0226
 1490 PLOG1=PLOG                                                        STMT0227
      ERROR1=STEAM(3)                                                   STMT0228
 1500 PRESS=PRESS*(1.0+DS*DPDS)                                         STMT0229
      IF (LINK-4) 1510,1510,1550                                        STMT0230
 1510 IF (ABS(DS)-.000005) 1640,1120,1120                               STMT0231
 1520 LINK=5                                                            STMT0232
      X=H                                                               STMT0233
      Y=S                                                               STMT0234
      I=198                                                             STMT0235
      J=3                                                               STMT0236
      GO TO 1370                                                        STMT0237
 1530 TEMP=Z                                                            STMT0238
      DTDS=SLOPE                                                        STMT0239
      X=PLOG                                                            STMT0240
      Y=H                                                               STMT0241
      I=165                                                             STMT0242
      J=4                                                               STMT0243
      GO TO 1370                                                        STMT0244
 1540 DTDH=SLOPE                                                        STMT0245
      GO TO 1300                                                        STMT0246
 1550 TEMP=TEMP+DS*DTDS                                                 STMT0247
      IF (ABS(DH)-.005) 1610,1560,1560                                  STMT0248
 1560 DELTA2=DH-ERROR2                                                  STMT0249
      IF (ERROR2) 1570,1590,1570                                        STMT0250
 1570 IF (ABS(DELTA2)-.005) 1600,1600,1580                              STMT0251
 1580 DTDH=(TEMP1-TEMP)/DELTA2                                          STMT0252
```

```
1590 TEMP1=TEMP                                                          STMT0253
     ERROR2=DH                                                           STMT0254
1600 TEMP=TEMP+DH*DTDH                                                   STMT0255
     GO TO 1320                                                          STMT0256
1610 IF (ABS(DS)-.000005) 1640,1600,1600                                 STMT0257
1620 WRITE (6,1630) NI,XI,YI                                             STMT0258
1630 FORMAT (I3,2E14.8,13H OUT OF RANGE)                                 STMT0259
     STOP                                                                STMT0260
1640 RETURN                                                              STMT0261
     END                                                                 STMT0262
```

BIOGRAPHY

The author was graduated from the U. S. Naval Academy in 1960. From 1960-1964 he served in various engineering capacities including Engineer Officer of U.S.S. ROBERT A. OWENS (DD827). He underwent naval nuclear power training and served as Material Officer for Destroyer Squadron Two prior to coming to Massachusetts Institute of Technology in 1967. He received the degree of Master of Science in Mechanical Engineering and the degree of Naval Engineer in 1970 with a thesis in the area of two phase turbulent mixing in boiling water reactors. He is presently a Lieutenant Commander in the United States Navy.

134726

Thesis
R2765 Reese
v.2
Analysis of a hydrogen-oxygen semiclosed rankine cycle propulsion plant for deep submersibles.